Volcanological and Environmental Studies of Mount Erebus, Antarctica

Philip R. Kyle
Editor

American Geophysical Union

ANTARCTIC RESEARCH SERIES

Physical Sciences

American Geophysical Union

ANTARCTIC RESEARCH SERIES

EREBUS

Keeper of the Southern Gateway, grim, rugged, gloomy
and grand;
Warden of these wastes uncharted, as the years sweep
on, you stand.
At your head the swinging smoke-cloud; at your feet
the grinding floes;
Racked and seared by the inner fires, gripped close by
the outer snows.
Proud, unconquered and unyielding, whilst the untold
æons passed,
Inviolate through the ages, your ramparts spurning
the blast,
Till men impelled by a strong desire, broke through
your icy bars;
Fierce was the fight to gain that height where your
stern peak dares the stars.
You called your vassals to aid you, and the leaping
blizzard rose,
Driving in furious eddies, blinding, stifling, cruel
snows.
The grasp of the numbing frost clutched hard at their
hands and faces,
And the weird gloom made darker still dim seen
perilous places.
They, weary, wayworn, and sleepless, through the long
withering night,
Grimly clung to your iron sides till with laggard Dawn
came the light:
Both heart and brain upheld them, till the long-drawn
strain was o'er,
Victors then on your crown they stood and gazed at
the Western Shore;
The distant glory of that land in broad splendour lay
unrolled,
With icefield, cape, and mountain height, flame rose
in a sea of gold.
Oh! Herald of returning Suns to the waiting lands
below;
Beacon to their home-seeking feet, far across the
Southern snow.
In the Northland in the years to be, pale Winter's first
white sign
Will turn again their thoughts to thee, and the glamour
that is thine.

<div align="right">NEMO.</div>

Volcanological and Environmental Studies of Mount Erebus, Antarctica

Philip R. Kyle
Editor

CONTENTS

The Antarctic Research Series:

STATEMENT OF OBJECTIVES

The Antarctic Research Series provides for the presentation of detailed scientific research results from Antarctica, particularly the results of the United States Antarctic Research Program, including monographs and long manuscripts.

The series is designed to make the results of Antarctic fieldwork available. The Antarctic Research Series encourages the collection of papers on specific geographic areas within Antarctica. In addition, many volumes focus on particular disciplines, including marine biology, oceanology, meteorology, upper atmosphere physics, terrestrial biology, geology, glaciology, human adaptability, engineering, and environmental protection.

Topical volumes in the series normally are devoted to papers in one or two disciplines. Multidisciplinary volumes, initiated in 1990 to enable more rapid publication, are open to papers from any discipline. The series can accommodate long manuscripts and utilize special formats, such as maps.

Priorities for publication are set by the Board of Associate Editors. Preference is given to research manuscripts from projects funded by U.S. agencies. Because the series serves to emphasize the U.S. Antarctic Research Program, it also performs a function similar to expedition reports of many other countries with national Antarctic research programs.

The standards of scientific excellence expected for the series are maintained by the review criteria established for the AGU publications program. Each paper is critically reviewed by two or more expert referees. A member of the Board of Associate Editors may serve as editor of a volume, or another person may be appointed. The Board works with the individual editors of each volume and with the AGU staff to assure that the objectives of the series are met, that the best possible papers are presented, and that publication is timely.

Proposals for volumes or papers offered should be sent to the Board of Associate Editors, Antarctic Research Series, at 2000 Florida Avenue, N.W., Washington, D.C. 20009. Publication of the series is partially supported by a grant from the National Science Foundation.

Board of Associate Editors
Antarctic Research Series

FOREWORD

I had the great pleasure of taking part in the scientific exploration of Mount Erebus during the period 1973 to 1979. Now it is my pleasure to write the foreword for this book, which contains the results of 20 years of study carried on at this exceptional volcano.

Mount Erebus is a unique volcano. Unique, in present geological times at least, because nowhere in the world is there an active volcano with phonolite magma containing abundant giant anorthoclase phenocrysts. Even in past geological times, only Mount Kenya, Mount Kilimanjaro and a few other volcanoes have erupted this rare variety of rock, appropriately named "kenyte". But Mount Kenya, where in 1948 I built an eskimo igloo on the Equator and where I was stricken by snow blindness, is unfortunately a spent volcano. Mount Erebus is the only volcano currently erupting this exceptional anorthoclase phonolite (kenyte) magma.

The type of eruptive activity exhibited by Mount Erebus is also extremely rare, characterized as it is by the presence of a permanent molten lava lake. Such lava lakes constitute anomalous behavior in that they reflect (semi)permanent eruptive activity. Less than a handful of the many thousands of potentially active volcanoes scattered around the world have developed, or are presently developing, semipermanent eruptive activity.

The persistence of eruptive activity constitutes a second anomaly. Over 90% of the presently active volcanoes fall into repose immediately after releasing the gas and lava that have accumulated during the preceding period of repose. The remaining few percent (i.e., a dozen or so of the permanently eruptive volcanoes) continue their eruptive activity even when the bulk of the magma has been erupted. Why?

The answer I proposed a few decades ago postulates that the frequency of eruptive periods depends mainly on the local tectonic situation. By this I mean the number and width of the different fault trends which intersect under the volcano. The combined width of the fractures may determine the ease with which magmas can eventually reach the surface.

Volcanoes located on a single fault are normally, as A. Rittmann named them, monogenetic, i.e., volcanoes that become extinct after a single eruption. I believe the reason is that the magma solidifies as a massive plug within the conduit. Such a plug is so strong that further eruptive energy cannot reopen this fissure which, henceforward, is blocked forever.

Monogenetic fissure eruptions generate flood basalts as well as tiny cinder cones. When eruptive activity resumes on such a fault, magma reaches the surface either at a different spot on the same fissure or through a new fissure, parallel to the previous one, broken open by tectonic and magmatic stresses. This mechanism accounts for the huge flood basalts, known from every continent, and the basalts erupted from the oceanic rifts.

Large polygenetic volcanoes, on the other hand, are located above intersecting fractures, a *sine qua non* for renewed activity that needs feeder channels wide enough to inhibit complete solidification during repose periods. Permanently and semipermanently erupting volcanoes are all polygenetic. Most seem to be located where several fractures of various trends intersect. Because the cooling and eventual solidification of a magma body below the surface is controlled largely by its thickness and depth, the wider the channel, the longer the duration of the molten or plastic state. This allows longer periods for the resumption of eruptive activity. A molten or partially molten magma plug is incomparably easier to overcome, especially when the channels are wide enough, than a solidified and crystallized one, particularly when the conduits are narrow.

Mount Erebus poses many scientific problems. To solve them is a scientifically exciting challenge. From the standpoint of volcanology, many questions related to the eruptive behavior remain. What are the physical and chemical characteristics of its eruptive gas phase? What are the dynamics of the convective currents observed on the surface of the lava lake? What are the magma volumes involved? What is the composition of gas within vesicles, and what are the chemical reactions when they escape into the air? What are the thermodynamics and kinetics involved? What chemical equilibria exist in the magmatic gas phase?

Using a broader definition of volcanology some other questions should be tackled by volcanologists. What are the local tectonics that allow the permanent eruptive

activity? How many fault trends intersect beneath Mount Erebus? Do all these faults result from extensional pull or are other stresses involved? What is the width of the resulting feeder pipe(s)? What are the tectonic and magmatic relationships with the surrounding volcanoes on Ross Island and the more distant ones such as Mount Discovery and the active Mount Melbourne?

All these questions and many others were nested in my mind during the four visits I made to the crater of Mount Erebus. Our first goal, at the time, was only to climb down into the Inner Crater to reach the lava lake shores in order to make physical and mechanical measurements and to sample the volcanic gas. Unfortunately, we failed to achieve our hopes. Consequently, this type of investigation, among many others, is still open to any team willing to utilize the unique opportunities offered by the continuous volcanic activity at Mount Erebus. It should be carried out with the instrumentation and facilities which modern volcanology now has available, but which were not available to me and my colleagues 15-20 years ago. The instrumentation should be used by multidisciplinary teams who are scientifically competent as well as mentally and physically prepared to carry on such a difficult, yet stimulating, program.

One and a half centuries have elapsed since Captain James Ross and his men gazed in wonder from the decks of H.M.S. *Erebus* and H.M.S. *Terror* at the erupting volcano they named after one of their ships. Three quarters of a century has passed since a team of hardy explorers, belonging to Ernest Shackleton's South Pole expedition, made the first ascent of the volcano. Since the early 1970s important scientific observations and data have been collected, some of which are published here. This volume, therefore, constitutes a basic step leading to the understanding of the unique, fundamental place of Mount Erebus on Earth.

Haroun Tazieff
Paris, France

PREFACE

In January 1841 Captain James Clark Ross sailed in his two small ships *Erebus* and *Terror* into the then unknown southern Ross Sea and discovered and named Mount Erebus. In his journal Ross noted:

> ...it proved to be a mountain twelve thousand four hundred feet of elevation above the level of the sea, emitting flame and smoke in great profusion; at first the smoke appeared like snow drift, but as we drew nearer, its true character became manifest.

On January 28, 1841, Ross reported:

> At 4 P.M. Mount Erebus was observed to emit smoke and flame in unusual quantities, producing a most grand spectacle. A volume of dense smoke was projected at each successive jet with great force, in a vertical column, to the height of between fifteen hundred and two thousand feet above the mouth of the crater, when condensing first at its upper part, it descended in mist or snow, and gradually dispersed, to be succeeded by another splendid exhibition of the same kind in about half an hour afterwards, although the intervals between eruptions were by no means regular. The diameter of the columns of smoke was between two and three hundred feet, as near as we could measure it; whenever the smoke cleared away, the bright red flame that filled the mouth of the crater was clearly perceptible; and some of the officers believed they could see streams of lava pouring down its sides until lost beneath the snow...

Thus began the exploration and the first observations of the world's southernmost active volcano. The observations of the volcanic activity of Mount Erebus made by Ross and his officers are among the first geologic observations ever made in Antarctica. Even today the report is very relevant to our understanding of the eruptive history of Mount Erebus and should be viewed as historically one of the significant events in Antarctic exploration. This volume was inspired by the report of

Ross and commemorates the 150th anniversary of his discovery.

Mount Erebus is one of the unique volcanoes in the world. Its uniqueness is not derived from its southern locality, but rather from the unusual volcanic activity and lava type. The convecting lava lake of anorthoclase phonolite magma differs from the better known and well-studied lava lakes in Hawaii. Many of the Hawaiian lava lakes form when craters or vents are filled with lava which then slowly cool. They represent ponds of lava. In all respects the Hawaiian lava lakes are, as the name implies, lakes of lava, magma that has been erupted. Mount Erebus on the other hand has a convecting magma lake with magma circulating from a chamber deep in the volcano. The Mount Erebus lava lake therefore gives us a window into the magma chamber and an opportunity to study the internal plumbing of a volcano.

This volume is the first to describe various aspects of the volcanology and environmental impact of Mount Erebus. It presents the most recent and authoritative accounts available. The harsh environment and short field season limit the scope of research which is possible. Yet this collection of papers shows that high-quality research is possible and in some cases is innovative by world standards. The volume comprises a group of papers which clearly illustrate the broad spectrum of investigations made by modern researchers at active volcanoes. The subjects covered include remote sensing, seismology, estimates and characterization of gas and aerosol emissions, magma crystallization and evolution, deformation studies, and the chemical record left by the gas emissions in the snow surrounding the volcano. As these contributions clearly illustrate, the scope of work at Mount Erebus has been truly multidisciplinary involving volcanologists, glaciologists, geophysicists, atmospheric chemists, petrologists and many others.

Mount Erebus poses many fundamental questions which relate both to Antarctica and to volcanology in general. In recent years it has been recognized that Mount Erebus is an important natural source of gases and aerosols to the Antarctic atmosphere and that these eventually end up in the snow and ice of the Antarctic ice sheets. As anthropogenic effects are starting to be

recognized in this once pristine environment, it becomes essential to understand and evaluate the natural sources of gases and aerosols. Considerable speculation has circulated in the popular media surrounding the possibility that Mount Erebus could be a source of chlorine that destroys the ozone layer over Antarctica each spring. Such speculation is not supported by current observations made at Mount Erebus, but it is important that the scientific community not dismiss the idea out of hand without making the appropriate scientific observations and evaluations. On the volcanological side, Mount Erebus has much to offer in our understanding of the origin, evolution, behavior, eruptive activity and life of active convecting lava (magma) lakes.

Much remains to be learned about the volcanic activity and magmatic processes at this beautiful and interesting volcano. In the 25 years of modern scientific observations and investigations we have only scratched the surface, but in doing so we have come to appreciate the dynamic nature of Mount Erebus and its special place among the world's volcanoes. This volume gives the scientific community an opportunity to learn of the progress a small but devoted group of scientists has made in understanding Mount Erebus.

As editor I extend my thanks to the numerous authors for their manuscripts and also for their patience. I thank the reviewers for their thorough and insightful comments and suggestions which helped improve the quality of the papers. David Elliot, as series editor, has held the whole volume together. Funding from the Office of Polar Programs, National Science Foundation through Grants OPP-8716319 and OPP-9118056 has helped defray editorial expenses.

This volume is dedicated to Ray Dibble as he enters retirement after a career of teaching in the Department of Geology at Victoria University of Wellington. We wish him well and are delighted to see him continue an active role in field work and seismological observations on Mount Erebus.

Philip R. Kyle
New Mexico Institute of Mining and Technology
Socorro

THE VELOCITY STRUCTURE OF MOUNT EREBUS, ANTARCTICA, AND ITS LAVA LAKE

R. R. Dibble and B. O'Brien

Victoria University of Wellington, Wellington, New Zealand

C. A. Rowe

Geophysical Institute, University of Alaska, Fairbanks, Alaska

Mount Erebus, Ross Island, contains an active phonolite lava lake in its summit crater which erupts in a strombolian fashion occasionally each day. The velocity structure of the volcano has been studied using three seismic refraction lines up to 1.4 km long, six large seismic shots, and the frequent strombolian explosions recorded by video surveillance and a 10-station seismic net. The surface permafrost layer on the summit cone has a velocity of about 3 km/s and prevents critically refracted arrivals from subsurface layers of lower velocity. Seismic shots in unfrozen ground near the summit show a layer below the permafrost up to 100 m thick with velocity ranging from 1 to 2 km/s. The underlying refractor has lateral velocity changes from 1.3 to 4 km/s along the line of fumaroles from Side Crater to the somma rim. The six large seismic shots were recorded over distances of 4 to 38 km. Seismic wave arrival times limit the surface layer thickness to between 220 and 650 m and the velocities to 1.3 to 3.1 km/s. The surface layer is underlain by 5 km of massive volcanics of a velocity of 4.3 km/s and in turn is assumed (from marine seismic surveys in McMurdo Sound) to be underlain by 3–5 km of Cenozoic sediments with velocity of 4.1–5.5 km/s. A low-velocity layer probably underlies the volcanics, unless the volcanic load has sufficiently increased the seismic velocity of the sediments. The basement below the volcano has a velocity of 6.5 km/s, in agreement with seismic surveys in McMurdo Sound. Several multiplets of strombolian explosion earthquakes with cross-correlation coefficients between waveforms exceeding 0.7, and lag times between events which are constant within 0.03 s at each station, have been recorded. The time and location of the explosions were simultaneously recorded by video surveillance. The stacked seismic onsets and video explosion instants are reliable to within 0.1 s, and the earthquake foci lie within 100 m of each other. They show that the explosions occur 0.47 ± 0.1 s before the intercept time of the seismic time/distance curve and that the apparent velocity is 4.1 ± 0.1 km/s over the distance range 0.7 to 10 km. The refraction lines show that a seismic delay of such magnitude is not occurring on the flanks of the volcano. It must occur in and around the low-velocity lava lake, magma column, and magma chamber of the volcano.

INTRODUCTION

Mount Erebus, a phonolitic volcano 3794 m high and 1670 km^3 in volume, has an active lava lake in its summit crater. Study of the velocity structure of Mount Erebus began in December 1974 from a temporary five-station seismic network of 2-km aperture (Figure 1).

Kyle et al. [1982] reported a peak at 1.4 km/s in the histogram of apparent velocities of local earthquake waves across the net and suggested this was the true velocity. *Dibble et al.* [1984] used the same 1974 recordings to obtain apparent velocities of 1.6 ± 0.2 km/s between 0.25 and 1.25 km distance from the strombolian explosions which were assumed to be the source of the
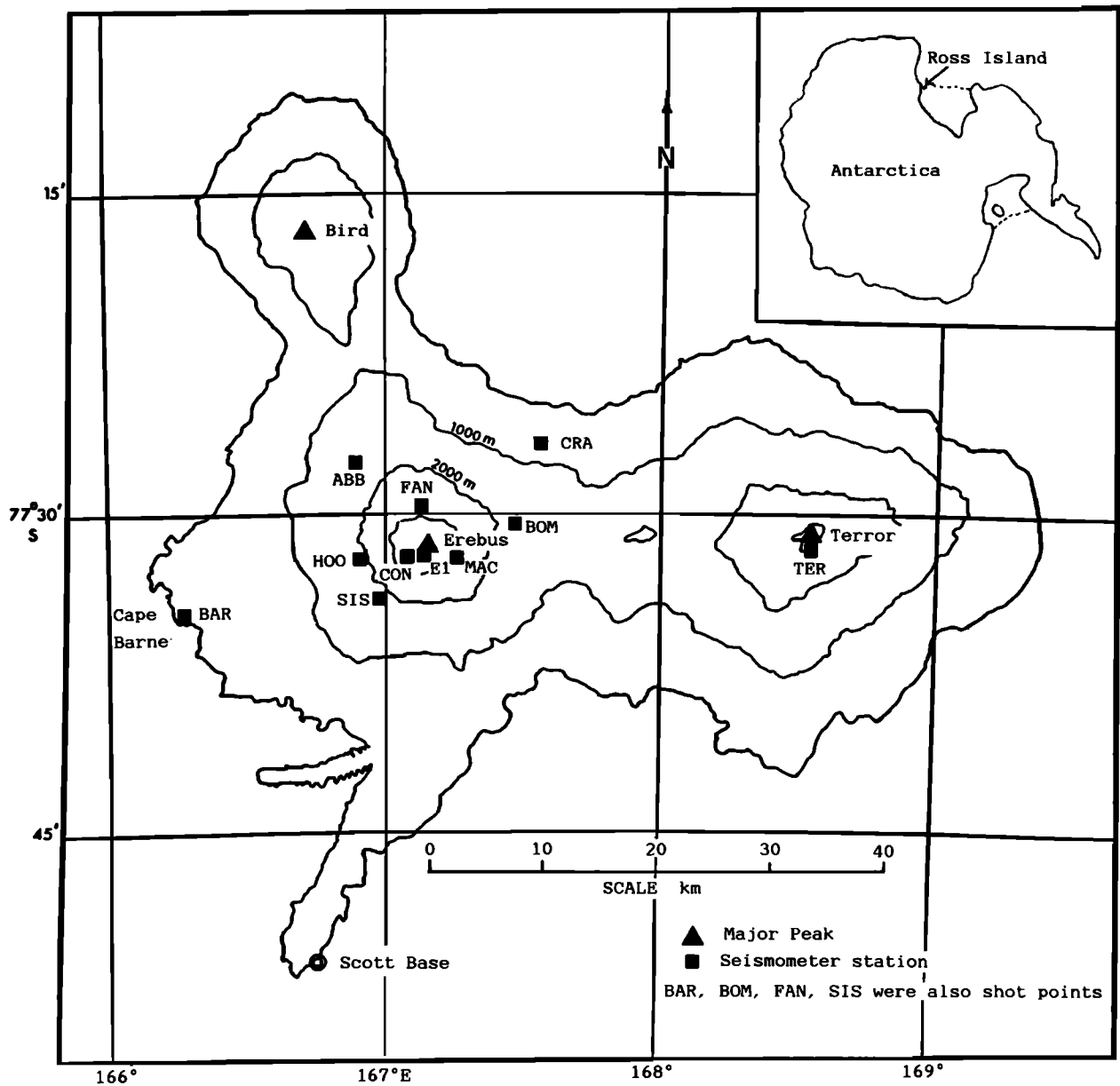
Fig. 1. Map of Ross Island, showing Mount Erebus and the telemetry seismic stations. BAR, BOM, FAN, and SIS were close to the shot points for the large seismic explosions.

accompanying earthquakes. Using the 1.6-km/s velocity in a homogeneous model gave foci at shallow depths, clustered within 1 km of the lava lake. There were numerous nonlocatable earthquakes outside the net.

Better data began to accumulate after 1980 when a permanent four-station telemetry seismic network of 16-km aperture was installed by the International Mount Erebus Seismic Study (IMESS) project. *Shibuya et al.* [1983] located 162 events recorded during the 1981–

1982 field season. They found that a homogeneous earth model of velocity 2.1 km/s gave the smallest rms errors. The resulting locations of earthquakes associated with strombolian explosions in the lava lake were between 850 and 4000 m from the explosions. *Shibuya et al.* [1983] and *Kienle et al.* [1983] proposed that the earthquakes were separate from the explosions in time and place, and the earthquakes may have triggered the explosions. However, *Dibble* [1985] showed that the

durations of explosion earthquakes and infrasonic signals from the strombolian explosions were correlated. This would not be expected if the earthquakes merely triggered the eruptions.

Dibble et al. [1984] estimated the vertical velocity through Mount Erebus from changes in the arrival time of distant earthquakes versus station height (from sea level to 3800 m). The mean of six determinations was 4.5 ± 1.3 km/s, after omitting two outlier values of 1.4 and 13.4 km/s. *Dibble et al.* [1984] also obtained an apparent velocity of 7.5 km/s below the basement from a shot offset 40 km from the Erebus seismic net. Unfortunately, the shot instant was unreliable and prevented reliable interpretation of depth to the material.

Within McMurdo Sound, near the flank of Mount Erebus, *McGinnis et al.* [1983] measured seismic refraction velocities of 2 to 4.7 km/s in 3-km-thick Cenozoic sediments. The sediments were older than Mount Erebus [*Moore and Kyle*, 1987] and appeared to underlie it. The seismic basement had velocities of 5 and 6.5 km/s.

SEISMIC REFRACTION SURVEYS
ON THE SUMMIT PLATEAU

An attempt to shoot seismic refraction lines on the summit area was made in January 1985 (J. Kienle and R. R. Dibble, unpublished data). Line A-A´ (Figure 2) was a 165-m spread laid out on snow west-southwest (WSW) from a 12-channel Nimbus 1210F digital seismograph operating in the Erebus lower hut. Shot points (flagged and surveyed by V. Belgrave of the New Zealand Department of Lands and Survey) were offset in an anticlockwise direction around the plateau. The spread was end shot with 1 kg of Nitromon at 1-m depth in both directions and gave a surface layer velocity of 2400 m/s. However, the arrivals were highly attenuated and unreadable beyond 90 m, as if a thin surface layer was underlain by lower-velocity material which refracted the ray paths downward. Shots at 2-m depth in snow were fired at distances of 214 m and 810 m (9-kg shot) off the WSW end of the spread. Again, the arrivals were extremely poor but were consistent with an unreversed velocity of 1500 to 2000 m/s with small intercept time, suggesting an underlying lower-velocity layer. Even when 2-m-deep shot holes were drilled close beside lava outcrops, the holes always bottomed in fairly hard ice of undetermined depth. The only certain result from line A-A´ was that there was no 4-km/s refractor within about 300 m of the surface.

To avoid the ice, and the difficulty of drilling in frozen ground, a survey in November 1989 used repeated sledge hammer blows and explosions of 1.5-m lengths of detonating cord laid on the surface. These were stacked and recorded on a Nimbus 1210F digital seismograph in the Erebus upper hut. Seismic line B-B´, 330 m long on the exposed scoria of the summit cone between the upper hut and Nausea Knob (Figure 2), was end shot for each length and direction. A velocity of 3000 ± 300 m/s was found on the undisturbed volcanic cone, and 2100 ± 300 m/s was found on the slump erroneously known as Camp Flow on which the hut stands. Both time-distance lines had approximately zero intercept time, indicating that they were surface velocities. A minimum of five shots of detonating cord had to be stacked to record at 330 m distance, but although the improvement over the 1985 records was spectacular, no refracted arrivals were recorded.

It was clear that the surface permafrost layer on the scoria cone had a higher velocity (3 km/s) than that initially accepted for the volcano as a whole (2.1 km/s) and that lower-velocity layers might not be detected unless the shots were fired in warm ground. Consequently, in November 1990 a seismic refraction survey was made on the summit plateau over a 1.4-km line (C-C´, Figure 2) between shot points at the bottom of Side Crater and the very edge of the summit plateau near CON seismic telemetry station. Three contiguous 330-m spreads of the Nimbus 1210F digital seismograph (kept warm with a 20-W heater and an insulated box) were laid out from the CON end of the line and shot from each end of the line, using shots up to 10 kg in 1-m-deep holes. The line was close and parallel to Tower Ridge, a line of small craters and active fumaroles which must be underlain by warm ground. This was expected to have velocities as low as any other part of the solid edifice. Warm ground was not exposed at the edge of the plateau. The shots were in very hard snow there and appeared to be just off and level with the top of a cliff under the snow, which may be the top of a slump scar.

The arrivals were weak but readable at nearly all the geophones, although on some records the third half cycle was the first visible arrival. This was recognized from the recordings on neighboring geophones between contiguous spreads (Figure 3). In all cases the times of peaks and troughs in the waveform were read and corrected to the time of first onset using the empirical square root relationship between period and travel time found by *Ricker* [1953]. At Mount Erebus the period varied unevenly with travel time, from 17 ms at 20-m distance to 100 ms at 1400 m, and the relationship was fitted to each homogeneous section of the time-period curve. The resulting uncertainty in adopted arrival times was usually within 40 ms. The apparent velocities were more reliable.
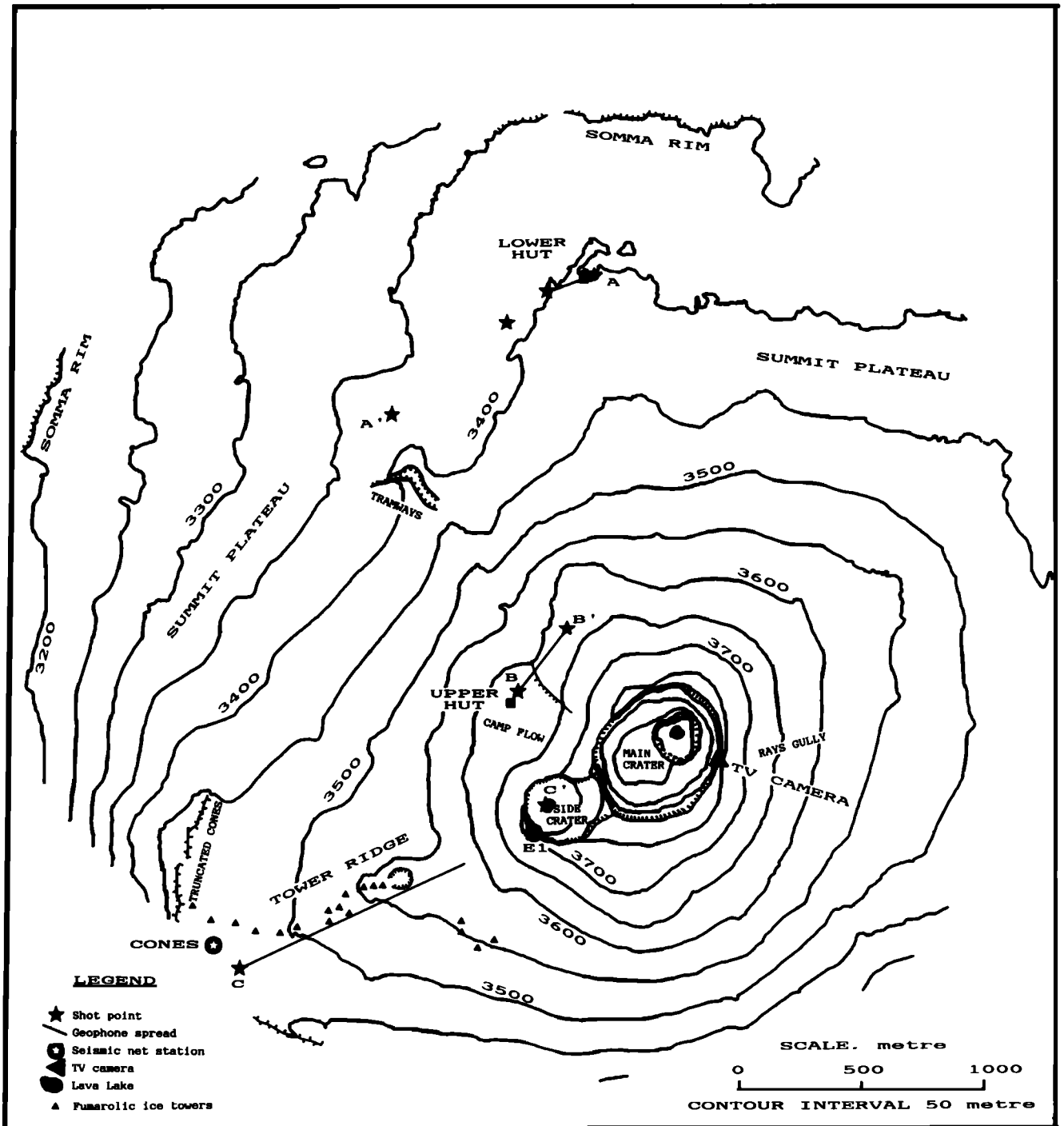
Fig. 2. Map of the Erebus plateau and summit cone showing the seismic refraction lines observed in 1984–1985 (A-A´), 1989 (B-B´), and 1990 (C-C´), the seismic telemetry stations E1 and Cones, and the TV camera site (modified from AP 1253 by the New Zealand Department of Lands and Survey, from aerial photography flown December 24, 1979, by the U.S. Navy).
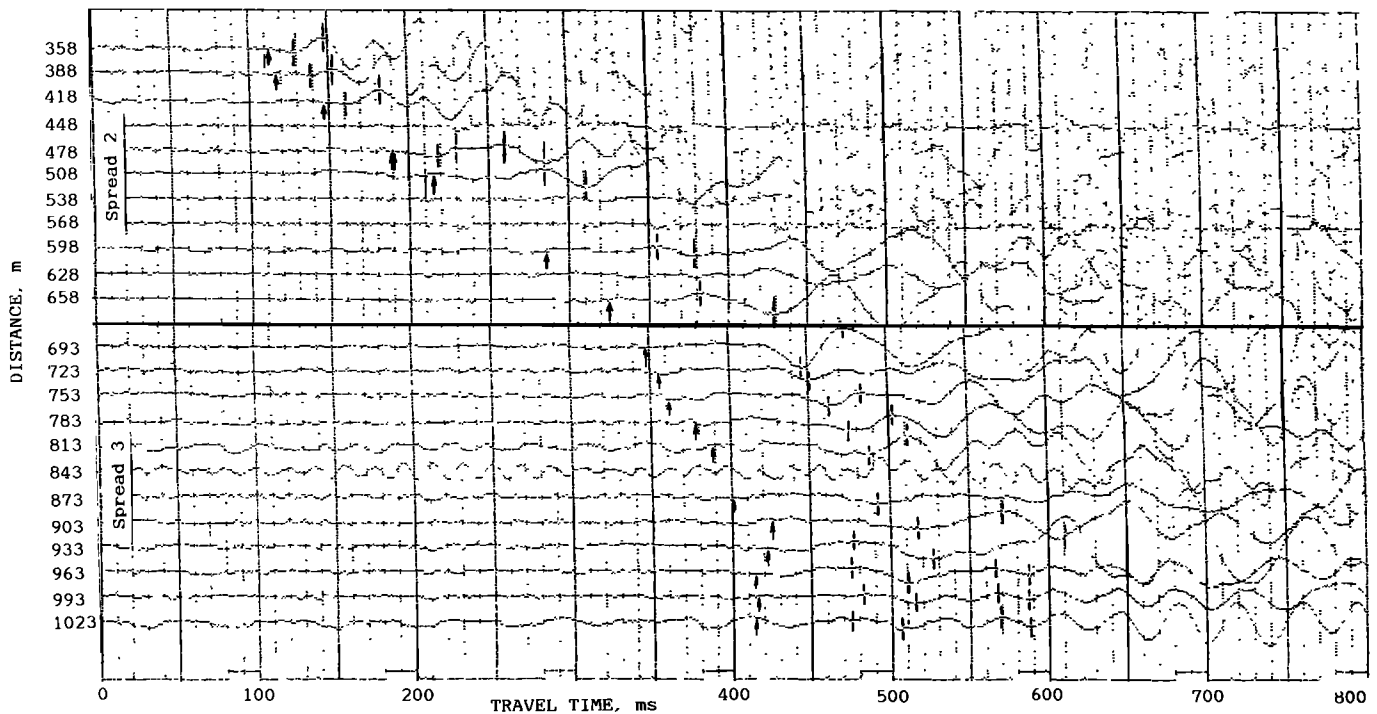
Fig. 3. Seismograms from shot point C (Cones) on refraction line C-C', showing the picks on the contiguous spreads 2 and 3. On the near geophones of spread 3 the third half cycle was the first visible arrival. Arrows mark the times corrected to the compressional onset which is downward on the record.

The time-distance graph (Figure 4b), which shows times relative to 4 km/s, has been interpreted by obtaining a preliminary model of refractor depth and lateral velocity variation by Hagedoorn's [1959] plus-minus method, and adjusting it by ray tracing using RAYAMP-PC, 2.3 [Crossley, 1989] as shown in Figure 4a. A subpermafrost near-surface layer up to 90 m thick with lateral velocity variations of 1.0 to 1.9 km/s overlies a refractor with lateral velocity variations between 1.3 and 4.0 km/s. The lowest velocities were found below the active fumaroles of Tower Ridge, immediately downhill from Western Crater. Most of the ice towers are underlain by caves [Giggenbach, 1976], which may contribute to the low apparent velocities. A second arrival of high apparent velocity recorded in the middle of the line from shots in Side Crater may be a reflection from a surface about 1 km deep, dipping steeply outward from Main Crater. If so, the rays leave the shot point at angles exceeding 90° (i.e., backward) and cannot be traced using RAYAMP.

LARGE-SCALE SEISMIC EXPERIMENT

In the 1984/1985 austral summer, IMESS [Kienle et al., 1985] fired nine shots of 5 to 300 kg of Nitromon in crevasses and the sea at four sites greater than 4 km from the summit. They were recorded on an eight-station seismic net to determine the velocity structure. Each shot site was close to a seismic telemetry station so that the shot instant could be transmitted to the recorder as a pulse on the geophone signal. Unfortunately, the pulse obscured the arrival at that geophone, so that the closest station which recorded the first arrival was at least 4 km from each shot point, precluding determination of shallow structure. The shot parameters are given in Table 1, and the locations of the seismic telemetry stations are given in Table 2. Both the shot points and the seismic stations are shown in Figure 1.

Kaminuma et al. [1987] published without substantiation a tentative P velocity structure of 2.9 km/s in the top 0.5 km, 4.7 km/s in the next 1.5 km, 6.2 km/s below
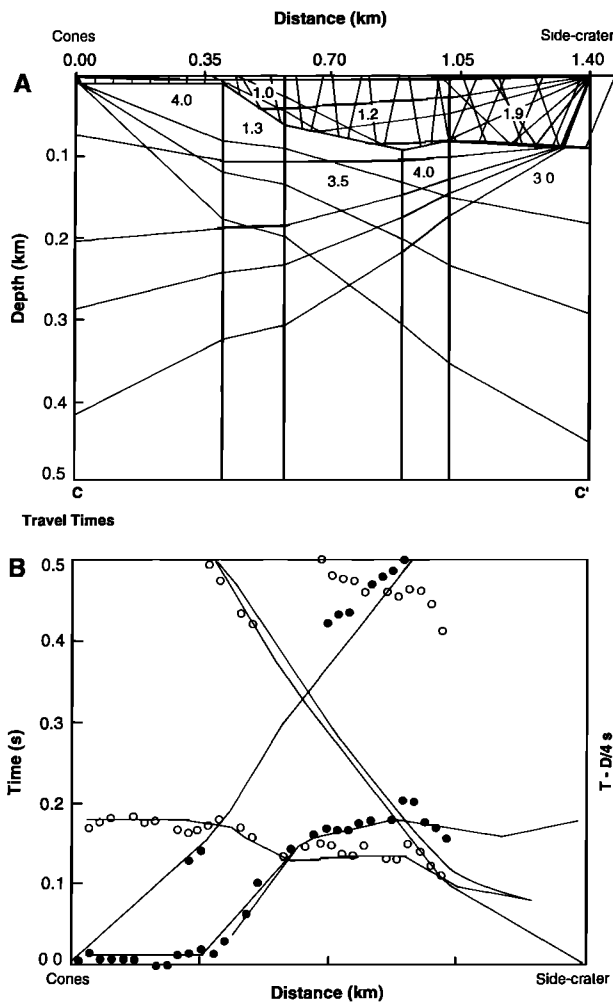
Fig. 4. The refraction line C-C' between E1 and Cones: (a) the ray paths and interpreted structural cross section, with velocities in kilometers per second; and (b) reversed time-distance graph reduced by 4.0 km/s, showing observed times (open symbols from Cones and solid symbols from E1) and lines calculated by RAYAMP-PC V.2.3.

2 km, and 7.0 km/s below 4.5-km depth. *Rowe* [1988] interpreted the time-distance graph shown in Figure 5 (in which slant distances are used) as three conical layers parallel to the mountain slope. Regretably, a 272-m survey error in the position of CON station discovered in 1990 necessitates a recalculation. The least squares fitted time-distance lines for Figure 5 (excluding points with residuals of more than twice the standard deviation of *t*) are as follows:

$$t_1 = (0.32 + x/4340) \pm 0.12 \text{ s}$$

where *x* is 3.95- to 13.54-km distance and

$$t_2 = (2.14 + x/6170) \pm 0.08 \text{ s}$$

where *x* is 17.45- to 29.95-km distance. The homogeneous plane layer interpretation using 2.8 km/s as the surface layer velocity is as follows: below ground surface, 2.8 km/s; below 0.58-km depth, 4.3 km/s; and below 6.1-km depth, 6.2 km/s.

Rowe [1988] found that the shot positions were more accurately relocated by HYPOELLIPSE [*Lahr*, 1982], if the top two layers were replaced by a single layer with a velocity gradient from 3.6 km/s at the summit to 4.6 km/s at 7-km depth. This was underlain by a 6.1-km/s half-space. The relocation errors averaged 0.8 ± 1.1 s in origin time, 1.3 ± 1.6 km in position, and 1.5 ± 0.6 km in depth. The reliability of this result suffers from the limitations that (1) HYPOELLIPSE cannot accurately incorporate the large range in the seismograph station elevations, (2) recordings at short distances are lacking, and (3) the survey location of CON station was 272 m in error.

The least reliable parameter in a layered model is the mean near-surface velocity. The only certain result from the large seismic experiment is that it does not exceed 3.1 km/s. Line C-C' showed a complex structure with near-surface velocities as low as 1 km/s. The mean near-surface velocity is unknown, but adopting 2.0 km/s for Rowe's calculation, the depths to 4.3- and 6.2-km/s material would be 0.36 km and 5.9 km, respectively. Tentatively, the surface layer is uncompacted volcanics, and the deepest is igneous basement.

Next we examine the assumption of the single 4.3-km/s layer between the surface layer and the basement by incorporating marine seismic studies around Ross Island. *Northey et al.* [1975] found by reflection profiling that the upper 150 m of the sediments under McMurdo Sound appeared to abut against volcanic material in the 900-m-deep moat along the west coast of Ross Island, and that the deeper strata appeared to extend beneath the volcanics off Cape Barne at the same dip as the seafloor (1.35°). A refraction survey from the sea ice across McMurdo Sound by *McGinnis et al.* [1983] found layers nearly parallel to the seafloor which averaged 2.5 km/s below the seafloor, 3.3 km/s below 0.35 km under the seafloor, 4.1 km/s below 1.70 km under the seafloor, 5.0 km/s below 3.05 km under the seafloor (basement?), and 6.5 km/s below 5.25 km under the seafloor (subbasement?). As all but the 2.5-km/s layer are interpreted by *Wong and Christoffel* [1981] and *McGinnis et al.* [1983] as older than Erebus, it is probable that the 3.3-, 4.1-, 5.0-, and 6.5-km/s layers extend right under Erebus (but not necessarily with these velocities) and that the top two form a low-veloci-

TABLE 1. 1984 Shot Locations, Times, and Sizes

Name	Latitude	Longitude	Height, m	Date	Time, MST	Size, kg
Fang	77.48748°S	167.14126°E	2578	Dec. 4	0121	4.5
	77.48748°S	167.14126°E	2578	Dec. 4	0211	4.5
	77.48748°S	167.14126°E	2578	Dec. 4	0308	36.3
	77.48671°S	167.13954°E	2552	Dec. 4	0414	45.4
Barnes	77.57134°S	166.23138°E	0	Dec. 10	0955	72.6
Sisters	77.56483°S	166.98621°E	1733	Dec. 7	0206	22.7
	77.56483°S	166.98621°E	1733	Dec. 19	0139	226.8
Bomb	77.51111°S	167.40956°E	2040	Dec. 20	0308	294.8
Lake*	77.52700°S	167.16450°E	3570			

*No date, time, or size is given because Lake shots occurred on many occasions.

ty layer beneath the 4.3-km/s material of the volcano.

Using gravity, radio echo sounding, and seismic reflection surveys southeast of Ross Island, *Stern et al.* [1991] consider that the island had subsided a maximum of 1.8 km because of isostasy. Marine reflection lines on three sides of Ross Island show that the basement dips toward Erebus at about 1°, but this can be partly explained by the north-northwest (NNW) trending Terror Rift which underlies Ross Island [*Cooper et al.*, 1991]. This rift, which has not yet been adequately modeled, may date from the late Mesozoic [*Rowe and Kienle*, 1986].

To see if the Erebus seismic experiment can put limits on the isostatic subsidence and the rift, ray-tracing models with and without isostatic subsidence were compared. Figure 6 is a ray-tracing model without subsidence, in which Erebus is assumed to rest at sea level on

the velocity structure of McMurdo Sound as determined by *McGinnis et al.* [1983], but reduced in depth by the water depth. In this model the observed times from the Cape Barne shot (at sea level) were corrected to a recording plane at elevation 2 km and plotted at map distances (and now lie on a 6.4-km/s line with a late arrival at CRA Station). The times from the Bomb/Fang/Sisters shots were plotted without altitude correction at slant recording distances from a notional source position 15 km from Cape Barne. The calculated times of basement refractions from Cape Barne are 0.1–0.2 s later than the observed times. Isostatic subsidence would add volcanic rock below sea level and depress the sediments, making the calculated times later still. This indicates either that the depth to basement taken from *McGinnis et al.* [1983] is too great or more probably that the velocity in the underlying sediments is higher than *McGinnis et al.*

TABLE 2. Locations of Seismic Telemetry Stations on Erebus and Slant Distances to the Erebus Lava Lake

Name	Latitude	Longitude	Height, m	Slant Distance, m	Depth, m
Lake	77.52700°S	167.16450°E	3,570	0	128
E1	77.53058°S	167.14047°E	3,708	723	0
CON	77.53464°S	167.08514°E	3,476	2,092	237
FAN	77.49225°S	167.12564°E	2,687	4,099	1,026
HOO	77.53158°S	166.93236°E	2,121	5,824	1,592
SIS	77.56531°S	166.98219°E	1,721	6,420	1,992
BOM	77.50894°S	167.44017°E	2,012	7,136	1,701
ABB	77.45700°S	166.90908°E	1,789	10,120	1,924
CRA	77.4445°S	167.55917°E	830	13,545	2,878
BAR	77.57300°S	166.25478°E	46	22,771	3,667
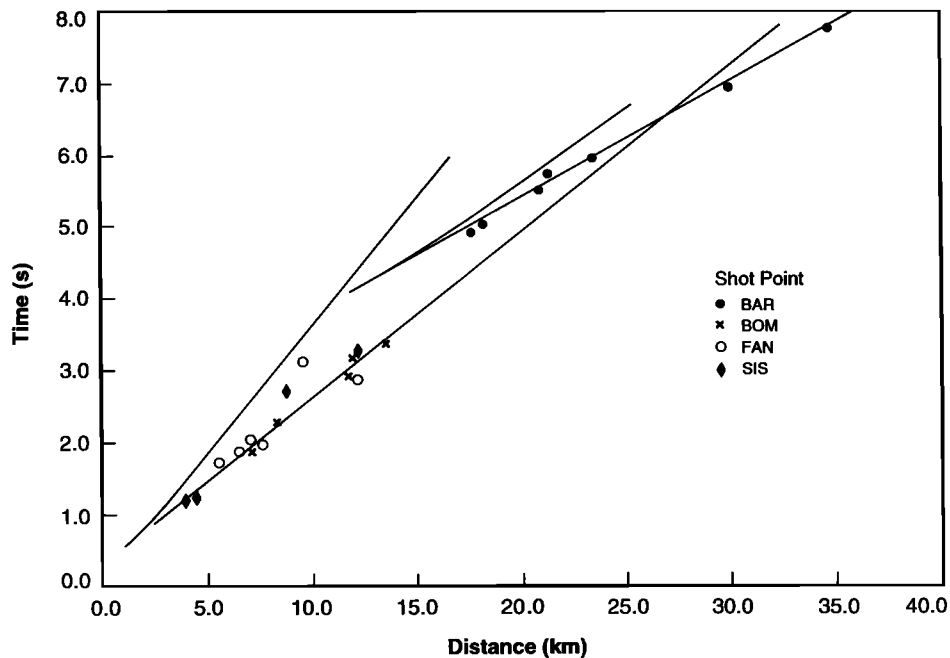
Fig. 5. Composite time-distance graph of arrivals at the eight seismic telemetry stations from the four principal shot points used in 1984–1985. Slant distances and unreduced times are shown [after *Rowe*, 1988].

[1983] estimated, because of the load pressure of the volcano. It seems that the structure below Erebus cannot be determined uniquely from the available Erebus data.

The velocity structure and bathymetry found in McMurdo Sound [*Northey et al.*, 1975; *Wong and Christoffel*, 1981; *McGinnis et al.*, 1983] and under the Ross Ice Shelf [*Stern et al.*, 1991; *Beaudoin et al.*, 1992] have been extrapolated under the volcano. Figure 7 is a structural cross section from New Harbour through Erebus and Windless Bight to the Ross Ice Shelf. Simple curved surfaces can join up the velocity boundaries in the sediments on each side of Erebus with no marked disconformities in thickness or velocity and can incorporate isostatic subsidence.

Figure 8 shows a ray-tracing model based on Figure 7, in which the volcano replaces the top 150 m of sediments in McMurdo Sound, and has depressed the lithosphere by 1.8 km so that the base of the volcano is 1.5 km below sea level at the center. This deflection was calculated by T. Stern (personal communication, 1991) for a 10-km-thick lithosphere of flexural rigidity 10^{23} N m and was chosen by us because the maximum dip of the lithosphere (1.35°) agreed with the dip of the McMurdo Sound seafloor. To obtain agreement between calculated and observed times, the added load pressure of about 72 MPa from the volcano must be invoked to raise the sedimentary velocities by about 20% of their difference from the subbasement velocity, taken as 6.5 km/s. This is clearly

possible according to *Faust* [1951], who showed that sedimentary velocity increased as the one-sixth power of depth, other parameters being constant. The load from Erebus is equivalent to a 2.9-km depth of sediments, but the velocity increases required to fit calculated to measured times from the IMESS shots correspond to only 1 km according to Faust's formula. The discrepancy may be due to the relatively recent application of the load. *Gardner et al.* [1974] show that density and therefore layer thickness should also change proportional to the one-fourth power of the velocity, but the change is only 2% and can be neglected in the model. To avoid a misleading appearance of reliability, the layered sedimentary structure has been replaced by a single unit with a linear velocity gradient of 0.28, giving the model in Table 3.

The base of the volcano can be set deeper below sea level without disturbing the fit, by assuming that it replaces more of the top of the sedimentary velocity gradient, and the thickness of underlying sediment in the model can be increased by raising the sediment velocity nearer to the maximum possible due to load. With these assumptions the maximum depth to basement is about 8 km.

VOLCANIC EXPLOSIONS TIMED BY TV SURVEILLANCE

In November 1986 a video surveillance camera (Philips LDH 0600, B&W PAL) and TV transmitter

(NZ BCTTX, Channel 9) operating from a solar cell/battery supply were permanently installed on the Main Crater rim to monitor the activity in the lava lake. The picture was displayed and videotaped at Scott Base and showed real time in hours, minutes, and seconds from a code generator synchronized hourly with the seismic telemetry clock. Frame by frame playback between the changes in the seconds display enabled sudden events to be timed to 0.04 s because the PAL system runs at 25 frames per second. S. I. D. Barrett (Seismic and video telemetry studies of Mount Erebus, Antarctica, unpublished project for B.Sc. Honours, Victoria University, Wellington, New Zealand, 1987) found that the strombolian explosions preceded the calculated origin times of the accompanying earthquakes, and Dibble et al. [1988] realized that similar explosions produced a multiplet of similar earthquake waveforms (Figure 9), which could be correlated to improve the reliability of the seismic onset times. For nine strong explosion earthquakes between December 16, 1986, and January 9, 1987, they obtained an apparent velocity of 4.06 ± 0.09 km/s, with an intercept time of 1.43 ± 0.06 s after the TV origin time. However, the intercept time contained a 1-s error, caused by the IRIG time code [Inter-Range Instrumentation Group, 1964], and was in fact 0.43 s. An independent "phase-matched" time-distance graph by Rowe [1988] showed a slope of 3.64 km/s for the same explosions, indicating that the real errors in visual correlations are of the order of 400 m/s in this case.

Subsequently, these analog tape records were digitized and stacked with weighting required to normalize the ambient noise levels immediately prior to the explosions, so as to obtain the time-distance diagram in Figure 10. The stacked waveforms are shown superimposed. The least squares line has a velocity of 4.07 ± 0.1 km/s, an intercept time of 0.47 ± 0.1 s, and a correlation coefficient of 0.99 when all six stations within 10.1 km of the source are included. The velocity is consistent with that from the large seismic experiment within the margins of error, even though it is determined over shorter distances. No consistent slower or faster arrivals are evident, but some explosions were preceded by weak lower-frequency vibrations similar to those reported by Dibble et al. [1984] which were reduced in the stack. They were either separate preliminary events, as interpreted by Kaminuma et al. [1988] or accompanied the observed bulging of the lava lake surface leading up to an explosion. The stacked result of the inconsistent earlier events in Figure 10 is evident only at E1, the closest station.

Real time digital recordings of the Erebus seismic telemetry net began in November 1988, using a personal computer based system, but the size and frequency of
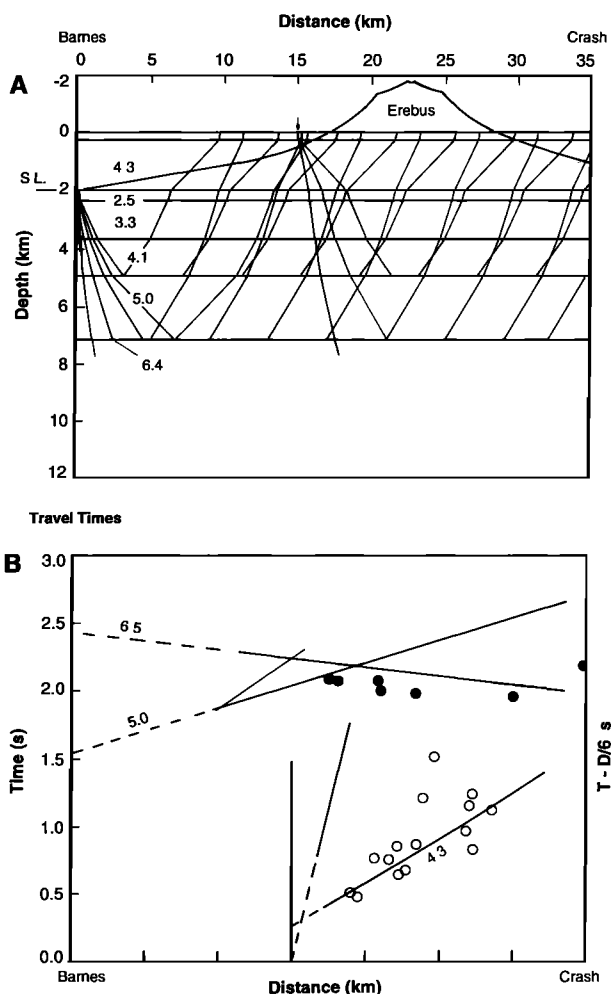
Fig. 6. (a) Ray-tracing model of Erebus assumed to be sitting without subsidence on top of the velocity structure of McMurdo Sound sediments determined by McGinnis et al. [1983]. Velocities are in kilometers per second. (b) Calculated and observed travel times (solid symbols for Barnes shot) are reduced by 6 km/s. The Barnes data are corrected for a shot at sea level, and geophones at 2000-m elevation. For other shots, uncorrected times are plotted at slant distances along the datum line from a notional position 15 km from the Barnes shot.

explosion earthquakes had decreased considerably by then, and only two more explosion earthquake multiplets have been found to confirm Figure 10. The best of these is shown in Figure 11.

E1 at a slant distance 723 m from the lava lake has arrival times of 0.69 s. If this is the direct ray, the mean velocity to E1 would be 1050 m/s. The lowest measured velocity on Erebus is 1 km/s (line C-C'), but most are higher than this. The large seismic shots have shown that only 0.16 s of the 0.47-s intercept time is due to the
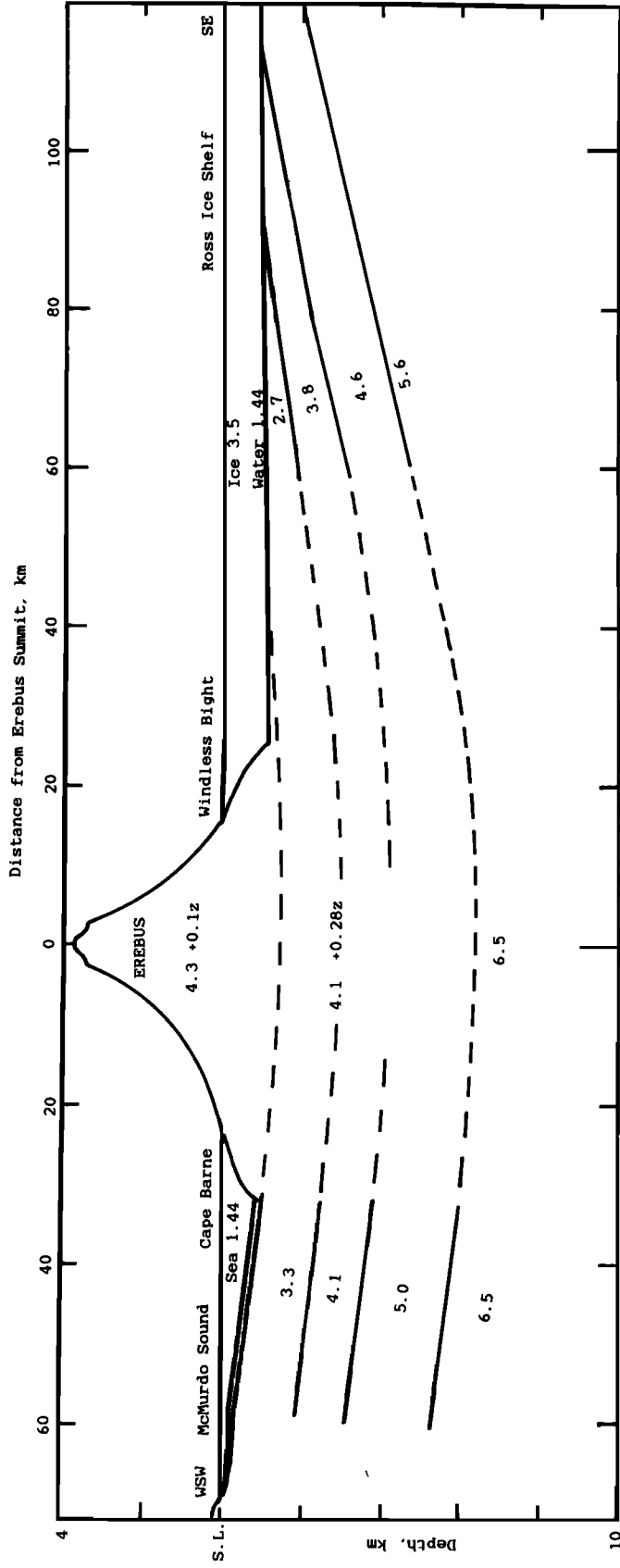
Fig. 7. Cross section through Erebus summit from WSW to southeast, derived from *McGinnis et al.* [1983] and *Northey et al.* [1975] seismic surveys under McMurdo Sound, *Beaudoin et al.* [1992] seismic survey of the Ross Ice Shelf, *Stern et al.* [1991] seismic survey of Windless Bight, and calculations of isostatic subsidence. Velocities are in kilometers per second.
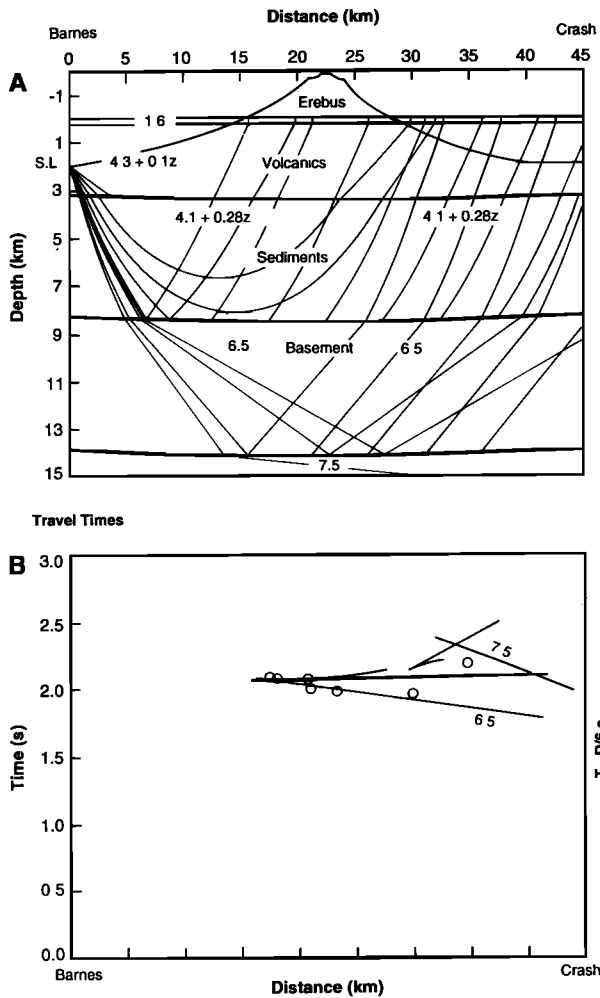
Fig. 8. (a) Ray-tracing model of Erebus with base 1500 m below sea level due to isostatic subsidence and underlain by sediments as determined by *McGinnis et al.* [1983] in McMurdo Sound, minus the top 150 m. The isostatic subsidence model is by T. A. Stern (personal communication,1991). The increased sediment velocity due to loading was chosen to fit the times from the Cape Barne shot. Velocities are in kilometers per second. (b) Calculated and observed travel times from Cape Barne, corrected for shot at sea level and geophones at 2000 m elevation, are reduced by 6 km/s.

surface layer at the recording stations. If the magma column was surrounded by 0.7-km radial thickness of scoria, say, its velocity would have to be 1500 m/s to explain the extra 0.31-s delay. Figure 12 is a model incorporating both these possibilities. However, it ignores the fact that the explosions occur in a vesicular lava lake, which *Aki et al.* [1978] noted could have a much lower velocity. *Dibble* [this volume] has interpreted the 0.47-s intercept time in terms of velocities ranging from 23 m/s in surface magma with 75% vesicles,
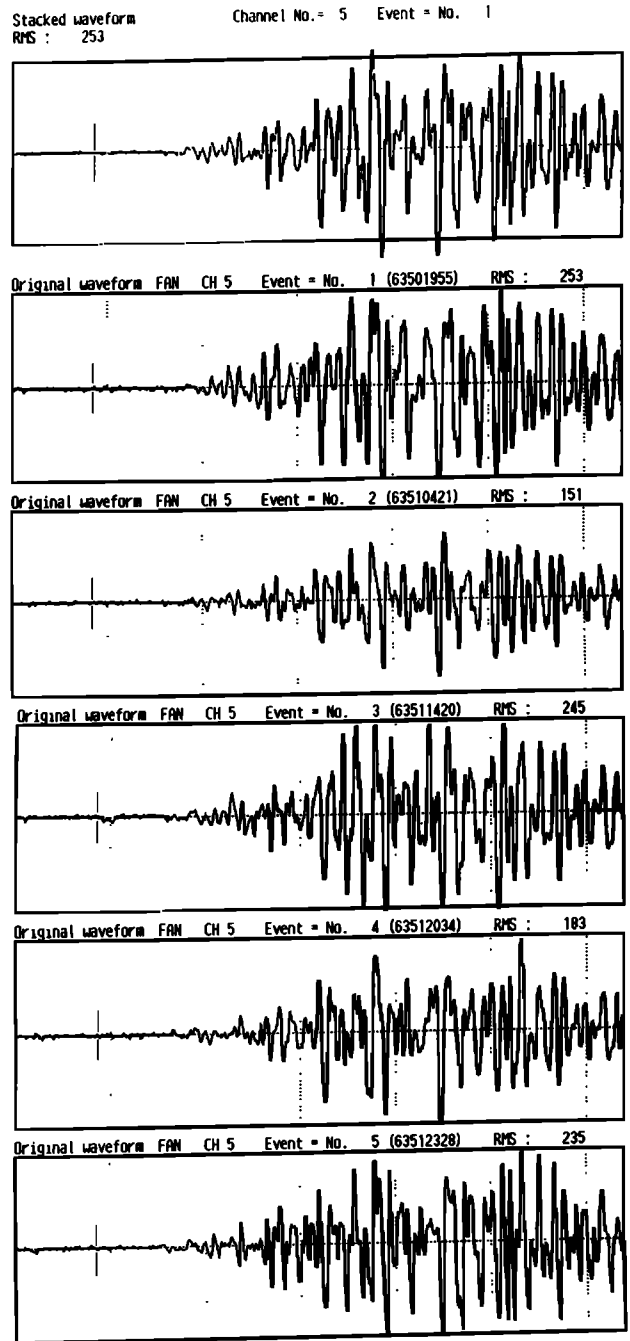
Fig. 9. Aligned waveforms of five of the family of nine similar explosion earthquakes as recorded at FAN telemetry station, compared with the stacked waveform at the top. The TV explosion times marked on each record are seen to be aligned within the accuracy of measurement. The scale is 2 s per division.

increasing with depth in the rising convection limb at up to 100 m s^{-1} m^{-1}, to 2300 m/s below the depth of nucleation at about 60 m.

TABLE 3. Velocity Structure in the Solid Material of Erebus Volcano, the Underlying Sediments, and Basement

Depth, km			
Below Summit	Below Sea Level	Velocity, km/s	Remarks
0	−3.8	2	adopted mean
0.35	−3.45	$4.3 + 0.1z$	compact volcanics
5.3	1.5	$4.1 + 0.28z$	tertiary sediments
10.3	6.5	6.5	basic igneous basement
16.2	12	7.5	unreversed, minimum depth

DISCUSSION

The principal difficulties in determining the velocity structure of Mount Erebus have been the poor quality of many of the seismic onsets, the small number of seismic stations, the permafrost, and the novel features of the structure. The poor onset quality of volcanic explosion earthquakes, which is partly due to their low earthquake magnitudes and wave frequencies, resulted in the onset times being read progressively later at increasing distances and for decreasing magnitudes. Apparent velocities were then erroneously low, leading to low velocities in the model. Consequently, the larger better recorded explosion earthquakes showing high apparent velocities have been interpreted as being several kilometers deep in the past. *Ishihara* [1985], who observed that explosions of Sakurajima Volcano were triggered by slightly earlier earthquakes a few kilometers below the explosion site, seems to support this. With sufficient seismic stations the shape of the seismic time-distance curve would have revealed the error, but underinstrumentation is endemic to the youthful science of geophysical volcanology.

The velocity structure revealed in this paper is built
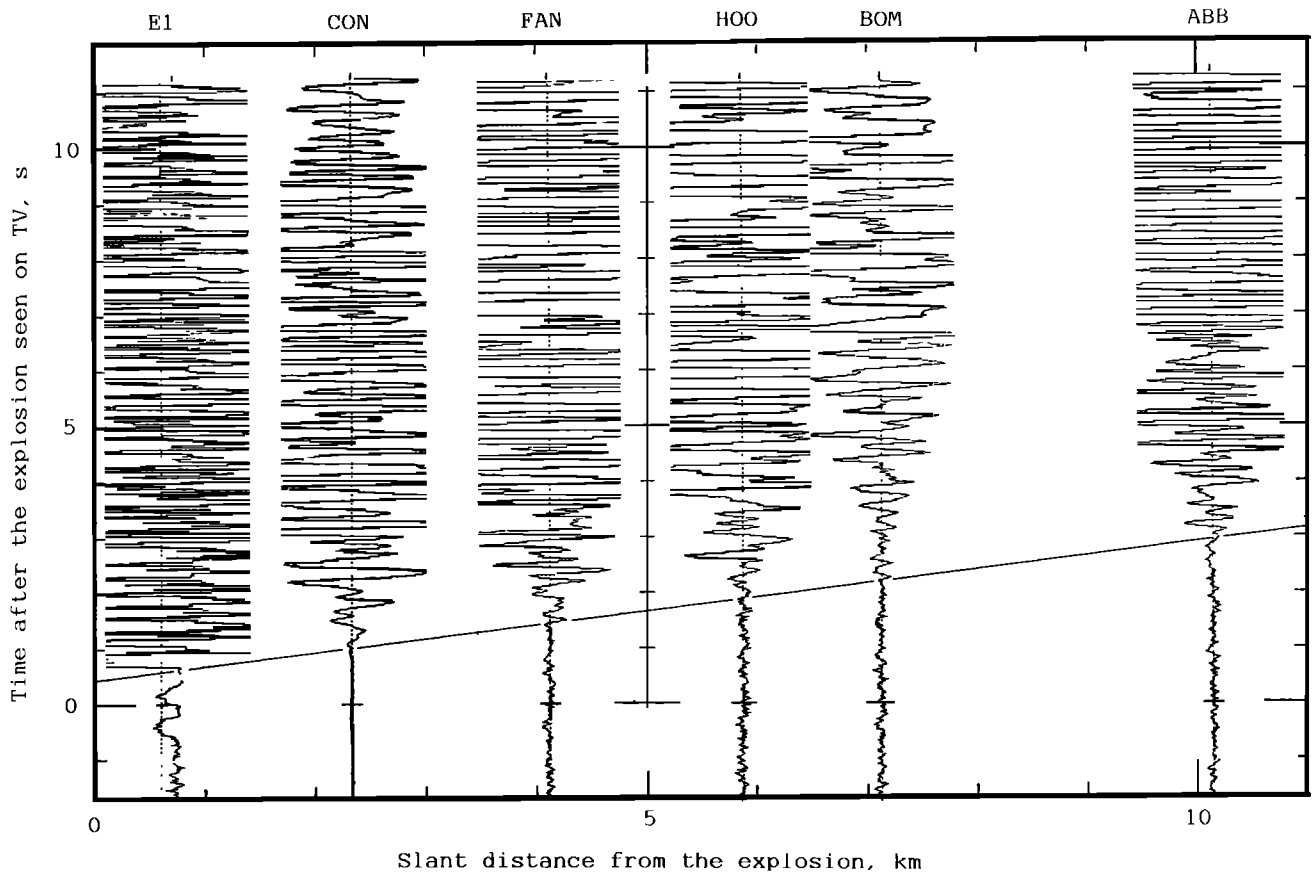
Fig. 10. Time-distance diagram showing digitally stacked seismograms of the explosion earthquake family of December 1986 to January 1987 positioned at slant distances from the explosion point. The time zero is set at the TV explosion time, which was consistent within 0.1 s for all nine explosions in the family.
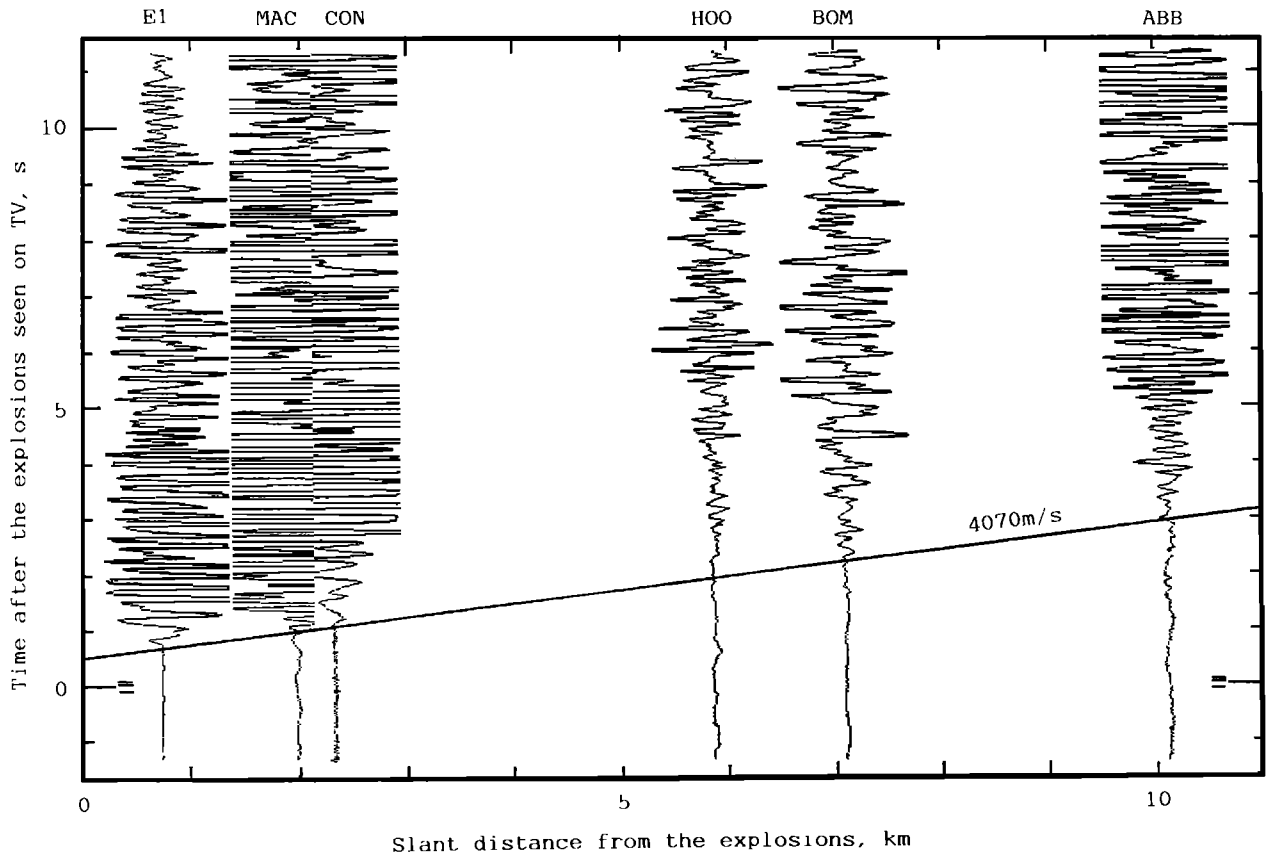
Fig. 11. Time-distance diagram showing stacked seismograms of the explosion earthquake family of December 1989. All but three of these explosions were obscured by cloud on the TV, but their infrasonic records showed they were explosions. Individual explosion instants are marked as short lines near the adopted zero of the time scale.

up from several lines of evidence. Working downward from the outer surface, short-range recordings of crater activity and refraction lines have shown velocities of about 3 km/s in the surface permafrost, sometimes underlain by low velocities of 1.0 to 2.4 km/s to average depths of about 360 m, but with wide variability. The maximum delay time along line C-C' relative to a homogeneous 4-km/s model is only 0.21 s (compare the 0.32-s intercept for the 4.3-km/s arrival in *Rowe*'s [1988] model) and shows that only a third of the 0.47-s intercept time for explosions in the lava lake originates under the summit plateau. The C-C' refraction line traversed the widest and most thermally active part of the summit plateau, which might be expected to delay the seismic arrivals to CON more than at other stations.

Below this, both the large-range seismic experiment and the seismic study of volcanic explosions timed and located by TV surveillance show velocities of 4.1–4.3 km/s. This velocity is observed between 1 and at least

14-km distance from seismic explosions and appears to increase with distance and therefore with depth (represented by velocity gradient 0.05 s^{-1} in the adopted model). It belongs to a layer up to 5.5 km thick, which represents massive phonolitic lava flows forming the bulk of the volcano. The 3–4 km of Cenozoic sediments of velocity 2.5–5.5 km/s previously determined in McMurdo Sound almost certainly underlie Mount Erebus as low-velocity and hidden layers, and so cannot be measured by the seismic network. The velocity in these sediments must be adjusted upward for the effect of the load of the volcano in order to fit the seismic data. There should be radial variations of velocity in these sediments under the flank of Erebus. The sediments are underlain by a basement of a velocity of 6.5 km/s which is probably basaltic, because granitic xenoliths have not been found in the volcanic rocks on Ross Island (J. A. Gamble, personal communication, 1991).

The consistent TV evidence that explosions slightly
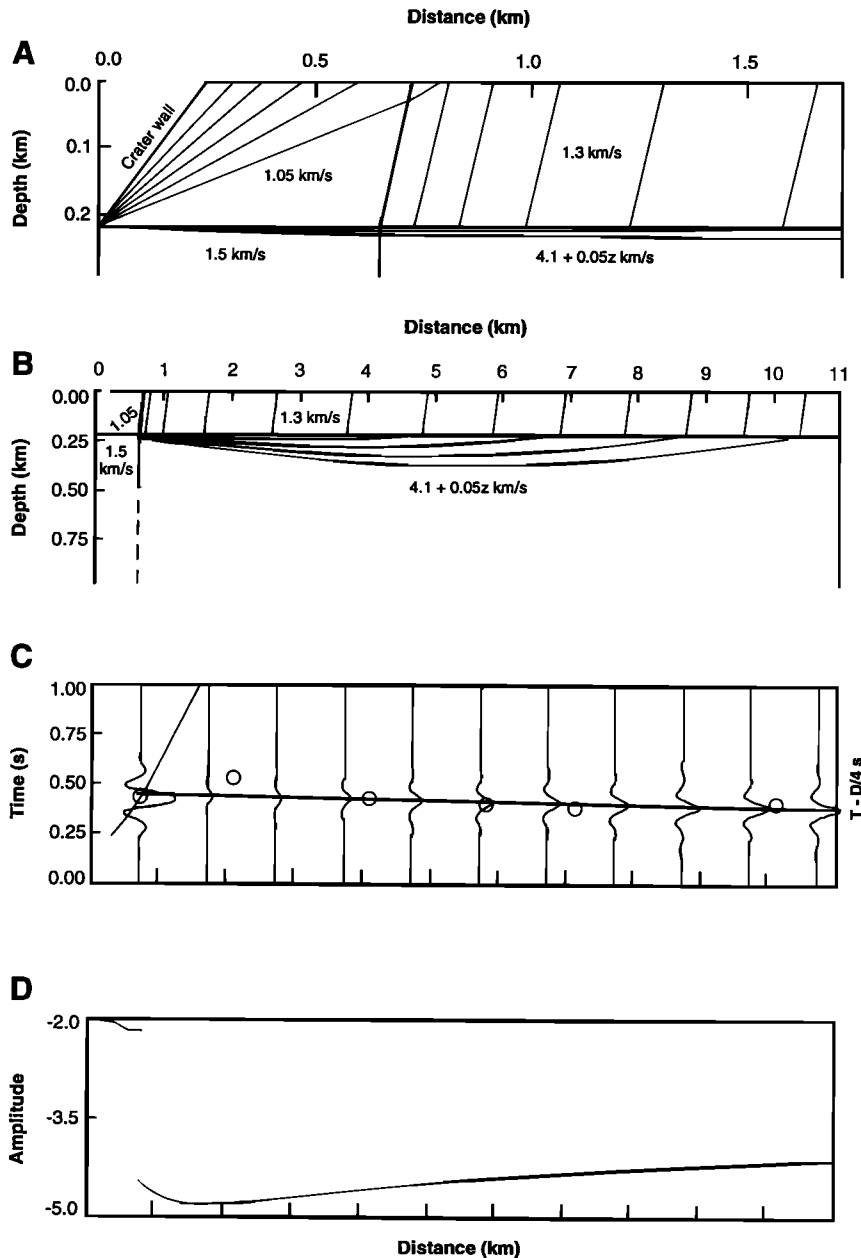
Fig. 12. (a) Simplistic ray-tracing model for explosion earthquakes, ignoring the magma but using a 700-m radius column of scoria with velocity 1500 m/s and a direct ray path of 1050 m/s as alternatives to explain the intercept time. Velocities are in kilometers per second, and the scale is expanded. (b) The same model is shown as in Figure 12a but with a distance scale as in the time-distance plot below. (c) Calculated and observed travel times (reduced by 4 km/s) are plotted at their slant distances from the explosion site. (d) Relative amplitude (log scale) versus distance is also shown.

preceded the earthquakes, even prior to the improvement of the seismic onsets by stacking, was crucial to accepting the normally shallow origin and common source of the explosion and earthquake. The 0.47-s intercept time can be explained by lower than normal velocities in or around the magma column. Although some of the explosion earthquakes have forerunning vibrations [*Dibble et al.*, 1984] and the lava lake often

begins to bulge and cause an infrasonic signal prior to the explosion, these phenomena are not consistent. They appear to accompany the accelerating failure of the lid on the overpressurized volume, rather than to cause or trigger it, and are practically always weaker and less reliably located than the stacked earthquake families originating close to the lava lake.

REFERENCES

Aki, K., B. Chouet, M. Fehler, G. Zandt, R. Koyanagi, J. Colp, and R. G. Hay, Seismic properties of a shallow magma reservoir in Kilauea Iki by active and passive experiments, *J. Geophys. Res.*, *83*(B5), 2273–2282, 1978.

Beaudoin, B. C., U. S. TenBrink, and T. Stern, Characteristics and processing of seismic data collected on thick floating ice: Results from the Ross Ice Shelf, Antarctica, *Geophysics*, *57*, 1359–1372, 1992.

Cooper, A. K., F. J. Davey, and K. Hinz, Crustal extension, sedimentary basins beneath the Ross Sea, and the Ross Ice Shelf, Antarctica, in *Geological Evolution of Antarctica*, edited by M. R. A. Thomson, J. A. Crame, and J. W. Thomson, pp. 285–291, Cambridge University Press, New York, 1991.

Crossley, D., RAYAMP-PC, 2.3, computer program, McGill Univ., Montreal, Que., Canada, 1989.

Dibble, R. R., New eruption parameters and spectral relationships between seismic and infrasonic signals from Erebus Volcano, Antarctica, in *Proceedings of 5th Symposium on Antarctic Geoscience, Mem. 37*, pp. 22–28, National Institute of Polar Research, Tokyo, 1985.

Dibble, R. R., Velocity modeling in the erupting magma column of Mount Erebus, Antarctica, this volume.

Dibble, R. R., J. Kienle, P. R. Kyle, and K. Shibuya, Geophysical studies of Erebus Volcano, Antarctica, from 1974 December to 1982 January, *N. Z. J. Geol. Geophys.*, *27*, 425–455, 1984.

Dibble, R. R., S. I. D. Barrett, K. Kaminuma, S. Miura, J. Kienle, C. A. Rowe, P. R. Kyle, and W. C. McIntosh, Time comparisons between video and seismic signals from explosions in the lava lake of Erebus Volcano, Antarctica, *Bull. 38*, pp. 49–63, Disaster Res. Inst., Kyoto Univ., Uji, Japan, 1988.

Faust, L. Y., Seismic velocity as a function of depth and geologic time, *Geophysics*, *16*, 192–206, 1951.

Gardner, G. H. F., L. W. Gardner, and A. R. Gregory, Formation velocity and density: The diagnostic basis for stratigraphic traps, *Geophysics*, *39*, 770–780, 1974.

Giggenbach, W. F., Geothermal ice caves on Mt Erebus, Ross Island, Antarctica, *N. Z. J. Geol. Geophys.*, *19*, 365–372, 1977.

Hagedoorn, J. G., The plus-minus method of interpreting seismic-refraction sections, *Geophys. Prospect.*, *7*, 158–182, 1959.

Inter-Range Instrumentation Group, IRIG standard time formats, *Doc. 104-60*, rev. 1, 26 pp., Range Commanders Council, White Sands Missile Range, White Sands, N. M., 1964.

Ishihara, K., Dynamical analysis of volcanic explosion, *J. Geodyn.*, *3*, 327–349, 1985.

Kaminuma, K., K. Shibuya, J. Kienle, and R. R. Dibble, A preliminary report of explosion seismic experiments in Mount Erebus, Antarctica, *Proc. NIPR Symp. Antarct. Geosci.*, *1*, 193, 1987.

Kaminuma, K., S. Miura, and R. R. Dibble, A process of Mount Erebus eruption, *Proc. NIPR Symp. Antarct. Geosci.*, *2*, 7–16, 1988.

Kienle, J., D. L. Marshal, P. R. Kyle, K. Kaminuma, K. Shibuya, and R. R. Dibble, Volcanic activity and seismicity of Mount Erebus, 1982–1983, *Antarct. J. U. S.*, *18*(5), 41–44, 1983.

Kienle, J., C. A. Rowe, P. R. Kyle, W. C. McIntosh, and R. R. Dibble, Eruption of Mount Erebus and Ross Island seismicity, 1984–1985, *Antarct. J. U. S.*, *20*(5), 25–28, 1985.

Kyle, P. R., R. R. Dibble, W. F. Giggenbach, and J. R. Keys, Volcanic activity associated with the anorthoclase phonolite lava lake, Mount Erebus, Antarctica, in *Antarctic Geoscience*, edited by C. Craddock, pp. 735–745, University of Wisconsin Press, Madison, 1982.

Lahr, J., HYPOELLIPSE/VAX: A computer program for determining local earthquake hypocentral parameters, magnitude, and first motion patterns, *U.S. Geol. Surv. Open File Rep.*, *80-59*, 1982.

McGinnis, L. D., D. D. Wilson, W. J. Burdelik, and T. H. Larson, Crust and upper mantle study of McMurdo Sound, in *Antarctic Earth Science*, edited by R. L. Oliver, P. R. James, and J. B. Jago, pp. 204–208, Australian Academy of Science, Canberra, 1983.

Miksis, M. J., and L. Ting, Viscous effects on wave propagation

in a bubbly liquid, *Phys. Fluids, 30*(6), 1683–1689, 1987.

Moore, J. A., and P. R. Kyle, Volcanic geology of Mt. Erebus, Ross Island, Antarctica, *Proc. NIPR Symp. Antarct. Geosci., 1*, 46–65, 1987.

Northey, D. J., C. Brown, D. A. Christoffel, H. K. Wong, and P. J. Barrett, A continuous seismic profiling survey in McMurdo Sound, Antarctica, *Dry Val. Drilling Proj. Bull. 5*, pp. 167–179, N. Ill. Univ., DeKalb, 1975.

Ricker, N., The form and laws of propagation of seismic wavelets, *Geophysics, 18*, 10–40, 1953.

Rowe, C. A., Seismic velocity structure and seismicity on Mount Erebus Volcano, Ross Island, Antarctica, M.S. thesis, 156 pp., Univ. of Alaska, Fairbanks, 1988.

Rowe, C. A., and J. Kienle, Seismicity in the vicinity of Ross Island, Antarctica, *J. Geodyn., 6*(1–4), 375–385, 1986.

Shibuya, K., M. Baba, J. Kienle, R. R. Dibble, and P. R. Kyle, Study of the seismic and volcanic activity of Mount Erebus, Antarctica, 1981–82, in *Proceedings of 3rd Symposium on Antarctic Geoscience, Mem. Natl. Inst. Polar Res. Tokyo Spec. Issue, 28*, 54–66, 1983.

Stern, T. A., F. J. Davey, and G. Delisle, Lithospheric flexure induced by the load of Ross Archipelago, southern Victoria Land, Antarctica, in *Geological Evolution of Antarctica*, edited by M. R. A. Thomson, J. A. Crame, and J. W. Thomson, pp. 323–328, Cambridge University Press, New York, 1991.

Wong, H. K., and D. A. Christoffel, A reconnaissance seismic survey of McMurdo Sound and Terra Nova Bay, Ross Sea, in *Dry Valley Drilling Project, Antarct. Res. Ser.*, vol. 33, edited by L. D. McGinnis, pp. 37–62, AGU, Washington, D. C., 1981.

R. R. Dibble and B. O'Brien, Department of Geology, P.O. Box 600, Victoria University of Wellington, Wellington, New Zealand.

C. A. Rowe, Geophysical Institute, University of Alaska, Fairbanks, AK 99775-0800.

VELOCITY MODELING IN THE ERUPTING MAGMA COLUMN OF MOUNT EREBUS, ANTARCTICA

R. R. Dibble

Victoria University of Wellington, Wellington, New Zealand

Television surveillance of explosions in the Mount Erebus lava lake has shown that explosions originate 0.5 s earlier than expected from the time-distance diagram of the accompanying earthquakes, assuming that (1) the sources were at the explosion sites, (2) the volcano was homogeneous, and (3) the stacked seismograms of families of similar explosion earthquakes accurately define the seismic arrivals. Lava bombs show that the lava lake is vesicular, which markedly reduces the seismic velocity, and can cause the delay. The velocity structure in the vesicular lava column has been calculated using models of bubble growth in rising basaltic magmas with 0.5%, 0.75%, and 1% water and the theoretical acoustic velocity in bubbly liquids. The calculated velocities range from 20 m/s in surface magma with 50% vesicles, increasing with depth at up to 100 m s^{-1} m^{-1} to 2.3 km/s below the depth of nucleation. Ray path modeling shows that seismic rays originating in such media are curved strongly upward and have difficulty escaping into surrounding solid lava walls. At Mount Erebus, the best fitting model has 0.5% water, 75% surface porosity, and 10 m explosion depth. The rays recorded on the seismic net originate steeply downward and escape below 50 m depth.

INTRODUCTION

The seismic and eruptive activity of Mount Erebus, Ross Island, Antarctica, has been studied by cooperating scientists from the United States, Japan, and New Zealand, since 1980, using a network (Figure 1) of permanently installed radiotelemetry geophones and infrasonic microphones, and from 1986 to 1990, using television surveillance of the strombolian eruptions from the lava lake in the active crater. The results have been described by *Kyle et al.* [1982], *Dibble et al.* [1984, 1988], *Dibble* [1985], *Kaminuma et al.* [1985], *Kaminuma* [1987], *Kaminuma and Dibble* [1988], and *Kienle et al.* [1985] and in annual reports in the *Antarctic Journal of the United States* from 1981 through 1985, such as *Kienle et al.* [1985] above. The explosion earthquakes accompanying the strombolian eruptions (Figure 2) first appeared to be distributed in a column extending to about 4 km below the crater. This was interpreted as showing that the earthquakes triggered the eruptions from a distance.

However, the TV surveillance, using the same clock as the seismic recordings, showed *Dibble et al.* [1988] that the explosions began about a second earlier than the earthquakes. Stacked seismograms of a family of similar explosion earthquakes showed that the seismic velocity in the volcano was higher than that used to locate the earthquakes. Either the explosions were the source of the earthquakes or the explosions triggered the earthquakes at a distance, rather than the reverse assumption.

TIME-DISTANCE FUNCTION FOR EXPLOSION EARTHQUAKES

The seismic recordings of the explosion earthquakes at Mount Erebus (Figure 3a) usually had emergent onsets and were without clear *S* wave arrivals. A few of them were preceded by precursory tremor or earthquakes by up to 45 s, similar to those reported by *Peterschmitt and Tazieff* [1962] and *Kasahara et al.* [1975], and these have been interpreted by *Dibble et al.* [1984] as preparation for eruption, separate from the explosion itself. Little consistency was obvious in the initial time-distance diagrams for apparently similar explosions in the lava lake, but for nine similar explosions in the period November 20, 1986, to January 10, 1987, the waveforms digitized from the FM tape records had cross-correlation coefficients of between 0.7 and 0.9 for each and every pair of events at any one station (Figure 3a). The coeffi-
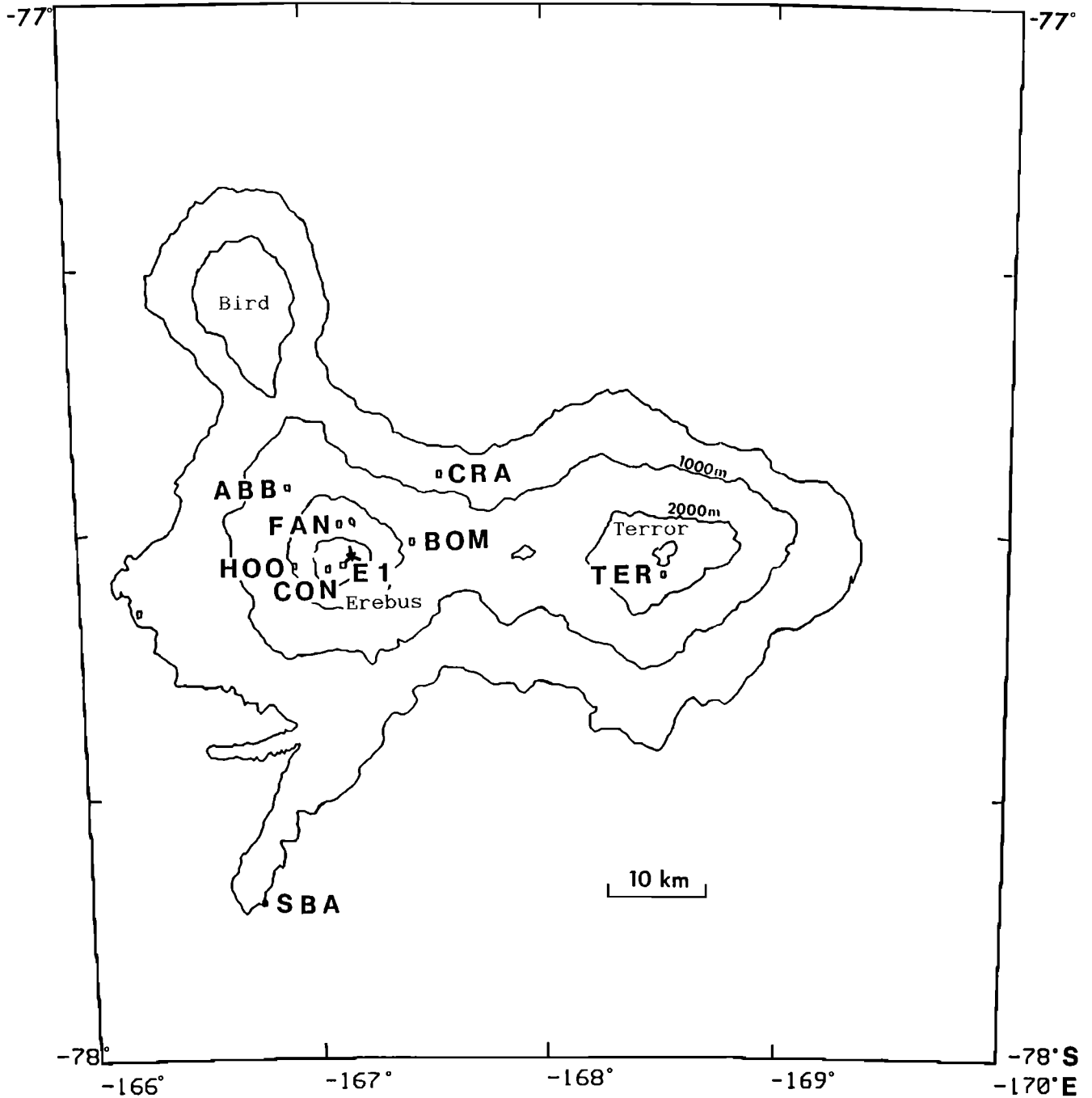
Fig. 1. Ross Island, near the west coast of the Ross Sea, Antarctica, showing the telemetry stations recorded at Scott Base (SBA). The position of the Erebus lava lake is marked with a star, near E1. Station TER is on the inactive volcano Terror.

cients remained high, and the time offsets for best cross correlation remained the same to 20 ms over the entire duration of the events (Figure 3b). Furthermore, this time offset was the same within 30 ms at all seven seismograph sites (Table 1), showing that the time-distance

graphs and therefore the source positions were the same within 120 m. It follows that the nine recordings could be stacked to obtain a threefold improvement in signal to noise ratio (Figure 4). Thus the onsets became clear out to 10-km distance, and a reliable apparent velocity of
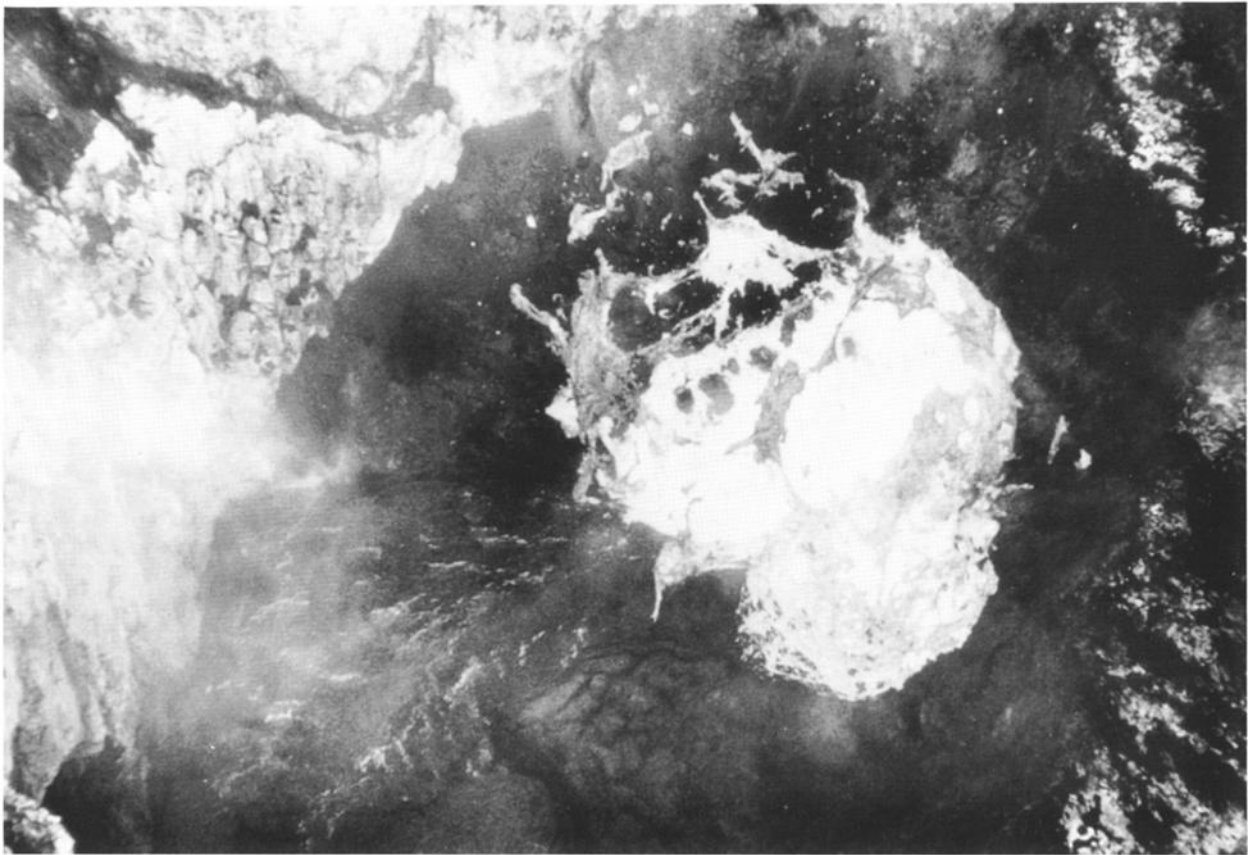
Fig. 2. An eruption from the lava lake of Erebus volcano in 1984. A large bubble is bursting. Glowing cracks can be seen in the degassed crust on the 50-m-diameter lake. The view is steeply downward from the north rim of the crater. The photograph is by J. R. Keys.

4070 ± 100 m/s was obtained for the P arrival. The precursory tremors, on the other hand, were neither well correlated nor consistent and were reduced along with the noise by the stacking process.

The explosion instants from the TV videotapes, defined as the time of the frame which first showed outburst from the updoming lava surface, could also be stacked within the accuracy of their determination (40 ms). That is, the time differences between TV explosion instants were about the same as the offset times for best cross correlation between seismic waveforms. This supported the assumption that the TV explosion instant could be adopted as the explosion earthquake origin time, enabling a travel time versus distance function (Figure 5) to be defined for the stack of the nine best recorded explosions.

Except for the small low-frequency precursory tremor on the stacked waveform at the closest station, E1, all the first arrival times versus slant distance from the explosion point lie on a straight line of inverse slope 4.07 ± 0.10 km/s with intercept time 0.47 ± 0.1 s.

INTERPRETATION

At first, no difficulty was anticipated in interpreting the data as a surface source on a low-velocity surface layer of constant thickness, underlain by a homogeneous half space of velocity 4 km/s. Data from *Dibble et al.* [1984] suggested that surface velocities were in the range 0.9–1.6 km/s, and a 217- to 409-m-thick layer would explain the 0.47-s time intercept. However, the seismic refraction experiments [*Dibble et al.*, this volume] carried out in 1984 and 1990 showed that the time terms at the geophone sites were only of order 0.10–0.16 s, leaving at least 0.31 s at the source. Furthermore, the source explosion was in a vesicular liquid lava lake, which needed to be modeled seismically.

Many observations have been made of the dramatic reduction of acoustic velocity caused by gas bubbles in water and other liquids. At large ratios of gas to liquid volumes as in foams, the mixture behaves as a heavy gas, and the velocity falls well below that in either of
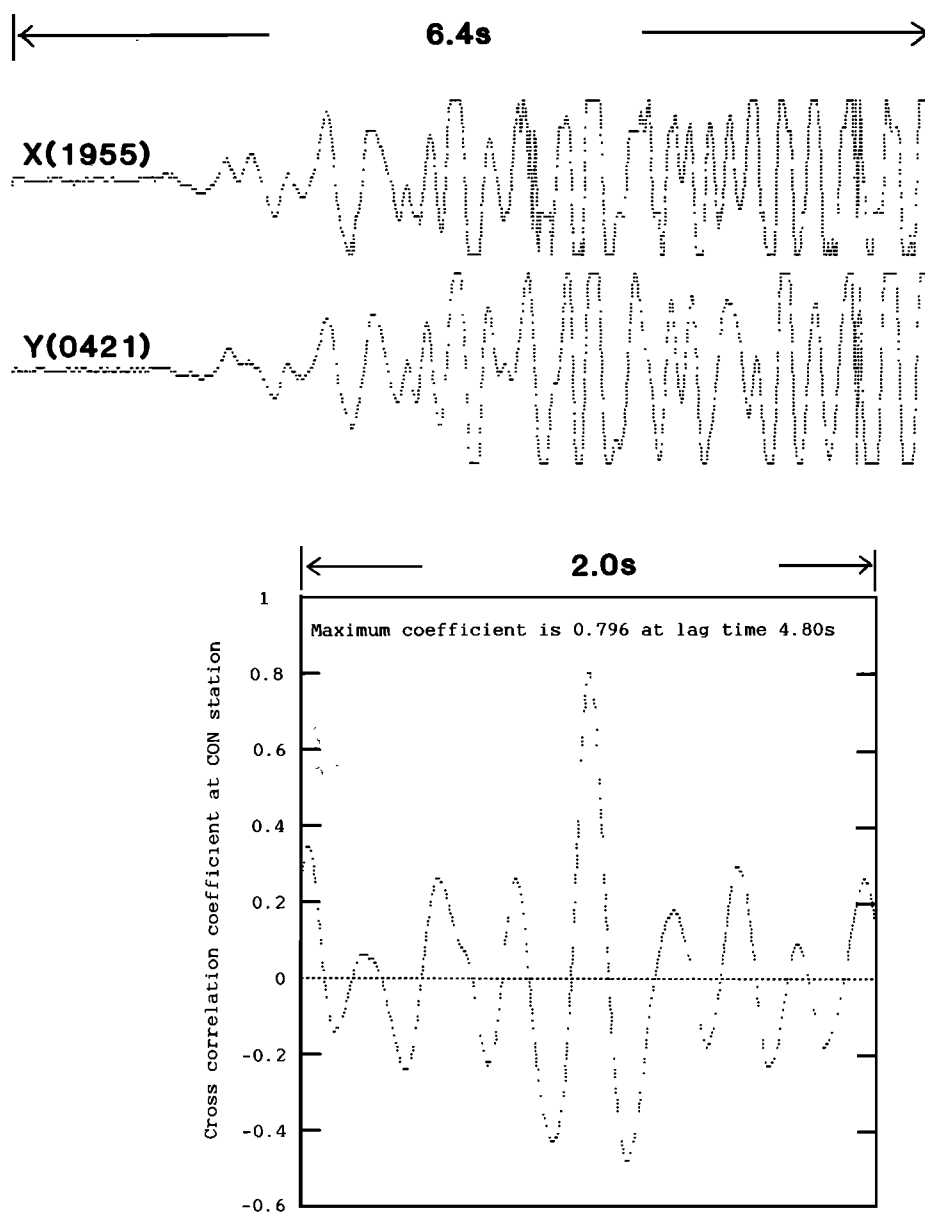
Fig. 3a. Aligned waveforms and cross-correlation function between the onsets of two of the 1986–1987 family of explosion earthquakes, as recorded at CON station.

the separate phases. *Wood* [1946] wrote the first correct equation for this effect, and *Dibble* [1972] used it to suggest that vesiculation of the Mauna Ulu lava lake in Hawaii lowered the seismic velocity to a few tens of meters per second. He was uncertain of this because viscosity was ignored, and the gas fraction versus depth in the lava was unknown. As described below, *Sparks* [1978] has since calculated the latter, and *Miksis and Ting* [1987] have considered the effect of viscosity on the acoustic velocity in bubbly fluids. *Aki et al.* [1978] also used the equation of *Wood* [1946] to calculate a *P*

velocity of 300 m/s in melt with 5% vesicles during their seismic experiments on the solidified crust of the Kilauea Iki lava lake.

THE BUBBLE FRACTION VERSUS DEPTH FUNCTION

The nucleation of bubbles in magma is promoted by supersaturation of dissolved gases such as water and carbon dioxide and by sites of easy nucleation such as

Earthquake coda

6.4s

2.0s

Maximum coefficient is 0.828 at lag time -4.82s

Cross correlation coefficient at CON station
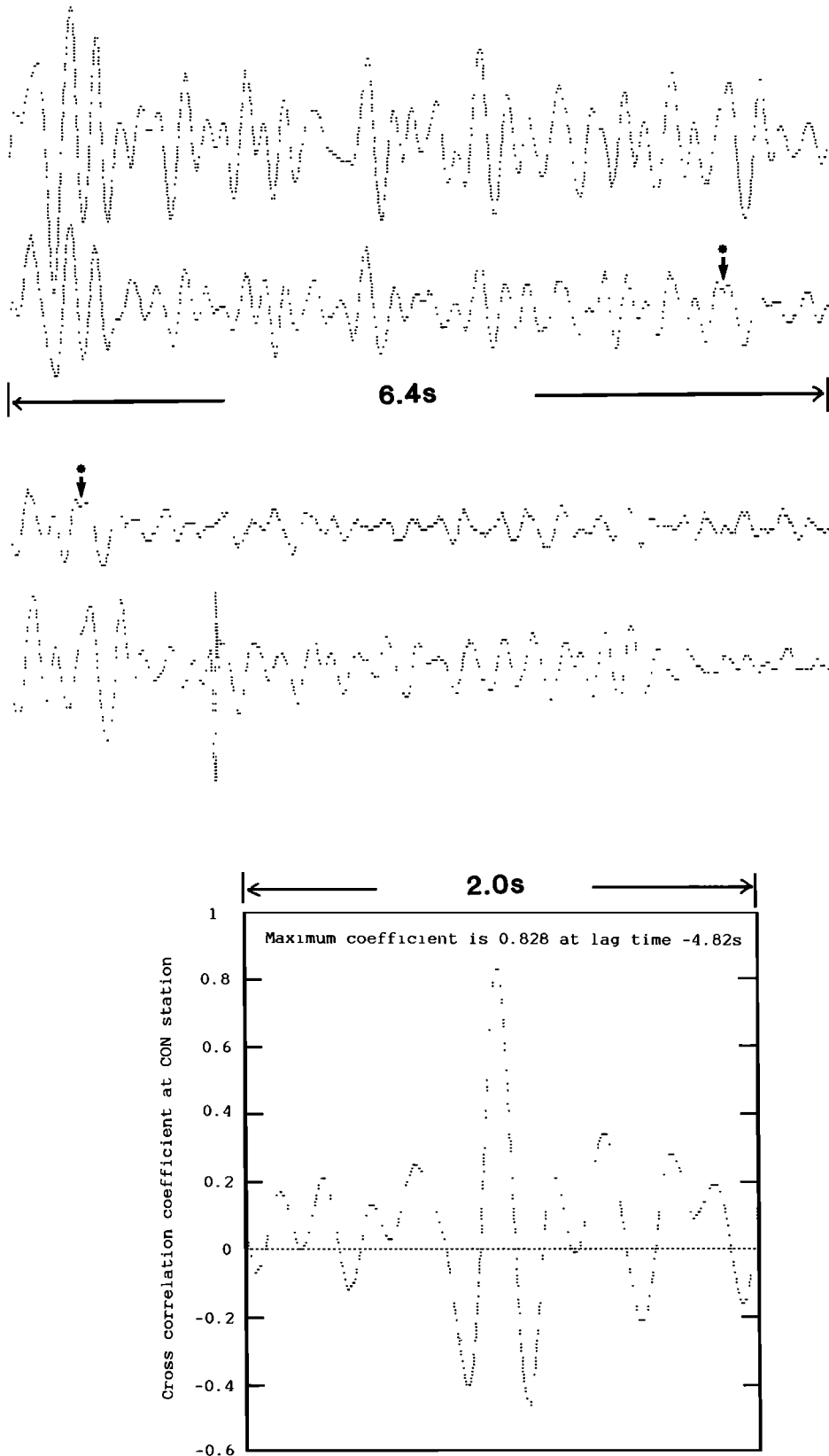
Fig. 3b. The similarity of waveform continues throughout the coda, and the lag giving maximum correllation coefficient stays the same within 20 ms. All the family members exhibit these similarities, which are consistent with their sharing a similar focal position.

TABLE 1. Lag Times of Best Cross Correlation Between Each Family Member and the Reference Event at Day 350, 1986, 1955 UT, for Each Geophone Site

Event			Geophone Site								
Year	Day	Time, UT	E1H	CON	CRA	FAN	BOM	HOO	ABB	E1Z	Range dt
1986	351	0421	NR	479	482	480	481	480	481	480	3
1986	351	1420	NR	390	393	390	391	392	392	391	3
1986	351	2034	NR	573	576	574	574	574	575	576	3
1986	351	2328	NR	248	249	248	248	249	249	248	1
1986	355	0646	319	318	319	319	319	318	320	319	2
1986	355	2320	275	275	276	276	276	275	276	274	2
1986	356	1042	NR	463	461	462	464	463	462	462	3
1987	007	0056	NR	451	NR	NR	451	452	451	453	2

Units are in 0.01 s. NR means no record.

reentrants on phenocrysts. The degree of saturation increases with the weight fraction of dissolved gas and with reduction of pressure. Within a bubble, pressure is increased above the static head by surface tension, and for bubbles below a critical size the increase is enough to make the bubble dissolve again. If water was the only volatile, magma would be free of bubbles below a pressure depth proportional to the square of the water content and would contain millions of bubbles per cubic meter above that depth. However, carbon dioxide is much less soluble than water and begins to exsolve in small quantities at depths of tens of kilometers. This complication is ignored here.

Above the depth of nucleation, bubbles grow by diffusion of volatiles through the shell of depletion around each bubble, so as to equate the vapor pressure of dissolved gas at the bubble wall with the gas pressure. The expansion is resisted by the viscosity of the liquid, and by its yield strength if it behaves like a Bingham body. *Shaw et al.* [1968] showed that liquid basalt in the Makaopuhi lava lake in Hawaii was a Bingham body with a yield strength of 700–1400 dyn/cm^2. At the stage when the depletion shells of neighboring bubbles come in contact with each other, growth almost stops, except by coalescence or by reduction of pressure due to outflow of magma in eruptions, because the rate of rise of small bubbles through viscous magma is very slow.

Sparks [1978] took these factors into account in calculating the growth of single isolated bubbles in various magmas which were ascending toward a free surface at various constant rates. Of the models he considered, that of basaltic magma of viscosity 1000 P, temperature 1373 K, ascent velocity 5 cm/s, initial water contents 0.25, 0.5, 0.75 and 1 wt %, solubility constant 0.13, diffusion coefficient 1.5 x 10^{-6} cm^2/s, and 200 kPa excess bubble pressure (relative to hydrostatic pressure) is closest to the conditions at Mount Erebus. The initial water content of the Erebus phonolite magma is unknown, but *Dunbar* [1991] measured 0.16% in degassed matrix glass and 0.2% in melt inclusions within anorthoclase crystals erupted in lava bombs. She suggests that the volatile contents of matrix and crystals are similar because the cystals may have grown under near-surface conditions. Thus the initial water content is probably between 0.25 and 1%. *Sparks* [1978] assumed that the ascending magma was erupted from the conduit, but it could also be the ascending limb of a convection system. Magma can often be seen to be convecting in the Erebus lava lake. Figure 6 shows *Sparks'* [1978] graph of bubble radius versus pressure depth. With 0.5% water, nucleation begins at 1.4-MPa pressure depth (above atmospheric pressure), and bubbles grow to a maximum radius of 7 mm at zero pressure depth.

To obtain the number of bubbles per cubic meter of initial liquid, a porosity range of 50 to 75% at zero depth has been adopted on the basis of bombs collected at Erebus. The bombs vary from spheroidal foams with vesicles intact to stringy hollow masses with all the macrovesicles coalesced. The very large bombs erupted in 1984 [*Kyle,* 1986] had a large hole in the center, surrounded by stringy coalesced foam. The porosity range and the theoretical 7-mm-radius bubbles at zero depth require between 700,000 and 2,000,000 bubble nucleii per cubic meter of initial liquid with 0.5% water. This will expand to between 2 and 4 m^3 of vesicular magma of average density 650 to 1300 kg/m^3 when the bubbles have expanded to 7 mm. The parameters for water contents of 1, 0.75, and 0.5% are given in Tables 2, 3, 4, and 5. The pressure depths used by Sparks for isolated bubbles were converted into true depth below free surface, using the computed average density of vesicular magma at each pressure depth, to obtain porosity versus true depth for each water content and bubble number.
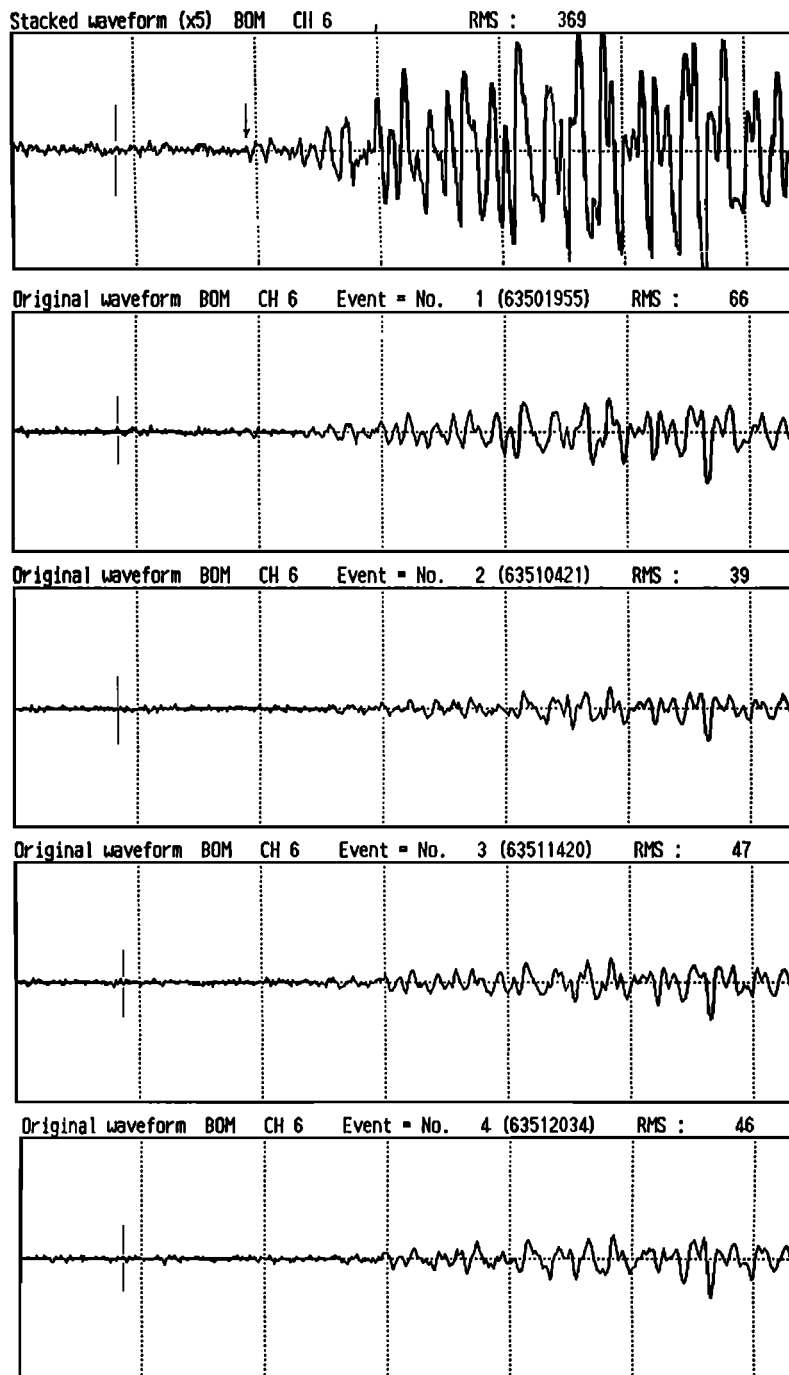
Fig. 4. The stacked waveform (at BOM) of all the members of the family of similar earthquakes is shown at the top. Some of the individual members are shown aligned below. Note the improved signal to noise ratio and clearer onset (arrow).
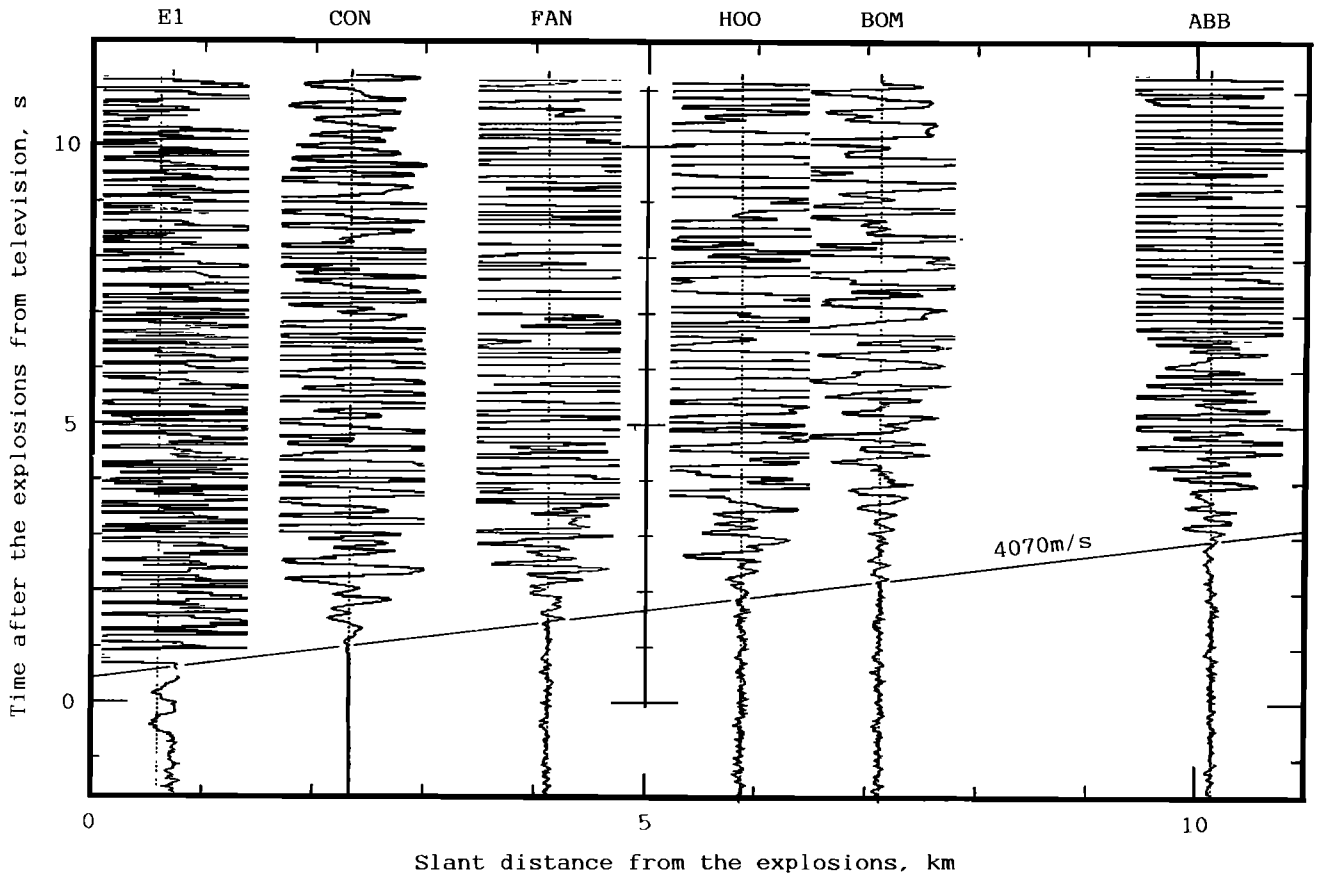
Fig. 5. The stacked waveforms at each station, arranged as a time-distance graph. The origin time
is the average explosion outburst time on television which also stacked with good precision. The
intercept time is 0.47 ± 0.10 s relative to this. The weak earlier arrivals at E1 did not stack well and
accompanied bulging of the lake before the outburst.

ACOUSTIC VELOCITY IN VESICULAR MAGMA

Wood [1946] calculated the velocity of sound in bub-
bly liquids by assuming it is the same as in a homoge-
neous fluid of the same mean density and mean elastici-
ty as the mixture. Then

$$c^2 = \frac{KfKg}{\{BKf + (1-B)Kg\}\{BDg + (1-B)Df\}} \quad (1)$$

where

    c acoustic velocity, m/s;

    Kf incompressibility of fluid, 1.4 x 10^{10} Pa for
        basalt;

    Kg incompressibility of gas, Pa;

    Df density of the fluid, 2600 kg/m^3 for basalt;

    Dg density of the gas, kg/m^3;

    B volume fraction of gas in fluid.

For adiabatic conditions, $Kg = \gamma P$ where P is the gas
pressure in pascals and γ is the ratio of specific heats (γ =
1.29 for steam), but *Crespo* [1969] deduced that the bub-
bles behave isotropically except when they are large, the
liquid viscosity is low, and the sound frequency is high.
In the present case with an incandescent liquid of high
viscosity, isothermal conditions apply and $Kg = P$ Pa.
Taking steam as the gas, its density Dg is given by

$$Dg = P/RT \text{ kg/m}^3 \quad (2)$$

where R = 461.51 J/(kg K) is the gas constant for steam
and T = 1273 K is the assumed temperature of the
magma. Adopting *Murase and McBirnie*'s [1973] val-
ues of 2.3 km/s for the velocity and 2600 kg/m^3 for the
density in bubble-free tholeiitic basalt at 1200 K, the
values of velocity and density versus pressure in the
vesicular magma were calculated and converted into
values versus depth given in Tables 2, 3, 4, and 5.

Figure 7 shows the curves of velocity versus true depth. Velocity gradients with depth were calculated and carefully smoothed and adjusted so that the straight line segments met without steps.

Aki et al. [1978] made similar calculations, except that they assumed adiabatic conditions in the bubbles, and noted that the level of their seismic signals was below the yield strength. Both these conditions increase the seismic velocity. Our calculations apply to strong signals, in which the yield strength is greatly exceeded, and the velocity is lower.

Miksis and Ting [1987] have deduced the effects of viscosity on the velocity, for the assumptions of small gas volume fraction (<<1), and bubble diameter and separation distance much less than the acoustic wavelength. For small amplitudes of motion, propagation is linear, and the acoustic velocity varies monotonically between *Wood*'s [1946] value for zero Reynolds number *Re* (infinite viscosity and/or zero bubble diameter) and *Crespo*'s [1969] value c_c for infinite *Re*. *Miksis and Ting* [1987] quote the Crespo value for the case of zero gas density as

$$c_c^2 = \gamma P(1 + 3B)/DB$$

where γ is ratio of specific heats of the gas, P is the gas pressure in the mixture, B is the bubble fraction, and D is the density of the liquid. For the conditions adopted at the Erebus lake surface, $c_c = 25.5$ m/s and 23.8 m/s for $B = 0.5$ and 0.75, respectively, which are hardly different from the values 20.1 and 23.2 m/s from Wood's equation. Fifty percent porosity gives the lowest possible velocity in basalt magma at low pressure.

The amplitude of oscillation relative to bubble diameter has an important effect on attenuation and linearity, because large amplitudes cause translation of bubbles through the liquid, owing to the density contrast and differential acceleration forces, and result in elliptical bubbles. *Miksis and Ting*'s [1987] solution is complex and approximate. Acoustic velocity varies during each cycle from the Crespo limit at maximum particle velocity to the Wood's limit at zero particle velocity. Propagation is nonlinear, with compressional onsets becoming smoothed (emergent) and dilational ones becoming steepened.

MODELING CALCULATIONS

For modeling purposes the volcano is regarded as a radially symmetrical cone with vertical axis and can be represented as a two-dimensional radial section. The magma column was initially assumed to have the same
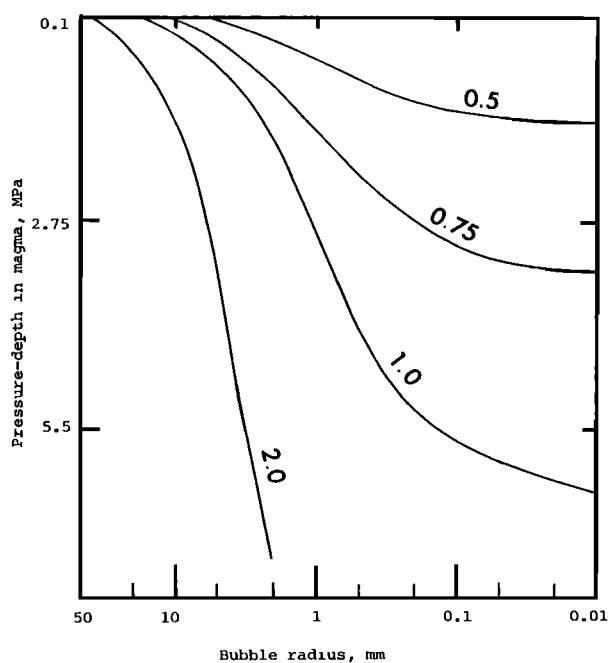
Fig. 6. Curves of bubble radius versus pressure depth in basalt magma rising at 5 cm/s, calculated by *Sparks* [1978] for several values of water content (weight percent). Other conditions were as follows: solubility constant, 0.13; diffusion coefficient, 1.5×10^{-6} cm²/s; supersaturation pressure, 2 bars; viscosity, 1000 P.

radius as the main crater (500 m), on the assumption that the inner crater and lava lake mark the top of the ascending limb of a convection system and that the descending limb has crusted over to form the main crater floor. Subsequently, it was found that the radius was not critical and could be quite small. A radius of 50 m has been adopted, similar to that of the inner crater.

Program RAYAMP-PC [*Crossley*, 1989] was used for the modeling. The program defines the measurement plane to be horizontal, unlike the sides of the volcano. An unsuccessful attempt was made to tilt the model so that the volcano sides were horizontal, and the layering in the lava lake was tilted. Instead, the sides and the lava lake were made horizontal, and slant distances were adopted as in the time-distance graph. The errors are small provided that the source of the earthquakes is shallow relative to the recording distances. Models with a concentric descending convection limb of lower vesicularity than the rising limb were attemped, but RAYAMP-PC could not correctly calculate the ray path times for rays which penetrated two vertical boundaries between different media in succession. It was necessary to model the entire magma column as laterally homoge-

TABLE 2. Magmastatic Pressure, Bubble Radius, Porosity, Specific Gravity, Acoustic Velocity, and Vertical Velocity Gradient Versus True Depth in Bubbly Magma Rising at 5 cm/s

Depth, m	Pressure, kPa	Radius, mm	Porosity, %	Specific Gravity	Velocity, m/s	Gradient, s^{-1}
0	263	20.0	75	0.650	23.22	0.3602
21.1	537.7	10.8	32.1	1.766	30.8	2.2164
34.5	812.4	6.41	9.50	2.355	60.5	4.5431
46.1	1087	4.53	3.37	2.512	113.2	6.7545
57.1	1362	3.44	1.50	2.561	187.5	8.8716
68.0	1636	2.75	0.774	2.580	284.2	11.5505
78.9	1911	2.25	0.425	2.589	410.1	13.9444
89.7	2185	1.89	0.252	2.593	560.7	18.2037
100.5	2457	1.58	0.148	2.596	757.3	21.4444
111.3	2735	1.33	$8.81E^{-2}$	2.598	988.9	22.5278
122.1	3010	1.135	$5.48E^{-2}$	2.598	1232.2	24.7407
132.9	3284	0.956	$3.27E^{-2}$	2.599	1499.4	22.0648
143.7	3559	0.810	$1.99E^{-2}$	2.599	1737.7	18.1667
154.5	3834	0.685	$1.20E^{-2}$	2.599	1933.9	13.6759
165.3	4109	0.575	$7.29E^{-3}$	2.600	2081.6	8.5741
176.1	4383	0.488	$4.36E^{-3}$	2.600	2174.2	5.7130
186.9	4658	0.409	$2.57E^{-3}$	2.600	2235.9	3.5463
197.7	4933	0.338	$1.45 E^{-3}$	2.600	2274.2	2.1389
208.5	5207	0.272	$7.55E^{-4}$	2.600	2297.3	1.1574
219.3	5482	0.213	$3.62E^{-4}$	2.600	2309.8	0.6019
230.1	5757	0.158	$1.48E^{-4}$	2.600	2316.3	0.2963
240.9	6031	0.098	$3.53E^{-5}$	2.600	2319.5	0.0833
251.7	6306	0.043	$2.98E^{-6}$	2.600	2320.4	0.0093
262.5	6581	0.006	$8.10E^{-9}$	2.600	2320.5	0.0000

The initial water content is 1%, with 90,000 bubble nucleii per cubic meter. The notation E^{-2} means $\times 10^{-2}$.

TABLE 3. Magmastatic Pressure, Bubble Radius, Porosity, Specific Gravity, Acoustic Velocity, and Vertical Velocity Gradient Versus True Depth in Bubbly Magma Rising at 5 cm/s

Depth, m	Pressure, kPa	Radius, mm	Porosity, %	Specific Gravity	Velocity, m/s	Gradient, s^{-1}
0	263	11.45	75	0.650	23.22	0.5429
19.1	537.7	5.422	24.1	1.972	33.59	2.5953
31.8	812.4	3.458	7.63	2.402	66.55	6.4204
43.1	1087.1	2.242	2.20	2.543	139.1	12.4364
54.1	1361.8	1.510	0.683	2.578	275.9	19.5278
64.9	1636.5	1.085	0.255	2.593	486.8	26.3426
75.7	1911.2	0.8200	0.110	2.597	771.3	39.8333
86.5	2185.9	0.5977	$4.26E^{-2}$	2.599	1201.5	45.6262
97.2	2460.6	0.4272	$1.56E^{-2}$	2.600	1689.7	35.3148
108.0	2735.3	0.2923	$5.00 E^{-3}$	2.600	2071.1	16.3981
118.8	3010.0	0.1916	$1.41E^{-3}$	2.600	2248.2	5.6204
129.6	3284.7	0.1056	$2.35E^{-4}$	2.600	2308.9	1.0463
140.4	3559.4	0.0304	$5.61E^{-6}$	2.600	2320.2	

The initial water content is 0.75%, with 477,000 bubble nucleii/m³. E^{-2} means $\times 10^{-2}$.

TABLE 4. Magmastatic Pressure, Bubble Radius, Porosity, Specific Gravity, Acoustic
Velocity, and Vertical Velocity Gradient Versus True Depth in Bubbly Magma Rising at 5 cm/s

Depth, m	Pressure, kPa	Radius, mm	Porosity, %	Specific Gravity	Velocity, m/s	Gradient, s^{-1}
0	263	7.0	75	0.65	23.22	0.4059
10.1	400	3.61	29.1	1.842	27.3	3.2687
16.8	538	2.28	9.4	2.355	49.2	8.4561
22.5	675	1.49	2.81	2.527	97.4	15.3818
28.0	812	1.03	0.947	2.575	182.0	28.3395
33.3	950	0.72	0.325	2.591	332.2	51.4727
38.8	1087	0.49	0.103	2.597	615.3	86.5741
44.2	1224	0.33	$3.14E^{-2}$	2.599	1082.8	122.0926
49.6	1362	0.205	$7.50E^{-3}$	2.600	1742.1	92.2453
54.9	1499	0.10	$8.7E^{-4}$	2.600	2231.0	16.4815
60.3	1636	0.015	0.0	2.600	2320.0	

The initial water content is 0.5%, with 2,088,000 bubble nucleii/m^3. E^{-2} means $\times$ 10^{-2}.

neous, which is an unfortunate oversimplification.

Successful models fitting the observed time-distance graph were possible using the velocity-depth functions for 0.5% water. Figure 8 shows the solution for 75% surface porosity based on Table 4. A depth of 10 m to the seismic source is required in this case. A model with 0.5% water and 50% surface porosity based on Table 5 was also tested. Zero depth to the source was best here, but the calculated times averaged 0.12 s larger than the observed times. A marginal increase in water content and/or surface porosity would optimize the fit. In both models the volcano surrounding the magma column was modeled as two layers on the basis of the interpretation

of the large seismic refraction experiment [Dibble et al., this volume]. The surface layer of velocity 1.3 km/s and thickness 220 m overlies a thick layer of 4.1 km/s. The calculated times were very sensitive to depth of source (Figure 9), but relatively insensitive to the radius of the magma column provided it exceeded 10 m (Figure 10). The lava lake is normally smaller than this, but the solid crust can be seen to overhang when the lava level falls temporarily after an explosion, and at these times, lava has been seen to flow horizontally in and out under the overhang.

Figure 11 is an enlargement of the ray paths within the lava lake, showing that only paths leaving the source

TABLE 5. Magmastatic Pressure, Bubble Radius, Porosity, Specific Gravity, Acoustic
Velocity, and Vertical Velocity Gradient Versus True Depth in Bubbly Magma Rising at 5 cm/s

Depth, m	Pressure, kPa	Radius, mm	Porosity, %	Specific Gravity	Velocity, m/s	Gradient, s^{-1}
0	263	7.00	50.00	1.300	20.1	2.2500
7.5	400	3.61	12.10	2.286	38.1	8.4000
13.4	538	2.28	3.34	2.513	79.9	14.1667
18.8	675	1.49	0.955	2.575	165.2	32.0000
24.3	812	1.00	0.291	2.592	325.0	39.6667
29.7	950	0.72	0.109	2.597	562.8	87.0000
35.1	1087	0.49	0.034	2.599	997.9	94.5000
40.4	1224	0.33	0.010	2.600	1565.2	100.0000
45.8	1362	0.20	0.003	2.600	2068.8	36.8333
51.2	1499	0.10	0.000	2.600	2289.5	6.0000
56.6	1636	0.02	0.000	2.600	2320.0	0.0300

The initial water content is 0.5%, with 696,000 bubble nucleii/m^3.
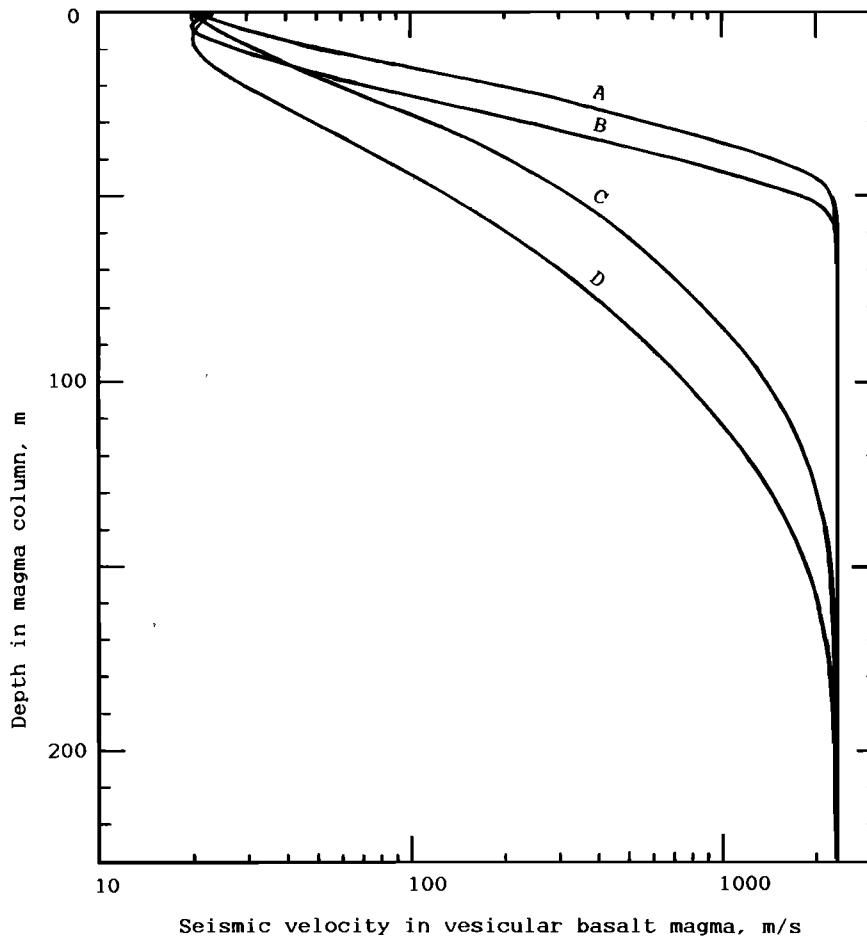
Fig. 7. Acoustic/seismic velocity versus depth in vesicular magma. Curve A represents 0.5% water and 50% surface porosity (700,000 bubbles/m^3); curve B, 0.5% water, 75% surface porosity (2,090,000 bubbles/m^3); curve C, 1% water, 50% surface porosity (30,000 bubbles/m^3); and curve D, 1% water, 75% surface porosity (90,000 bubbles/m^3).

at near vertically downward trajectories can easily penetrate the wall of the magma chamber and reach the geophones. Theoretically, rays leaving by much less steep paths can be reflected from the surface one or more times so as to meet the wall horizontally and pass through, but the reflection coefficient between vesicular magma and massive wall rock is high because of the velocity and density contrasts, and the escaping rays are highly divergent. One other efficient path can be recognized. If the lava lake is covered with a crust of normal velocity, rays originating in the lava lake can be critically refracted along its lower surface and pass through the crater wall to the geophones, so as to be the first arrival at short distances. The amplitude of such rays can be expected to be small and variable when the crust is thin, because the solid angle available for their propagation is

small. The small precursors at E1 which do not stack well cannot result from such a path. They probably result from the updoming of the lake prior to the explosion. Dibble et al. [1984] ascribed the emergent infrasonic precursors to explosion airwaves to such updomings.

EXPLOSION EARTHQUAKE MECHANISM

The mechanism of explosion in vesicular and highly viscous lava having an appreciable yield strength (Bingham body) is complex and incompletely understood, but it is obvious from the bulging of the lake surface before an explosion that a volume within the lake becomes overpressurized. This pressure is present at the bottom of the volume before the explosion occurs. The
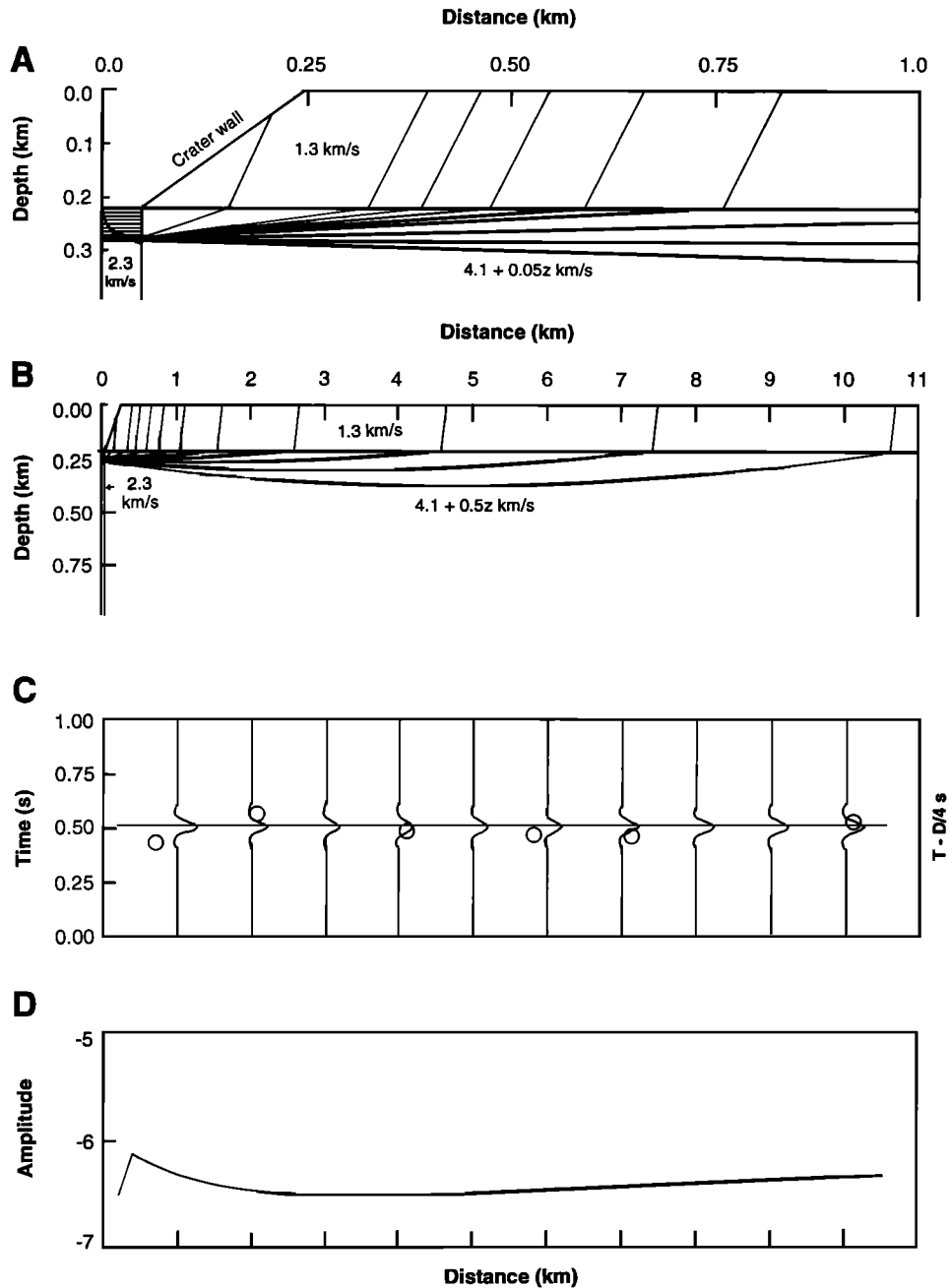
Fig. 8. Seismic ray paths and travel times through a model of Erebus, for a source 10 m deep in a vesicular lava lake with 0.5% initial water. The RAYAMP program dictated a horizontal recording plane (the tilted mountain side) and a horizontally stratified lava lake. (a) The enlarged view of the ray paths to 1 km is shown. Velocity versus depth in the apparently layered part of the lava lake is shown in Figure 8b. (b) Ray paths out to 11 km slant distance are shown. A velocity gradient of 0.05 km/s per kilometer of depth Z is assumed in the 4.1-km/s layer. (c) Reduced travel times versus slant distance show synthetic seismograms, a calculated time-distance line, and observed times (symbols). Times T were reduced by 0.25 s per kilometer of distance D, so that 4-km/s lines become horizontal. (d) Calculated amplitude times D versus slant distance D are shown on a log scale. Horizontal lines have $A_0 \propto 1/D$.
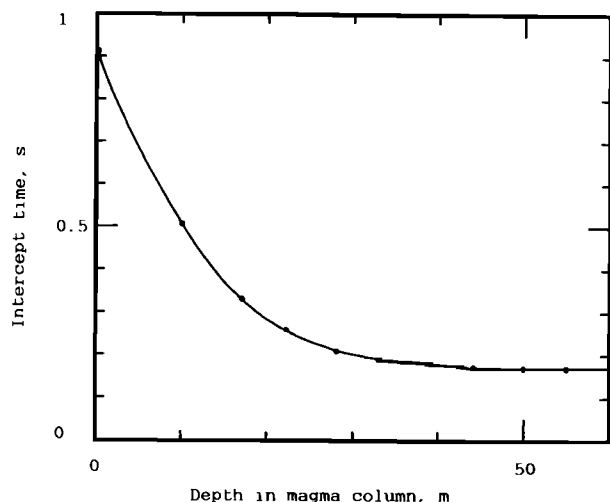
Fig. 9. The time intercept of the 4.1-km/s time-distance line versus the depth of the source in the model shown in Figure 8.

Fig. 10. Time intercept versus radius of the magma column for explosions at a constant depth of 10 m. As radius is reduced, the rays exit the magma at shallower depth, but the times are hardly affected until the radius of the column is less than 10 m.

volume may be a large bubble, as in those cases when clear gas and discrete bombs are erupted, or contain lava foam, as in cases when incandescent gas and ash are erupted. In many eruptions, both large bubbles and foam may be involved.

At Erebus the first sign of impending explosion is a bulging of the lake surface over the eruption site, beginning about a second before the explosion. Until then the exploding volume is controlled by the viscous and elastic yield stresses in the magma around it and by surface tension on bubble walls. It is also controlled by depth pressure and of course by the strength of the roof. This must be considerable and laterally very variable to allow strong explosions and convection to occur close together in space and time. It may be due to rewelding and cooling of the collapsed lava foam after the vesicles have burst near the surface to provide the column of fume rising from the lake. Kyle et al. [1991, this volume] report SO_2 outputs of 15–230 Mg/d, and fast forward video shots in the TV documentory "Expedition to Erebus" by Martin [1987] show the fume rising from the convecting lava lake. The author's TV surveillance of explosions shows they usually occur from a stagnant nonfuming lake.

An explosion occurs when the roof fails in tension, and a mass of bombs, ash, and gas is erupted, releasing the pressure so that the bottom half of the volume (crater) implodes. How then is the force of the explosion applied downward so that compressional seismic waves are recorded at a distance, as, for instance, at Sakurajima Volcano [Yamasato, 1987]? Possibilities include tensional rebound in the walls around the erupting volume from

the lip of the new vent toward its bottom, lateral spreading of erupted gas pressure over the surface of the lava lake around the vent, and gravitational slumping of the sides of the vent as releveling begins. Thus the source location of the downwardly propagating compressional seismic waves is not the bottom of the transient hole in the lava lake, but a ring around its sides at about the level of the center of the erupted volume. Nevertheless, the horizontally propagating waves should be dilational, and this was observed by Kasahara et al. [1976] on the rim of the crater of Miharayama Volcano, Izu-Oshima, and explained by an "asymmetrical push cone type model." The flying bombs do not push the bottom of the vent down by reaction forces any more than an arrow pushes the tips of the bow backward when it is released.

The model has similarities to that of MacIntyre [1972] for air bubbles bursting on a water surface, except that surface tension is the main driving force in such small bubbles. Using high-speed photography and dye, he observed a surface shear flow wave on the bubble wall traveling at close to its phase velocity (2.3 m/s) from the rupture point toward the bottom of the bubble. The convergence of the wave there caused a visible water spout, and the dye revealed that a downward jet also occurred below the bubble, in a classic example of action and reaction. The upward spouts are characteristic of boiling
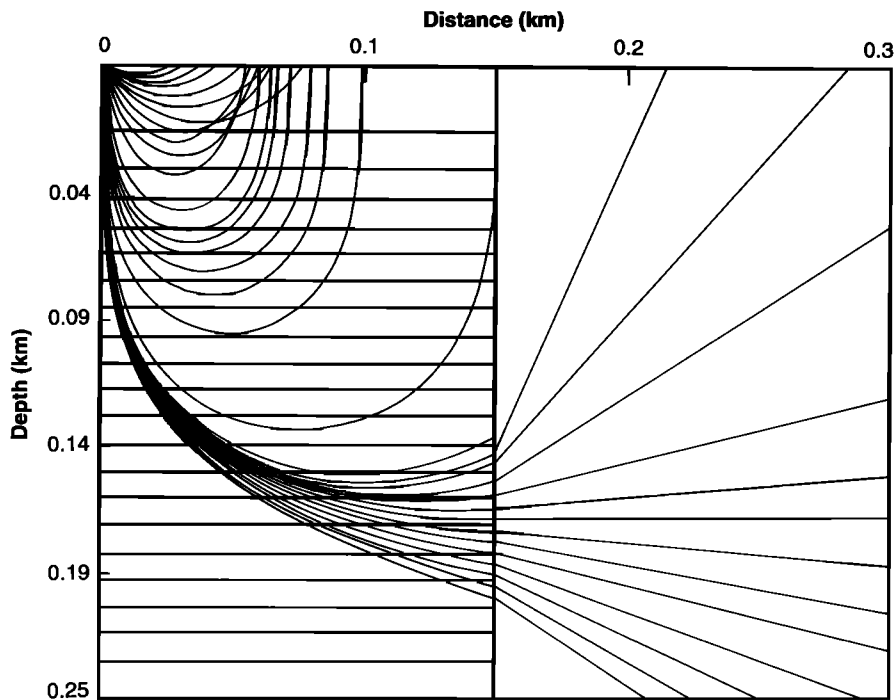
Fig. 11. An enlarged plot of the ray paths through a lava lake with 1% water as in curve C of Figure 7 and where the volcanic edifice is homogeneous 4-km/s material.

mud in geothermal areas and were seen in less perfect form by *Dibble* [1972] during degassing of the Mauna Ulu lava lake in Hawaii. They may also explain the observations of *Wilson* [1980] and *Dibble et al.* [1988] that the bombs are ejected a small fraction of a second after the gas cloud from strombolian explosions.

If the exploding volume is full of highly vesicular magma, a decompressional wave propagates downward through it at the acoustic velocity of the mixture, causing bubbles at increasing depth to expand and burst, each releasing seismic energy as for a big bubble, until a depth is reached where the bubble walls are too thick and the vesicular magma is no longer disrupted. In this scenario the power of the downward seismic wave increases over an appreciable time as the eruption propagates downward, and its effective source is ill defined but may be the center of the erupted volume. In both of the above cases the initial seismic motion is at the surface, although the center of energy release is effectively the center of the exploding volume. Thus the best fit depth of 10 m might be interpreted as an error in the velocity model for the lava lake. Certainly, the velocity model can not be regarded as sufficiently accurate to give the depth of the source to 10 m.

It is important to note that it is not the "application"

of a reaction force to the eruption of mass or of gas pressure to the bottom of the hole which produces the downward seismic motion, but the removal of upward forces on the rims of bursting bubbles allowing elastic rebound of tensional strain together with gravitational collapse. The mass, together with the low acoustic velocity, controls the time duration of disruption, and thus of rebound, and therefore the peak seismic power and the spectral peak. It is concluded that no matter how deep the bubble extends, surface effects are always important, and that the effective seismic source is at or above the equator through the erupted volume.

SUMMARY

The velocity structure of convecting vesicular basalt magma columns during eruption has been determined by using *Sparks'* [1978] calculations for the growth of bubbles in rising magma columns and *Wood's* [1946] equation for the velocity in bubbly liquids. *Miksis and Ting* [1987] found Wood's equation to be valid for high-viscosity liquids with small Reynolds numbers. For basalt with bubbles of radius less than 20 mm, Re is less than 0.006.

Aki et al. [1978] reported very low velocities in

Hawaiian magma caused by this mechanism but modified by weak shear strength as for Bingham bodies. The present author uses it at Mount Erebus to explain a 0.5-s delay in the seismic times relative to the video time of an explosion, because the source is clearly within a low-velocity medium of considerable vertical extent forming a vertical waveguide. Here we consider only strong waves which exceed the strength and assume a maximum porosity of 50 to 75% in the magma column at zero depth.

Acoustic velocity is about 20 m/s at the top of the column and increases rapidly downward at gradients up to 100 s^{-1} until the depth of bubble nucleation is reached. For basalt with 0.5% initial water, this is about 60 m.

Ray paths originating from strombolian explosions at the top of the column have been determined using the personal computer version of RAYAMP [*Crossley*, 1989]. They curve strongly upward and are inhibited from penetrating into the wall rock by large values of critical angle and high reflection coefficients.

Legitimately escaping rays originate very steeply downward and enter the wall near the bottom of the vesicular layer. Normally, they produce the first arrivals at a distance but are weak because they are sourced from a small solid angle. Their time intercept for an otherwise simple model of the volcano is of the order of 0.5 s, but this is not obvious in typical data, because the lack of a clear S wave prevents reliable origin time determination. The intercept time is not strongly dependent on the radius of the conduit, provided it is above 10 m.

The modeling of vesicular lava columns as having very low surface velocity and very high vertical velocity gradients gives a satisfactory explanation of the data on explosion earthquakes in the Erebus lava lake and must be a real phenomenon in strombolian activity. However, the theory for the present velocity-depth curve assumes small bubble fractions, and the curve is unreliable for high bubble fractions. The theoretical difficulties are daunting, and experimental data on acoustic velocity in spheroidal foams of high bubble fraction and viscosity are -necessary. The growth rate of bubbles in magma foams is also uncertain when the bubble fraction is high, because *Sparks* [1978] considered only isolated bubbles of water vapor. When other gases are included, the vesiculation will extend deeper, and at large bubble fractions the depression of velocity may be less than modeled here. The seismic effects may be modified but not eliminated. The best fit depth of 10 m for an explosion which originates at the surface may be a measure of the accuracy of the velocity model.

REFERENCES

Aki, K., B. Chouet, M. Fehler, G. Zandt, R. Koyanagi, J. Colp, and R. G. Hay, Seismic properties of a shallow magma reservoir in Kilauea Iki by active and passive experiments, *J. Geophys. Res., 83*, 2273–2282, 1978.

Crespo, A., Sound and shock waves in liquids containing bubbles, *Phys. Fluids, 12*(11), 2274–2282, 1969.

Crossley, D., RAYAMP-PC, 2.3, computer program, McGill Univ., Montreal, Que., Canada, 1989.

Dibble, R. R., Seismic and related phenomena at active volcanoes in New Zealand, Hawaii and Italy, Ph.D. thesis, 557 pp., Victoria Univ. of Wellington, Wellington, New Zealand, 1972.

Dibble, R. R., New eruption parameters and spectral relationships between seismic and infrasonic signals from Erebus Volcano, Antarctica, in Proceedings of 5th Symposium on Antarctic Geoscience, *Mem. 37,* pp. 22–28, Natl. Inst. of Polar Res., Tokyo, 1985.

Dibble, R. R., J. Kienle, P. R. Kyle, and K. Shibuya, Geophysical studies of Erebus Volcano, Antarctica, from 1974 December to 1982 January, *N. Z. J. Geol. Geophys., 27,* 425–455, 1984.

Dibble, R. R., S. I. D. Barrett, K. Kaminuma, S. Miura, J. Kienle, C. A. Rowe, P. R. Kyle, and W. C. McIntosh, Time comparisons between video and seismic signals from explosions in the lava lake of Erebus Volcano, Antarctica, *Bull. 38,* pp. 49–63, Disaster Prev. Res. Inst., Kyoto Univ., Uji, Japan, 1988.

Dibble, R. R., B. O'Brien, and C. A. Rowe, The velocity struc-

ture of Mount Erebus, Antarctica, and its lava lake, this volume.

Dunbar, N. W., Low pressure crystallisation of anorthoclase crystals from phonolitic melt, Mount Erebus, Antarctica: Evidence from volatile contents of melt inclusions, in *Abstracts, Sixth International Symposium on Antarctic Earth Sciences*, p. 129, National Institute of Polar Research, Tokyo, 1991.

Kaminuma, K., Seismic activity of Erebus Volcano, Antarctica, *Pure Appl. Geophys.*, *125*, 993–1008, 1987.

Kaminuma, K., and R. R. Dibble, An eruption process of Mount Erebus, Antarctica, in *Kagoshima International Conference on Volcanoes 1988, Proceedings*, pp. 66–70, Kagoshima Prefectorial Government, Japan, 1988.

Kaminuma, K., M. Baba, K. Shibuya, and R. R. Dibble, Explosion earthquakes of Mount Erebus, Antarctica, in Proceedings of 5th Symposium on Antarctic Geoscience, *Mem. 37*, pp. 40–47, Natl. Inst. of Polar Res., Tokyo, 1985.

Kasahara, M., A. Kubotera, and Y. Tanaka, Simultaneous observations of the eruptions at the Miharayama Volcano, Izu-Oshima, by a seismometer and an infrared radiation thermometer, 1, Observational results (in Japanese), *Kazan*, *20*(2), 87–101, 1975.

Kasahara, M., A. Kubotera, and Y. Tanaka, Simultaneous observations of the eruptions at the Miharayama Volcano, Izu-Oshima, by a seismometer and an infrared radiation thermometer, 2, Analytical research of the characteristics of the isolated type eruption tremors and preliminary examinations of their source mechanism (in Japanese), *Kazan*, *21*(2), 81–93, 1976.

Kienle, J., C. A. Rowe, P. R. Kyle, W. C. McIntosh, and R. R. Dibble, Eruption of Mount Erebus and Ross Island seismicity, 1984–1985, *Antarct. J. U. S.*, *20*(5), 25–28, 1985.

Kyle, P. R., Volcanic activity of Mount Erebus, 1984–1986, *Antarct. J. U. S.*, *21*(5), 7–8, 1986.

Kyle, P. R., R. R. Dibble, W. F. Giggenbach, and J. R. Keys, Volcanic activity associated with the anorthoclase phonolite lava lake, Mount Erebus, Antarctica, in *Antarctic Geoscience*, edited by C. Craddock, pp. 735–745, University of Wisconsin Press, Madison, 1982.

Kyle, P. R., L. Sybeldon, G. Zreda-Gostynska, D. Finnegan,

and W. C. McIntosh, Volcanic emission rates from Mount Erebus, Antarctica, in *Abstracts, Sixth International Symposium on Antarctic Earth Sciences*, p. 338, National Institute of Polar Research, Tokyo, 1991.

Kyle, P. R., L. Sybeldon, W. C. McIntosh, K. Meeker, and R. Symonds, Sulfur dioxide emission rates from Mount Erebus, Antarctica, this volume.

MacIntyre, F., Flow patterns in breaking bubbles, *J. Geophys. Res.*, *77*, 5211–5228, 1972.

Martin, B., Expedition to Erebus, *KENW-TV Documentary*, Portales, New Mexico, 1987.

Miksis, M. J., and L. Ting, Viscous effects on wave propagation in a bubbly liquid, *Phys. Fluids, 30*, 1683–1689, 1987.

Murase, T., and A. R. McBirnie, Properties of some common igneous rocks and their melts at high temperatures, *Geol. Soc. Am. Bull.*, *84*, 3563–3592, 1973.

Peterschmitt, E., and H. Tazieff, Sur un nouveau type de secousse volcanologique enregistree au Stromboli, *C. R. Seances Acad. Sci.*, *255*, 1971–1973, 1962.

Shaw, H. R., D. L. Peck, T. L. Wright, and R. Okamura, The viscosity of basaltic magma: An analysis of field measurements in Makaopuhi lava lake, Hawaii, *Am. J. Sci., 266*, 225–264, 1968.

Sparks, R. S. J., The dynamics of bubble formation and growth in magmas: A review and analysis, *J. Volcanol. Geotherm. Res., 3*(1), 1–37, 1978.

Wilson, L., Relationships between pressure, volatile content and ejecta velocity in three types of volcanic explosion, *J. Volcanol. Geotherm. Res., 8*, 297–313, 1980.

Wood, A. B., *A Textbook of Sound*, 578 pp., G. Bell and Sons, London, 1946.

Yamasato, H., Distribution of the initial motions of explosion earthquakes at Sakurajima Volcano (in Japanese), *Kazan, 32*, 289–300, 1987.

R. R. Dibble, Department of Geology, P.O. Box 600, Victoria University of Wellington, Wellington, New Zealand.

THE SEISMIC ACTIVITY OF MOUNT EREBUS IN 1981-1990

Katsutada Kaminuma

National Institute of Polar Research, Tokyo, Japan

The seismic activity of Mount Erebus was monitored from December 1980 until December 1990. Seismicity during the period can be divided into four stages: (1) high activity (December 1980 to September 1982), (2) precursor to increased explosive activity (October 1982 to August 1984), (3) increased explosive activity (September to December 1984), and (4) low activity (1985-1990). From December 1980 to August 1984, the number of volcanic earthquakes around Mount Erebus averaged 20-150 per day, including several earthquake swarms. A marked increase in volcanic activity which began on September 13, 1984, and lasted until the end of December 1984 had more frequent and larger strombolian explosions. This increased eruptive activity was accompanied by a distinct decrease in the intensity of background seismic activity, and only a few earthquakes per day were subsequently recorded. The number of seismic events during 1985-1990 averaged less than 20 per day, with only one or two earthquake swarms in 1985 and 1986. An aseismic zone in the southwestern part of Mount Erebus attenuates the higher-frequency seismic waves and might indicate a magma reservoir which continuously supplies fresh magma to the lava lake in the Erebus crater.

1. INTRODUCTION

This paper summarizes the seismic activity of Mount Erebus from 1981 to 1990. A seismic network was established on Mount Erebus (77°37'S, 167°09'E, 3794 m), Ross Island, Antarctica, in December 1980 by the International Mount Erebus Seismic Study (IMESS). This collaboration between Japan, New Zealand, and the United States studied the seismic activity of Mount Erebus until December 1986 [*Kienle et al.*, 1981, 1982; *Takanami et al.*, 1983; *Kaminuma et al.*, 1986, 1987; *Kaminuma*, 1987]. During IMESS the number of seismic stations ranged between three and ten (Figure 1). Later the network which consisted of six seismic stations was used by the International Mount Erebus Eruption Mechanism Study (IMEEMS) of New Zealand and Japan [*Kaminuma and Murakami*, 1989; *Dibble*, this volume]. The objective of IMEEMS was to study the eruption mechanism and the seismic activity of Mount Erebus.

Signals from the Mount Erebus seismic network (Figure 1) were transmitted to New Zealand's Scott Base by radio telemetry and recorded on a 14-channel FM data recorder and monitored using a one-channel chart recorder. Five additional temporary stations were operated during the 1984-1985 field season for recording

during an explosion seismic experiment.

Infrasonic microphones were installed in 1980 near the main crater of Mount Erebus to record explosive eruptions. The infrasonic signals were recorded on the FM data recorder via the radio telemetry [*Dibble*, 1985].

A video camera was installed from December 1986 to December 1990 on the rim of the main crater of Mount Erebus to observe eruptions from the lava lake [*Dibble*, this volume]. The solar-powered camera and associated TV transmitter usually operated from September to April each year, but corrosion by volcanic gases of the glass camera window obscured the pictures between September and December [*Dibble et al.*, 1988] until an acrylic window was fitted in December 1988.

A new phase of volcanic activity started on September 13, 1984, and lasted until late December 1984. It was characterized by larger and more frequent strombolian eruptions. Significant changes in seismicity within Ross Island and Mount Erebus were recognized both before and after the increased eruptive activity.

2. SEISMICITY IN 1981-1990

Four types of earthquakes are recognized on the seismic records: (1) teleseisms, (2) volcanic earthquakes, (3) icequakes, and (4) local earthquakes in the region

IMESS SEISMIC NETWORK
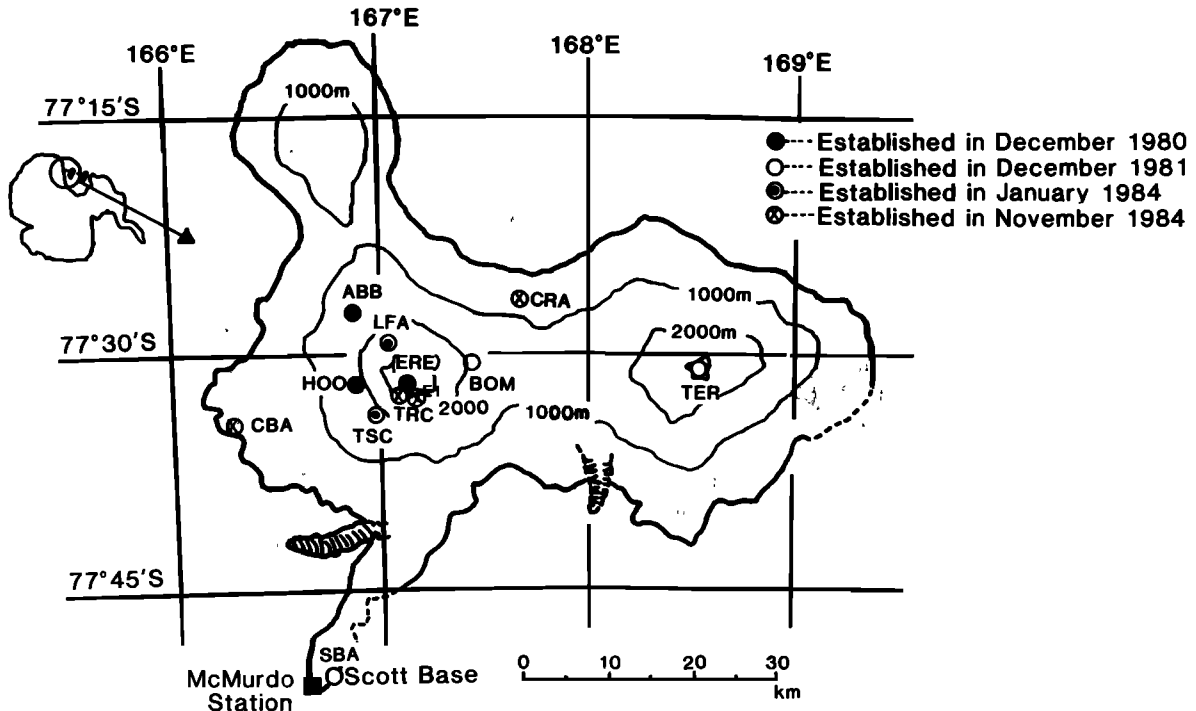
Fig. 1. Locations of seismic stations in 1984. Abbreviations are as follows: ABB, Abbott Peak; BOM, Bomb Peak; CBA, Cape Barne; CRA, Crash Nunatak; ERE, Erebus Summit; HOO, Hoopers Shoulder; SBA, Scott Base; TER, Mount Terror Summit; LFA, Lower Fang Ridge; TRC, Truncated Cone; and TSC, Three Sisters Cones. The Erebus summit station (ERE) was destroyed in September 1984 and was replaced by station E1, which was situated at the E1 Trig station on the south side of the Side Crater.

surrounding Ross Island. Figures 2 and 3 show examples of seismograms of a volcanic earthquake, a teleseism, an icequake, and a local earthquake recorded at Hoopers Shoulder station (HOO). Volcanic earthquakes and icequakes are easy to distinguish from teleseisms and local earthquakes because the latter two have a lower frequency and longer duration. Only a few local earthquakes have been recognized on the network.

Figures 4 and 5 show the daily number of earthquakes per day between 1982 and 1986 as counted on the seismograms from HOO. Only earthquakes with S-P time less than 10 s and volcanic earthquakes as shown in Figure 2 (no clear S phases) and amplitude greater than 4 mm on the monitoring seismogram at HOO were counted. Teleseisms and local events, which were estimated to occur outside of Ross Island, were not counted. Icequakes (Figure 3) which have high frequencies and shorter durations [*Kaminuma and Haneda*, 1979] were not counted.

Figure 6 shows the daily number of volcanic earth-

quakes counted at the Truncated Cones station (TRC) and the Erebus E1 Trig station (E1) between 1987 and 1990. Counts using HOO could not be used during this period, as the number of seismic events had decreased and their amplitudes were too small. Stations TRC and E1 are both located in the summit area. Seismic station E1 replaced station ERE, which was damaged by a volcanic bomb during the 1984 eruptive activity. Using seismic records from a week in 1987, *Kaminuma and Murakami* [1989] counted the daily number of earthquakes on the HOO and TRC stations. They found 4 times more earthquakes per day at TRC than at HOO. The daily number of earthquakes at E1 was about the same as at TRC. In Figure 6 the estimated daily number of earthquakes at HOO is also shown along the *Y* axis for easy comparison with the numbers at TRC/E1.

The magnitudes of the volcanic earthquakes were very small in most cases. Although the magnitudes have not been determined quantitatively, the seismic events shown in Figures 4–6 are estimated from their ampli-

HOOPER
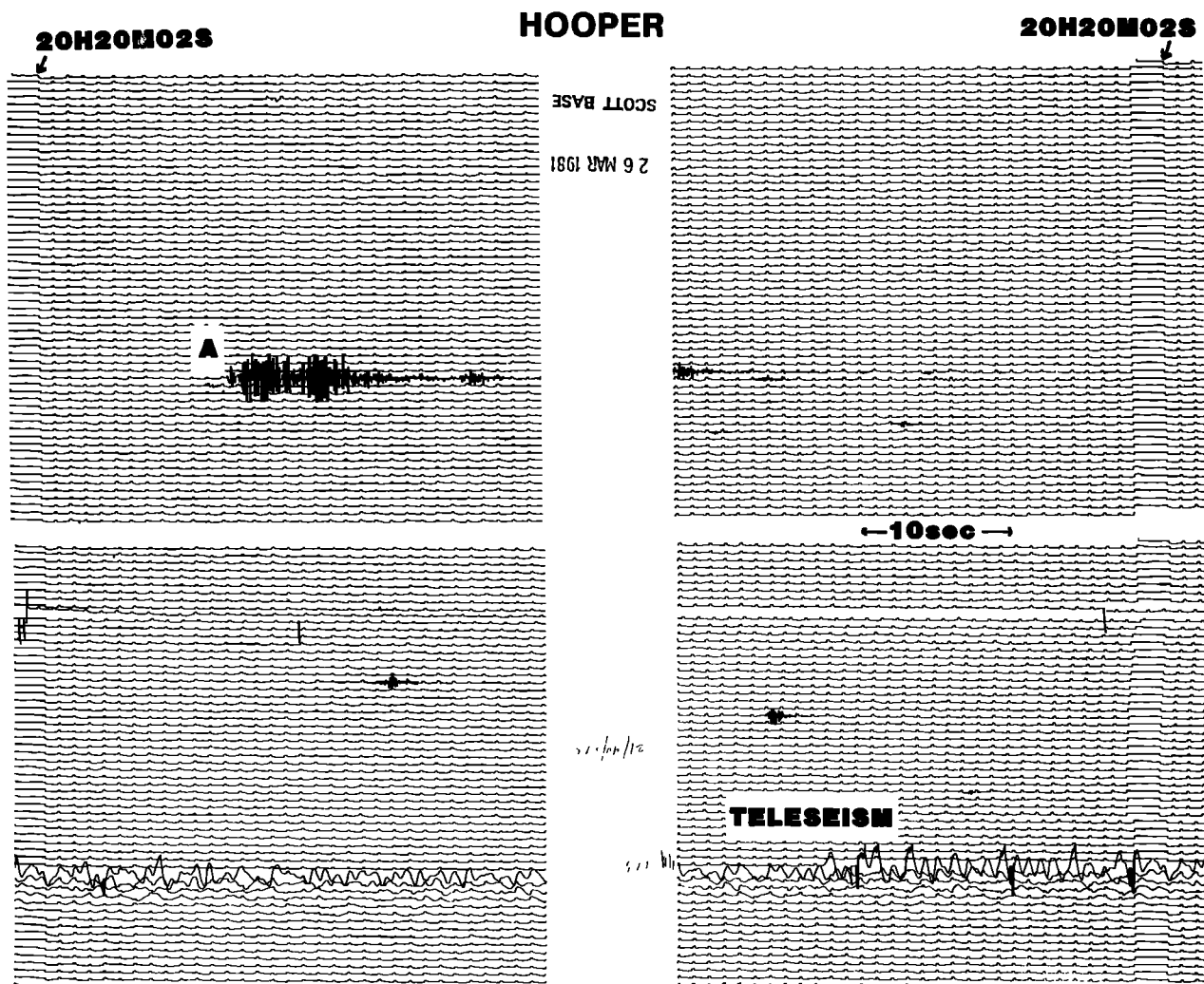
Fig. 2. A typical record of a volcanic earthquake (A) and a teleseism as recorded on the long-term recorder used to monitor the activity. Each horizontal trace represents 1 min, and each block represents 1 hour. The horizontal traces are split into two sections with 5-s overlap at the end of each block.

tudes on seismograms to have magnitudes of less than 2 [*Ueki et al.*, 1984; *Dibble*, 1985].

A remarkable change in the seismicity of Mount Erebus occurred before and after the 1984 activity. The seismic activity before the 1984 volcanic activity was characterized by 60–150 earthquakes per day, as counted at HOO. However, after the 1984 activity the daily earthquake counts at HOO gradually declined (Figures 4, 5, and 6). At HOO there was an average of 64 earthquakes per day in 1982, 134 in 1983, and 146 in January–July 1984. In 1985 and 1986, following the activity, the average number of earthquakes was about 20 per day. The average daily counts at TRC in 1987 and 1988 were 64 and 15, respectively, which would

correspond to 16 and 4 earthquakes at HOO. The number of earthquakes at (mainly) E1 in 1989 was 47 per day, equivalent to 12 at HOO. In 1990 the daily earthquake count at TRC was 12, equivalent to 4 at HOO.

3. HYPOCENTER DISTRIBUTION

Numerous studies of the earthquake hypocenters were made as part of IMESS and IMEEMS using various models of *P* wave velocity structure [e.g., *Takanami et al.*, 1983; *Kienle et al.*, 1984; *Kaminuma et al.*, 1986, 1987; *Kaminuma*, 1987; *Dibble et al.*, this volume]. *Takanami et al.* [1983] used an empirical structure model with an estimated Poisson's ratio of σ– = 0.25.
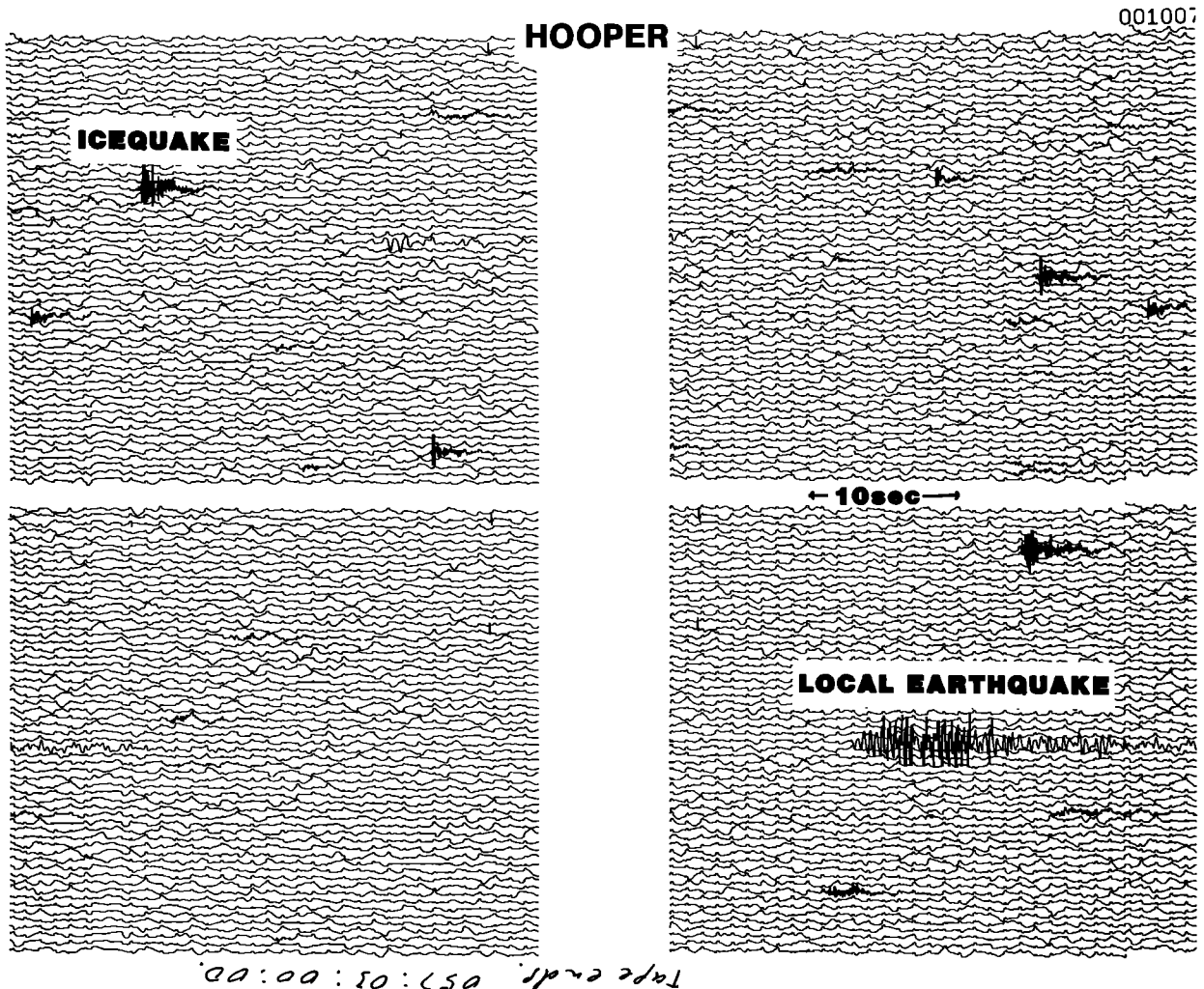
Fig. 3. A typical record of icequakes and local earthquakes on the monitoring seismogram.

Kienle et al. [1984] located earthquakes using "hypoellipse," a computer program developed by the U.S. Geological Survey. *Rowe* [1988] developed a structure model using data from explosion seismic experiments made in December 1984 [*Kaminuma et al.*, 1985*a*]. Rowe's model had a linear gradient in *P* wave velocity ranging from 3.55 km/s at the Erebus summit to 4.6 km/s at a depth of 7 km below the summit, which overlay a homogeneous half-space with a velocity of 6.1 km/s.

Kaminuma and Shibuya [1991] also developed a velocity structure using the same explosion seismic experiments as *Rowe* [1988] but with additional data from some temporary seismic stations. They proposed a first layer 2.2–2.4 km thick with a seismic velocity of 3.07 km/s. The boundary between the first and second layers was slightly inclined, with the thickness of the

second layer ranging from 4.2 to 4.4 km and a velocity of 4.67 km/s. The velocity of a third layer was 6.27 km/s starting at a depth of 6.6 km below the summit. *Kaminuma and Shibuya* [1991] determined the earthquake hypocenters using *P* wave arrival times from five or more stations. The accuracy of phase readings was better than 0.05 s. The hypocenter locations have horizontal and vertical errors of less than 3 km. An example of a seismogram used for hypocenter determinations is given in Figure 7. The event in the figure was observed to be an explosion in the lava lake. The infrasonic signal associated with the explosion was recorded on the infrasonogram as shown at the top of Figure 7. The *P* phases identified and scaled as the arrival times are shown with arrows in the figure.

Figure 8 shows the distribution of earthquake epicenters and their focal depth projected onto a vertical NE-
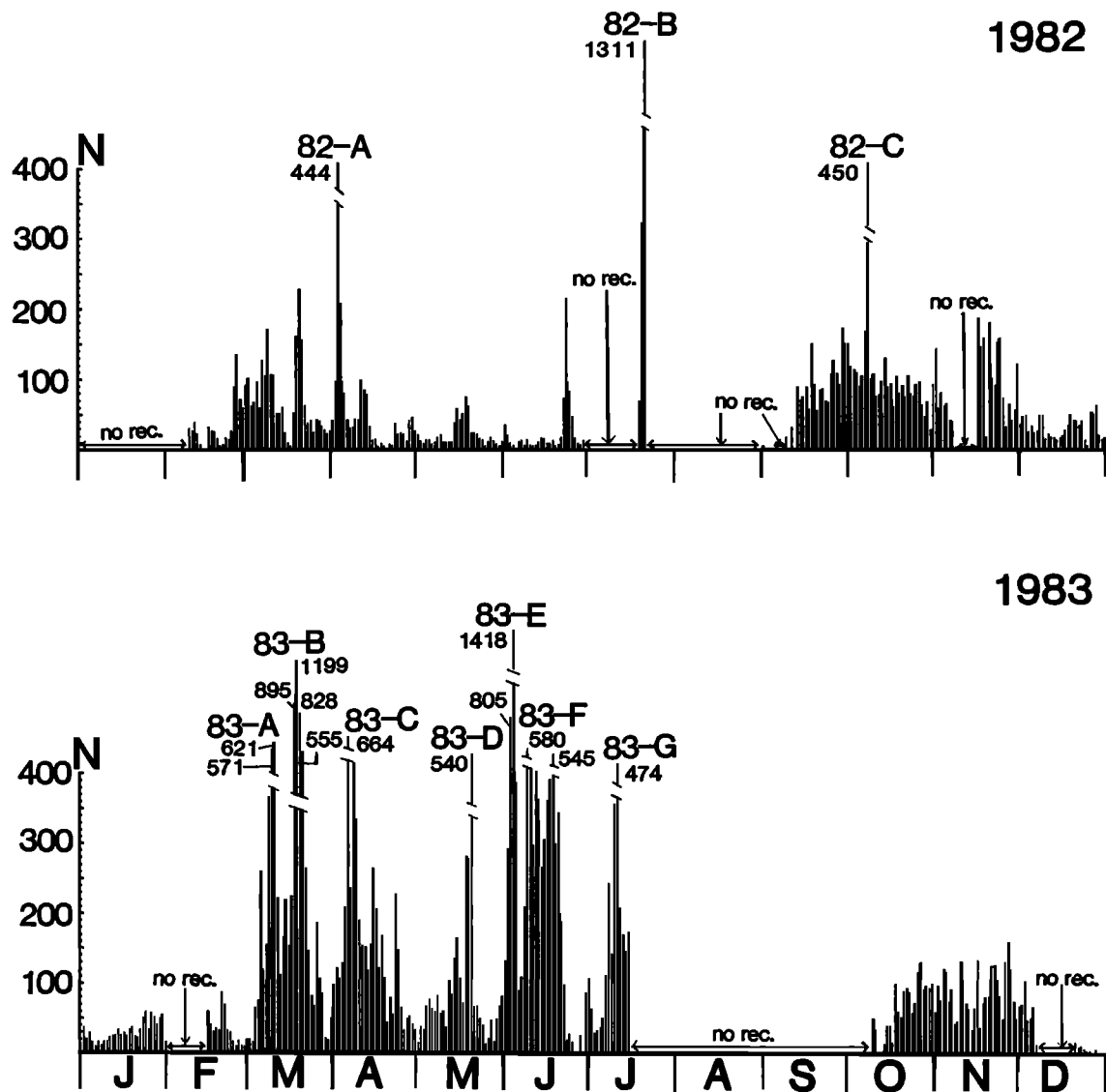
Fig. 4. Daily number of earthquakes in 1982 and 1983 at Mount Erebus and vicinity as counted at Hoopers Shoulder station (HOO). Earthquake swarms are labeled 82-A, 83-B, etc.

SW section across Ross Island. Over 200 events were used in the hypocenter calculations (Figure 8) for the period January 1982 to September 1984 (that is, prior to the 1984 eruptive activity). Although the hypocenters scatter widely around Mount Erebus, there is a slight concentration in the area northwest of the central cone (between E1 and lower Fang Glacier (LFA) (Figure 3)). Most of the earthquakes located in the northwest area occurred in earthquake swarm 82-C [*Kaminuma et al.*, 1985*b*].

The focal depth distribution of explosion earthquakes as defined by *Shibuya et al.* [1983] and *Ueki et al.*

[1984] ranges from 0 to 4 km below the summit. Other earthquake types are distributed up to 15 km in depth. An aseismic zone with few earthquakes is located in the area southwest of the summit (ERE). Such an aseismic zone was also reported by *Shibuya et al.* [1983], *Ueki et al.* [1984], and *Kaminuma et al.* [1985*b*].

Figure 9 shows the distribution of earthquake epicenters for the period between September 1984 and December 1987 and their focal depth projected onto a vertical NE-SW section across Ross Island. About 230 earthquakes are located in Figure 9, and their horizontal and vertical errors are within 3 km. Almost all earth-
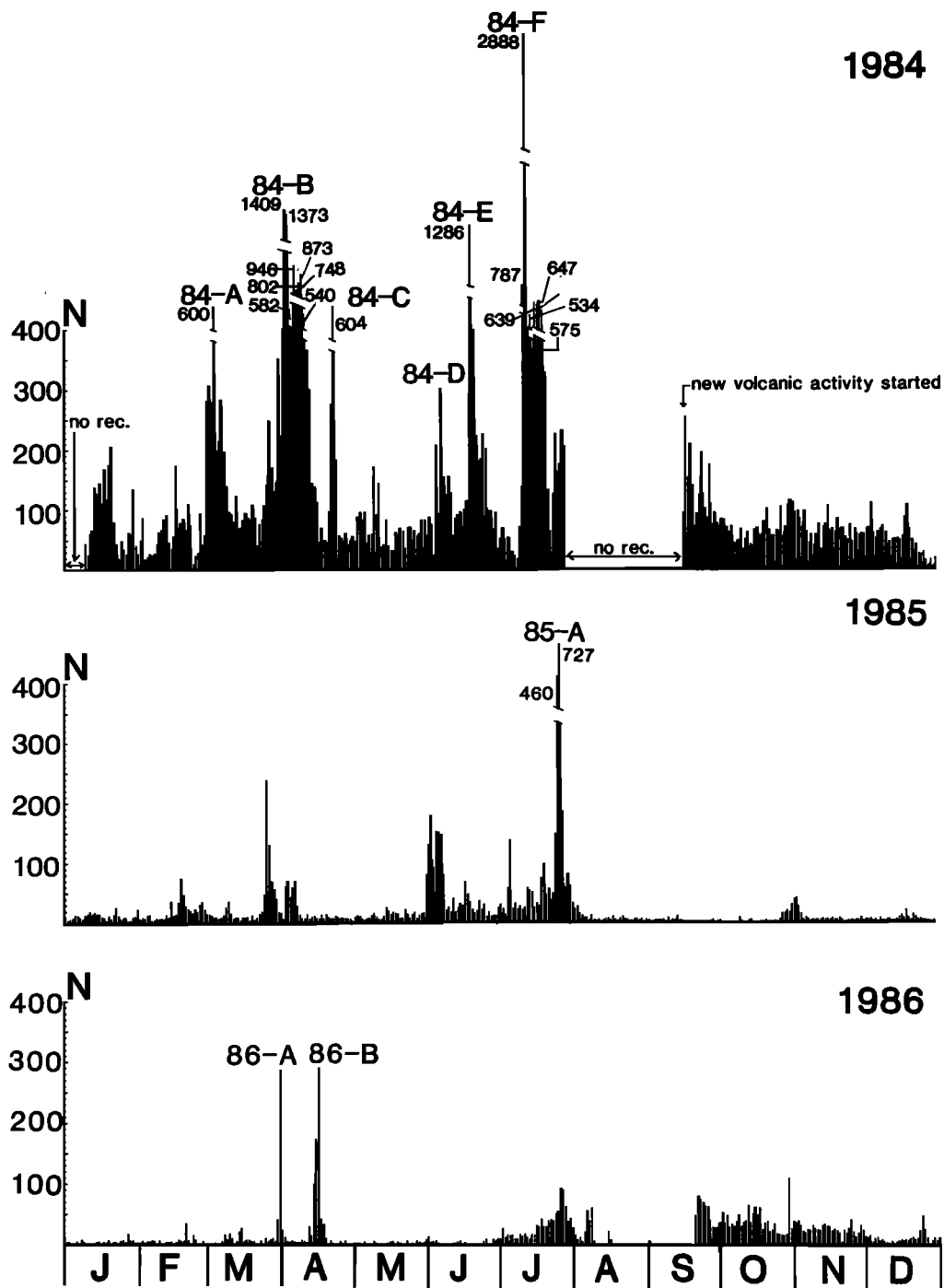
Fig. 5. Daily number of earthquakes in 1984, 1985, and 1986 at Mount Erebus and vicinity as counted at HOO. Earthquake swarms are labeled 84-A, 85-B, etc.
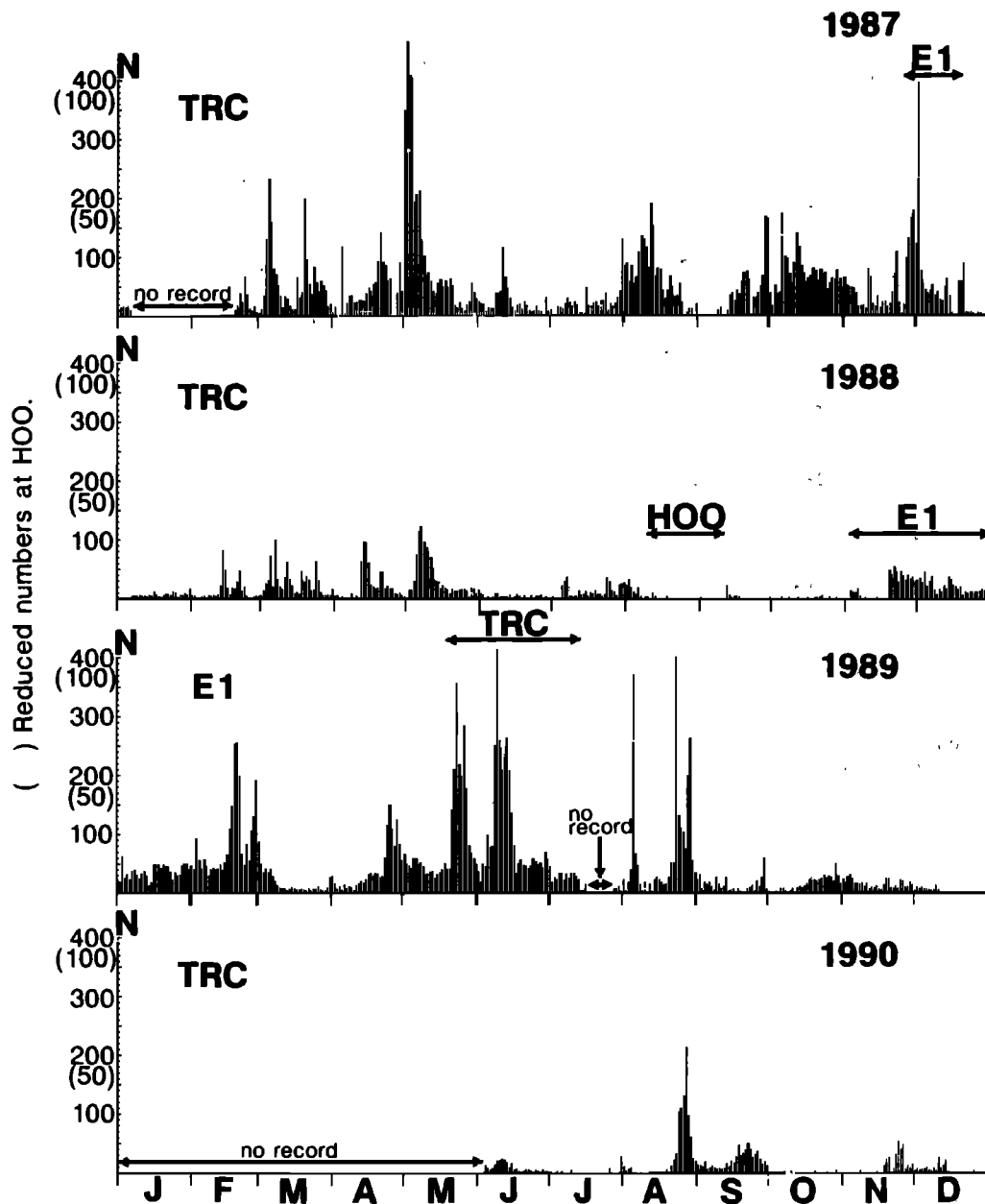
Fig. 6. Daily number of earthquakes from 1987 to 1990 at Mount Erebus and vicinity as counted at TRC or E1. The numbers in parentheses on the Y axis are the numbers reduced to HOO.

quakes in Figure 9 clustered within a 5-km distance of the summit. However, prior to the 1984 eruptive activity the earthquakes were located more extensively throughout Mount Erebus (Figure 8).

The existence of the aseismic zone beneath the summit of Erebus becomes clearer when 5 years of observations are considered (Figure 10). The aseismic zone is shown shaded in Figure 10, which also shows the hypocenters of earthquakes. This aseismic zone might indicate a magma reservoir which supplies continuously fresh magma to the lava lake at the Erebus summit.

Figures 11a–11c show seismograms and spectra for three typical earthquakes which were not accompanied by an eruption of Mount Erebus. The locations of each event are shown by a double circle on the figures. The earthquake shown in Figure 11a was located near the
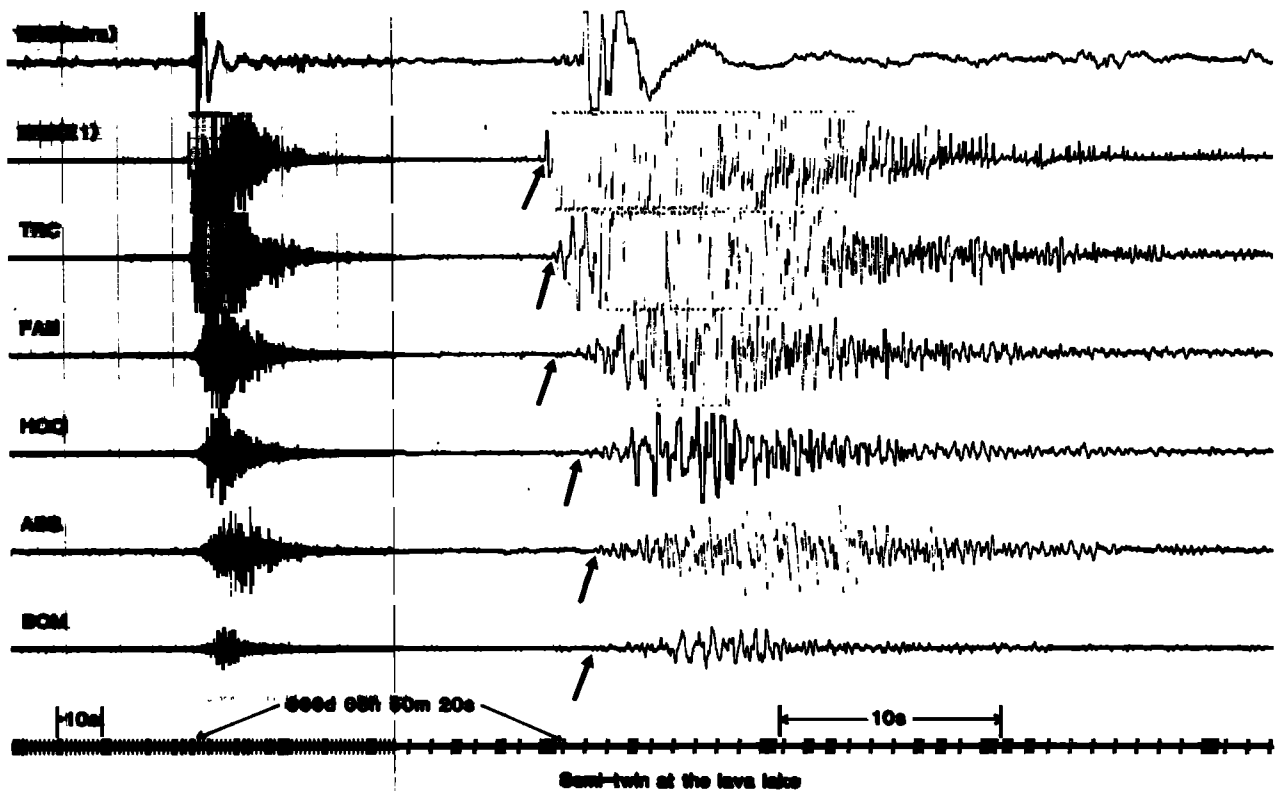
Fig. 7. An example of seismograms resulting from an explosion in the lava lake as recorded on the six stations used for the hypocenter determination. P wave arrival times used in the calculations are shown with arrows. FAN was a temporary station located at Fang Ridge. The top line of the figure shows the infrasonogram of the explosion sound.

aseismic zone, and the seismic ray path toward HOO might pass through the aseismic zone. The spectra of the seismic waves observed at the three stations on the flank of Mount Erebus (HOO, ABB, and BOM) and at TER are given in Figure 11a for comparison with each other. The spectra of the seismic waves at ABB, BOM, and TER have peaks in the range of 1–7 Hz. However, in contrast, the spectra at HOO have peaks in the lower-frequency range of 1–3 Hz.

The seismic waves of the earthquake shown in Figure 11b are characterized by narrow spectra whose peaks are in the range of 1–3 Hz. This event has longer hypocentral distances to the four stations than the events in Figure 11a. The earthquake shown in Figure 11c has spectral peaks in the range of 5–25 Hz, which is higher than the peaks for the other two examples (Figures 11a and 11b).

The hypocenters suggest there may be an aseismic zone beneath the southwestern flank of Mount Erebus (Figure 10). Seismic waves passing through the aseis-

mic zone seem to have strongly attenuated higher frequencies (Figure 11a), which suggests that the zone is a magma reservoir [Kaminuma et al., 1985c; Baba et al., 1985].

4. EARTHQUAKE SWARMS

An earthquake swarm is here defined as 250 or more seismic events occurring within a 24-hour period. Events occurring within a day on either side of the 250-event days are also considered part of the swarm [Ueki et al., 1984]. An example seismogram of an earthquake swarm is given in Figure 12.

Nineteen earthquake swarms were detected from 1982 through 1990 (Figures 4–6). However, 16 of the swarms occurred during 30 months in 1982–1984 [Ueki et al., 1984; Baba et al., 1985] and are labeled 82-A, 83-B, 84-C, etc., in Figures 4 and 5. Only one earthquake swarm occurred in 1985, and two occurred in 1986. No earthquake swarms were recorded in 1987 [Kaminuma

January 1982 – September 12, 1984
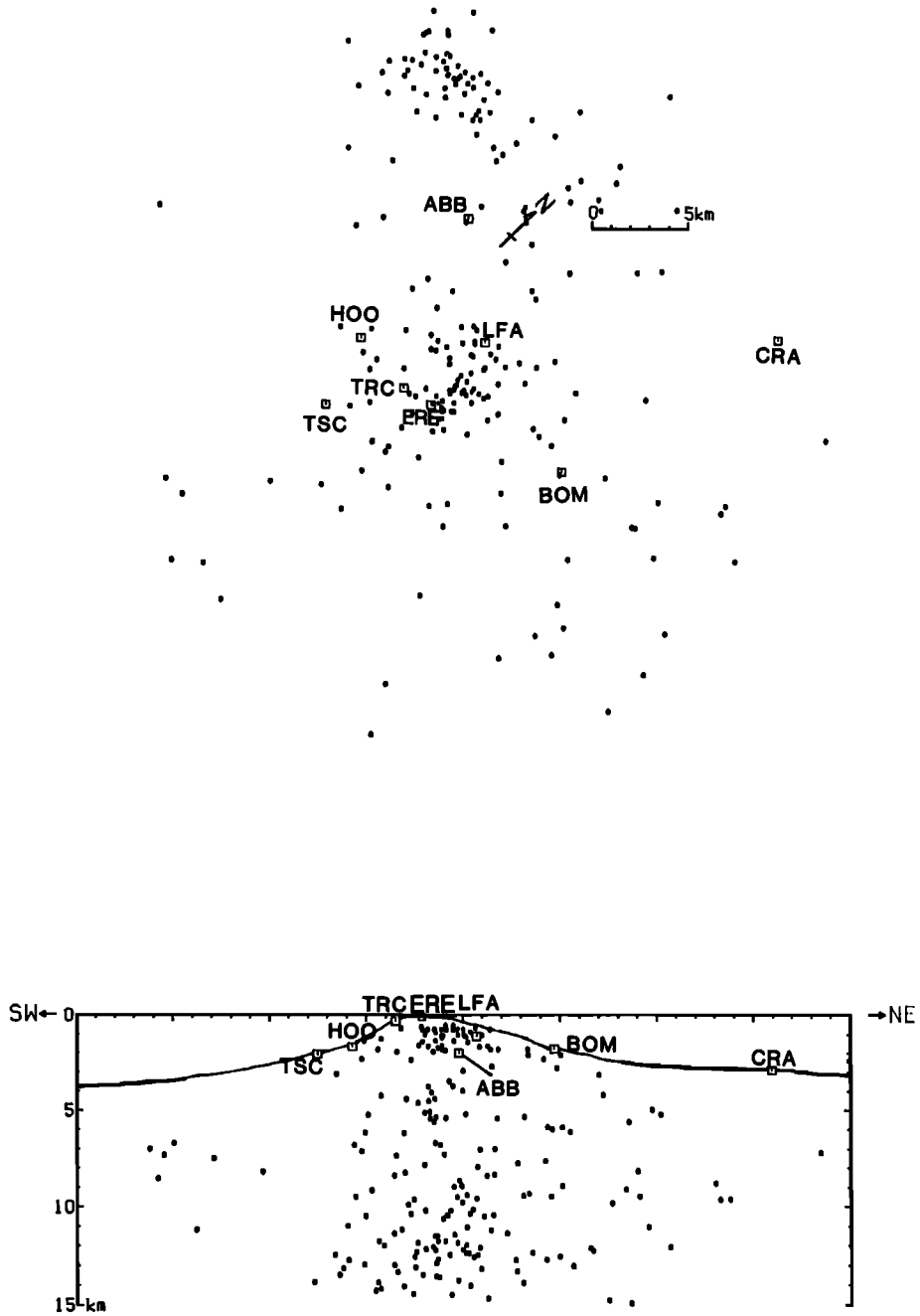
Fig. 8. Hypocenters and epicenters of earthquakes recorded between January 1982 and September 12, 1984.

September, 1984 - December, 1987
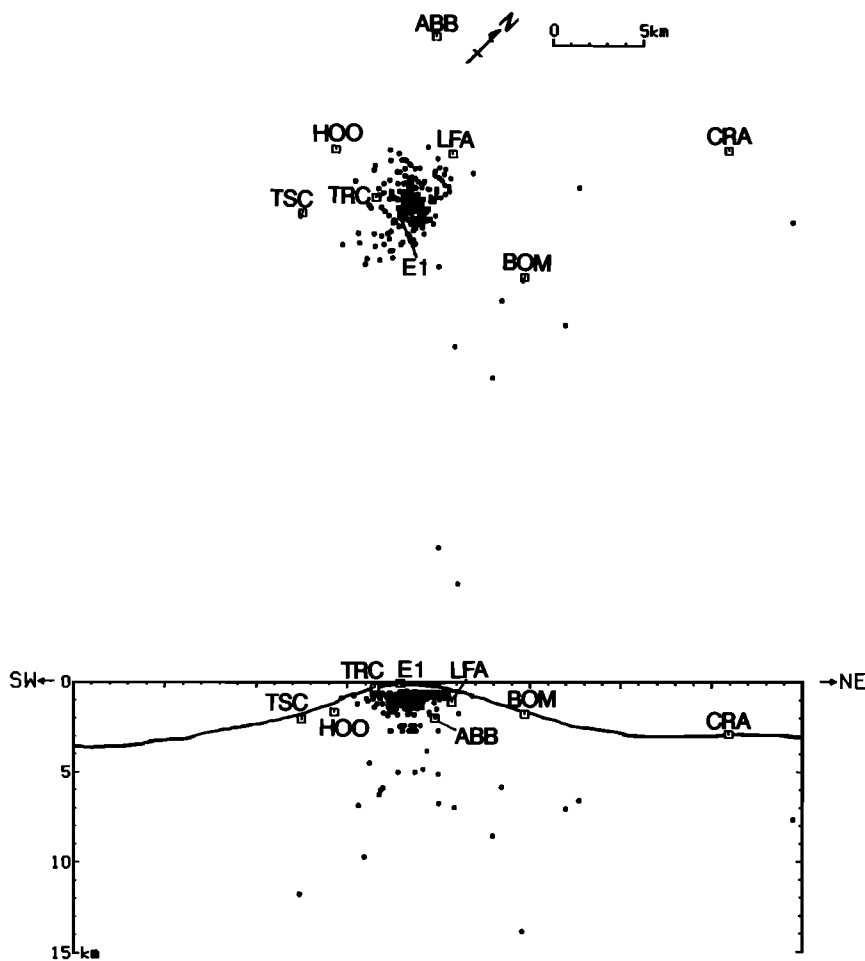
Fig. 9. Hypocenters and epicenters of earthquakes recorded between September 13, 1984, and December 1987.

and Murakami, 1989], 1988, 1989, or 1990 (Figure 6).

Frequency Variation

Figure 13 shows the duration, number of earthquakes, and average hourly number of earthquakes for the 19 identified earthquakes swarms. The largest number of earthquakes recorded on a single day was 2888 on July 12, 1984, during swarm 84-F . The number of days on which the daily number of earthquakes exceeded 1000 was only seven. Such swarms occurred once in 1982, twice in 1983, and 4 times during three swarms in 1984.

The largest hourly number of earthquakes among the swarms was 37 for swarm 82-B, which occurred in 1982 between 1200 hours on July 20 and 1100 hours on July

22. Unfortunately, the network stopped its operation, owing to a lack of battery power, on July 22 after a day in which 1311 events were recorded (Figure 4). Therefore the duration and number of earthquakes in swarm 82-B are unknown.

Swarm 82-C was characterized by a very sudden onset and a very rapid decrease in seismic activity [*Kaminuma et al.*, 1985*b*]. The 36-hour duration is the shortest among the 19 recognized swarms; however, the individual events were larger than those in the other swarms.

Swarms 83-C and 83-F were characterized by longer durations and a smaller average hourly number of earthquakes. The duration of swarm 83-C was 276 hours, the third longest of the 19 swarms. The duration of swarm
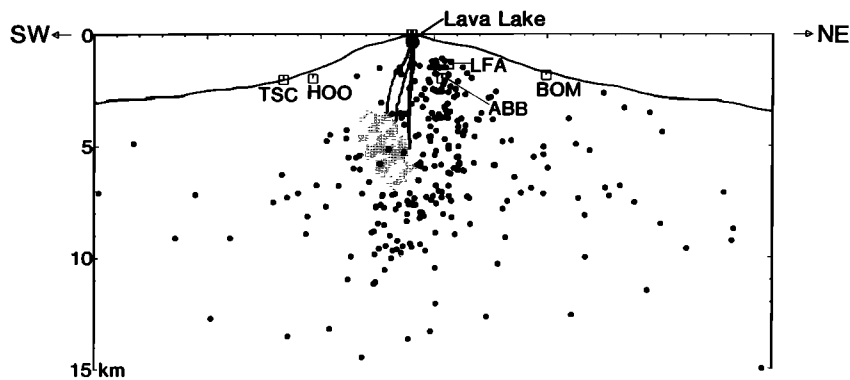
Fig. 10. The hypocenters of earthquakes recorded between 1980 and the 1984 eruptive activity. The shaded area shows an aseismic zone, which may represent a magma reservoir.

83-F was 325 hours, the second longest of the swarms, and its total number of earthquakes was about 5000, the third largest.

Swarm 84-B lasted for 365 hours from 0300 hours on March 29 to 0800 hours on April 13 and consisted of 9601 earthquakes, averaging 26 events per hour. This swarm had the longest duration and the largest number of earthquakes among the 19 swarms. Swarm 84-F lasted 261 hours and had about 8000 earthquakes.

The total number of earthquakes and the duration of the earthquake swarms in 1985 and 1986 were smaller than those in 1982–1984 [*Kaminuma et al.*, 1988; *Kaminuma and Murakami*, 1989]. Not only the daily counts but the swarm activities decreased after the 1984 activity.

Locations

Most of the swarms consisted of microearthquakes with magnitudes of less than 1. Therefore only a few locations could be determined for earthquakes in the swarms. The errors of the hypocenter determination are 3 km in both the vertical and the horizontal direction; so it seems that the swarms occurred beneath the Erebus summit within a depth range of 0 to 9 km.

The earthquakes of swarm 82-A had very small amplitudes and were only recorded at HOO; thus no locations could be determined. However, the large value of the Ishimoto-Iida coefficient "*m*" is consistent with this swarm being of volcanic type.

Three stations (BOM, ERE, and HOO) were operating during swarm 82-B; however, ABB was not working, and TER and SBA were more than 25 km from the estimated epicentral area. No locations were determined for swarm 82-B.

Using the seismic records for HOO, ABB, and BOM, hypocenters for swarm 82-C were located near the

Abbott Peak seismic station (ABB) on the northwestern flank of Mount Erebus. The swarm is assumed to have no direct relation with any surface volcanic activity [*Kaminuma et al.*, 1985b].

Three stations (ABB, HOO, and BOM) were operating during swarms 83-A and 83-B, but the earthquake amplitudes were too small to accurately identify the arrival times of *P* waves.

The summit station (ERE) did not work during swarm 83-C, and only 11 earthquakes were recorded at HOO, ABB, BOM, and TER. Although the accuracy of the earthquake locations is not high, they were located mostly to the east of the summit.

No locations for earthquakes in swarms 83-D, 83-E, 83-F, 83-G, and 84-F could be determined, as only two stations (HOO and SBA) were working.

During swarm 84-B, eight stations were working, although most of the earthquakes were recorded at only two or three stations. Six earthquakes of this swarm were located, and their hypocenters are shown by stars in Figure 14. These six earthquakes are characterized by having their maximum amplitudes at lower Fang station (LFA) (see Figure 1).

Four earthquakes were located for swarm 86-A, and seven were located for 86-B (Figure 15).

5. SUMMARY OF SEISMIC ACTIVITY

The monthly mean number of earthquakes counted at and reduced to HOO is shown in Figure 16. The seismic activity for 1981 to 1990 is divided into four stages. The daily number of explosions during each stage is not discussed because explosions could only be recognized from audiovisual, video, and infrasonic observations, which are much less continuous than the seismic observations.
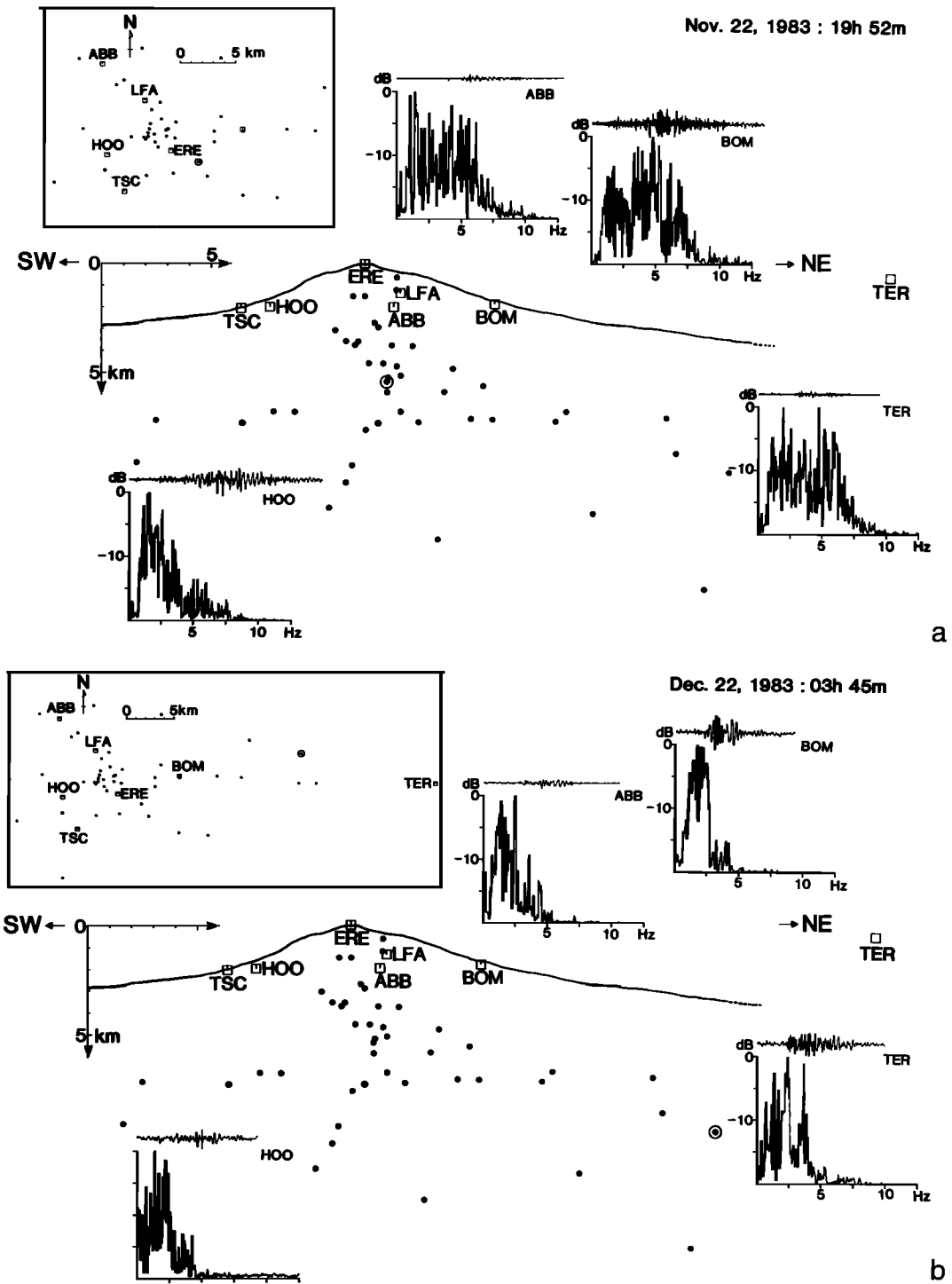
Fig. 11. Spectra of seismograms for three types of earthquakes which were not accompanied by eruptions. Locations of the earthquakes are given by double circles. Solid circles in the box (top left) of each figure indicate epicenter locations. Vertical cross sections (center) show focal depth.
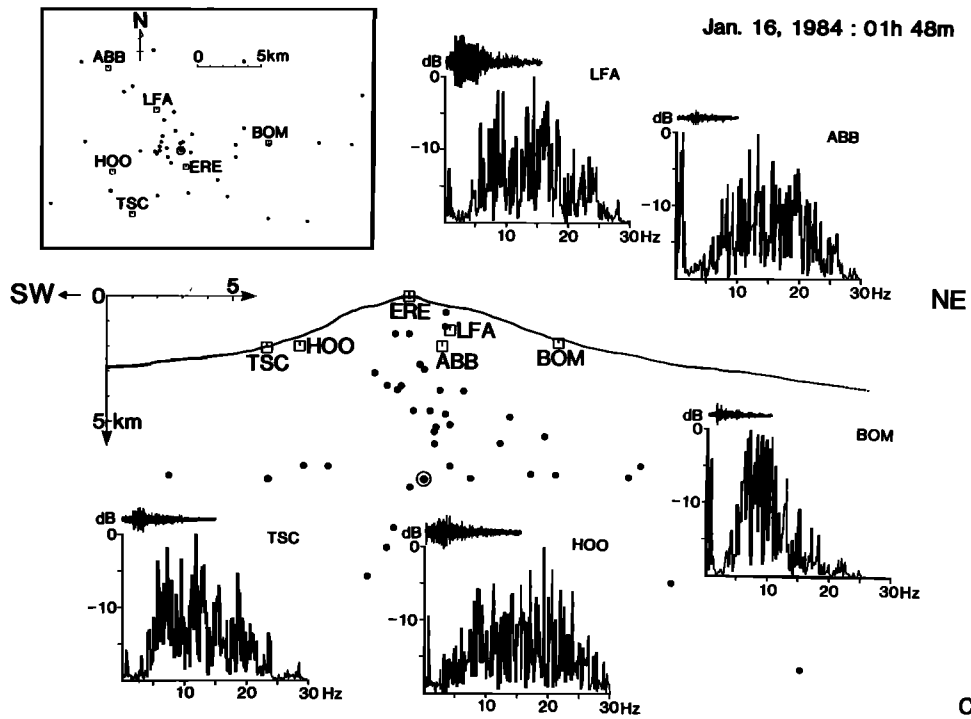
Fig. 11. (continued)
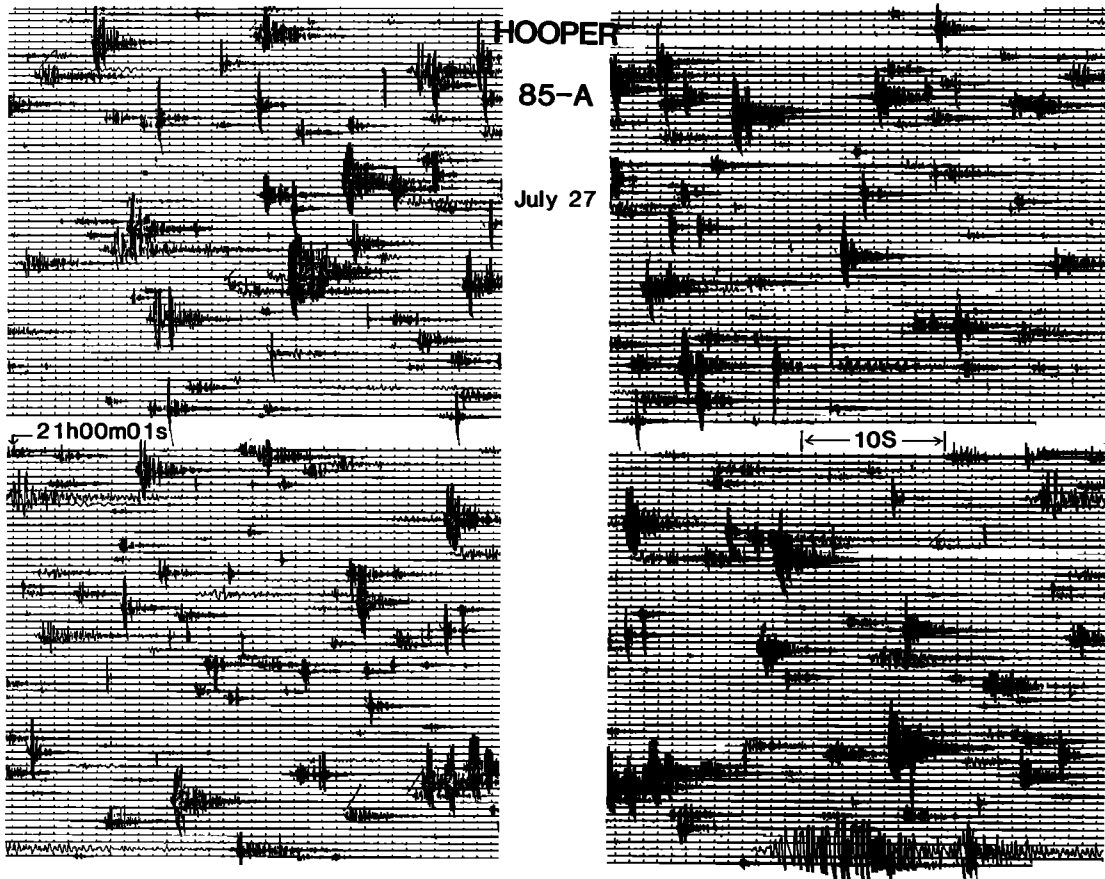
Fig. 12. Seismogram record of an earthquake swarm. The seismogram shows the events of swarm 85-A recorded at HOO for 2000–2200 hours on July 27, 1985.
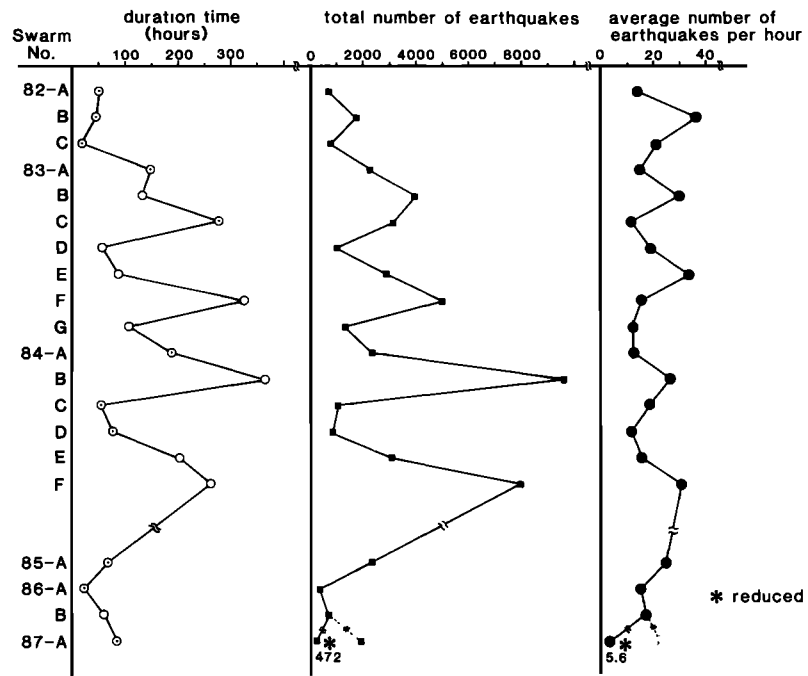
Fig. 13. The duration, total number, and average hourly number of earthquakes of 19 earthquake swarms.

84-B
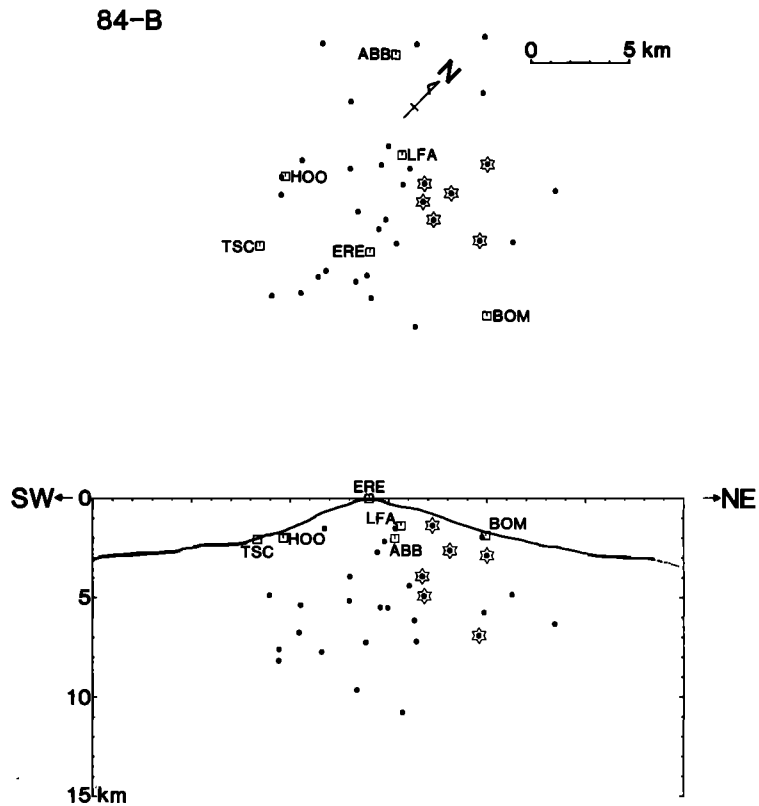
Fig. 14. Earthquake locations of swarm 84-B (stars) and of the other type of events (solid circles).

86 Swarm A, B

▲------86 Swarm A

●----86 Swarm B
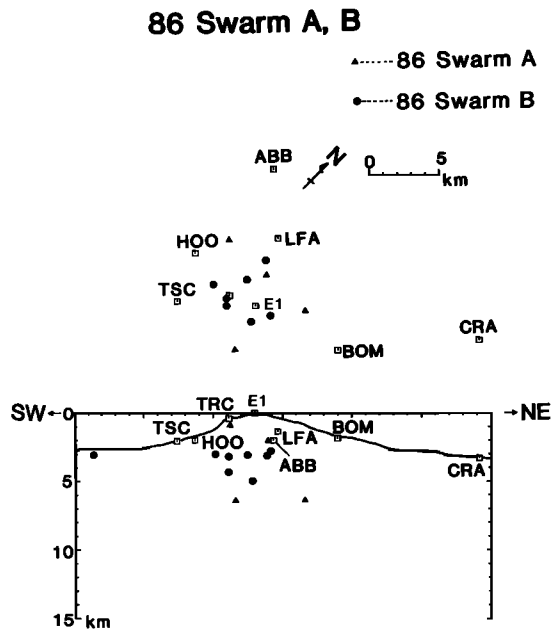
Fig. 15. Earthquake locations during swarms 86-A (solid triangles) and 86-B (solid circles).

High activity (December 1980 to September 1982). The daily counts of earthquakes were 50–100 with one or two earthquake swarms per year. The earthquakes were located throughout Mount Erebus and the surrounding area. This stage may have started before December 1972, when the lava lake was first recognized and was expanding [Kyle et al., 1982].

Preceding the new phase (October 1982 to August

1984). This stage started with the earthquake swarm in October 1982 [Kaminuma et al., 1985b]. Energy for the 1984 eruptive activity was accumulating, and the size of the lava lake was maximum at this stage. The seismic activity was very high; the daily counts were over 100, and several earthquake swarms occurred every year. The earthquakes were located throughout Mount Erebus and the surrounding area.

New phase in activity (September to December 1984). Many large explosions with volcanic ejecta occurred, and there were major changes in the inner crater [Kyle, 1986; Kaminuma, 1987]. The lava lake in the Inner Crater was buried by ejecta.

Low seismic activity (1985–1990). A 20-m-diameter lava lake was exhumed within the inner crater in 1985 [Kyle, 1986]. During this period the daily earthquake counts were less than 20, and the earthquake epicenters were located only in the summit area.

6. CONCLUSION

An international cooperative project between Japan, New Zealand, and the United States continuously monitored the seismic activity of Mount Erebus from 1981 to 1990. During the observation period, a large increase in eruptive activity commenced in September 1984 and lasted to the end of the year. A distinct change in the background seismicity was recognized before and after the 1984 activity.

The number of volcanic earthquakes around Mount Erebus averaged 20–150 per day, including several
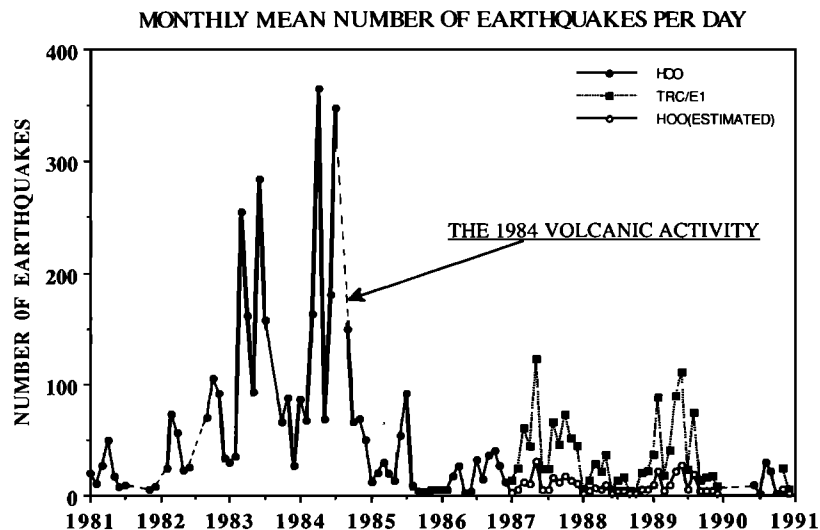
Fig. 16. The monthly mean number of earthquakes per day counted at HOO from 1981 to 1986 and at TRC or E1 from 1987 to 1990. The reduced number to HOO is also shown in 1987–1990.

earthquake swarms in every year before the 1984 erup-
tive activity. The number of seismic events after the
activity during 1985–1990 averaged less than 20 per
day. Only one and two earthquake swarms were record-
ed in 1985 and 1986, respectively, and no earthquake
swarms occurred from 1987 to 1990.

An aseismic zone is recognized in the southwestern
part of Mount Erebus. The seismic waves passing
through the aseismic zone seem to be strongly attenuat-
ed at higher frequencies. It is suggested that the zone
might be a magma reservoir which supplies magma to
the lava lake in the Erebus crater.

REFERENCES

Baba, M., K. Kaminuma, S. Ueki, and E. Koyama, Seismic
activity of Mount Erebus, Antarctica, in 1983–1984, *Mem.
Natl. Inst. Polar Res. Spec. Issue Jpn., 37,* 29–39, 1985.

Dibble, R. R., New eruption parameters and spectral relation-
ships between seismic and infrasonic signals from Erebus
volcano, Antarctica, *Mem. Natl. Inst. Polar Res. Spec. Issue
Jpn., 37,* 22–28, 1985.

Dibble, R. R., Velocity modeling in the erupting magma col-
umn of Mount Erebus, Antarctica, this volume.

Dibble, R. R., S. I. D. Barrett, K. Kaminuma, S. Miura, J.
Kienle, C. A. Rowe, P. R. Kyle, and W. C. McIntosh, Time
comparisons between video and seismic signals from explo-
sions in the lava lake of Erebus volcano, Antarctica, *Bull.
Disas. Prev. Res. Inst. Kyoto Univ., 38,* 147–161, 1988.

Dibble, R. R., B. O'Brien, and C. A. Rowe, The velocity struc-
ture of Mount Erebus, Antarctica, and its lava lake, this vol-
ume.

Kaminuma, K., Seismic activity of Erebus volcano,
Antarctica, *Pure Appl. Geophys., 125,* 993–1008, 1987.

Kaminuma, K., and T. Haneda, Icequakes around Syowa
Station, Antarctica (in Japanese), *Antarct. Rec., 65,*
135–148, 1979.

Kaminuma, K., and K. Murakami, Seismic activity of Mount
Erebus in 1987, Proceedings of the NIPR Symposium,
Antarct. Geosci., 3, 13–19, 1989.

Kaminuma, K., and K. Shibuya, The structure and seismic
activity of Mount Erebus, Ross Island, in *Geological
Evolution of Antarctica,* edited by M. R. A. Thomson, J. A.
Crame, and J. W. Thomson, pp. 329–333, Cambridge
University Press, New York, 1991.

Kaminuma, K., K. Shibuya, and K. Niida, Geophysical studies
on Mount Erebus, *Antarct. J. U. S., 20(5),* 28–30, 1985a.

Kaminuma, K., S. Ueki, and J. Kienle, Volcanic earthquake
swarms at Mt. Erebus, Antarctica, *Tectonophysics, 114,*
357–369, 1985b.

Kaminuma, K., M. Baba, K. Shibuya, and R. R. Dibble,
Explosion earthquakes of Mount Erebus, Antarctica, *Mem.
Natl. Inst. Polar Res. Spec. Issue Jpn., 37,* 40–47, 1985c.

Kaminuma, K., M. Baba, and S. Ueki, Earthquake swarms on
Mount Erebus, Antarctica, *J. Geodyn., 6,* 391–404, 1986.

Kaminuma, K., J. Amino, and S. Miura, Seismic activity of
Mount Erebus in 1984–1985, Proceedings of the NIPR
Symposium, *Antarct. Geosci., 1,* 1–5, 1987.

Kaminuma, K., S. Miura, and R. R. Dibble, A process of
Mount Erebus eruption, Proceedings of the NIPR
Symposium, *Antarct. Geosci., 2,* 7–16, 1988.

Kienle, J., P. R. Kyle, S. Estes, T. Takanami, and R. R.
Dibble, Seismicity of Mount Erebus 1980–1981, *Antarct. J.
U. S., 16(5),* 35–36, 1981.

Kienle, J., D. L. Marshall, S. A. Estes, R. R. Dibble, K.
Shibuya, and P. R. Kyle, Seismicity of Mount Erebus
1981–1982, *Antarct. J. U. S., 17(5),* 29–31, 1982.

Kienle, J., K. Kaminuma, and R. R. Dibble, Seismicity of
Mount Erebus and vicinity, 1983–1984. *Antarct. J. U. S.,
19(5),* 25–27, 1984.

Kyle, P. R., Volcanic activity of Mount Erebus, 1984–1986,
Antarct. J. U. S., 21(5), 7–8, 1986.

Kyle, P. R., R. R. Dibble, W. F. Giggenbach, and J. Keys,
Volcanic activity associated with the anorthoclase phonolite
lava lake, Mount Erebus, Antarctica, in *Antarctic
Geoscience,* edited by C. Craddock, pp. 735–745,
University of Wisconsin Press, Madison, 1982.

Rowe, C. A., Seismic velocity structure and seismicity of
Mount Erebus Volcano, Ross Island, Antarctica, M.S. the-
sis, 156 pp., Univ. of Alas., Fairbanks, 1988.

Shibuya, K., M. Baba, J. Kienle, R. R. Dibble, and P. R. Kyle,
A study of the seismic and volcanic activity of Mount
Erebus, Antarctica, 1981–82, *Mem. Natl. Inst. Polar Res.
Spec. Issue Jpn., 28,* 54–55, 1983.

Takanami, T., J. Kienle, P. R. Kyle, R. R. Dibble, K.
Kaminuma, and K. Shibuya, Seismological observation on
Mount Erebus, 1980–1981, in *Antarctic Earth Science,* edit-
ed by R. L. Oliver, P. R. James, and J. B. Jago, pp.
671–674, Australian Acadamy of Science, Canberra, 1983.

Ueki, S., K. Kaminuma, M. Baba, E. Koyama, and J. Kienle,
Seismic activity of Mount Erebus, Antarctica, in
1982–1983, *Mem. Natl. Inst. Polar Res. Spec. Issue Jpn.,
33,* 29–40, 1984.

K. Kaminuma, National Institute of Polar Research, 9-10,
Kaga 1-chome, Itabashi-ku, Tokyo 173, Japan.

MONITORING MOUNT EREBUS BY SATELLITE REMOTE SENSING

D. A. Rothery and C. Oppenheimer

Department of Earth Sciences, The Open University, Milton Keynes, England

The harsh conditions at Mount Erebus make remote sensing an attractive means to help monitor its activity. Here we review previous attempts to determine conditions at the active vent of Mount Erebus by satellite-based infrared techniques using data of both high and low spatial resolution. Either resolution can reveal the presence of hot material exposed at the surface. By using the high-resolution data, it is possible to estimate the sizes and temperatures of the hot areas. Uncertainties are considerable, but they will be less for future generations of satellite instruments.

INTRODUCTION

An active lava lake of phonolitic composition was first observed at Mount Erebus in 1972 [*Giggenbach et al.*, 1973] and was present at the time of all reported observations until 1984. The maximum recorded diameter of the lake during this period was 60 m, but by October 1984 it had become buried by strombolian ejecta. Continued strombolian activity led to the reopening of vents and the exhumation of the former lake surface upon which one or more lakes up to about 20 m across have been present in all observations since December 1985.

Quite apart from their unusual geochemistry, Mount Erebus's long-lived lava lakes deserve monitoring because they represent an extremely rare phenomenon. Other sites where active lava lakes have persisted to a comparable extent are very few, notably Erta 'Ale, Ethiopia [e.g., *Le Guern et al.*, 1979], Nyiragongo, Zaire [e.g., *Tazieff*, 1984], Kilauea, Hawaii [e.g., *Tilling*, 1987; *Wolfe et al.*, 1987], and Masaya, Nicaragua [e.g., *Stoiber et al.*, 1986].

Direct visual observations of conditions within the summit crater of Mount Erebus have so far proved feasible only at intervals during the short Antarctic field season (usually restricted to the period October-January). These have been supplemented with recordings made by video cameras located on the crater rim [*Dibble*, 1989] and year-round seismic data that can be related to summit activity [*Kaminuma*, this volume]. Remote sensing from satellites is an additional tool that may become increasingly important because it offers the potential to monitor the thermal structure of Mount Erebus's lava lakes, vents, and fumaroles frequently and throughout the year, though only when the summit is not obscured by cloud.

MOUNT EREBUS AS A TARGET FOR SATELLITE REMOTE SENSING

Remote-sensing satellites are usually placed in polar orbits that take them to within about 10° of the poles. At the high southern latitude of Mount Erebus, adjacent orbital tracks converge markedly, and this increases the frequency at which the volcano falls within the image swath. For example, the conventionally quoted repeat time for coverage by a Landsat satellite is 16 days. However, this applies only near the equator, and in fact, Mount Erebus falls within the image swath nine times during the 16-day repeat cycle. Satellites recording at lower spatial resolutions but with broader imaging swaths, such as the National Oceanic and Atmospheric Administration (NOAA) polar orbiters, which give twice daily coverage near the equator, can cover Mount Erebus several times each day.

There are essentially two approaches to remote sensing of a high-temperature target such as Mount Erebus, where material at temperatures of around 1000°C is exposed; these are imaging in the conventional thermal infared region at low spatial resolution and high spatial resolution imaging in the short-wavelength part of the infrared spectrum. Both types of data are provided by satellites currently in orbit; the former is typified by Landsat and the latter by NOAA polar orbiters. We shall

review examples of each of these in turn. Data supplied in photographic form are sometimes adequate to confirm the presence of a high-temperature feature, but the original digital data must be examined, using an image-processing system, to identify anomalies that are spatially small or of low radiant magnitude and to perform the quantitative comparisons between spectral bands that allow temperature, area, and (ideally) heat flux to be estimated.

SHORT-WAVELENGTH INFRARED IMAGING AT HIGH SPATIAL RESOLUTION

The Landsat Thematic Mapper (TM) instrument records images in the short-wavelength infrared and visible region of the spectrum, with square pixels that are 30 m across. It also records a single channel in the longer-wavelength, conventional, thermal infrared, but with larger (lower resolution) pixels that are 120 m across. The ability of the TM's short-wavelength infrared sensors to record thermal radiance from hot volcanic targets was first demonstrated by *Francis and Rothery* [1987]. *Rothery et al.* [1988] went on to elaborate a technique for measuring the sizes and temperatures of the subpixel-sized thermal anomalies responsible for this radiance, and *Glaze et al.* [1989] suggested that such data could be used to estimate the thermal radiant flux emanating from a volcano, thereby offering a constraint on the energetics of the system. Subsequent work [e.g., *Oppenheimer*, 1991a; *Oppenheimer et al.*, 1993a, b] has indicated several limitations to, and uncertainties in, the derivation of radiant flux, but nevertheless, TM data remain a powerful means of detecting molten lava or high-temperature fumaroles and of estimating several thermally related parameters [*Pieri et al.*, 1990; *Oppenheimer and Rothery*, 1991; *Oppenheimer*, 1991b].

Only one example of Landsat TM data showing short-wavelength infrared radiance from Mount Erebus has been documented in the literature. This is an image recorded on January 26, 1985, for which *Rothery et al.* [1988] reported a clear radiant anomaly in the short-wavelength infrared TM bands: band 5 (1.55 to 1.75-μm wavelength) and band 7 (2.08 to 2.35-μm wavelength). There is also a radiant anomaly in the longer-wavelength infrared, TM band 6 (10.4 to 12.5-μm wavelength), within the conventional thermal infrared part of the spectrum. These data are illustrated in Plate 1 and indicate the clarity with which data of this kind can be used to demonstrate the presence of hot material within a summit crater such as that of Mount Erebus.

This image contains a cluster of six pixels that are radiant in band 5 as well as in band 7, surrounded by a halo of two or three pixels (i.e., up to about 90 m wide) that is radiant in band 7 only. For pixels in which both bands 5 and 7 are radiant, the "dual-band" calculation (outlined by *Rothery et al.* [1988]) demonstrates a temperature in the range 900°-1130°C in areas occupying about 0.1-0.2% of each pixel. This would be compatible with a crusted lava lake broken by incandescent cracks, though it predates the first direct observation of the renewed lava lake by 11 months. An alternative interpretation is that the data represent a situation more akin to an incandescent strombolian vent, and we note that situations can exist which can be regarded as transitional between the two types of phenomena, such as at Masaya in 1989 [*Smithsonian Institution*, 1989].

Temperatures that are derived by comparing spectral radiance at different wavelengths in the infrared (as in the dual-band method) are model-dependent. In this case, since we are using Landsat TM data where there are only two short-wavelength spectral bands available, a value has to be assumed for one of the "unknowns" in the dual-band equations. Furthermore, the model works only for surfaces where the temperature distribution within a pixel can be approximated to hot areas at a single temperature surrounded by a background at a lower uniform temperature. This problem may be approached in any of several ways: the background can be assumed to be too cold to be radiant in the short-wavelength infrared [*Rothery et al.*, 1988]; the temperature of either the hot component [*Oppenheimer*, 1991a] or the background material [*Pieri et al.*, 1990] can be assumed; or the dual-band equations can be solved for a range of possible hot component and background temperatures [*Oppenheimer et al.*, 1993a]. Further uncertainties are introduced by instrumental effects such as blurring associated with the sensor point spread functions, possible spatial misregistration between bands, resampling of the data during geometric correction (if any), and wavelength-dependent absorption and scattering of the upwelling radiation by the atmosphere. However, the demonstration that a small fraction of the surface was occupied by material at or near a magmatic temperature remains valid.

The warm halo surrounding the hottest part of the anomaly is more problematic. With only one useful radiance measurement in each pixel (band 7), the temperature of, and fractional area occupied by, the hot material cannot be calculated. However, it can be constrained to lie between a minimum of 240°C if the surface was at a uniform temperature and a maximum of 400°C if the hot material occupied 5% of each pixel, dispersed on a nonradiant (<160°C) background.
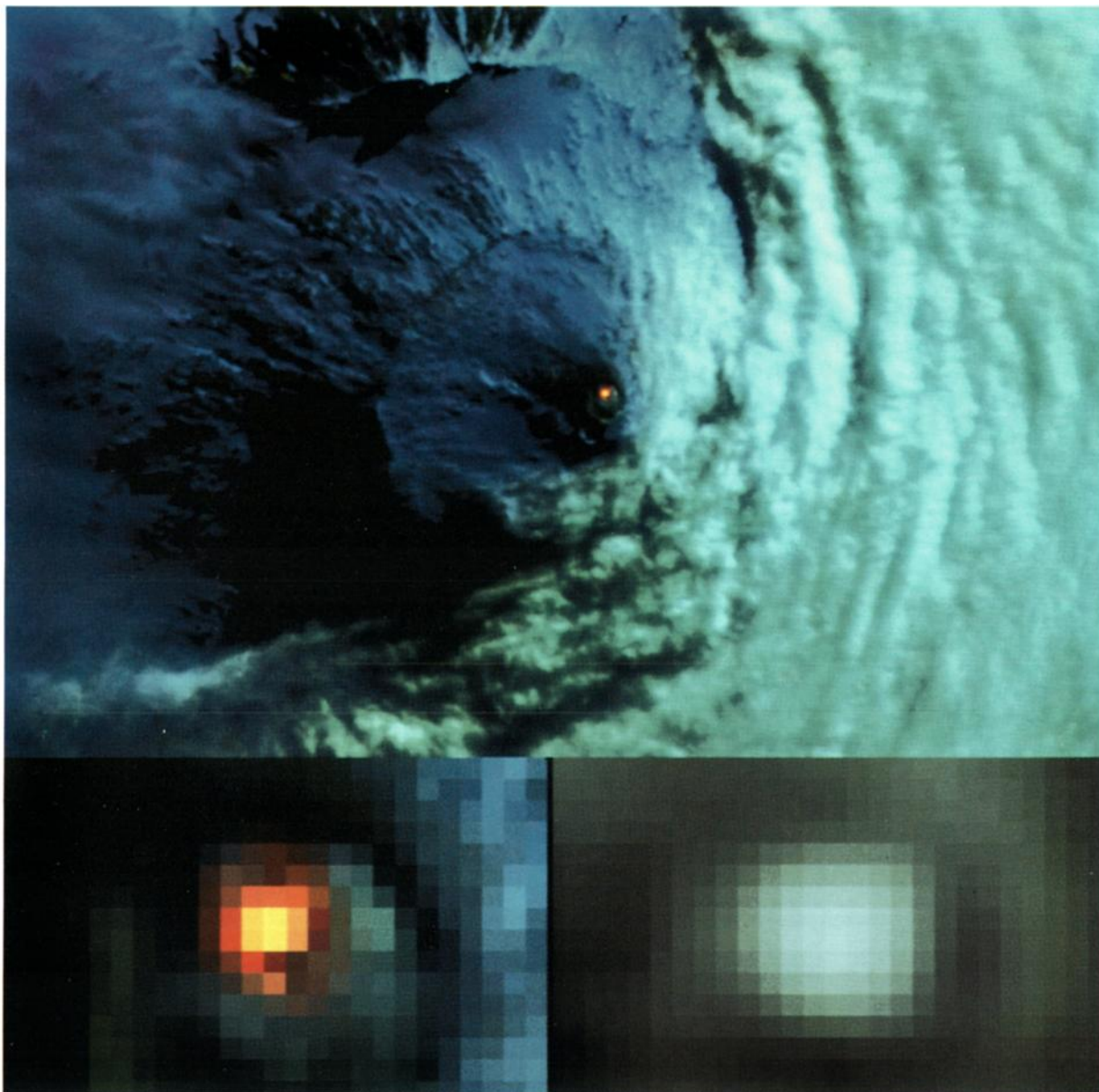
Plate 1. Details from a Landsat TM image of Mount Erebus, acquired on January 26, 1985. The main view is 15 km across and shows TM bands 7, 5, and 4 in red, green, and blue, respectively, and an enlargement of the central area is shown in the inset at the bottom left in which the 30-m by 30-m pixels can be distinguished. This combination of bands shows clouds as white and snow as blue, whereas the hottest areas, radiating thermally in bands 7 and 5, appear yellow, and less hot areas, radiating thermally in band 7 only, appear red. The inset at the bottom right shows the same area as the adjacent inset in band 6 only; there is less detail because this channel is recorded with 120-m by 120-m pixels, which have been resampled to 30 m by 30 m.

Rothery et al. [1988] suggested that this situation could be accounted for by recently erupted tephra, citing a seismic event at 1951:56 UT (5 min before the image was recorded) as evidence. Workers who are familiar with the normal conditions on Mount Erebus have cast doubt on the validity of this argument (e.g., P. R. Kyle, personal communication, 1989), and our own continued TM observations of other hot volcanoes show that it is common for a radiant anomaly to appear blurred in this manner, possibly as a result of forward scattering of radiation by the atmosphere or cross-sensor contamination.

Despite the uncertainty over how far the spectral radiances recorded in each pixel can be relied on to give a correct interpretation of the exact cause of a volcanic thermal anomaly, these data are certainly adequate to demonstrate the presence of incandescence in Mount Erebus's vent area, at a time when the only other information comes from seismic events. Short-wavelength infrared observations such as these could be made frequently for year-round monitoring. *Rothery and Oppenheimer* [1991] and *Oppenheimer et al.* [1993a] have demonstrated that such observations can be carried out successfully at night, with distinct advantages over the daytime data for estimating temperatures. Other works have described forthcoming satellite platforms more suitable for this kind of study than Landsat and the techniques that could be used to take advantage of them [*Mouginis-Mark et al.*, 1989, 1991; *Oppenheimer and Rothery*, 1991; *Rothery and Pieri*, 1993].

THERMAL INFRARED IMAGING AT LOW SPATIAL RESOLUTION

At present it is possible to monitor a target such as Mount Erebus more frequently and more cheaply using image data of low spatial resolution recorded by meteorological satellites, such as the NOAA polar orbiters that are equipped with a sensor system known as the Advanced Very High Resolution Radiometer (AVHRR). The resolution of the AVHRR is high only in a meteorological context, the pixels being 1.1 km across at nadir and considerably wider than this near the edges of each image swath. At this order of spatial resolution the short-wavelength infrared part of the spectrum becomes ineffective for detecting all but the largest volcanic thermal anomalies. However, many phenomena remain detectable at longer wavelengths, lying in the conventional thermal infrared part of the spectrum (wavelength greater than 3 μm).

The only account of satellite thermal infrared obser-

vations of Mount Erebus that we are aware of is that of *Wiesnet and D'Aguanno* [1982], who showed that the 3- to 5-μm AVHRR channel showed a thermal anomaly coincident with the summit. *Oppenheimer* [1989, 1991b] reexamined the image data that they used (Figure 1), in an attempt to see if the dual-band technique combining this channel with the 10.5- to 11.5-μm channel could be used to derive an estimate of the temperature at the center of the anomaly and of the total thermal radiant flux. Unfortunately, this does not appear to be realistic, because of physical problems (a uniform background temperature cannot be assumed) and sensor-related problems (streaking out of the anomaly along a scan line and bleeding of the anomaly between scan lines).

However, the ability of low-resolution satellite platforms to simply confirm the continuation of a thermal anomaly, such as that on Mount Erebus outside the active field season, is something that ought not to be overlooked, especially in view of the ready availability of such data, which could be received by direct transmission using equipment at McMurdo Sound or Scott Base. Some of the options for using meteorological satellites for volcano monitoring are reviewed by *Rothery* [1992].

OTHER USES OF SATELLITE DATA

It is expected that satellite data will become more abundant and more readily available in the future, as will the workstations and personal skills required to take advantage of them. Among the other potential contributions of satellite data for studies of Mount Erebus are mapping the distribution of newly erupted products by visible or near-infrared imaging, tracking eruption plumes by visible or thermal imaging, monitoring the SO_2 flux by ultraviolet atmospheric sounding, and measuring deformation by lidar altimetry or radar altimetry and interferometry. References to these techniques may be found in the work of *Mouginis-Mark et al.* [1989, 1991], *Rothery* [1992], and *Rothery and Pieri* [1993].

Fig. 1. (Opposite) The lava lake (arrow) on Mount Erebus detected as a hot thermal anomaly (dark in this rendering) on NOAA polar orbiter AVHRR images. The pixels on this image represent areas slightly more than 1 km across at (*a*) 1632 UT on January 13, 1980, and (*b*) 1808 UT on October 10, 1980.
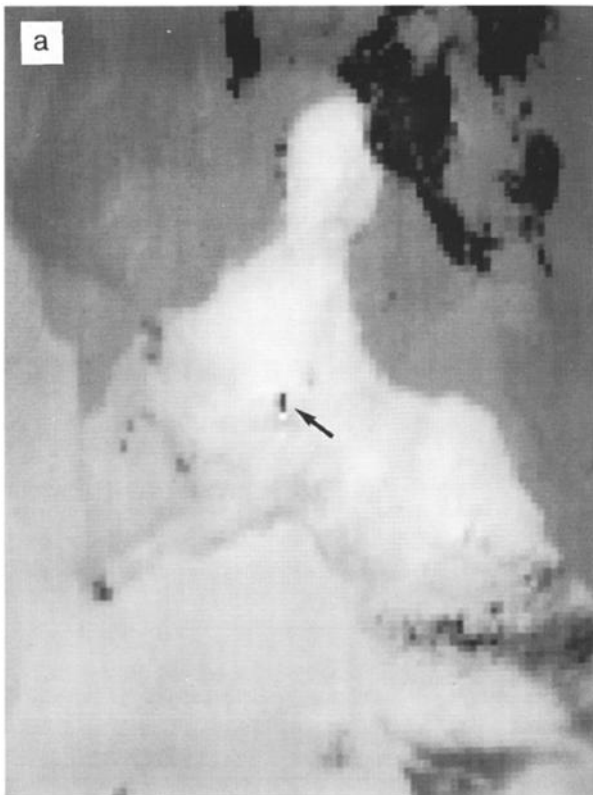
CONCLUSIONS

Satellite remote sensing has so far played only a minor role in volcanological studies of Mount Erebus. It has demonstrated the presence of exposed hot material within the summit crater at times when there were no other observations and has provided a crude estimate of the temperature of the active lava. However, as techniques improve, remote sensing will become a more highly valued volcanological tool. Except for the use of radar, remote sensing can be carried out only when the area of interest is clear of clouds. This difficulty is somewhat eased by the increased frequency at which a polar-orbiting satellite can image a high-latitude target such as Mount Erebus.

REFERENCES

Dibble, R. R., Infrasonic records of strombolian eruptions of Erebus, Antarctica March-December 1984, covering the jump in activity on 13 September 1984, in *Volcanic Hazards*, edited by J. H. Latter, pp. 536–553, Springer-Verlag, New York, 1989.

Francis, P. W., and D. A. Rothery, Using the Landsat thematic mapper to detect and monitor active volcanoes, *Geology*, *15*, 614–617, 1987.

Giggenbach, W. F., P. R. Kyle, and G. L. Lyon, Present volcanic activity on Mt Erebus, Ross Island, Antarctica, *Geology*, *1*, 135–136, 1973.

Glaze, L. S., P. W. Francis, and D. A. Rothery, Measuring thermal budgets of active volcanoes by satellite remote sensing, *Nature*, *338*, 144–146, 1989.

Kaminuma, K., The seismic activity of Mount Erebus in 1981–1990, this volume.

Le Guern, F., J. Carbonelle, and H. Tazieff, Erta 'Ale lava lake: Heat and gas transfer to the atmosphere, *J. Volcanol. Geotherm. Res.*, *6*, 27–48, 1979.

Mouginis-Mark, P. J., D. C. Pieri, P. W. Francis, L. Wilson, S. Self, W. I. Rose, and C. A. Wood, Remote sensing of volcanos and volcanic terrains, *Eos Trans. AGU*, *70*(52), 1567–1575, 1989.

Mouginis-Mark, P. J., S. Rowland, P. Francis, T. Freidman, H. Garbeil, J. Gradie, S. Self, L. Wilson, J. Crisp, L. Glaze, K. Jones, A. Kahle, D. Pieri, H. Zebker, A. Kreuger, L. Walter, C. Wood, W. Rose, J. Adams, and R. Wolf, Analysis of active volcanoes from the Earth Observing System, *Remote Sens. Environ.*, *36*, 1–12, 1991.

Oppenheimer, C., AVHRR volcano hotspot monitoring, paper presented at 4th AVHRR Data Users' Meeting, EUMET-SAT, Rothenburg, Germany, Sept. 5–8, 1989.

Oppenheimer, C., Lava flow cooling estimated from Landsat thematic mapper data: The Lonquimay eruption (Chile, 1989), *J. Geophys. Res.*, *96*, 21,865–21,878, 1991a.

Oppenheimer, C., Volcanology from space: Applications of infrared remote sensing, Ph.D. thesis, 230 pp., Open Univ.,

Milton Keynes, England, 1991*b*.

Oppenheimer, C., and D. A. Rothery, Infrared monitoring of volcanoes by satellite, *J. Geol. Soc. London*, *148*, 563–569, 1991.

Oppenheimer, C., P. W. Francis, D. A. Rothery, R. W. Carlton, and L. S. Glaze, Infrared image analysis of volcanic thermal features: Láscar Volcano, Chile, 1984–1992, *J. Geophys. Res.*, *98*, 4269–4286, 1993*a*.

Oppenheimer, C., D. A. Rothery, and P. W. Francis, Thermal distributions at fumarole fields: Implications for infrared remote sensing of active volcanoes, *J. Volcanol. Geotherm. Res.*, *55*, 97–115, 1993*b*.

Pieri, D. C., L. S. Glaze, and M. J. Abrams, Thermal radiance observations of an active lava flow during the June 1984 eruption of Mount Etna, *Geology*, *18*, 1018–1022, 1990.

Rothery, D. A., Monitoring and warning of volcanic eruptions by remote sensing, in *Geohazards—Natural and Man-Made*, edited by G. J. H. McCall, D. J. Laming, and S. Scott, pp. 25–32, Chapman and Hall, London, 1992.

Rothery, D. A., and C. Oppenheimer, Monitoring volcanoes using short wavelength infrared images, in Proceedings of the 5th International Colloquium on Physical Measurements and Signatures in Remote Sensing, *Rep. SP-319*, pp. 513–516, Eur. Space Agency, Neuilly, France, 1991.

Rothery, D. A., and D. C. Pieri, Remote sensing of active lava, in *Active Lavas: Monitoring and Modelling*, edited by C. J. Kilburn and G. Luongo, pp. 203–232, University College London Press, London, 1993.

Rothery, D. A., P. W. Francis, and C. A. Wood, Volcano monitoring using short wavelength infrared data from satellites, *J. Geophys. Res.*, *93*, 7993–8008, 1988.

Smithsonian Institution, Masaya [Nicaragua]: Lava lake develops in new collapse crater, *SEAN Bull.*, *14*(2), 8–9, 1989.

Stoiber, R. E., S. N. Williams, and B. J. Huebert, Sulfur and halogen gases at Masaya caldera complex, Nicaragua: Total flux and variations with time, *J. Geophys. Res.*, *91*, 12,215–12,231, 1986.

Tazieff, H., Mt Nyiragongo: Renewed activity of the lava lake, *J. Volcanol. Geotherm. Res.*, *20*, 267–280, 1984.

Tilling, R. I., Fluctuations in surface height of active lava lakes during the 1972–1974 Mauna Ulu eruption, Kilauea Volcano, Hawaii, *J. Geophys. Res.*, *92*, 13,721–13,730, 1987.

Wiesnet, D. R., and J. D'Aguanno, Thermal imagery of Mt Erebus from the NOAA-6 satellite, *Antarct. J. U. S.*, *17*, 32–34, 1982.

Wolfe, E. W., M. O. Garcia, D. B. Jackson, R. Y. Koyangi, C. A. Neal, and A. T. Okamura, The Pu'u 'O'o eruption of Kilauea Volcano, episodes 1–20, January 3, 1983, to June 8, 1984, in Volcanism in Hawaii, *U.S. Geol. Surv. Prof. Pap.*, *1350*, 471–508, 1987.

D. A. Rothery, Department of Earth Sciences, The Open University, Milton Keynes MK7 6AA, England.

C. Oppenheimer, Department of Geography, University of Cambridge, Downing Place, Cambridge, CB2 3EN, England.

VOLCANIC DEFORMATION MONITORING ON MOUNT EREBUS: METHODS AND RESULTS OF GEODETIC SURVEYS, 1980–1985

P. M. Otway

Volcanology Programme, Institute of Geological and Nuclear Sciences, Wairakei, New Zealand

G. H. Blick

Earth Deformation Section, Institute of Geological and Nuclear Sciences, Lower Hutt, New Zealand

B. J. Scott

Volcanology Programme, Institute of Geological and Nuclear Sciences, Wairakei, New Zealand

A program to monitor volcanic deformation about the active summit crater of Mount Erebus was conducted from December 1980 to December 1985. Precise triangulation, trilateration, and tilt-leveling surveys were made annually in conjunction with the International Mount Erebus Seismic Studies project. Observed volcanic deformation has been restricted to a relatively minor expansion across the 500-m-wide crater totaling 50 ± 20 mm. Most of this deformation was recorded in 1982 and 1984 coinciding with increased seismic and volcanic activity, respectively. The deformation is interpreted as minor inflation associated with the increased gas and heat flux beneath Main Crater. There was no evidence for a substantial volume change in magma stored at shallow levels or a blockage in the conduit during the monitored period. The geodetic data also suggest a shallow rift system extending southwest from Main Crater through Side and Western craters. Short-term deformation detected during early December 1984 could not be correlated with ongoing eruptive activity. Downhill creep of Camp Flow about the old Erebus hut was monitored, confirming its origin as a glacier rather than a lava flow. The survey techniques and equipment used proved satisfactory in the Antarctic environment, although problems with benchmark instability, thought to be related to the effect of solar or geothermal heat on surface or underlying ice, restricted the effectiveness of the tilt-leveling surveys and resulted in noise levels of about 20 µrad.

INTRODUCTION

Geodetic surveys were conducted annually from December 1980 to December 1985 in the summit area of Mount Erebus to assess the nature and level of volcanic deformation associated with ongoing volcanic activity. The work, although separately funded, complemented the International Mount Erebus Seismic Studies (IMESS) project. Deformation at active volcanoes can reflect volume changes in stored magma at shallow depths or a buildup of gas due to conduit blockage. A measurement program was introduced at Erebus to help refine volcanological models based on seismological data. Of almost equal importance, the surveys also pro-

vided a unique opportunity to test and refine geodetic monitoring techniques, both at a continuously active volcano and in the extreme environmental conditions of Antarctica.

Horizontal deformation was monitored by triangulation and trilateration of a network established about the active crater (Main Crater) and the portion of the summit to the north and west (Figures 1 and 2a). Vertical deformation was monitored by four small-aperture tilt-leveling patterns (dry tilt arrays) in the same region (Figure 1). Minor surveys were made to assess deformation of the Main Crater floor, possible short-term deformation associated with elevated volcanic activity in 1984, and suspected downhill creep of Camp Flow on
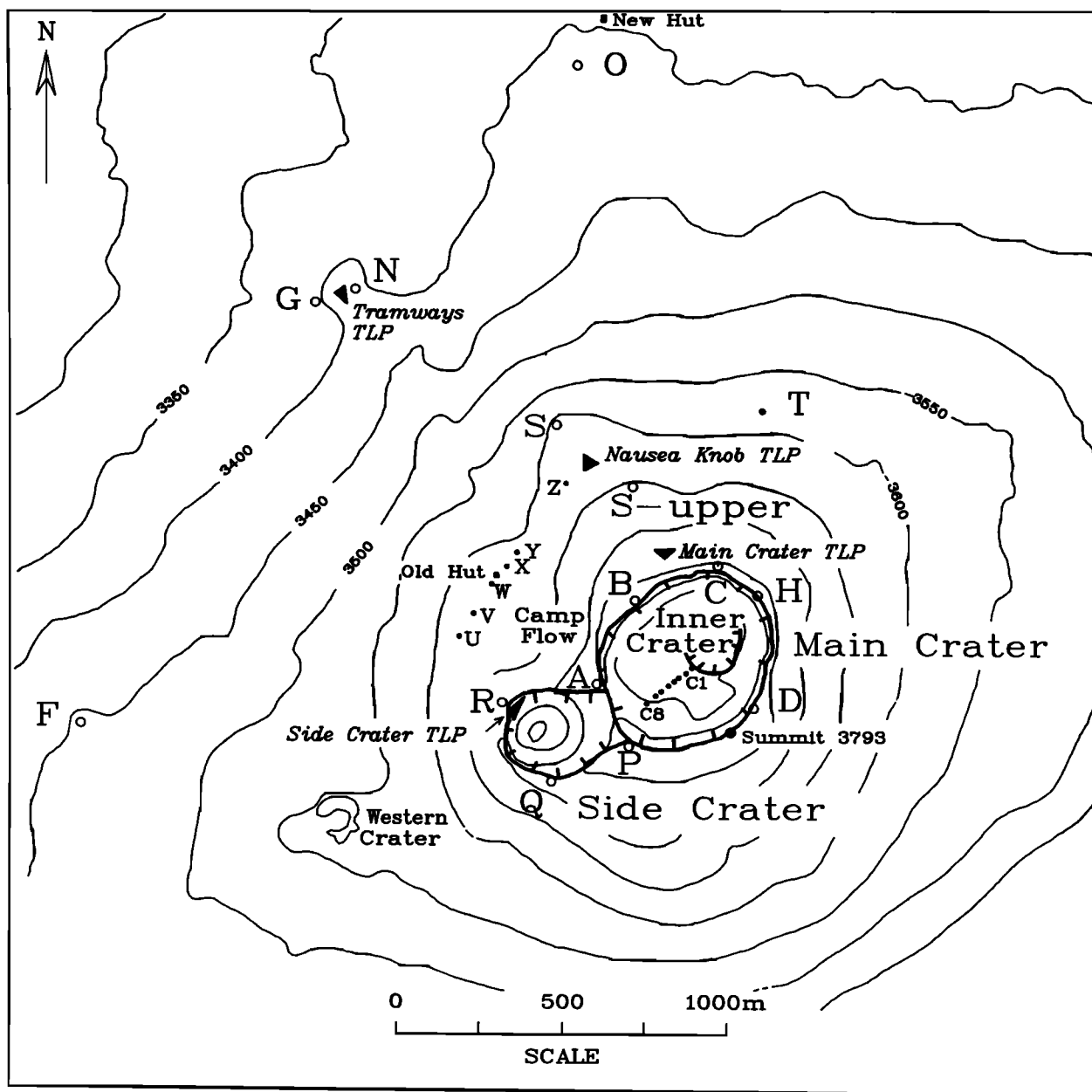
Fig. 1. Mount Erebus summit topography showing the locations of major survey stations (open circles), alignment marks (dots), and tilt-leveling patterns (TLP) (heavy triangles). Contours are in meters above sea level.

which the old Erebus Hut is located (Figure 2b) to determine whether its origin was primarily glacial or volcanic.

SUMMIT MORPHOLOGY AND ACTIVITY

Mount Erebus is an active anorthoclase phonolite stratovolcano of 3794 m elevation. The summit Main Crater is 500–550 m in diameter with a mainly flat floor, 140 m below the crater rim (Figure 1). Situated at the northeastern end is Inner Crater, a subcrater 250 m wide and 100 m deep, that has contained a lava lake since at least December 1972. Strombolian-type eruptions, observed to average more than three per day, have occurred from the lava lake and surrounding vents since 1974 [*Giggenbach and Lyon*, 1973; *Kyle and Otway*, 1982; *Kyle et al.*, 1982; *Dibble et al.*, 1984]. Eruptive activity in September-October 1984 was significantly

more explosive than any previously observed, with many eruptions throwing lava bombs up to 500 m from the crater. The presence of similar but older bombs in the ballistic fall field indicates earlier episodes of this style of activity. The 1984 activity buried the lava lake beneath ejecta and modified the topography of Inner Crater [*Kyle*, 1984]. By December 1985 a small lava lake was again visible on the floor of Inner Crater. The alignment of four craters, Inner, Main, Side, and Western (Figure 1), and Tower Ridge, a 500-m-long linear fumarolic feature, suggests the presence of a rift system trending at 060° (east of grid north).

HISTORY AND SCOPE OF SURVEYS

The project was approved by the Ross Dependency Research Committee in 1979 with the understanding that it would be carried out in cooperation with the IMESS project. Surveyors were supplied each season by the New Zealand Geological Survey, Department of Scientific and Industrial Research (now the Institute of Geological and Nuclear Sciences Ltd.) with field assistance from the New Zealand Antarctic Research Program (NZARP). The survey team benefited from sharing the logistics with IMESS.

The original ground marks were installed around the rim of Main Crater and the northwestern portion of the summit area in December 1980, and the initial survey was completed by early January 1981. Assistance was provided by members of both the NZARP and the IMESS groups (P. M. Otway, unpublished report on 1980/1981 deformation survey, 1981). The location and description of all survey marks have been recorded [*Blick*, 1986]. Five repeat surveys were made and reported annually in the *New Zealand Volcanological Record 11-15* [*Otway*, 1982, 1984, 1985; *Scott and Otway*, 1987; *Blick*, 1987], and the results were summarized and discussed by *Blick et al.* [1989]. The fifth survey commenced 2 months after enhanced eruptive activity began in September-October 1984 [*Kaminuma and Dibble*, 1990] and provided a rare opportunity to test the monitoring techniques and examine the data for correlation of deformation with volcanic activity [*Scott and Otway*, 1985]. The final survey of the series was made in 1985 [*Blick and Williams*, 1986]. It is hoped that further surveys can be conducted to define any long-term trends.

DESCRIPTION OF SURVEYS

The main components of the surveys were as follows: (1) The horizontal deformation of the summit area was monitored by a network centered on the rim of Main Crater connected to stations to the northwest (Figure 2*a*). The network was strengthened and extended to include Side Crater and the Nausea Knob area in 1984. (2) The vertical deformation of the summit area was monitored by three tilt-leveling patterns to the northwest aligned radially to Main Crater and by one to the southwest on Side Crater (Figure 1). (3) The horizontal and vertical deformation of Main Crater floor were monitored from 1981 to 1983 by an eight-marker alignment before it was destroyed by the 1984 activity (Figure 2*b*). (4) The short-term deformation was monitored during the declining activity in December 1984 by repeat electronic distance measurements (EDM) of four lines on the outer slopes of Main Crater (Figure 2*b*). (5) A survey was conducted to determine whether the area known as Camp Flow is a lava flow or an active glacier. It was monitored by an alignment of six stations near the old Erebus Hut from 1980 to 1985 (Figure 2*b*).

Horizontal Deformation Surveys

This aspect of the project was given maximum priority, being regarded as the technique most likely to detect surface deformation related to pressure changes in a shallow magma or gas source. Four survey stations (A, B, C, and D) were initially installed on Main Crater rim within approximately 200 m of the lava lake (Figure 2*a*). Station H was installed in 1981 but survived for only three surveys before falling victim to lava bombs in 1984. The crater rim stations were connected to stations F and G, 1.5 km to the west and northwest to provide a reference scale away from the active crater. The enhanced activity in 1984 necessitated a major modification to the network due to the risk of working on the crater rim and the need to extend the network, particularly across Side Crater. This modification served the dual purpose of expanding coverage in case of extensive eruptive activity and further examining deformation associated with the rift system suggested by *Scott and Currie* [1984]. Stations N, O, and S were added beyond Nausea Knob to compensate for the lack of observations at stations B, C, and D, located on the crater rim. Stations P, Q, and R were added to Side Crater.

Each survey mark consists of 12-mm-diameter reinforcing steel rod ("rebar") 1.5 m long, driven to about 1 m depth or refusal, leaving 0.5 m above ground level and surrounded by a small cairn of rocks. The mark was secured in place by "Antarctic cement," warm water applied liberally. This quickly becomes permanently frozen by the low air temperature, which never exceeds about −15°C. Marks installed prior to 1984 were fitted
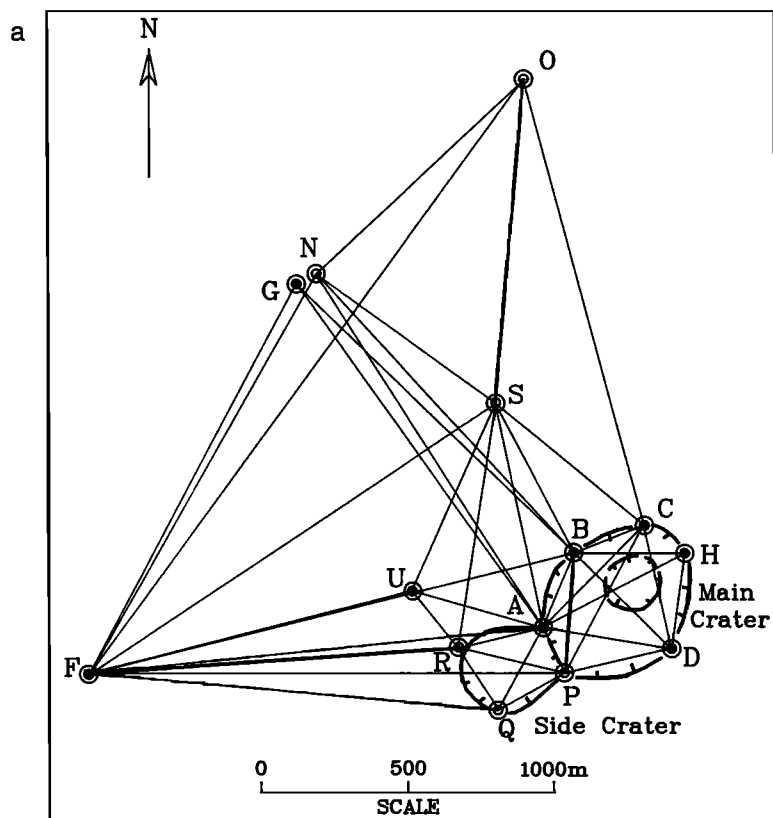
Fig. 2. Mount Erebus summit horizontal deformation monitoring networks. (a) Stations A–H and U (double circles with solid centers) were installed in 1980 and 1981, and stations N–S (open centers) were installed in 1984. Not all rays were observed during each survey. (b) The map shows minor monitoring patterns. Minor or alignment marks are shown as circles (solid prior to 1982; otherwise open) and commonly observed rays. Major stations are as for Figure 2a (Main Crater network is shown in the inset).

with a 19-mm-diameter sleeve to provide a sighting target. Subsequently, marks were modified and had a 5/8-inch stainless steel Whitworth thread attached to the top to enable forced centering of the EDM reflectors. The stability of each mark was assessed during each survey by measuring to two reference marks (30-cm-long rods driven in flush with the ground) approximately at right angles, 3 to 5 m away. These precautions paid off during the 1984 survey when marks A, B, and C were found to be damaged by lava bomb strikes. All were easily reestablished relative to the reference marks. Any small remaining displacements were computed and applied as eccentric corrections.

The first four surveys were made solely by triangulation using line F–G as a baseline to control scale (Figure 2a). This line was measured in 1981 using EDM equipment borrowed from a team carrying out mapping control. The 1984 and 1985 surveys were strengthened by

EDM measurement of all lines, in addition to the direction observations, made possible by the acquisition of new EDM equipment. Vertical angles were observed to determine station heights in order to reduce measured distances to the horizontal. All angle observations were made directly to the station marks using a Wild T2 theodolite optically plumbed over each station. Six sets of horizontal directions and three sets of vertical angles were recorded. The precision of the horizontal directions was estimated to be 2.5 seconds of arc and, for vertical angles, 5 seconds [Blick and Scott, 1986; Blick and Williams, 1986]. Distance measurements in 1981 were made by Geodimeter 14A and in 1984 and 1985 by Wild DI20 Distomat infrared EDM. Meteorological parameters were measured at each end of the lines to correct for ambient air temperature and pressure. The precision of distance measurements was estimated to be 5 mm ± 3 ppm [Blick and Scott, 1986; Blick and Williams, 1986].
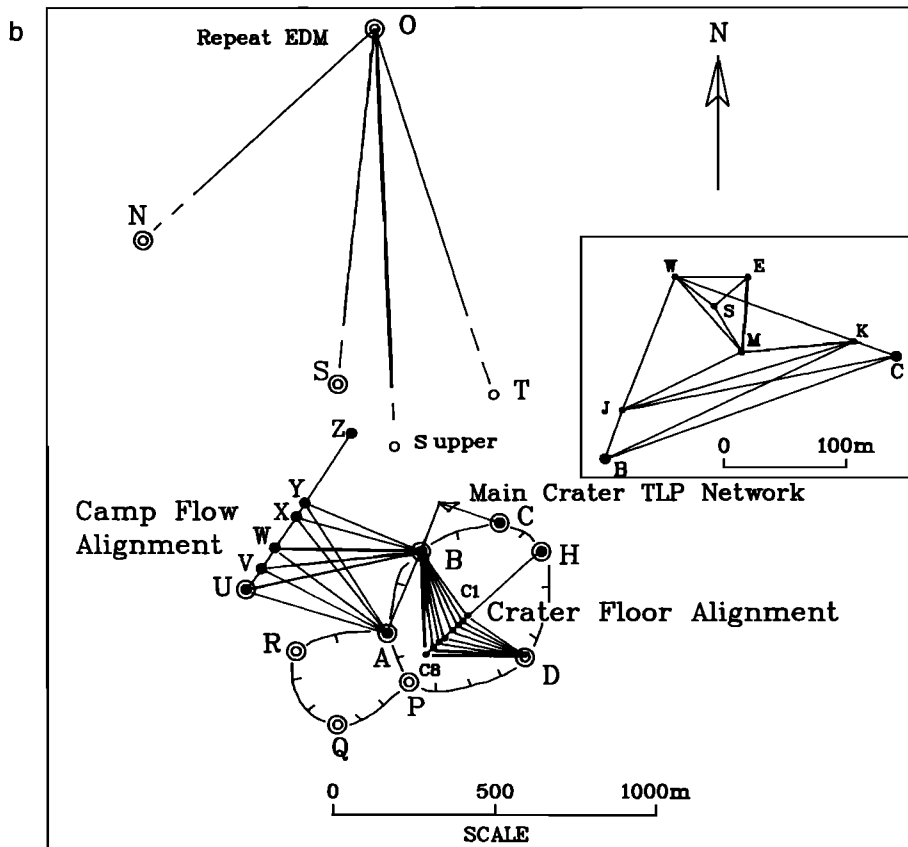
Fig.2. (continued)

Scale in 1981, 1984, and 1985 was provided by distance measurements. The measured distances of F–G showed no significant difference; therefore F–G was held fixed at the 1981 derived length for adjusting the 1982 and 1983 surveys. As direction observations were not completed from F and G during 1980 because of adverse observing conditions, and distances were not measured, the length of A–B was held at the 1981 value when adjusting the initial survey and calculating displacements.

The observed deformation of the summit portion of Erebus can be modeled in different ways. It was first done by studying horizontal displacements around Main Crater. An "intrinsic" displacement solution for stations around Main Crater rim is shown in Figure 3, in which the translation and rotation of the network between surveys is calculated to minimize the sum of squared lengths of the displacement vectors of the stations. Apparent displacements between the Main Crater and the outer stations have been ignored in this model, being generally below the standard error (SE). The SE of the displacements about Main Crater is estimated at ±15 mm. The results indicate displacements between consecutive surveys that are generally less than 20 mm, although cumulative displacements

between December 1981 (the first survey with adequate scale control) and December 1985 range from 20 to 45 mm. This represents extension between opposing stations of 50 ± 20 mm, or a proportional length change of about 100 ppm. Examination of the annual changes shows about 40% of the total extension occurring during 1982 (Figure 3). Most of the remaining extension occurred during 1984, concurrent with increased activity. Further outward movement occurred at station C the following year. The station displacements have also been resolved into the line length changes (with SE) of lines A–B, B–D, and C–D (Figure 4). The computations assumed a fixed baseline A–B between the 1980 and the 1981 surveys. The extension across the crater rim in 1982 and 1984 is interpreted as minor inflation as there was no evidence of station instability.

An alternative technique was to model the deformation by estimating the parameters of a uniform shear strain model. The method of simultaneous adjustment was used to compute the station coordinates and the parameters of a uniform shear strain following the method of *Bibby* [1973, 1982]. The values quoted below are the magnitude of maximum shear strain rate in engi-
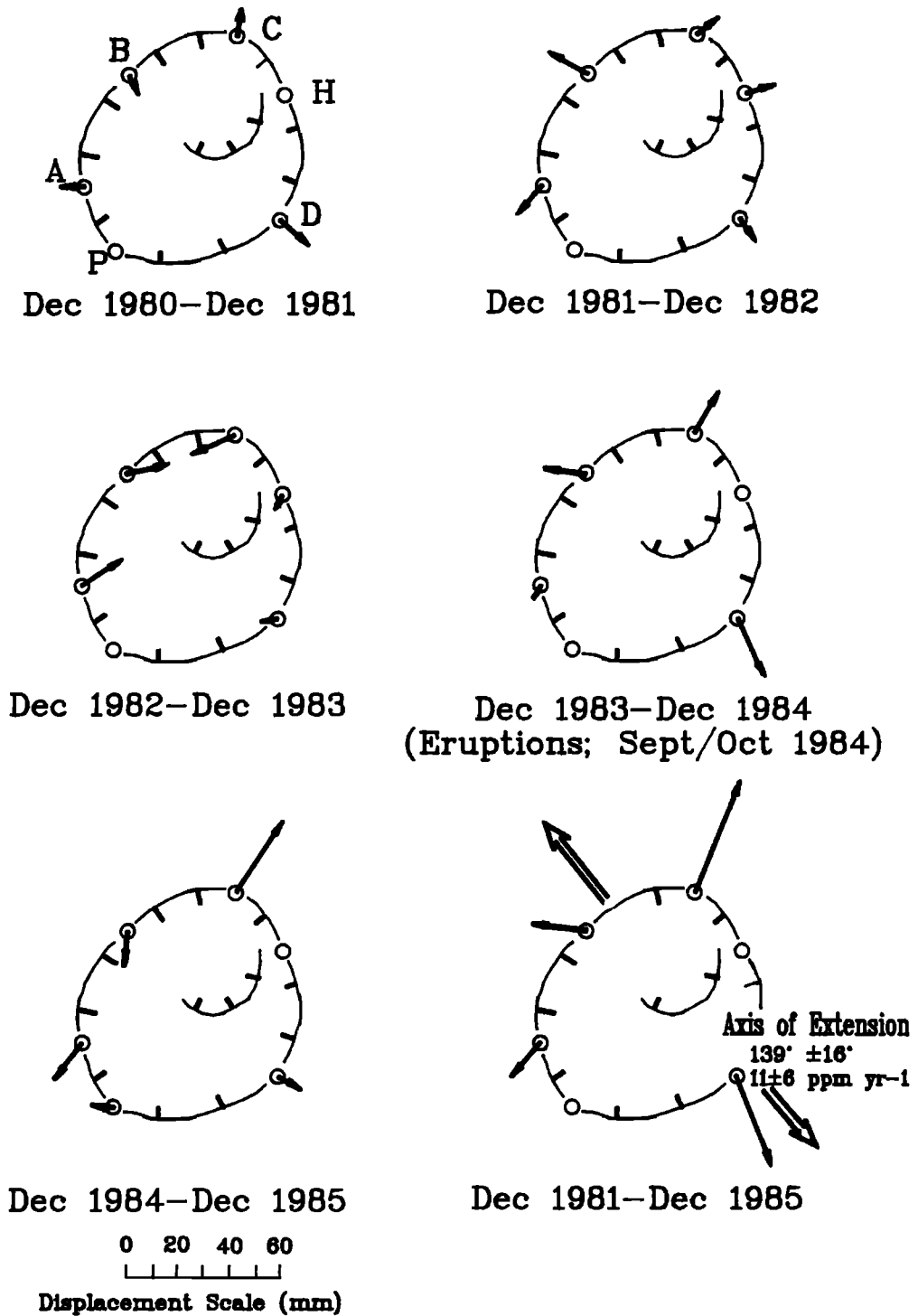
Fig. 3. Time series plots of horizontal displacement vectors in millimeters of the Main Crater rim stations. Standard error on displacements is assessed at ±15 mm.
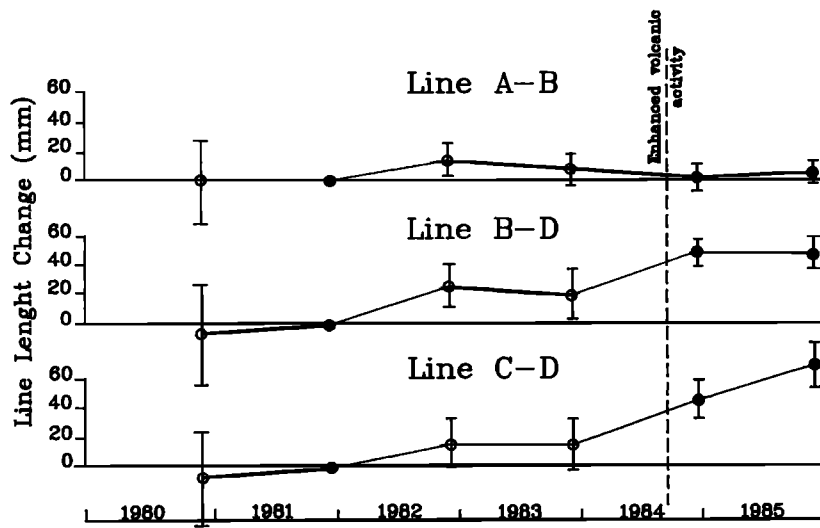
Fig. 4. Line length changes across Main Crater [after *Blick et al.*, 1989]. Results were derived from angle data only in 1980, 1982, and 1983 (open circles) by holding scale on line A–B in 1980 and line F–G in 1982 and 1983. Angle and distance data were used in 1981, 1984, and 1985 (solid circles). The December 1981 survey held as the origin. Bars indicate a single standard error.

neering units and the azimuth of relative extension, each followed by the half width of its 95% confidence interval. Direction observations from all surveys were combined in the adjustment, but as distance data were available only in the 1984 and 1985 surveys, a dilatation value was not computed. The azimuth of maximum relative extension for the whole pattern is computed as 139° ± 16° (east of grid north), and the shear rate is computed as 11 ± 6 ppm yr^{-1}. The azimuth of the extension is thus almost perpendicular to the alignment of Main, Side, and Western craters and the Tower Ridge fumaroles beyond (Figures 1 and 3).

Tilt-Leveling Surveys

Vertical deformation about the summit was monitored by precise leveling of small-aperture tilt-leveling (dry tilt) patterns [*Otway*, 1979, 1986]. Three patterns were located on a northwest trending line radial to Main Crater at distances of 270 m, 600 m, and 1500 m from the lava lake. A fourth pattern was located 600 m toward the southwest (Figure 1). This array of patterns was intended to estimate the approximate plan position and depth of pressure fluctuations within a shallow magma body.

The preferred pattern design is an equilateral triangle with side lengths of 50 m observed from a single instrument position in the center. Only one pattern, Nausea Knob, achieved this configuration. Steep terrain and the

absence of stable rock in suitable locations resulted in the remaining patterns becoming more elongated and thus more susceptible to error on the shortest axis. All benchmarks were installed in pairs (as the main and check benchmarks) in order to assess their stability. The marks generally comprised 12-mm-diameter, 0.9-m-long sections of reinforcing steel, hammered in almost flush with the ground surface and secured with "Antarctic cement." Relative heights within each pattern were observed by a Wild NA2 automatic level, equipped with a parallel plate micrometer, to a hand-held 3-m Invar staff. Triangle closing errors were usually restricted to <0.2 mm over observing distances of up to 50 m. Noise levels induced by leveling errors and benchmark instability have been assessed at 5–10 μrad between surveys, depending on the pattern configuration. These results are slightly worse than results obtained under more favorable conditions in New Zealand [*Otway*, 1979, 1986].

Computed annual tilts from the Nausea Knob and Tramways patterns during the period December 1980 to December 1984 (expressed as vectors in Figure 5) were generally within the assessed noise level. During the same period, Side Crater recorded approximately twice as much annual tilt, but as it was primarily in an east-west direction (the most weakly defined component because of the pattern configuration; see Figure 1), it was also considered to be mainly noise. The 1985 survey recorded approximately double the previous appar-
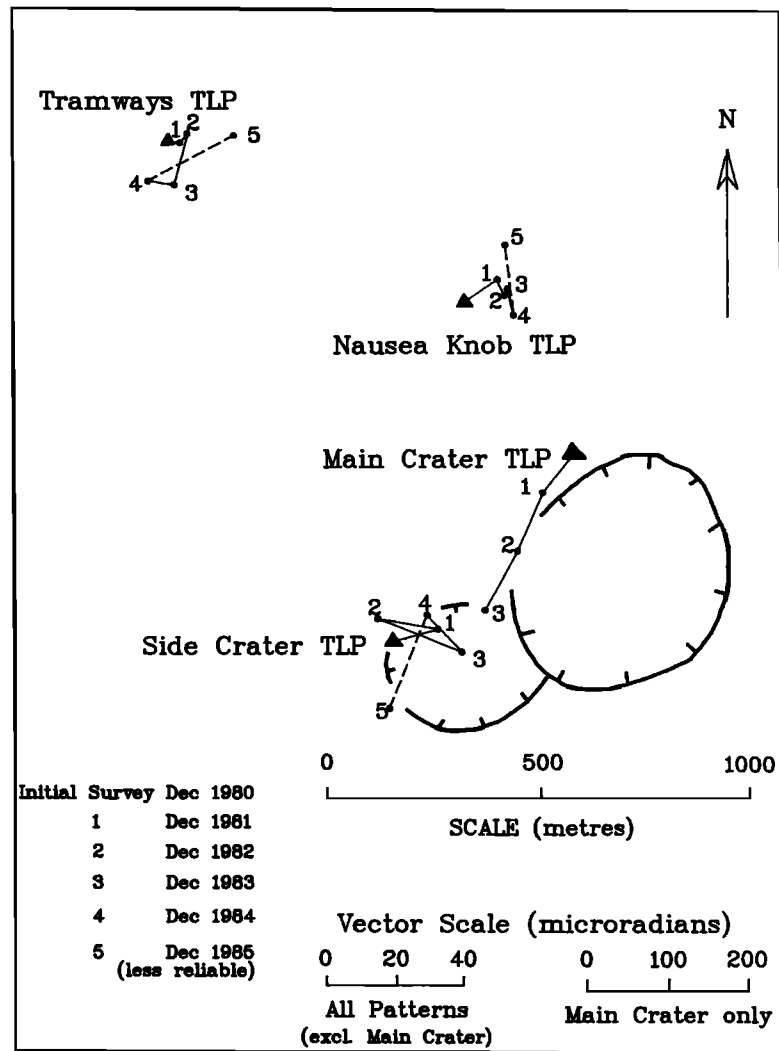
Fig. 5. Wander plots showing apparent (downward) tilt between consecutive surveys. (Note the different scale adopted for the Main Crater tilt-leveling pattern (TLP) and the less reliable result at other patterns for the year to December 1985.) The center of each pattern (solid triangle) is shown in its correct map location.

ent tilt at all three patterns, but a reexamination of the data disclosed unusually large discrepancies (0.4–1.0 mm) between some of the main and check benchmarks, thought to be related to the particularly mild temperatures encountered that summer. The effect of these discrepancies was tested by recomputation of the tilt by excluding the suspect benchmarks. This adjustment was found to substantially reduce the apparent tilt at all patterns in 1985.

Tilt recorded at the Main Crater pattern was by contrast both consistent and large, averaging 145 ± 20 µrad yr⁻¹ at 210° ± 10°, more or less tangential to the lava lake (Figure 5). Bomb strikes and ongoing activity in 1984 rendered this pattern unusable. Measurement between the three main benchmarks and their check marks indicated relatively close agreement with discrepancies of up to 0.5 mm, compared with the total annual changes of about 5 mm across the pattern, ruling out benchmark instability as the cause of the high tilt rate. The site itself (a 20° northwest facing slope composed of old ejecta) was checked for downslope movement by installing a network of three temporary stations in December 1982 (Figure 2b) to connect the tilt-leveling pattern to stations B and C on the crater rim. Observa-

tions made in 1982 and 1983 showed no significant change, suggesting that downslope creep was unlikely to be a major factor in such rapid tilt almost perpendicular to the slope. Lack of consistency with any other patterns also eliminated volcanic deformation as a primary cause. It was finally concluded that the tilt observed may have been the effect of geothermal activity in the crater wall on deep underlying ice. Surface cracking near the crater rim, 60 m upslope of the pattern, lends support to this theory.

Despite precautions the noise levels of all tilt-leveling patterns were higher than expected, indicating stability problems when attempting precise measurements in an area of contrasting ground temperatures and underlying ice. None of the recorded tilts have the characteristics of previously documented volcanic deformation. It is apparent that volcanic deformation in the zone 300–1500 m from the active crater did not exceed the 15- to 20-μrad noise level prior to 1985 or 30 μrad during that year. In a separate exercise to study the feasibility of recording tilt continuously, in December 1982 a pendulum borehole tiltmeter was installed adjacent to station A on Main Crater rim. No satisfactory results were obtained.

Crater Floor Surveys

In December 1981 eight steel (Dexian) marker stakes were installed radial to the lava lake on the floor of Main Crater as an experiment to measure gross deformation close to the lava lake. The markers were placed in line starting 10 m from the edge of Inner Crater and extending southwestward for 190 m (Figure 2b). Each 1.2-m-long stake was hammered into the ground (a mixture of fresh bombs and hard ice) to refusal, leaving 0.2–0.8 m exposed and standing near vertical. Although a high mortality rate through bomb strikes was anticipated, it was also hoped that enough markers would survive to enable an assessment of any deformation. Theodolite observations from B, H, and D located the markers to within about 100 mm horizontally and vertically. When reobserved in November/December 1982, four of the markers were found upright, two were slightly bent and leaning away from the crater, and two were badly bent and lying close to the ground. Observations were made to all markers, sighting to their bases where necessary in an endeavor to determine their true ground positions. The 1983 survey team found little further damage and repeated the observations. By December 1984 all markers had been buried by ejecta, and the project was abandoned.

Computations show that the three markers within 60 m of the rim of Inner Crater behaved in a different fashion from the more distant ones. In December 1982 the closest markers showed horizontal displacements of up to 200 mm generally away from the lava lake while dropping 200-300 mm. In 1983 they showed no significant horizontal displacement (10-60 mm), although they continued to drop a further 90-180 mm. As the large displacements observed in 1982 involved markers damaged during the same period, little reliance can be placed on these results. Hence the lesser displacements observed in 1983 may be a truer indication of the upper limits of deformation. Of the three markers at the far end of the line (all apparently untouched), two show random movements of 100 mm each year, while the third one, 200 m from the crater, shows a consistent 150- to 250-mm southerly movement and a 500-mm drop.

In summary, this experiment indicates that, in 1983 at least, the southwestern crater floor within 60 m of the edge of Inner Crater subsided by up to 180 mm with negligible horizontal movement. Further from the crater the random localized movements are thought to reflect the influence of fumarolic activity on ice underlying the crater floor in that area.

Repeat EDM Observations for Short-Term Deformation in 1984

An experimental scheme was operated from November 28 to December 8, 1984, to test for possible short-term deformation occurring over intervals of several hours to several days associated with the ongoing enhanced strombolian eruptions. Station O was adopted as the instrument base station from which frequent EDM observations were made to stations N, S, S upper, and T, 1000–1300 m away on the northwestern slopes of Main Crater (Figure 2b). Reflectors were left set up to alleviate unnecessary traveling. Eight measurement sessions lasting up to 17 min were made. The first session took place on November 28, with another one on December 3, four on December 7 (spanning 6 hours), and two on December 8. A log of significant eruptions seen or heard was kept from November 24 to December 8 to facilitate a comparison between activity and any observed deformation [Blick and Scott, 1986]. Although a number of apparently large explosive events were seen or heard, infrasonic recordings [Dibble, 1989] later revealed that acoustic energy release during this period had declined dramatically since October.

Distances measured from O to T (radial to the crater) decreased by 5 mm between November 28 and 1330 hours on December 7. The distance to S upper (also radial) decreased by 18 mm, with most of this decrease occurring December 3 to 7. Distances to N (tangential to the crater and therefore less likely to be affected by inflation or deflation) showed no more than 3 mm change. (S was not installed until December 7.) By comparison, the frequent measurements from 1330 hours on December 7 to the end of the observations at 2020 hours on December 8 recorded changes on all four lines (O to N, S, S upper, and T) averaging only 5 mm, independent of time. The estimated error on EDM lines of this length, assuming meteorological observations are made at both ends, is normally about 8 mm. Only two observations (both to S upper) out of a total of 29 exceeded this value and must therefore be regarded with caution, especially as none of the reflector stations were manned, resulting in incomplete meteorological data.

In summary, the results indicate little evidence of consistent deformation during the 11-day experiment. The changes of about 5 mm observed on most lines over the first 9 days are at about the normal instrumental error level while meteorological inconsistencies could be the source of the larger changes on the line to S upper. If deformation was occurring, therefore, it remained below the detection level of about 8 mm, i.e., 8 ppm.

Camp Flow Alignment Survey

This survey was initiated to help determine the true nature of the gently sloping area known as Camp Flow in the vicinity of the old Erebus Hut (Figure 1). Superficially, it has the characteristics of a lava flow, although the presence of small but active crevasses suggested the "flow" might be a small glacier with a surface coating of lava bombs. To try and resolve this ambiguity and monitor any movement, an alignment of five survey marks was installed in December 1980. A corner of the hut roof was adopted as an additional point. Theodolite observations, usually comprising one or two sets of horizontal and vertical angles, were made in 1980–1983 from A, B, U, and Z (Figure 2b). In 1984 and 1985 only station U was occupied, although EDM measurements were also made to all stations on the alignment.

Mean displacement rates and directions relative to stations A and Z have been computed from the mean annual changes in horizontal directions and vertical angles observed over the total observing period (Figure 6). All points, with the exception of X, exhibit a general northwesterly displacement (mean azimuth of 325 ± 10°) at a mean rate of 21 ± 7 mm yr^{-1} and a vertical rate

of -20 ± 7 mm yr^{-1}. Station X displays 70 mm yr^{-1} in a southwesterly direction, subsiding at 170 mm yr^{-1}, and was clearly affected by its close proximity to a northeast-southwest fracture associated with Camp Cave ice towers and caves, an area of geothermal activity and subsiding ice to the southeast. In conclusion, the general northwesterly downslope movement strongly supports the theory that Camp Flow is an active, although slow moving, glacier probably influenced by the geothermal activity on its upper side.

DISCUSSION

In general, the survey procedures and equipment used performed well and produced acceptably precise results, despite the temperatures (down to -30°C) producing uncomfortable observing conditions. The equipment was sometimes operated below the manufacturer's recommended temperature range, although only minor problems were encountered, such as the theodolite becoming stiff to operate and difficult to keep level because of spirit bubble instability in the temperature extremes, or the requirement that the EDM battery be kept warm.

The pattern design proved satisfactory and allowed for the modifications imposed by the 1984 eruptions. Station mark design, particularly the threaded top to accept EDM reflectors and the nearby reference marks to check stability, was successful. The only problem was in the benchmarks adopted for the tilt-leveling patterns, where stability of <0.5 mm is important because of the short (50 m) baseline lengths. In retrospect the effect of surface freeze and thaw may not have been fully appreciated. To minimize this problem in future surveys under similar circumstances, a more reliable method for isolating the marks from any near-surface effect may need to be found. Alternatively, the patterns should be expanded, or even joined to form an integrated leveling network, but this would require considerably more effort for only a slight return. In summary, the methods adopted for Mount Erebus are recommended for use on similar volcanoes elsewhere, with the provision that attention be paid to developing the most appropriate form of benchmark design for the local conditions.

Any significant volcanic deformation appears to have been confined to Main Crater. The most reliable record of deformation comes from the small network of crater rim stations (A, B, C, and D) that survived the whole period, demonstrating a total 50 ± 20 mm extension of the crater rim (representing a proportional change in the crater diameter of about 100 ppm). The crater expansion
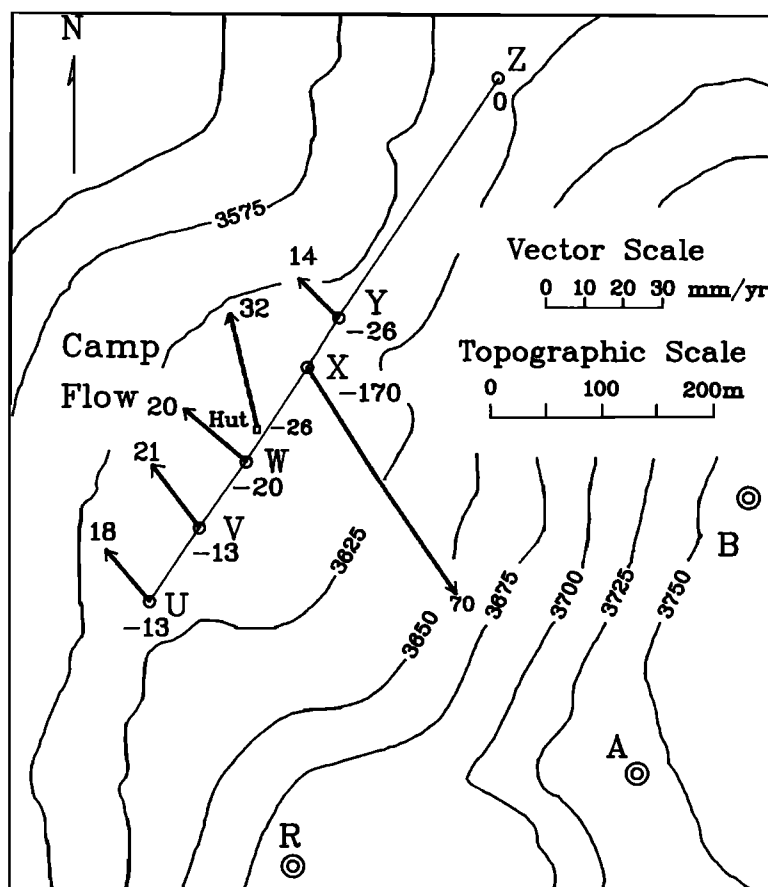
Fig. 6. Horizontal and vertical displacement rates and directions, Camp Flow alignment, December 1980 to December 1985. Horizontal rates (numbers at ends of vectors) and vertical rates (negative numbers near station symbols) are in millimeters per year relative to stations A, B, and Z. Contours are in meters above sea level.

occurred as two main pulses, the first in 1982 and a larger one in 1984. Maximum relative extension across the whole network occurred along an axis of 139°, approximately perpendicular to the alignment of Main, Side, and Western craters and the Tower Ridge fumaroles (about 245°). No tilt of volcanic significance was detected above the 15- to 30-μrad noise level in the monitored zone west of Main Crater. Results from experimental monitoring of markers on the floor of Main Crater close to the lava lake indicate 90- to 180-mm subsidence in 1983, although horizontal movement probably did not exceed the measurement error of 60 mm. In seeking a link with seismic and volcanic activity, we note that the first period of crater expansion, interpreted as inflation, coincided with a significant increase in the daily count of shallow earthquakes recorded in the latter half of 1982 [Kaminuma and Dibble, 1990]. The second, and greatest, inflation coincided with the enhanced volcanic activity and shallow

seismicity commencing in September 1984 with the possibility that it may have continued into 1985. In terms of the volcanic structure, the fact that relative extension is greatest in a direction almost perpendicular to the alignment of summit volcanic features appears to confirm a link between the intrusion paths and the geological structure of this portion of the volcano, although such a lineation has not been recognized in the seismicity [Kaminuma and Dibble, 1990].

By comparison with inflation and deflation observed to be associated with eruptions at similar shield volcanoes such as Mount Etna and those in Hawaii [Decker, 1986], the inflation recorded at Erebus appears to be both relatively localized about the vent and only weakly correlated with near-surface activity. The absence of more extensive preeruption inflation with no posteruption deflation in 1984 indicates that there was no substantial change in the size or pressure of the magma chamber at shallow levels in the summit region but does

not preclude changes below about 2–3 km. It seems probable that the magma conduit system stayed essentially open and stable during the study period allowing the lava lake to remain continuously active and open to the surface. The observed episodes of minor inflation are consistent with increased gas and heat flux into the lava lake and, possibly, also into a shallow rift system extending through Side Crater.

REFERENCES

Bibby, H. M., The reduction of geodetic survey data for the detection of earth deformation, *Rep. 84*, Geophys. Div., Dep. of Sci. and Ind. Res., Lower Hutt, New Zealand, 1973.

Bibby, H. M., Unbiased estimate of strain from triangulation data using the method of simultaneous reduction, *Tectonophysics, 82*, 161–174, 1982.

Blick, G. H., Site notes—Mt. Erebus volcanic monitoring pattern, *Immed. Rep. EDS 86/2*, Earth Deform. Sect., Dep. of Sci. and Ind. Res., Lower Hutt, New Zealand, 1986.

Blick, G. H., Mt. Erebus, Antarctica, volcanological observations and deformation survey, *N. Z. Volcanol. Rec., 15*, 52–55, 1987.

Blick, G. H., and B. J. Scott, Volcanic activity and deformation of the summit of Mt. Erebus, Antarctica, the 1984 survey; with appendix: Displacement analysis by P. M. Otway, *EDS Rep. 101*, 39 pp., Earth Deform. Sect., Dep. of Sci. and Ind. Res., Lower Hutt, New Zealand, 1986.

Blick, G. H., and R. O. Williams, The December 1985 survey of the Mount Erebus volcanic deformation monitoring pattern, *EDS Rep. 102*, 39 pp., Earth Deform. Sect., Dep. of Sci. and Ind. Res., Lower Hutt, New Zealand, 1986.

Blick, G. H., P. M. Otway, and B. J. Scott, Deformation monitoring of Mt. Erebus, Antarctica, 1980-1985, in *IAVCEI Proceedings in Volcanology*, vol. 1, *Volcanic Hazards*, edited by J. H. Latter, pp. 554–560, Springer-Verlag, New York, 1989.

Decker, R. W., Forecasting volcanic eruptions, *Annu. Rev. Earth Planet. Sci., 14*, 267–291, 1986.

Dibble, R. R., Infrasonic recordings of strombolian eruptions of Erebus, Antarctica, March/December 1984, covering the jump in activity on 13 September 1984, in *IAVCEI Proceedings in Volcanology*, vol. 1, *Volcanic Hazards*, edited by J. H. Latter, pp. 536–553, Springer-Verlag, New York, 1989.

Dibble, R. R., J. Kienle, P. R. Kyle, and K. Shibuya, Geophysical studies of Erebus Volcano, Antarctica, from 1974 December to 1982 January, *N. Z. J. Geol. Geophys., 27*, 425–455, 1984.

Giggenbach, W. F., and G. Lyon, Present volcanic activity on Mt. Erebus, Ross Island, Antarctica, *Geology 1*, 135–136, 1973.

Kaminuma, K. V., and R. R. Dibble, Seismic activity of Mount Erebus in 1981–1988, *Proc. Natl. Inst, Polar Res. Symp. Antarct. Geosci., 4*, 142–148, 1990.

Kyle, P. R., Mt. Erebus surprises Ross Island inhabitants, *Antarct. J. U. S., XIX(4)*, 1–3, 1984.

Kyle, P. R., and P. M. Otway, Volcanic activity of Mount Erebus, 1981–1982, *Antarct. J. U. S., XVII(5)*, 1982.

Kyle, P. R., R. R. Dibble, W. F. Giggenbach, and J. Keys, Volcanic activity associated with the anorthoclase phonolite lava lake, Mount Erebus, Antarctica, in *Antarctic Geosciences*, 1st ed., vol. 1, edited by C. Craddock, pp. 735–745, University of Wisconsin Press, Madison, 1982.

Otway, P. M., Tilt-level monitoring in the Taupo Volcanic Zone, *N. Z. Volcanol. Rec., 8*, 27–28, 1979.

Otway, P. M., Erebus volcanic deformation surveys, *N. Z. Volcanol. Rec., 11*, 49–50, 1982.

Otway, P. M., Erebus volcanic deformation surveys, *N. Z. Volcanol. Rec., 12*, 60–61, 1984.

Otway, P. M., Erebus deformation surveys (1982), *N. Z. Volcanol. Rec., 13*, 82–83, 1985.

Otway, P. M., Volcanic deformation surveys in Tongariro Volcanic Centre, in *Volcanic Hazards Assessment in New Zealand, Rec. 10*, edited by J. G. Gregory and W. A. Watters, pp. 35–40, Department of Scientific and Industrial Research, Lower Hutt, New Zealand, 1986.

Scott, B. J., and S. A. Currie, Mt. Erebus survey report, *EDS Rep. 84/7*, Earth Deform. Sect., Dep. of Sci. and Ind. Res., Lower Hutt, New Zealand, 1984.

Scott, B. J., and P. M Otway, Volcanic deformation studies - Mt. Erebus, *N. Z. Antarct. Rec., 6(2)*, 20–23, 1985.

Scott, B. J., and P. M. Otway, Erebus, Antarctica, volcanological observations and deformation survey, *N. Z. Volcanol. Rec., 14*, 62–69, 1987.

G. H. Blick, Earth Deformation Section, Institute of Geological and Nuclear Sciences, Lower Hutt, New Zealand.

P. M. Otway and B. J. Scott, Wairakei Research Centre, Institute of Geological and Nuclear Sciences, Private Bag 2000, Taupo, New Zealand.

SULFUR DIOXIDE EMISSION RATES FROM MOUNT EREBUS, ANTARCTICA

Philip R. Kyle, Lauri M. Sybeldon, William C. McIntosh, and K. Meeker

Department of Geoscience, New Mexico Institute of Mining and Technology, Socorro, New Mexico

Robert Symonds

Michigan Technological University, Houghton, Michigan

Volcanic emission rates of SO_2 have been measured at Mount Erebus annually between 1983 and 1991 by correlation spectrometer (COSPEC V). Between 1988 and 1991, high-precision (~±5%) measurements were possible by automating the COSPEC operations and the use of continuous video observations to determine vertical plume rise rates. In December 1983, SO_2 emissions were 230 Mg/d, but this value declined to 25 Mg/d in December 1984 following a 3-month period of sustained strombolian eruptions which buried a persistent, convecting, anorthoclase phonolite lava lake. Since 1985, there has been a general trend of increasing SO_2 emissions which correlates with the area of magma exposed in small magma pools in the crater. Annual SO_2 emission rates have ranged from a high of 84 Gg/yr in 1983 to a low of 6 Gg/yr in 1985. These rates are trivial in comparison with global volcanic SO_2 emissions but may be important on a local scale.

INTRODUCTION

Volcanic gas emissions provide important insights into the degassing processes occurring at and inside volcanoes. Volcanic gases can also have long- and short-range environmental impacts. Eruptions may be predicted by monitoring the amount and changes in SO_2 emission rates at volcanic vents [*Malinconico*, 1979; *Casadevall et al.*, 1981].

Generally, H_2O (35–90 mol %), CO_2 (5–50 mol %), and SO_2 (2–30 mol %) are the most abundant volatiles in basaltic and andesitic magmas [*Anderson*, 1975]. Sulfur can be analyzed more precisely than water or CO_2 in volcanic plumes and, unlike H_2O, is less likely to be subjected to contamination by groundwater, meteoric water, and air surrounding the vent [*Gerlach*, 1980]. The oxidizing conditions found at most volcanic vents result in nearly all volatile sulfur in plumes being present as SO_2 [*Gerlach and Nordlie*, 1975; *Jaeschke et al.*, 1982; *Symonds et al.*, 1990]. At the present time, because of the availability of correlation spectrometer (COSPEC) data, sulfur dioxide is the most sensitive of the major volatiles to use in monitoring gas plume associated with the degassing of magma.

Measured SO_2 emission rates from individual volcanoes are used to calculate the total output of other volatiles and particulate matter from the vent. They are also useful for the estimation of the total SO_2 output due to volcanoes on a global scale [*Stoiber et al.*, 1987].

The objectives of this study were as follows: (1) to quantify the amount of sulfur dioxide emitted from Mount Erebus using a correlation spectrometer, (2) to determine average SO_2 emission rates for annual budget estimates, and (3) to determine trends in the data and relate them to magma dynamics in the permanent lava lake.

Prior to COSPEC measurements, SO_2 emission rates at Mount Erebus were estimated by other methods in 1978 and 1980. *Polian and Lambert* [1979] reported an SO_2 flux of 3 Mg/d in 1978, using treated filters. In 1980, *Radke* [1982] made three SO_2 flux measurements using a flame photometer mounted in a LC-130 aircraft. These measurements ranged from 35 Mg/d on

November 14, 1980, to 155 Mg/d on November 5, 1980. The latter measurement was considered less reliable owing to high winds and turbulence. All of these measurements are considered inferior to the COSPEC measurements reported here.

VOLCANIC ACTIVITY

Mount Erebus, Ross Island, Antarctica (3794 m, 77.58°S, 167.17°E), is a composite intraplate stratovolcano. The summit crater is 550 m in diameter and 120 m deep and contains an Inner Crater 220 m in diameter and 100 m deep. A persistent, convecting lava lake of anorthoclase phonolite magma was first discovered in 1972 [*Giggenbach et al.*, 1973] making Erebus host to one of a very limited number of such features in the world. The lava lake at Erebus is the only known phonolitic lava lake.

Since the discovery of the lava lake, its size was monitored annually between 1972 and 1978 [*Kyle et al.*, 1982], at which time the lake size stabilized and remained constant until 1984. The motion of the magma in the lake was characterized by either slow convective movement or infrequent explosive eruptive activity. Eruptions ranged from strong explosions that emitted ash and bombs to weak explosions brought on by bubble ruptures within the lake. Nonexplosive eruptions that emitted dark ash from vents on the side of the lake were also common [*Dibble et al.*, 1988].

Sixty to 150 seismic events daily, as well as annual earthquake swarms (250 or more seismic events per day) occurred between December 1980 and August 1984 [*Kaminuma and Shibuya*, 1991]. Small strombolian eruptions occurred at a rate of 2–6 per day from 1972 until 1984 [*Kyle et al.*, 1982; *Dibble et al.*, 1984] and often spewed bombs and ejecta onto the crater rim. On September 13, 1984, stronger strombolian eruptions started and over the next four months were heard, seen, and recorded at Scott Base and McMurdo Station, 37 km away. Such violent activity had not been described since Sir James Ross discovered the volcano in 1841 [*Kyle et al.*, 1982]. During this period, bombs up to 10 m in diameter were ejected up to 1 km from the vent. Bombs and other ejecta engulfed the Inner Crater and buried the lava lake. Beginning in early 1985, seismic activity had decreased to less than its pre-1984 level [*Kaminuma and Shibuya*, 1991]. The lava lake has gradually exhumed itself and consists of several small lakes which show annual areal increases, except for 1988, when their area as well as the SO_2 emission rate decreased by 36%.

In January 1991 the position of the lava lakes and an adjacent small explosive vent known as the "active vent" were in similar configurations as prior to September 1984. Chemical and mineral analyses indicate that no change in the composition of the anorthoclase phonolite magma has occurred since 1972 [*Caldwell et al.*, 1989]. There have been no indications that the conduit system beneath Erebus has been altered in any way, which suggests it was stable during the study period.

ANALYTICAL METHODS

Sulfur dioxide emission rates were determined using a Barringer COSPEC V correlation spectrometer. The COSPEC operates by dividing ultraviolet light into several different spectral bands and measuring the intensity of energy in those bands. A telescope on the COSPEC (field of view 23 milliradians by 7 milliradians) scans incident solar radiation. Four masks containing seven gratings slit each filter and separate the light according to wavelength. Two bands of radiation are of particular interest; the first is the band of radiation of the wavelength where energy is absorbed by atmospheric sulfur dioxide. The second is the band of radiation where the presence of atmospheric sulfur dioxide produces energetic radiation [*Millan et al.*, 1985]. The ratio of the energy intensities of these two sets of radiation, in the absence of extraneous sulfur dioxide, provides a base line for the analysis. The energy intensity ratio is proportional to the amount of sulfur dioxide present. The COSPEC electronically produces an output voltage signal proportional to the ratio.

The COSPEC contains an automatic gain control (AGC) to correct for changes in the intensity of ultraviolet radiation during the day. The AGC adjusts the sensitivity of the instrument based on the intensity of the incoming radiation. The instrument is frequently calibrated by measuring the energy intensity ratio when a fused quartz chamber containing a known quantity of SO_2 is inserted into the field of view of the instrument against an SO_2-free background.

COSPEC data collected in 1983 were obtained using a LC-130 aircraft fitted with a quartz viewing window mounted in the crew escape hatch [*Rose et al.*, 1985]. All subsequent measurements were made on the ground in a stationary mode where the instrument remained in a fixed position and was then scanned across the volcanic plume [*Stoiber et al.*, 1983]. Data collected from 1984 to 1987 used the manual hand-held scan technique [*Stoiber et al.*, 1983; *Chartier et al.*, 1988]. This technique requires the constant presence and attention of the operator to provide a steady scan rate and scan angle for accurate SO_2 measurements. The data collected in this manner were recorded on a Hewlett-Packard strip chart

recorder and analyzed by calculating the area beneath the resulting curve, by using a planimeter or counting squares manually on the chart paper. The computed area was referenced to calibration data taken prior to and after each scan, then multiplied by the plume width to give an SO_2 cross section, in ppm m². The SO_2 cross section multiplied by the plume velocity gives the SO_2 emission rate for that scan.

Since the 1987/1988 austral summer field season, an automatic scanning head that provides constant scan angles and scan rates with minimal aberrations due to operator interaction was used to collect all of the data [Kyle and McIntosh, 1989]. In the automated technique, data were collected by mounting the COSPEC on an automatic scanner and recorded into the memory of a Toshiba T1200 HB lap-top computer utilizing the software program COSPEC. Data were reduced using the program ASPEC.

The distance from the COSPEC to the plume was determined using topographic maps. The scan angle for each data set was measured by means of an inclinometer or protractor mounted on the COSPEC. The distance to the plume and scan angle are used to calculate the width of the plume.

Much of the COSPEC data used in this study were accompanied by simultaneous video recordings of the plume shot from the COSPEC site. The video records allow accurate determination of the plume velocity. Owing to the small volume of the volcanic plume at Erebus and the distance from the COSPEC site to the plume (approximately 2 km), COSPEC data were mainly collected on windless days when the plume rose vertically. In this case, plume velocities depend only on thermal inertia.

The distance from the COSPEC/camera site at the lower Erebus Jamesway hut and the distance between topographical landmarks on the rim of Erebus are well known. Plume velocities were therefore calculated directly from video tapes. Some distinguishable feature of the plume (for example, a discoloration or the leading edge of a puff) was timed using a stopwatch as it traveled known distances on the video screen. When time and distance traveled are measured, the calculation of plume velocity is trivial. In circumstances where the video was unsuitable (owing to no visible plume, for instance) or when no video was shot, average plume velocities from COSPEC sessions immediately preceding and/or following the times of "video gaps" were used. Nearly all measurements of plume travel times made using this method have better than ±5% statistical error, thereby greatly improving accuracy in one of the greatest sources of error (Table 1) involved with correlation spectrometry observations.

TABLE 1. Uncertainties in COSPEC Measurements at Mount Erebus

Error Source	With Video, %	Without Video, %
Wind speed/rise rate	±5	±30
Distance to plume	±3	±3
Scan rate	±2	±2
Data reduction with ASPEC	±2	±2
Cumulative error (square route of the sum of the squares)	±2	±30

Error is based on reproducibility, except distance and scan rate errors, which are best estimates.

RESULTS

Sulfur dioxide emission rates have been measured by COSPEC at Mount Erebus annually since 1983. The number of days of observations, mode of measurement, and number of observations are given in Table 2. There has been a steady increase in the number of daily measurements, due principally to the introduction of the automatic scanner in December 1988. A large number of measurements is desirable, because it helps average out the variations seen in SO_2 emission rates over minutes, hours, and days when calculating long-term SO_2 emission rates.

1983

In December 1983, SO_2 emission rates were measured with the COSPEC mounted in an aircraft. The results of 27 SO_2 flux determinations were reported by Rose et al. [1985] as 230 ± 90 Mg/d. This result is important, as it precedes the increased explosive activity which started in September 1984. The anorthoclase phonolite lava lake remained uniform in size and behavior from 1976 to September 1984. During this period, visual observations showed no changes in the size of the plume, and the odor in the plume was also strong and uniform. We therefore suggest that the 1983 SO_2 flux is characteristic of Mount Erebus for the period 1976 to September 1984.

1984

SO_2 emission rates were measured using a tripod-mounted COSPEC on December 26 and 29, 1984; the average was 25 ± 10 Mg/d [Symonds et al., 1985] (Table 3). The biggest uncertainty in these measurements is the plume speed. Measured wind speeds were

TABLE 2. Correlation Spectrometer Measurements of SO_2 Emissions From
Mount Erebus

Month and Year	No. of Days	No. of Scans	Mode	Reference
December 1983	4	27	A	*Rose et al.* [1985]
December 1984	2	41	SH	*Symonds et al.* [1985]
December 1985	2	67	SH	this study
December 1986	5	244	SH	this study
December 1987	4	277	SH	this study
December 1988	4	941	SA	this study
December 1989	5	1405	SA	this study
January 1991	2	513	SA	this study

A, aircraft; SH, stationary hand scan; SA, stationary automatic scanner.

between 2 and 3 m/s with an error of 0.5–1 m/s. Therefore the precision in the individual SO_2 measurements is ±30–50%.

During the measurement period, activity was generally quiet as the large strombolian eruptions, characteristic of late 1984, had mainly subsided. A small vent containing magma was centered near the site of the former lava lake. It is likely that larger SO_2 emissions occurred during the height of explosive activity in September and October. However, we have no means of estimating them.

1985

Sixty-seven observations of the SO_2 emission rates were made over 3 days (Table 4), with an average of 15 ± 7 Mg/d. Plume velocities were measured by timing the rise rate of visually observed individual puffs; these

velocities varied from 2.5 to 5.0 m/s. All measurements were made during periods when the wind speed was low and the plume was rising vertically, driven by thermal inertia from the lava lake. On December 17, 48 SO_2 measurements were made between 1542 and 1943 hours (Figure 1). Although there is a break between 1717 and 1807 hours, the data suggest a cyclic behavior in emission rates. Three high values of SO_2 emissions just prior to 1700 hours resulted from turbulence in the vertically rising plume, thus causing it to double back on itself. These three measurements therefore overestimate the actual emission rates.

1986

In December 1986, SO_2 emissions were measured on 5 days (Table 5). The bulk of the measurements (195 of 244) was made on December 10, 11, and 21 by horizon-

TABLE 3. Average SO_2 Emission Rates From Mount Erebus, December 1984
(Megagrams per Day)

	Date			Cumulative Average
	Dec. 26	Dec. 29	Dec. 29	
Decimal time, hours	22.03–22.62	1.43–2.03	13.20–20.23	
Average	38	39	20	25
σ	3	4	6	10
n	8	8	25	41
Minimum	33	34	8	8
Maximum	44	46	36	46

Variables: σ, standard deviation; n, number of measurements.

TABLE 4. Average SO_2 Emission Rates From Mount Erebus, December 1985
(Megagrams per Day)

	Date			Cumulative Average
	Dec. 15	Dec. 16	Dec. 17	
Decimal time, hours	21.00–21.17	11.00–23.77	15.70–19.72	
Average	22	20	13	15
σ	...	8	6	7
n	2	17	48	67
Minimum	17	10	3	3
Maximum	28	40	35	40

Variables: σ, standard deviation; n, number of measurements.

tally scanning a vertically rising plume. On December 8 and 23, vertical scans were made through a horizontal plume carried by the prevailing wind. SO_2 emission rates measured on December 8 and 23 average 6 Mg/d compared with 21 Mg/d (Table 5) for the 3 other days. The prevailing winds usually cause horizontal plumes to be obscured by the crater rim, and thus COSPEC measurements only provide a minimum estimate of SO_2 emission rates. The average SO_2 emission of 21 ± 11 Mg/d (Table 5) was, therefore, calculated excluding December 8 and 23 measurements. For the vertical rising plume, video recordings were used to estimate the plume speed.

On December 21, 76 SO_2 emission rates, between 1314 and 2123 hours, averaged 22 ± 12 Mg/d. The SO_2 emissions show a steady increase over the first 2.5 hours, reaching 50 Mg/d, and then decrease to a steady

Fig. 1. Variations in SO_2 emission rates measured by COSPEC at Mount Erebus on December 17, 1985.

level of about 15 Mg/d (Figure 2). At 1846 hours (18.8 decimal time) a small eruption in the crater was heard from 2 km away. Immediately following the eruption, SO_2 emissions fell from 18 to 5 Mg/d and remained at consistently low values for about 40 min (Figure 2).

1987

SO_2 emissions were measured by horizontal stationary hand-driven scans across a vertically rising plume on 4 days (Table 6). The majority of the measurements were made over a 14-hour period on December 8, when 227 observations were made. On the other 3 days (December 7, 12, and 16) a total of 100 observations was made. Video recordings were used to estimate plume speeds.

The cumulative average SO_2 emission rate was 44 ± 27 Mg/d (Table 6), with daily averages ranging from 26 ± 14 Mg/d (December 12) to 91 ± 38 Mg/d (December 7). Because of the small number of observations made on December 7 and 12, the differences in the average are not considered significant. On December 8, when 227 observations were obtained, the minimum SO_2 emission was 11 Mg/d and the maximum was 117 Mg/d (Table 6, Figure 3). SO_2 emissions fluctuated mainly between 10 and 40 Mg/d, from 0900 to 1700 hours on December 8 (Figure 3). Emissions then increased systematically, reaching ~100 Mg/d when observations ceased at 2100 hours owing to low UV radiation.

1988

SO_2 flux measurements were made on December 14, 16, 17, and 21, 1988 (Table 7). The averages for December 14, 16, and 21 agreed very well at 27 Mg SO_2/d. Measurements made on December 17 were sig-

TABLE 5. Average SO_2 Emission Rates From Mount Erebus, December 1986 (Megagrams per Day)

	Date					Cumulative Average*
	Dec. 8	Dec. 10	Dec. 11	Dec. 21	Dec. 23	
Decimal time, hours	16.20–17.60	7.38–20.52	10.27–22.42	13.23–21.38	10.90–15.10	
Average	5	18	21	22	6	21
σ	3	10	12	12	3	11
n	9	51	68	76	40	195
Minimum	3	4	6	2	3	2
Maximum	13	42	61	67	14	67

Variables: σ, standard deviation; n, number of observations.
*The cumulative average excludes measurements made on December 8 and 23.

nificantly lower, averaging only 3.4 Mg/d. The December 17 data were collected when the plume was transparent, although clear sky and windless conditions prevailed. The low readings were made over a period of 2 hours and are statistically different from the other measurements. The December 17 measurements were not included in the cumulative average emission rate estimate for 1988 of 27 ± 9 Mg SO_2/d.

Daily variations in emission rates (Figure 4) were markedly smaller than those observed in previous years (Figures 1–3). The record for December 14 is fragmented; however, there is a weak trend of increasing SO_2 emissions from 1430 to 1600 hours (Figure 4).

1989

SO_2 flux measurements were made on December 3, 11, 18, 20, and 21 (Table 8). The average daily emis-

sions calculated for the 4 days excluding December 11 show excellent agreement between 48 and 54 Mg SO_2/d. The average of 93.2 ± 27.0 Mg/d for December 11 is significantly higher. All the data were measured over time intervals greater than 5 hours (Figure 5) and should constitute good daily averages.

1991

SO_2 flux measurements were made on January 13 and 22 (Table 9). The average daily emissions of 66 ± 20 Mg/d ($n = 114$) and 72 ± 20 Mg/d ($n = 399$) for the 2 days are in good agreement. The cumulative average SO_2 flux was 71 ± 20 Mg/d. On January 13, emission rates were relatively constant at ~80 Mg/d from 0900 to 1400 hours and decreased sharply to <40 Mg/d by 1500 hours (Figure 6). Emission rates then showed a steady increase until 1830 hours.

DISCUSSION

Yearly SO_2 Emission Rates

Average annual SO_2 emission rates have shown significant and systematic variations since the first COSPEC measurements in December 1983 (Table 10). The most significant change was the dramatic decline between 1983 and 1984, when SO_2 emissions dropped from 230 ± 90 to 25 ± 10 Mg/d. The drop occurred after the 4-month period of highly explosive strombolian eruptions which commenced in September 1984. These eruptions partially filled the inner crater with ejecta, burying the lava lake. Since 1985 there has been a trend of increasing SO_2 emissions (Figure 7); only 1988 deviates from this trend. Mount Erebus thus appears to be rejuvenating itself.

21 December 1986

Fig. 2. Variations in SO_2 emission rates measured by COSPEC at Mount Erebus on December 21, 1986.

TABLE 6. Average SO_2 Emission Rates From Mount Erebus, December 1987 (Megagrams per Day)

	Date				Cumulative Average
	Dec. 7	Dec. 8	Dec. 12	Dec. 16	
Decimal time, hours	16.41–19.17	8.95–20.98	9.33–14.97	15.13–15.80	
Average	91	43	26	45	44
σ	38	22	14	14	27
n	25	227	55	20	327
Minimum	37	11	4	26	4
Maximum	185	117	61	81	185

Variables: σ, standard deviation; n, number of observations.

The SO_2 emissions rates are proportional to the area of the lava lake (Figure 8). This relationship suggests that saturation of the sulfur gases (H_2S and SO_2) is not achieved until the magma reaches the surface of the lake. Sulfur content of the anorthoclase phonolite is low, of the order of 350 ppm (P. R. Kyle, unpublished data). No studies of S solubility in phonolitic magmas are available; however, in S-rich Hawaiian tholeiitic basalts, SO_2 saturation is not achieved until shallow depths [Gerlach, 1986].

Support for the near-surface saturation of S gases is also provided by observations of SO_2 emission following small strombolian eruption. Degassing of magma at depth results in the formation of gas bubbles: these bubbles coalesce, expand, and rise as larger bubbles [Sparks, 1977]. Upon reaching the surface of the lava lake or the active vent, the expanding bubbles burst explosively with a force dependent upon their size and rise rate. These bubbles therefore contain gas exsolved at depth. Several COSPEC observations have been made following strombolian eruptions. On three such occasions in 1984 there was no significant increase in SO_2 emissions. In 1986 (Figure 2) there was a significant decline in SO_2 emission. The absence of large increases in SO_2 fluxes following eruptions suggests that the gas exsolved at depth did not contain SO_2.

Rose et al. [1985] reported aircraft measurements of SO_2 emission from Mount Erebus in 1983 which contradict the above observations. On December 9, 1983, they recorded increased SO_2 emissions following an inferred eruption. They observed darkening of the plume from over 6 km away. Most small strombolian eruptions from the lava lake at Mount Erebus do not result in an increase of ash content in the plume; however, they do result in a larger and faster rising plume. Rare ash eruptions occur from the active vent and other fumarolic vents surrounding the lava lake. These eruptions could be due to near-surface accumulations of gas resulting

from shallow magma degassing which would contain S gases. The darkened plume reported by Rose et al. [1985] thus may have resulted from an atypical style of eruption.

An important consequence of the observed relationship between SO_2 emissions and lava lake area is that it allows us to predict emission rates at times when COSPEC measurements were not available. The lava lake(s) first observed at Mount Erebus in 1972 were small pools [Giggenbach et al., 1973] which over the next 6 years grew to a 60-m-diameter semicircular lake [Kyle et al., 1982]. Therefore we predict that SO_2 emission rates were low (<40 Mg/d) in 1972 but increased to about 230 Mg/d by 1978. The lake remained uniform in size between 1978 and September 1984 and probably emitted SO_2 at about 230 Mg/d based on our measurements in December 1983.

Previous estimates of SO_2 emission made in 1978 [Polian and Lambert, 1979] and in 1980 [Radke, 1982]
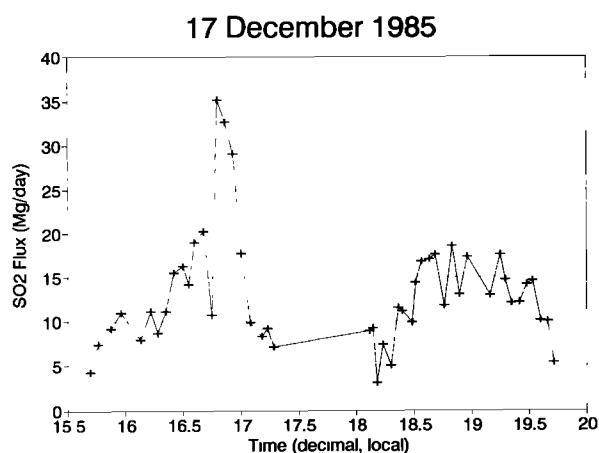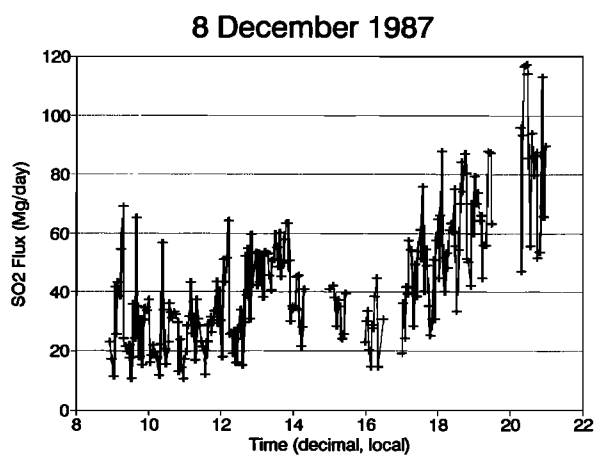

Fig. 3. Variations in SO_2 emission rates measured by COSPEC at Mount Erebus on December 8, 1987.

TABLE 7. Average SO$_2$ Emission Rates From Mount Erebus, December 1988 (Megagrams per Day)

	Date				Cumulative Average*
	Dec. 14	Dec. 16	Dec. 17	Dec. 21	
Decimal time, hours	9.92–20.39	13.67–21.09	9.66–12.67	15.47–17.15	
Average	28	27	3	26	27
σ	8	10	2	9	9
n	310	383	164	84	777
Minimum	11	1	1	10	1
Maximum	52	53	11	50	53

Variables: σ, standard deviation; n, number of observations.
*The cumulative average does not include measurements on December 17.

were 3 and 35 Mg/d, respectively. These values disagree with our inferred SO$_2$ emission rate of about 230 Mg/d. From 1978 to 1983, observations of the plume from the crater rim showed it to have a strong and distinct odor, consistent with our inferred estimates of high SO$_2$ emissions. Significant assumptions and estimates were involved in the measurements made by Radke [1982] and Polian and Lambert [1979], and thus they may contain considerable error.

Daily Emission Rates

SO$_2$ emission rates vary widely during a single day of observations (Figures 1 to 6). These variations are significant and greatly exceed the precision of measurements. Often emissions appear cyclic and have periods of 2.5 hours (Figure 1) and 6 hours (Figure 6). Such fluctuations in SO$_2$ emission rates must reflect the availability of magma to the lava lake. Qualitative observations have shown that during times of high SO$_2$ emission rates, activity within the lava lake is high and characterized by faster and more vigorous convection. Thus COSPEC observations may provide a means to monitor convection rates.

Variations in SO$_2$ emissions may also result from a heterogeneous distribution of volatiles in the convecting magma column. F/Cl ratios vary with time in volcanic gas samples collected on the crater rim of Mount Erebus using treated filters [Zreda-Gostynska et al., 1993]. One interpretation of the F/Cl variations is that they are due to batches of undegassed magma circulating into the lava lake. Degassing of this undegassed volatile-rich magma results in higher F/Cl ratios [Menyailov, 1975; Miller et al., 1990]. Such undegassed magma may also contain higher S contents.

Another feature seen in the daily SO$_2$ emission rate records (Figures 1–6) is large variations in emissions occurring over intervals of minutes. The spikes in the records are due to "puffing." Discrete bursts of gas emission are clearly seen visually and give the impression that the plume is pulsating. Such "puffs" of gas may be caused occasionally by the bursting of small degassing bubbles in the lava lake. At other times, there is an increase in noise as gas discharge increase from the lava lake and adjacent fumaroles. Puffing is not well understood, but it is a fundamental feature of many volcanoes (e.g., Etna [Andres, 1988] and Pu'u O'o, Kilauea, Hawaii [Sybeldon, 1991]). Undoubtedly, it is related to the mechanism of degassing, which, in turn, is related to bubble growth and ascent in the magma column. Apparently, degassing is not a steady state process. The puffing may be related to the development of instabilities possibly due to the rates of nucleation of gases within the convecting magma conduit.

Both puffing and longer-term variations in gas discharge contribute to the large standard deviations seen in daily averages of SO$_2$ emission rates (Tables 3 to 9). To overcome these variations and obtain a reasonable estimate of emission rates, we have significantly increased the rate of data collection by use of the automatic scanner. The results we have obtained are possibly the most detailed short-term records ever achieved at any volcano in the world.

SO$_2$ Emissions to the Antarctic Atmosphere

The short field season and often inclement weather conditions make continuous long-term observations of SO$_2$ emission from Mount Erebus impossible. However, even from the limited observations it is apparent that the magmatic system at Mount Erebus is very stable. Changes in the area and position of the lava lake are slow. Observations of the lava lake for periods of up to 6 months per year by a remote video camera show no significant fluctuations (R. R. Dibble, personal communication, 1992). Thus we believe that the SO$_2$ emission
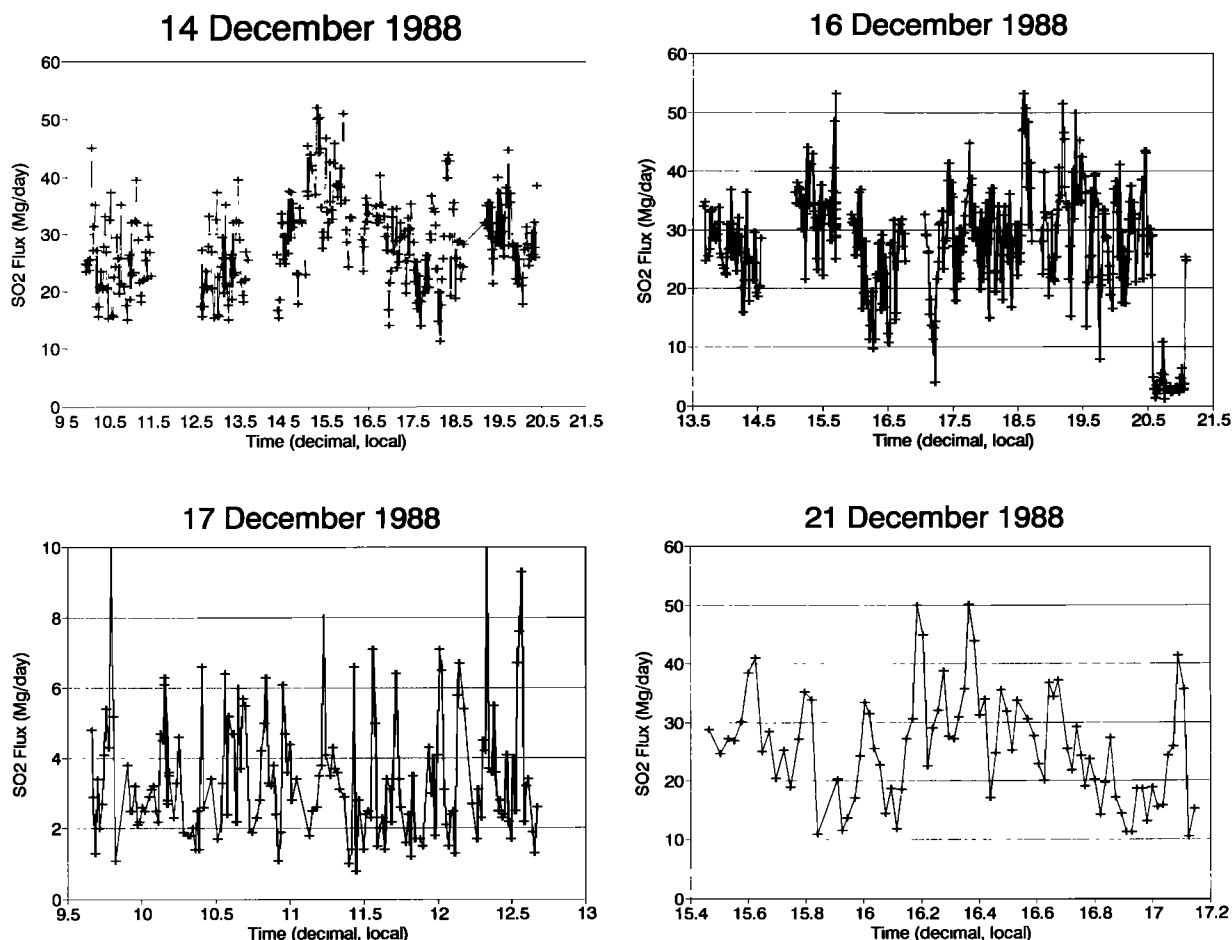
Fig. 4. Variations in SO_2 emission rates measured by COSPEC at Mount Erebus on 4 days during December 1988.

rates measured over a period of only 2 to 5 days are representative of a whole year.

SO_2 emission rates from Mount Erebus are extremely low in comparison with most passively degassing volca-noes [*Stoiber et al.*, 1987; *Berresheim and Jaeschke*, 1983]. This characteristic is a function of the highly evolved phonolitic composition with its low concentration of sulfur. Also, the low oxygen fugacity of the

TABLE 8. Average SO_2 Emission Rates From Mount Erebus, December 1989 (Megagrams per Day)

	Date					Cumulative Average*
	Dec. 3	Dec. 11	Dec. 18	Dec. 20	Dec. 21	
Decimal time, hours	11.08–14.5	9.55–14.01	9.63–17.34	9.78–20.32	14.87–20.23	
Average	52	93	48	54	54	52
σ	21	27	20	23	19	21
n	130	235	269	511	260	1170
Minimum	11	38	17	15	18	11
Maximum	104	218	99	137	130	218

Variables: σ, standard deviation; *n*, number of observations.
*The cumulative average does not include measurements made on December 11.
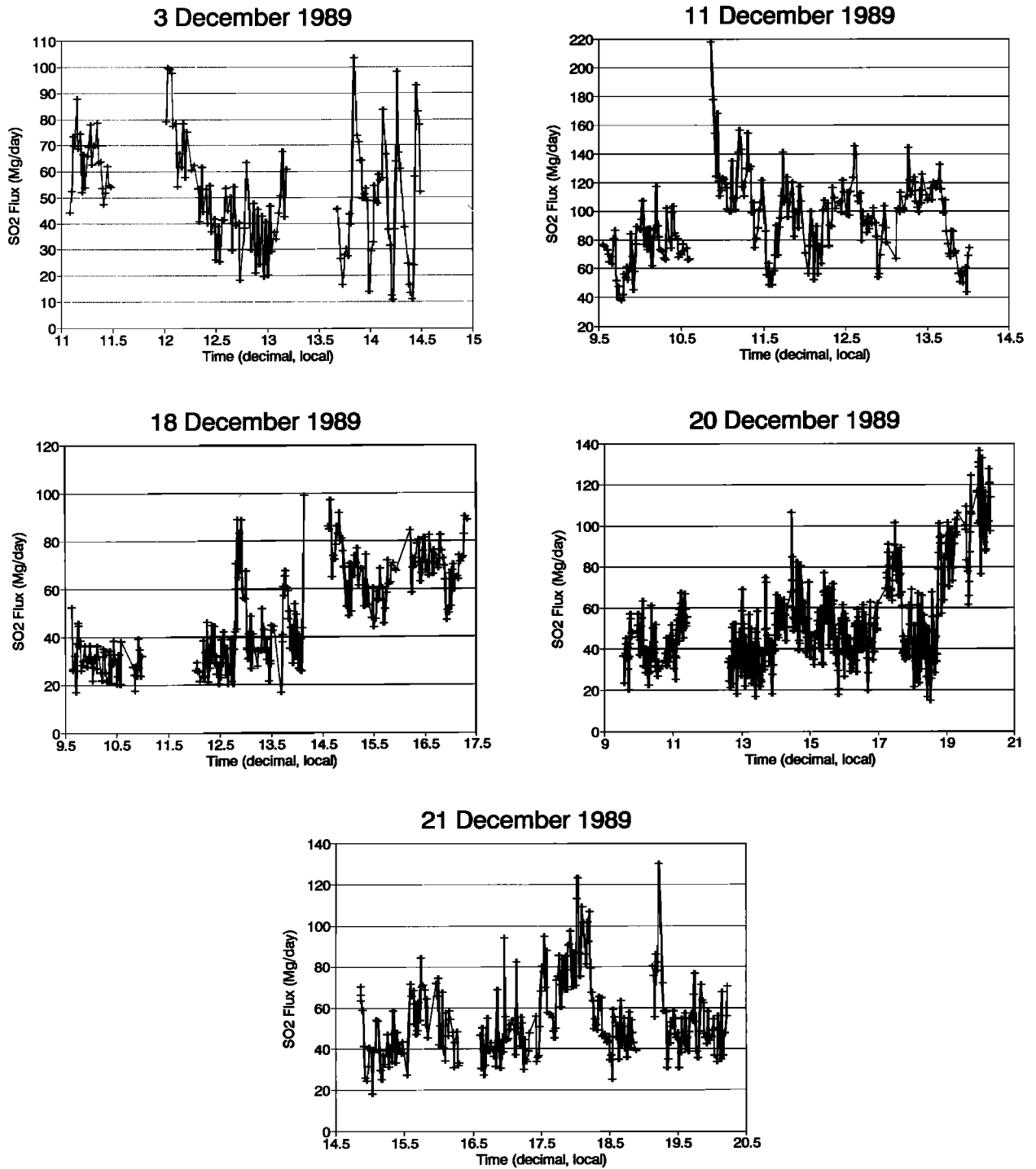
Fig. 5. Variations in SO$_2$ emission rates measured by COSPEC at Mount Erebus on 5 days during December 1989.

TABLE 9. Average SO_2 Emission Rates From Mount Erebus, January 1991 (Megagrams per Day)

	Date		Cumulative Average
	Jan. 13	Jan. 22	
Decimal time, hours	8.82–18.57	15.80–20.25	
Average	72	66	71
σ	20	20	20
n	399	114	513
Minimum	25	22	22
Maximum	126	144	144

Variables: σ, standard deviation; n, number of measurements.

magma [*Kyle*, 1977] results in removal of sulfur from the magma by the precipitation of pyrrhotite as a stable sulfide phase.

Estimates of global volcanic emission rates show a considerable range (Table 11). Of the global emissions given in Table 11, those of *Berresheim and Jaeschke* [1983] and *Stoiber et al.* [1987] are considered the most reliable. The highest annual emission rate measured at Mount Erebus was 84 Gg/yr in 1983 (Table 10), which is only 0.6% of the global emission rate of 15 Tg/yr [*Berresheim and Jaeschke*, 1983] or 0.5% of the 18 Tg/yr [*Stoiber et al.*, 1987].

On a more local scale, Mount Erebus may be a significant source of aerosols to the Antarctic atmosphere [*Zreda-Gostynska et al.*, 1993]. *Radke* [1982] suggested that Mount Erebus was the source of 32% of the Antarctic total sulfate budget. *Delmas* [1982] disputed

AVERAGE SO_2 EMISSION RATES

Fig. 7. Yearly averaged SO_2 emission rates from Mount Erebus. Note the steep decline in emissions following the intense period of eruptive activity which commenced in September 1984. Since 1985 there has been a trend of gradually increasing emission rates.

this suggestion and instead estimated, using *Radke*'s [1982] SO_2 emission rates, that the contribution of Erebus to the sulfur budget was only 3%. Most sulfate in the Antarctic atmosphere is derived from marine aerosols [*Delmas et al.*, 1982]. For 1983, our measured SO_2 emission rates are significantly higher than those used by *Radke* [1982] and represent ~10% of the Antarctic sulfur budget of *Delmas* [1982].

One feature of the Antarctic atmosphere is the long residence time for sulfate aerosols. *Delmas* [1982] and *Shaw* [1982] estimated that sulfate resided for about 50 days. Conversion of the volcanic SO_2 to sulfate typically occurs by homogeneous and heterogeneous processes at rates varying from 0.5–30%/hr [*Finlaysson-Pitts and*

Fig. 6. Variations in SO_2 emission rates measured by COSPEC at Mount Erebus on January 13, 1991.
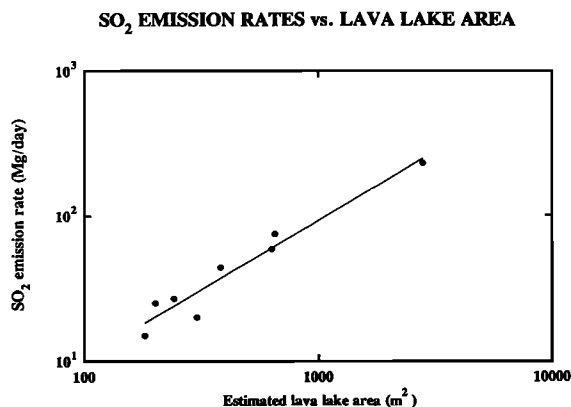
Fig. 8. Plot showing the close relationship between SO_2 emission rates and the estimated surface area of lava present in pools and small lakes within the inner crater of Mount Erebus.

TABLE 10. Annual Average SO_2 Emission Rates From Mount Erebus

Month and Year	SO_2 Output, Mg/d	Area of Lava Lake, m^2	Yearly SO_2 Output, Gg/yr	Reference
Dec. 1983	230 ± 90	2800	84	*Rose et al.* [1985]
Dec. 1984	25 ± 10	200	9	*Symonds et al.* [1985]
Dec. 1985	16 ± 7	180	6	*Kyle et al.* [1990]
Dec. 1986	21 ± 11	300	7	*Kyle et al.* [1990]
Dec. 1987	44 ± 27	380	16	this study
Dec. 1988	27 ± 9	240	10	this study
Dec. 1989	52 ± 21	630	19	this study
Jan . 1991	71 ± 20	650	26	this study

Pitts, 1986]. Water droplets and ash particles both provide major pathways for the oxidation of SO_2 [*Calvert and Stockwell*, 1984]. However, concentration of water and ash are lower than normal in the Antarctic atmosphere and plume at Mount Erebus, respectively. It is therefore probable that the aerosol from Mount Erebus is widely distributed.

CONCLUSIONS

Annual COSPEC measurements of SO_2 emissions from Mount Erebus have provided an excellent method to monitor quantitatively the ongoing volcanic activity associated with the anorthoclase phonolite lava lake. The COSPEC techniques used at Mount Erebus in 1988 and more recently have a much higher degree of sophistication than those used elsewhere and have resulted in a much larger set of data. We are therefore able to record short-term fluctuations in SO_2 with some precision and believe it is due to magma convection. It is apparent that degassing of the phonolitic magma is a complex process involving short-term degassing processes which result in puffing and longer-term magma convection rates. Thus the COSPEC may be a tool which can give indirect information on magma supply to the lava lake.

TABLE 11. Estimates of Global Volcanic SO_2 Emission Rates

Emissions, Tg/yr	Reference
47	*Naughton et al.* [1975]
7.5	*Cadle* [1975]
4.0	*Friend et al.* [1982]
10	*Le Guern* [1982]
15	*Berresheim and Jaeschke* [1983]
18	*Stoiber et al.* [1987]
50	*Lambert et al.* [1988]

The high precision emission rates for SO_2 are useful in allowing estimates of emission rates of other species such as Cl and F. Ratios of S to other species can be measured by direct sampling of fumaroles or by ground-based or aerial sampling using treated filters. Knowing this ratio and the S output from COSPEC, then it is possible to estimate other emissions.

REFERENCES

Anderson, A. T., Some basaltic and andesitic gases, *Rev. Geophys., 13*, 37–55, 1975.

Andres, R. J., Sulfur dioxide and particle emissions from Mount Etna, Italy, M.S. thesis, 159 pp., N. M. Inst. of Min. and Technol., Socorro, 1988.

Berresheim, H., and W. Jaeschke, The contribution of volcanoes to the global atmospheric budget, *J. Geophys. Res., 88*, 3732–3740, 1983.

Cadle, R. D., Volcanic emissions of halides and sulfur compounds to troposphere and stratosphere, *J. Geophys. Res., 80*, 1650–1652, 1975.

Caldwell, D. A., P. R. Kyle, and W. C. McIntosh, Compositions of 1972–1986 volcanic ejecta from Mount Erebus, Antarctica: Implications for the 1984 eruptive activity, *N. M. Bur. Mines Miner. Res. Bull., 131*, 36, 1989.

Calvert, J. G., and W. R. Stockwell, Mechanism and rates of the gas-phase oxidations of sulfur dioxide and nitrogen

oxides in the atmosphere, in *SO₂, NO and NO₂ Oxidation Mechanisms: Atmospheric Considerations*, edited by J. G. Calvert, pp. 1–63, Butterworth, Boston, Mass., 1984.

Casadevall, T. J., D. A. Johnston, D. M. Harris, W. I. Rose, Jr., L. L. Malinconico, R. E. Stoiber, T. J. Bornhorst, S. N. Williams, L. Woodruff, and J. M. Thompson, SO_2 emission rates at Mount St. Helens from March 29 through December, 1980, *U.S. Geol. Surv. Prof. Pap., 1250*, 193–200, 1981.

Chartier, T. A., W. I. Rose, and J. B. Stokes, Detailed record of SO_2 emissions from Pu'u O'o between episodes 33 and 34 of the 1983–1986 eruption, Kilauea, Hawaii, *Bull. Volcanol., 50*, 215–228, 1988.

Delmas, R. J., Antarctic sulfate budget, *Nature, 299*, 677–678, 1982.

Delmas, R. J., M. Briat, and M. Legrand, Chemistry of south polar snow, *J. Geophys. Res., 87*, 4314–4318, 1982.

Dibble, R. R., J. Kienle, P. R. Kyle, and K. Shibuya, Geophysical studies of Erebus volcano, Antarctica, from 1974–1981, *N. Z. J. Geol. Geophys., 27*, 425–455, 1984.

Dibble, R. R., S. I. Barrett, K. Kaminuma, S. Miura, J. Kienle, C. A. Rowe, P. R. Kyle, and W. C. McIntosh, Time comparisons between video and seismic signals from explosions in the lava lake of Erebus Volcano, Antarctica, *Bull. Disas. Prev. Res. Inst. Kyoto Univ., 38*, 147–161, 1988.

Finlaysson-Pitts, B. J., and J. Pitts, *Atmospheric Chemistry*, John Wiley, New York, 1986.

Friend, J. P., A. R. Bandy, J. L. Moyers, W. H. Zoller, R. E. Stoiber, A. L. Torres, W. I. Rose, M. P. McCormick, and D. C. Woods, Research on atmospheric volcanic emissions: An overview, *Geophys. Res. Lett., 9*, 1101–1104, 1982.

Gerlach, T. M., Evaluation of volcanic gas analyses from Kilauea Volcano, *J. Volcanol. Geotherm. Res., 7*, 295–317, 1980.

Gerlach, T. M., Exsolution of H_2O, CO_2, and S during eruptive episodes at Kilauea volcano, Hawaii, *J. Geophys. Res., 91*, 12,177–12,185, 1986.

Gerlach, T. M., and B. E. Nordlie, Temperature, atomic composition and molecular equilibria in volcanic gases, Part II, *Am. J. Sci., 275*, 377–394, 1975.

Giggenbach, W. F., P. R. Kyle, and G. Lyon, Present volcanic activity on Mt. Erebus, Ross Island, Antarctica, *Geology, 1*, 135–136, 1973.

Jaeschke, W., H. Berresheim, and H. Georgii, Sulfur emissions from Mt. Etna, *J. Geophys. Res., 87*, 7253–7261, 1982.

Kaminuma, K., and K. Shibuya, The structure and seismic activity of Mt. Erebus, Ross Island, in *Geological Evolution of Antarctica*, edited by M. R. A. Thomson, J. A. Crame, and J. W. Thomson, pp. 329–333, Cambridge University Press, New York, 1991.

Kyle, P. R., Mineralogy and glass chemistry of recent volcanic ejecta from Mt. Erebus, Ross Island, Antarctica, *N. Z. J. Geol. Geophys., 20*, 1123–1146, 1977.

Kyle, P. R., and W. C. McIntosh, Automation of a correlation spectrometer for measuring volcanic SO_2 emissions, *N. M.*

Bur. Mines Miner. Res. Bull., 131, 7, 1989.

Kyle, P. R., R. R. Dibble, W. F. Giggenbach, and J. Keys, Volcanic activity associated with the anorthoclase phonolite lava lake, Mount Erebus, Antarctica, in *Antarctic Geoscience*, edited by C. Craddock, pp. 735– 745, University of Wisconsin Press, Madison, 1982.

Kyle, P. R., K. Meeker, and D. Finnegan, Emission rates of sulfur dioxide, trace gases and metals from Mount Erebus, Antarctica, *Geophys. Res. Lett., 17*, 2125–2128, 1990.

Lambert, G., M.-F. Le Cloarec, and M. Pennisi, Volcanic output of SO_2 and trace metals: A new approach, *Geochim. Cosmochim. Acta, 52*, 39–42, 1988.

Le Guern, F., Les debits de CO_2 and SO_2 volcanoliques dans l'atmosphere, *Bull. Volcanol., 45*, 197–202, 1982.

Malinconico, L. L., Fluctuations in SO_2 emission during recent eruptions of Etna, *Nature, 278*, 43–45, 1979.

Menyailov, I. A., Prediction of eruptions using changes in composition of volcanic gases, *Bull. Volcanol., 39*, 112–125, 1975.

Millan, M. M., A. J. Gallant, Y. S. Chung, and F. Fanaki, COSPEC observation of Mt. St. Helens volcanic SO_2 eruption cloud of 18 May 1980 over southern Ontario, *Atmos. Environ., 19*, 255–263, 1985.

Miller, T. L., W. H. Zoller, B. M. Crowe, and D. L. Finnegan, Variations in trace metal and halogen ratios in magmatic gases through an eruption cycle of the Pu'u O'o vent, Kilauea, Hawaii: July–August, 1985, *J. Geophys. Res., 95*, 12,607–12,615, 1990.

Naughton, J. J., V. A. Greenberg, and R. Goguel, Incrustations and fumorolic condensates at Kilauea Volcano, Hawaii: Field, drill-hole and laboratory observations, *J. Volcanol. Geotherm. Res., 1*, 149–165, 1975.

Polian, G., and G. Lambert, Radon daughters and sulfur output from Erebus volcano, Antarctica, *J. Volcanol. Geotherm. Res., 6*, 125–137, 1979.

Radke, L. F., Sulphur and sulphate from Mt. Erebus, *Nature, 299*, 710–712, 1982.

Rose, W. I., R. L. Chuan, and P. R. Kyle, Rate of sulphur dioxide emission from Erebus volcano, Antarctica, December, 1983, *Nature, 316*, 710–712, 1985.

Shaw, G. E., On the residence time of the Antarctic ice sheet sulfate aerosol, *J. Geophys. Res., 87*, 4309–4313, 1982.

Sparks, R. S. J., The dynamics of bubble formation and growth in magmas: A review and analysis, *J. Volcanol. Geotherm. Res., 3*, 1–37, 1977.

Stoiber, R. E., L. L. Malinconico, and S. N. Williams, Use of the correlation spectrometer at volcanoes, in *Forecasting Volcanic Events*, edited by H. Tazieff and J. C. Sabroux, pp. 425–444, Elsevier, New York, 1983.

Stoiber, R. E., S. N. Williams, and B. Huebert, Annual contribution of sulfur dioxide to the atmosphere by volcanoes, *J. Volcanol. Geotherm. Res., 33*, 1–8, 1987.

Sybeldon, L., Sulfur dioxide emissions from Pu'u O'o vent, Kilauea, Hawaii and Mount Erebus, Antarctica, M.S. thesis, N. M. Inst. of Min. and Technol., Socorro, 1991.

Symonds, R. B., P. R. Kyle, and W. I. Rose, SO_2 emission

rates and the 1984 activity at Mount Erebus Volcano, Antarctica (abstract), *Eos Trans. AGU, 66,* 417, 1985.

Symonds, R. B., W. I. Rose, T. M. Gerlach, P. H. Briggs, and R. S. Harmon, Evaluation of gases, condensate, and SO_2 emissions from Augustine volcano, Alaska: The degassing of a Cl-rich volcanic system, *Bull. Volcanol., 52,* 355–374, 1990.

Zreda-Gostynska, G., P. R. Kyle, and D. L. Finnegan, Chlorine, fluorine, and sulfur emissions from Mount Erebus, Antarctica, and estimated contributions to the Antarctic atmosphere, *Geophys. Res. Lett., 20,* 1959-1962, 1993.

NM 87801.

K. Meeker, ENSR Consulting and Engineering, 14715 N.E. 95th Street, Redmond, WA 98052.

L. M. Sybeldon, Limmatauweg 8, CH 5400 Ennetbaden, Switzerland.

R. Symonds, Cascade Volcano Observatory, U.S. Geological Survey, Vancouver, WA 98661.

P. R. Kyle and W. C. McIntosh, Department of Geoscience, New Mexico Institute of Mining and Technology, Socorro,

COMPOSITIONS AND MASS FLUXES OF THE MOUNT EREBUS VOLCANIC PLUME

D. S. Sheppard

Institute of Geological and Nuclear Sciences, Lower Hutt, New Zealand

F. Le Guern

Centre des Faibles Radioactivités, Centre National de la Recherche Scientifique, Saclay, France

B. W. Christenson

Institute of Geological and Nuclear Sciences, Wairakei Research Centre, Taupo, New Zealand

In December 1989 and January 1990, gas and aerosol samples were collected in the plume of Mount Erebus to evaluate its impact on the Antarctic environment and to evaluate the processes and reactions occurring in the plume. Using an SF_6 injection technique, a flux of SO_2 of 2.4 Mg/d was determined, much lower than most other determinations. H_2S was detected at very low concentrations, whereas H_2SO_4 varied in concentration but at times exceeded SO_2. The presence of elevated levels of plume components in snow some distance from the crater indicates that processes removing material from the plume are significant. Elevated levels of CO_2 in soils and ice tower gases indicate that flank degassing does occur on the volcano.

INTRODUCTION

The chemical composition of volcanic plumes is studied for two reasons: first, to understand the mechanics of the volcanic cycle, for the ultimate purpose of prediction of activity and assessment of hazard; and second, to ascertain the plumes' significance in the biogeochemical environment through their contribution of matter to the biosphere.

We define a volcanic plume as that volume of the atmosphere associated with a volcano which contains material from the volcano. Volcanic plumes contain air and volcanic material of both a gaseous (e.g., H_2O, CO_2, SO_2) and a particulate nature (e.g., ash, aerosols, bombs), some of which may have been remobilized.

There have been many estimates of the fluxes of compounds and elements into the atmosphere from individual volcanoes (see, for example, *Rose et al.* [1986] and *Lambert et al.* [1988]) and for global volcanic emissions [e.g., *Nriagu*, 1989]. Volcanic sources are significant for some components; however, the compilations do not take into account the chemical form and, consequently, the residence time in the atmosphere of the various components. Such factors are worthy of further investigation, because of the suspected significance of volcanically derived material in such topical issues as stratospheric ozone depletion [*Johnston*, 1980; *Hofmann and Solomon*, 1989; *Arnold et al.*, 1990] and the greenhouse gas budget, particularly for CO_2, but also for sulphur gases [*Kellogg et al.*, 1972; *Stoiber et al.*, 1987].

The Antarctic atmosphere is remarkably "clean" compared with the rest of the globe, particularly away from the coasts. This is due to factors such as (1) the existence of the Antarctic vortex (a wind and current system in and above the southern ocean which serves to insulate the continent from the invasion of air masses); (2) the low ratio of land to ocean and the small amount of industrialization in the southern hemisphere; and (3) the absence of large internal sources of contamination in Antarctica (although this is changing [see *Boutron and Wolff*, 1989]). Because the cleanliness of the Antarctic atmosphere provides the best available environment for

TABLE 1. Collection and Analytical Techniques Used for Plume, Fumarole, Soil Gas, and Snow Samples, 1989-1990

Species	Method	Reference
SO_2	$Zn(Ac)_2$ paper and colorimetry	*Faivre-Pierret* [1983], *Bel* [1972]
H_2S	$AgNO_3$ paper and fluorimetry	*Natusch et al.* [1972]
H_2SO_4	PDA-Br paper and colorimetry	*Dasgupta et al.* [1979]
HCl, HF	LiOH paper and potentiometry	*Faivre-Pierret* [1983]
Radioisotopes	cellulose filter and α counting	*Polian and Lambert* [1979], *Le Cloarec et al.* [1986]
SF_6	plastic bag and ECD-gas chromatography (GC)	
Particulates	Casella cascade impactor and PIXE analysis	*Cadle* [1975]
Fumarolic gases	evacuated flasks and GC analysis	*Sheppard and Giggenbach* [1985]
Snow	AAS (cations) and ion chromatography (anions)	
CO_2 in soils	portable CO_2 analyzer (SERVOMEX)	

ECD, electron captive detector; AAS, atomic absorption spectrophotometry.

studies of both current and historic global atmospheric compositions, the assessment of the nature and variability of internal sources which do exist assumes a greater importance than elsewhere.

Active volcanism (in the sense of degassing from surficial features at temperatures elevated above the ambient) is known to occur at four sites within the Antarctic continent and near offshore islands: Mount Erebus, Mount Melbourne, Mount Berlin, and Deception Island [*LeMasurier and Thomson*, 1990]. Of these, Mount Erebus is the "most active volcano in Antarctica and the southernmost active volcano on earth" [*Moore and Kyle*, 1990, p. 103]. The volcano contains a persistent, convecting, anorthoclase phonolite lava lake, or lakelets more recently, and undergoes small Strombolian degassing eruptions.

Not all gaseous emissions from volcanoes occur from the central vent or lava lakes. Most volcanoes have associated fumaroles, diffuse gas effusions, and hydrothermal systems. While the scarcity of liquid water may be a limitation on the size and extent of hydrothermal systems on Mount Erebus, ice towers (formed by the freezing out of moisture in warmed air from below the ground surface) suggest their presence [*David and Priestley*, 1909, 1914; *Holdsworth and Ugolini*, 1965; *Lyon and Giggenbach*, 1974; *Giggenbach*, 1976]. Fumaroles exist within the Main and Inner craters. Areas of bare rock and soil, supporting life-forms, are present on the upper slopes, suggesting subsurface warmth and possible effusion of volcanically derived gases. The mass of gases transferred to the atmosphere by diffuse degassing through the flanks of some volcanoes is very large [*Allard et al.*, 1989, 1991]. The CO_2 flux from Mount Erebus may also be very high compared to most volcanoes [*Gerlach*, 1991a, b].

The composition and fluxes of volcanic material in the Mount Erebus volcanic plume have been measured by a number of workers [*Polian and Lambert*, 1979; *Delmas*, 1982; *Radke*, 1982; *Symonds et al.*, 1985; *Rose et al.*, 1985; *Chuan et al.*, 1986; *Meeker*, 1988; *Chuan and Palais*, 1989; *Meeker et al.*, 1989; *Kyle et al.*, 1990]. Other studies of interest include those examining the composition of surface salts from Mount Erebus [*Keys*, 1980; *Keys and Williams*, 1981] and snow compositions affected by the plume [*Palais and Mosher*, 1989; *Palais et al.*, 1989].

The current period of activity, arising from the presence of the lava lake(s), has persisted since at least 1972 [*Giggenbach et al.*, 1973]. The area of the lava lake(s) and the volumes of SO_2 in the plume correlate [*Kyle et al.*, 1990]. An activity peak occurred 1983, with an SO_2 flux of 230 Mg/d, and a minimum occurred in 1984 (20 Mg/d) increasing to 70 ± 20 Mg/d in January 1991 [*Rose et al.*, 1985; *Kyle et al.*, 1991]. The plume close to the volcano has S/Cl of about 0.7 and Cl/F of about 2 (P. R. Kyle, personal communication, 1992); this chloride and fluoride may be significant components of the inland Antarctic snow anion content [*Kyle et al.*, 1990]. Polonium 210 has been found to be relatively high and of significance in the low radioactive environment of Antarctica [*Polian and Lambert*, 1979].

Particles containing gold, chromium, arsenic, and carbon have been postulated as characterizing the Mount Erebus plume [*Meeker*, 1988; *Chuan and Palais*, 1989; *Palais et al.*, 1989; *Kyle et al.*, 1990; *Palais et al.*, 1991]. The Mount Erebus plume contributes a small fraction of the total sulphate flux into Antarctica according to *Delmas* [1982], but this opinion is still under debate [*Radke*, 1991].

Chuan et al. [1986] identified both elemental sulphur and sulphuric acid in aerosols collected 13.5 km downwind of the volcano. They reported that sulphuric acid

was generally not found close to the volcano, except during small eruptions, despite its ubiquity in plumes elsewhere [e.g., *Martin et al.*, 1986; *Stoiber et al.*, 1980, 1981, 1986; *Rose et al.*, 1986; *Varekamp et al.*, 1984, 1986]. Further, the study by *Chuan et al.* [1986] suggested mechanisms by which various components are extracted or change character within the plume; for example, many of the salts identified at the crater rim by *Keys* [1980] and *Keys and Williams* [1981] were presumed to be deposited from the plume, or by reaction of plume components with rock. These observations indicate that studies of the Mount Erebus plume chemistry, if they are to be of significant use in the assessment of local sources of atmospheric contaminants within Antarctica, must investigate not only the chemical and physical state of the plume components but also the chemical reactions and physical processes that affect their transportation from their source.

SAMPLE COLLECTION

The Mount Erebus plume was sampled in December 1989 for a range of components simultaneously, using a combination of techniques and samplers as detailed in Table 1. Impregnated filters were used to trap and preserve reactive gases. Particulate components were collected on ultrapure polystyrene targets in a four-stage cascade impactor and analyzed by energy dispersive analysis of X rays (EDAX), scanning electron microscope (SEM), and particle-induced X ray emission (PIXE) analysis of the collector films. Radioisotopes in particulates were collected and analyzed by measurement of emitted radiation trapped on paper filters after high-volume collection; analyses were by M. F. Le Cloarec at Centre des Faibles Radioactivités, Gif sur Yvette, France.

An SF_6 tracer method was used to assess the fluxes of plume components. The intention was to lower cylinders containing compressed SF_6 to near the lava lake surfaces and trigger the release of the gas at a preset rate, collecting samples of the plume in plastic bags (polylaminate wine cask) at the crater rim for later analysis. Samples were collected for periods of up to 12 min per bag. It proved impossible to get the SF_6 cylinders to the bottom of the crater; instead, a cylinder was lowered from the floor of Main Crater into Inner Crater, to a depth of 70 m, which was about 70 m above the floor of Inner Crater. The concentration of SF_6 in the bag samples and the known release rate were used to calculate the flux of other plume components collected on filters at the same time and place.

All collections were made on the crater rim, on the northwest side (Figure 1). Weather conditions tended to be quite still during the expedition (wind speed less than 15 knots (7.7 m/s)), which generally meant that sampling on the rim resulted in the sampling of the margins of the plume.

Samples of snow were taken at points at various distances from the lava lake (from inside Main Crater, beside Upper National Science Foundation (NSF) Hut, on Fang Glacier, and on Cape Bird) for analysis of major and minor components, with the aim of determining the nature of the fallout from the plume as a function of distance. The detailed results of this study are to be published elsewhere; however, some preliminary results and comments are provided here.

Soil CO_2 fluxes were determined after drawing air across a covered $1\text{-}m^2$ area at a known rate and measuring the CO_2 concentration of that air, using a portable IR analyzer, after entrainment of any gases emanating from the soil. Soil CO_2 concentrations were determined by inserting a 6-mm tube into a hole made in the soil as far as was possible without disturbing the soil unduly (usually about 10 cm) and pumping the soil gas into the IR analyzer which was calibrated against air.

RESULTS AND DISCUSSION

Fluxes determined during a SF_6 release period of some 90 min on January 1, 1990, were determined to be as follows:

SO_2	2.4 Mg/d
H_2S	3.1 kg/d
H_2SO_4	0.19 to 7.1 Mg/d
Cl	6.5 Mg/d

Fluoride was determined at 0.021 Mg/d, but the low levels of fluoride on the filters were very close to that on the blanks, so there is little confidence in this result. These values are calculated in relation to the weighted mean dilution of the sampled SF_6 over the time periods listed in Table 2, which also lists the derived plume concentrations of the samples, that is, the mass of the component divided by the volume sampled. The H_2SO_4 concentrations determined were unexpectedly high and variable.

Details of the compositions of the plume particulates are given in Tables 3 and 4.

The measured SO_2 flux of 2.5 Mg/d is very low in comparison with a value for "December 1989" of 52 ± 21 Mg/d SO_2 (P. R. Kyle, personal communication, 1991). The SF_6 technique relies upon a number of assumptions, not all of which may have been satisfied.
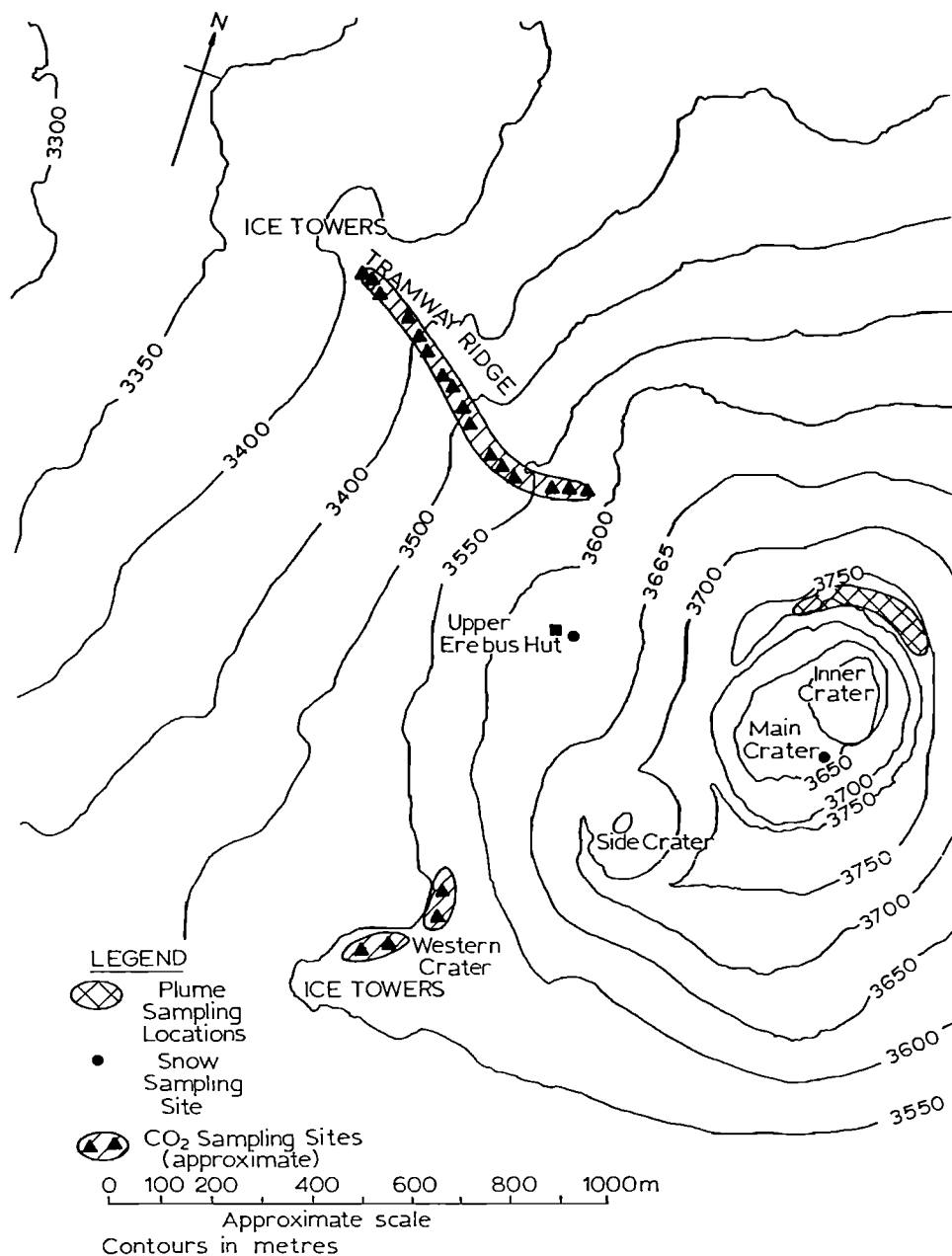
Fig. 1. Map of the upper slopes of Mount Erebus, showing the major features and the various sites mentioned in the text.

The accuracy of the calculated fluxes relies on an assumption of thorough mixing of the SF_6 with the volcanic plume and the homogeneity of the plume (other than by dilution with air). It is considered unlikely that the SF_6 mixed completely in the plume because of the high injection point, and that the portions that were sampled were more likely to contain more SF_6 than would have been the case if the plume was fully mixed, because of the proximity of the injection and sampling points. Our calculated fluxes are therefore likely to be low.

The SO_2 flux is nowadays usually measured with the use of the correlation spectrometer (COSPEC). Comprehensive reviews of the application of the technique to volcanic SO_2 emanations have been published elsewhere [e.g., Stoiber et al., 1987]. Kyle et al. [this

TABLE 2. Measured Concentrations of Plume Components and SF_6 Tracer Gas Collected on January 1, 1990

SF_6 Concentration, ppbv	SF_6 Duration, min	SO_2 Concentration, mg/m³	SO_2 Duration, min	Cl Concentration, mg/m³	Cl Duration, min	H_2S Concentration, μg/m³	H_2S Duration, min	H_2SO_4 Concentration, mg/m³	H_2SO_4 Duration, min	F Concentration, μg/m³	F Duration, min
0.47	2										
2.2	3	0.29	22	–	–	0.23	23	0.253	20	3.6	21
0.43	5										
1.6	10										
–											
1.4	10	0.30	20	0.55	21	0.57	20	0.063	20	1.3	20
0.79	10										
3.2	12	0.30	20	1.19	20	0.46	21	2.380	20	–	–
1.53	10	0.38	23	–	–	–	–	–	–	3.3	23

The SF_6 discharge rate was 0.915 g/s, determined by total weight loss over the discharge period. Cl and F analyses were performed by R. X. Faivre-Pierret, CEA, Grenoble, France. SO_2 analyses were by M. F. Le Cloarec, CFR, Gif sur Yvette, France. SF_6 analyses were by T. Clarkson, Meteorological Service, Wellington, New Zealand. H_2S and H_2SO_4 analyses were by D. Sheppard. The table is divided horizontally to represent the approximate comparable time periods over which the different samples were collected.

TABLE 3. Observations From SEM/EDAX Examinations of Particulates Collected on the Four-Stage Casella Cascade Impactor on January 2, 1990

Normal Size Range, μm	Maximum Particle Size Observed, μm	Nature	Core Composition	Surface Composition	Comments
0.4 to 0.7	6	Shards and grains	Mostly silicate?	Fe, S, Cu, Cl, Na, .K, Si. Up to 70% Cu, 35% Pb, 35%Fe, 25% S on surfaces.	Much very fine material, less than 0.1 μm.
0.7 to 2.0	8	Shards and grains	Silicates and salts Splattered droplet	Si, Cl, S, Cu, K, Ca, Mg Cl, S, Fe, Na, Si	
2.0 to 7.0		Rounded grains, agglomerates	Salts? Silicates Apatite	Pb, S, Al, Cu Na, Si, K, Cl, Ca, S Ca, P	
7.0 to 20	>100	Splattered deposit Shard	NaCl core 4 μm Phonolitic; Na, Al, Si, K, Ca, Fe	– –	Largely clear slide with large grains
		Splattered deposit Splattered deposit	Na, Si, Cl, Ca, Mg Na, Si, Cl, Ca, Mg, S	S, Cl, K, Na – –	usually coated with smaller grains.

volume] give a summary of all previous SO_2 flux estimations for Mount Erebus, all of which, with the exception of that of *Polian and Lambert* [1979], give fluxes considerably higher than those determined by us. It is likely that our results are inaccurate in terms of assessment of the fluxes; however, they have some validity in giving indications of compositions and compositional variations within the plume.

The mean [210]Po:SO_2 ratio measured on samples taken by us in the Mount Erebus plume was 167 pCi/mg, very much higher than that found for any other volcano for which measurements are known (M.-F. Le Cloarec, personal communication, 1991). Using our measure of SO_2 output of 2.4 Mg/d, Mount Erebus contributes about 0.4 Ci/d as [210]Po to the Antarctic atmosphere which is close to a determination in 1977 of 0.3 Ci/d [*Polian and Lambert*, 1979]. At an SO_2 flux of 52 Mg/d the [210]Po flux would be 8.7 Ci/d.

The particulates collected were dominantly very fine, less than 1 μm. Table 3 summarizes SEM and X ray analysis of the particles collected. The larger particles (some were greater than 100 μm) showed evidence of silicate glass shards; cubic crystal forms, composed of Na and Cl, presumably halite; splattered droplets up to perhaps 50 μm original diameter, containing both Cl

and S; and phases rich in Pb, Cu, and Fe associated with S, particularly in the finer fraction. S and Cl are almost ubiquitous in and on particles examined, sometimes as components of powdery coatings on larger grains.

PIXE analyses of targets from the cascade impactor are listed in Table 4. Cr has been noted as being anomalously high in some shards [cf. *Chuan and Palais*, 1989], but although Au has been found to be characteristic and ubiquitous in the Mount Erebus plume [*Meeker*, 1988; *Kyle et al.*, 1990; *Chuan and Palais*, 1989], it did not show up in our samples despite the PIXE method's being particularly sensitive to Au. Missing from the PIXE analyses are Na and F for instrumental reasons. These have been identified as almost always present in significant quantities on nucleopore filters collected on the crater rim (R. Lefevre, personal communication, 1990).

The Mount Erebus volcanic plume comprises four generically different components of different compositions. These are (1) the gas that escapes from the lava lakes' surfaces; (2) gas which emerges from the large and noisy fumarole(s) on the Inner Crater floor; (3) gas from smaller, cool (<100°C) fumaroles on the Main Crater floor and walls; and (4) air. Since the last two of these are very low in the sulphur- and metal-containing

TABLE 4. Elemental Quantities on Particulates Collected on the Different Stages of the Casella Cascade Impactor on January 2, 1990, as Determined by PIXE Analysis

Element	0.4–0.7 μm	0.7–2 μm	2–7 μm	7–20 μm
Si	18.7	18.2	17.9	91.2
K	288.4	36.7	11.2	17.3
Ca	2.3		1.9	13.8
Fe	12.8	3.7	3.2	12.6
P		1.4		11.4
S	258.2	54.4	10.9	10.9
Cl	159.7	21.3	12.7	12.9
Ti	0.7	0.23	4.21	1.76
V		0.06		
Cr		0.06		0.17
Co			0.01	0.19
Ni	0.02	0.01	0.35	0.21
Cu	0.18		0.08	1.64
As	3.48			
Br	5.45	0.44		
Rb	1.51	0.34		
Zr				0.91
Hg		0.20		
Pb	24.58	2.88	0.93	0.30

Analyses by L. Malmqvist, University of Lund, Sweden. Units of measure are nanograms.

components, they may be regarded as acting merely as dilutants (the fumaroles will contribute CO_2 and water vapor). The composition of the other two components must be expected to differ and to be modified by reaction with wall rock, particle agglomeration and precipitation, and heterogeneous reactions on particles carried in the plume as it rises. The presence of sublimed salts, contaminated snow, and staining on wall rocks and experiments on other volcanoes [Le Guern and Bernard, 1982] indicate that these processes not only occur but also must be considered as likely to be significant in the removal of some components, particularly metals, chloride, and sulphur.

Snow Composition

The incorporation of plume components into snow may be influenced by a number of mechanisms, such as the source of the snow (falling or blown), its location in relation to the volcanic center, the prevailing wind, and subsequent processes, as well as the state of the volcano itself. The variability in the concentrations with depth of snow at one site are presented in Figures 2a–2g. The sampling location, about 50 m from upper hut on Erebus, was in a 1-m-wide covered crack in a snowfield, about 0.5 km from the edge of Main Crater, and northwest of it. The ice cave may very well be the system explored in 1972 and 1974 [Lyon and Giggenbach, 1974; Giggenbach, 1976]. The walls of the crack below about 2 m from the surface were smooth and hard, as if eroded by warm air. Large clusters of ice crystals, each a few centimeters in diameter, at the top of the crack (which was about 5 m deep) attested to a long period of undisturbed circulation of moisture-laden air. Samples were taken from the walls of the crack, to its base, but the analyses presented in Figure 2 are from the top 1.4 m only and represent a continuous sampling over that interval. The deuterium composition of the ice shows that a complete annual cycle is probably represented in this interval, which is assumed to be an annual cycle, although this would seem to be a large accumulation for 1 year.

Large changes in concentration of most components analyzed are evident in the section sampled, with a general trend toward lower concentrations of all components with depth. This may well reflect an increase in volcanic degassing rates, and hence perhaps volcanic activity, but such analysis awaits the availability of seismic data covering that period. Other processes will influence the concentrations in the snow, such as dilution by incoming snow and surface sublimation of ice, as well as climatic effects (e.g., wind direction), while the nature of the components will be affected by reactions within the plume and differential fallout rates.
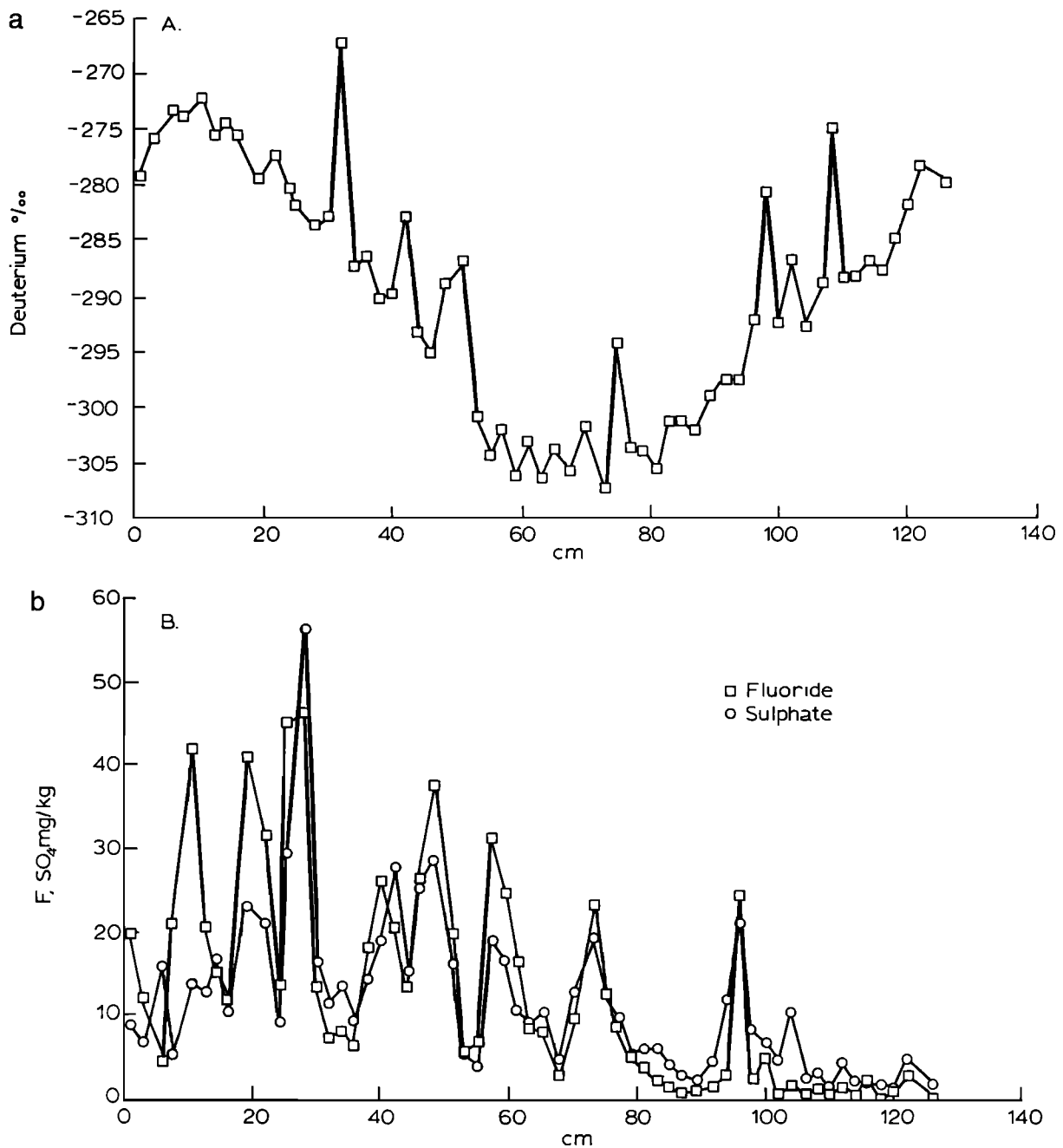
Fig. 2. Depth concentration profiles for snow samples taken from the snow cave near the upper hut, Mount Erebus.

Some observations can be made about the data presented in Figures 2a–2g. Most of the components show similar patterns suggesting that they travel and are deposited together, from the same source. Component ratios are not linear in any case. For example, the Na/K mass ratio is about 1.15 for samples containing less than 10 mg/kg Na, but at higher concentrations the ratio is lower and is quite variable; also, the F/SO$_4$ mass ratio is about 1.7 at SO$_4$ concentrations above 10 mg/kg. It is perhaps significant that Cl bears no constant relationship to either F or SO$_4$. In no case, though, does the F to Cl ratio fall below 0.25. Nor is chloride simply related to Na or K as might be expected if the dominant species containing these components were the chloride salts.

c

d
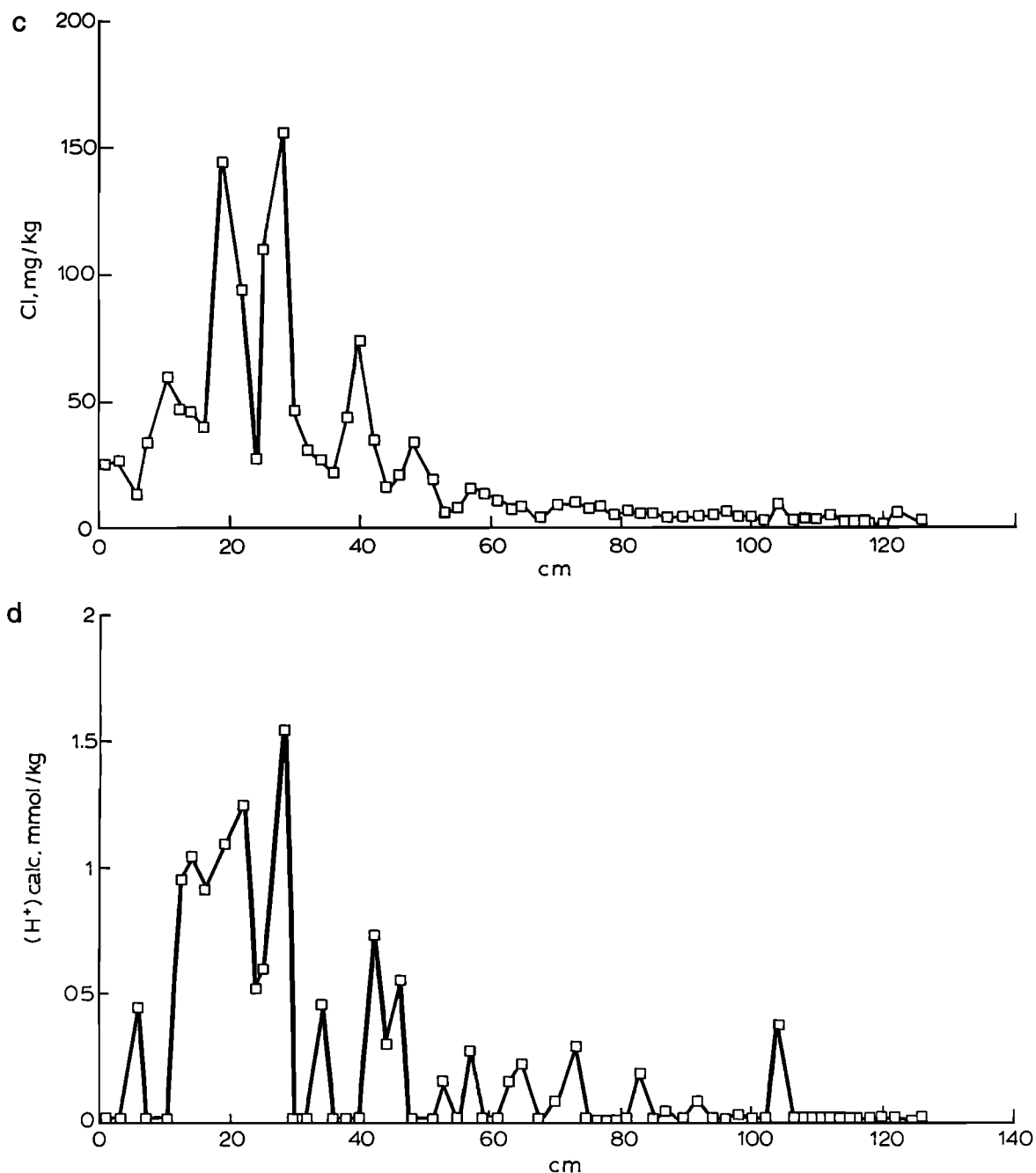
Fig. 2. (continued)

Where there is significant acidity (as calculated from solution pH), and less than 50 mg/kg Cl, the molar ratio of H⁺ to Cl is about 0.75 with a clear linear relationship, suggesting that the dominant acid in the snow is HCl at times, but when concentrations are higher, the other acid gases (HF and H_2SO_4) become significant. We specifically detected high levels of sulphuric acid in the plume,

a new finding for the Mount Erebus plume but normal for other volcanoes.

Flank Degassing

The ice towers and warm ground on the flanks of the Main Crater of Mount Erebus attest to mass transport of

e

□ Iron
o Aluminium

f

□ Sodium
o Potassium
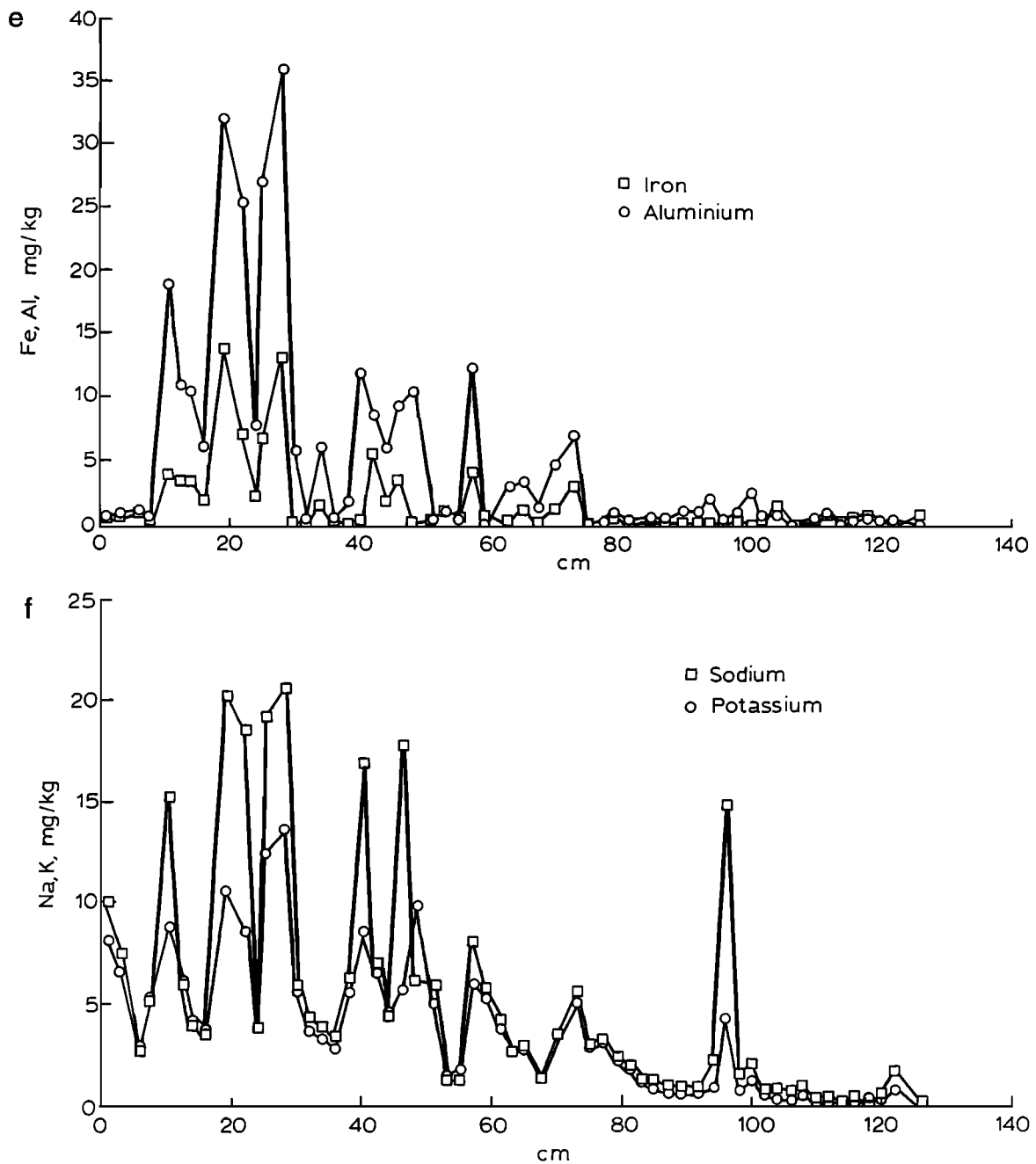
Fig. 2. (continued)

vapors to the ground surface. No reports of the composi-
tions of these vapors have been presented. The only
chemical analysis known showed the presence of a little
excess CO_2 in air (W. F. Giggenbach, personal commu-
nication, 1991); a sample of fumarolic gas collected by
one of us (F.L.G.) in 1977 from an outer crater fumarole
has been analyzed for the δD composition of the H_2O

(approximately -140 per mil, in the middle of the local
meteoric water range [*Allard*, 1983]).

Attempts were made to measure CO_2 diffusion rates
through the flanks of the main crater, and the gases
entering the base of the ice towers were sampled. The
measurement of CO_2 flux directly, in snow free areas of
fine soils, did not detect any flow above the background
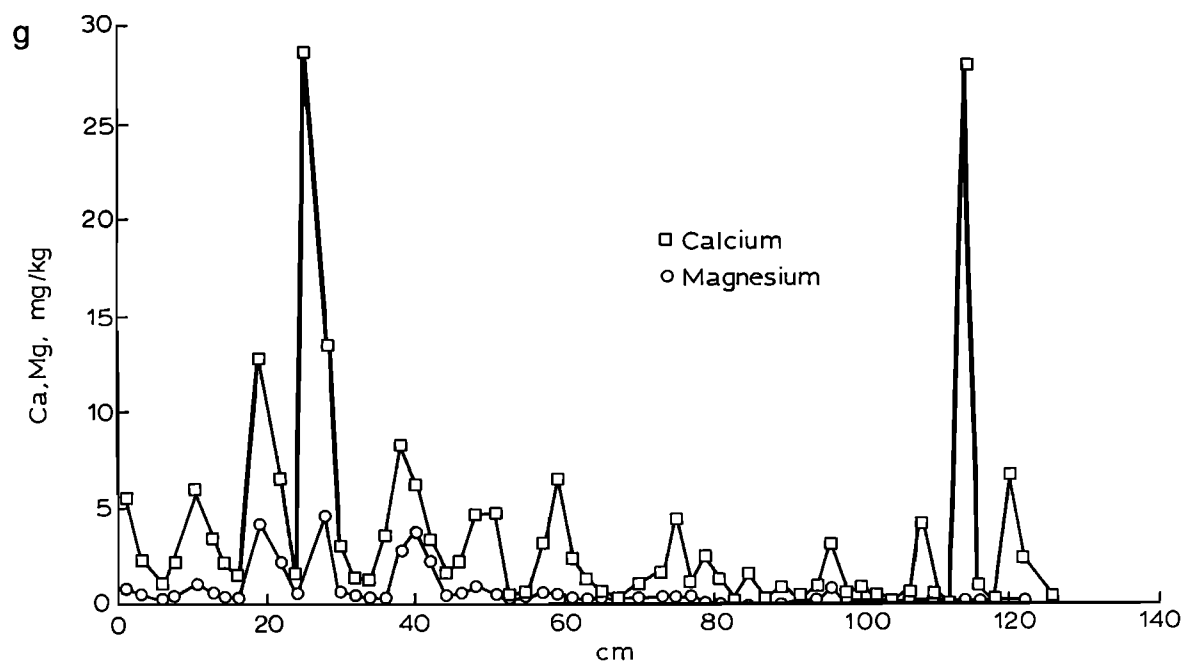
Fig. 2. (continued)

rate measured on scree-covered permafrost on Black Island of about 0.002 m³ CO_2/(m² h). This was attempted in two areas near Western Crater (Figure 1), close to an alignment of ice towers, but we did not measure concentrations significantly different from air. However, at four sites within these areas (out of six sites tested), concentrations of CO_2 within the soil were significantly above the ambient air concentrations, at up to 0.6%. These observations are interpreted to show that there is a buildup of CO_2 in the soils but that the rate of flow from these soils is too low to be detected by the equipment that we had available. Further surveys on Tramway Ridge (Figure 1) in scree with hard underlying ice, as well as in areas of rust-colored fine powdery soil, gave no indications that CO_2 was elevated in the surface layer above that of air, despite this ridge's containing an alignment of ice towers.

The analyses of a 42°C gas sample collected in an ice tower on Tramway Ridge gave an air composition with 1.34% (by volume) of CO_2 An 80°C fumarole on the Main Crater wall contained 4.0% CO_2. Together with the evidence of elevated CO_2 levels in the soils, and assuming the CO_2 to be of volcanic origin, which, given the absence of life-forms in the places sampled, seems a reasonable assumption, these findings suggest that Mount Erebus does degas through its upper flanks, but that this degassing is not as diffuse as that of Mount Etna [Allard et al., 1991], is restricted by underlying ice

sheets to areas and lineations marked by the ice towers and some bare soil areas, and is at a comparatively low rate. The gases may derive from recent lava flows, which are postulated to be the heat sources for the ice towers (P. R. Kyle, personal communication, 1992).

The composition of the magma in the lava lakes changes with time, particularly in relation to the volatiles, as the rate of injection of fresh magma and/or magmatic gases into the lake varies, and consequently, the composition of the gases evolved varies. This may be reflected in the activity of the volcano, gentle effusion or violent eruption, for instance. The rate of degassing through an orifice will affect in particular the quantity of volcanic glass, rock fragments, and encrustation material that is entrained into the plume. In large eruptions this "ash" can be the major component; in steady fumaroles it can be practically absent. The Erebus plume generally contains minor quantities of these materials, such as shards, and aggregates of typical fumarolic or vent-lining materials, for example, sulphur, NaCl, and Na_2SO_4 [Chuan et al., 1986; Meeker, 1988]. During the periodic eruptions that are heard from the volcano, volcanic bombs are injected into the plume, some several meters in diameter. Most of these fall back into the crater. It is likely that a complete size range of particles enters the plume from the volcano at some time, but generally, only the fine particles make it over the crater rim.

The effect on plume chemistry caused by the diminution in extent of the lakes may be that peripheral fumaroles will tend to cool, and the evolved gas compositions will change, principally as components are deposited out on surfaces. One likely effect would be an increase in the proportion of H_2S in the plume from such peripheral fumaroles [Giggenbach and Sheppard, 1989]. Not only do the hot gases react with surrounding rocks by depositing sublimates, but they are also able to extract components from rocks as they pass through or over them; typical components are the volatiles, such as H_2O, S, Cl, and, by reaction, metals, such as volatile halides and sulphides. The extent of such interactions is dependent upon the extent of physical interaction with the rocks, the temperature and composition of the gases, and the composition of the rocks.

Interaction of the magma with groundwaters within Mount Erebus may be minimal at the shallow levels (i.e., above sea level) given the lack of liquid water able to recharge the system. The mountain is composed substantially of ice, at least in its outer layers. The consequent absence of freely percolating groundwaters within the volcano is an unusual situation which may have significant effects on the magma chemistry and hence on the plume chemistry. Chuan et al. [1986] have commented that the dry atmosphere may have affected the production of H_2SO_4 within the plume, as a consequence of the air temperature. Our findings have shown that H_2SO_4 is produced at least on the periphery of the plume, possibly because this is where the influence of cooler and wetter fumaroles is greatest.

The chemical composition of a volcanic plume derived from hot magma is dramatically affected by interaction with air because of oxidation reactions. Reduced sulphur burns about fumarole vents [Rose et al., 1986] to produce SO_2, and probably SO_3, which in turn reacts with water to produce H_2SO_4. The latter forms, or is formed in, the aerosol particles which are the cause of the blue smoke, or haze, characteristic of volcanic fumaroles and plumes [Cadle et al., 1967; Cadle and Frank, 1968; Naughton et al., 1974]. Not all reactions are due to direct oxidation; they can be due to nucleation and formation of aerosols, a consequence of cooling. Subsequent reactions between solid and gas phases, for example the formation of metal sulphides by reactions such as

$$PbCl_{2(s)} + H_2S_{(g)} <=> PbS_{(s)} + 2HCl_{(g)}$$
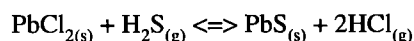
[Bernard and Le Guern, 1986], provide the source of the halogen acids (HCl, HF, HBr) found in volcanic plumes and fumaroles, but not in the magma. Many components are deposited from plumes, as sublimates,

after the gases leave the magma or fumarole. The nature of these is dependent upon temperature and the availability of oxygen. These components will end up in the surface snows on Mount Erebus, as we have found, and as we have shown, these snows include components such as alkali earth metals, and aluminium and iron in significant quantities (Figures 2f and 2g).

The fallout of solid materials from a plume obviously affects the composition of the plume, by the simple act of removing material; falling ash and aerosol particles also take with them finer materials and liquid droplets as adhering phases, nucleated on the aerosol particle. Agglomeration of finer particles is an active process within the atmosphere and volcanic plumes and leads to the fallout of, for instance, large sulphur particles. Such processes need to be taken into account in the assessment of the contribution of material to the Antarctic biosphere from the Mount Erebus plume, or indeed, from any volcano.

CONCLUSIONS

An initial investigation of the input of components into the Antarctic atmosphere from the Mount Erebus volcano has provided some new data. There is a need for more work to be done to ascertain what, how far, and in what form the various components are dispersed. Problems which need to be addressed include (1) sampling in such a manner as to take account of inhomogeneity in the plume, at the crater rim level; (2) measuring quantitatively the compounds formed in the plume and how they change with time and distance; (3) measuring the deposition from the plume and the variations caused by factors such as the activity of the volcano, the season, the climatic conditions, and the sampling location; and (4) quantifying the fluxes of components emitted from locations other than the inner crater, such as the ice towers, warm ground, and flanking craters.

We have been able to provide new data on the nature and quantities of many components emitted and deposited, such as the sulphur species. While we confirmed that H_2S is present in minor amounts, our evidence is also that H_2SO_4 is present in the plume at the crater rim. The SO_2 flux calculated by use of tracer injection on one day was very much lower than would have been expected from other measurements of SO_2 flux. This may have been due to plume inhomogeneity, so that the samples taken at the crater rim were not representative of the plume as a whole.

Snow samples collected within 500 m of the crater rim show heavy contamination with volcanic plume components, in a manner which may allow the elucidation of the speciation of plume fallout components. The

composition of snows from more sites at different distances from the crater will also give information on the processes leading to fallout and hence some indication of what components of the plume are dispersed widely and in what quantities.

We established that CO_2 is present in elevated concentrations in soils at some sites on the main crater flanks, but were unable to measure the flux from this source. Ice towers are discrete sources of volcanically derived gases to the atmosphere.

REFERENCES

Allard, P., The origin of hydrogen, carbon, sulphur, nitrogen and rare gases in volcanic exhalations: Evidence from isotope geochemistry, in *Forecasting Volcanic Events*, edited by H. Tazieff and J. C. Sabroux, pp. 337-386, Elsevier, New York, 1983.

Allard, P., J. C. Baubron, J. Carbonelle, D. Dajlevic, J. Le Bronec, M. C. Robe, P. Zettwoog, and J. P. Toutain, Diffuse soil degassing from volcanoes: Geochemical and volcanological implications (abstract), in Proceedings of the General Assembly on Continental Magmatism: International Association of Volcanology and Chemistry of Earth's Interior, *Bull. 131*, p. 3, N. M. Bur. of Mines and Miner. Resour., Socorro, 1989.

Allard, P., J. Carbonnelle, D. Dajlavic, J. Le Bronec, P. Morel, M. C. Robe, J. M. Maurenas, R. Faivre-Pierret, D. Martin, J. C. Sabroux, and P. Zettwoog, Eruptive and diffuse emissions of CO_2 from Mount Etna, *Nature, 351*, 387-391, 1991.

Arnold, F., T. Bürke, and S. Qiu, Evidence for stratospheric ozone-depleting heterogeneous chemistry on volcanic aerosols from El Chichón, *Nature, 348*, 49-50, 1990.

Bel, M.-J., Contribution à l'étude d'une méthode d'échantillonnage sur support sec du dioxyde de soufre en pollution atmosphérique, D.Pharm. thesis, 68 pp., Univ. Paul Sabatier, Toulouse, France, 1972.

Bernard, A., and F. Le Guern, Condensation of volatile elements in high temperature gases of Mount St. Helens, *J. Volcanol. Geotherm. Res., 28*, 91-105, 1986.

Boutron, C. F., and E. W. Wolff, Heavy metal and sulphur emissions to the atmosphere from human activities in Antarctica, *Atmos. Environ., 23*, 1669-1675, 1989.

Cadle, R. D., *The Measurement of Airborne Particles*, 342 pp., John Wiley, New York, 1975.

Cadle, R. D., and E. R. Frank, Particles in the fume from the 1967 Kilauea eruption, *J. Geophys. Res., 73*, 4780-4783, 1968.

Cadle, R. D., A. F. Wartburg, E. R. Frank, and J. P. Lodge, Particles in volcanic fume, *Nature, 213*, 581, 1967.

Chuan, R. L., and J. Palais, Do gold, chromium oxide, and carbon-containing particles provide tracers of Mount Erebus emissions?, Review, *Antarct. J. U. S., 24*, 215-217, 1989.

Chuan, R. L., J. Palais, W. I. Rose, and P. R. Kyle, Fluxes, sizes, morphology and compositions of particles in the Mount Erebus volcanic plume, December 1983, *J. Atmos. Chem., 4*, 467-477, 1986.

Dasgupta, P. K., G. L. Lundquist, and P. W. West, Specific deter-

mination of aerosol sulfuric acid in the presence of ammonium sulfate: A laboratory study, *Atmos. Environ., 13*, 767-774, 1979.

David, T. W. E., and R. E. Priestley, Notes in regard to Mount Erebus, in *The Heart of the Antarctic*, vol. 2, edited by E. H. Shackleton, pp. 308-310, William Heineman, London, 1909.

David, T. W. E., and R. E. Priestley, Glaciology, physiography, stratigraphy, and tectonic geology of south Victoria Land, in Reports on the Scientific Investigations of the British Antarctic Expedition 1907-09, *Geology, 1*, 319 pp., 1914.

Delmas, R. J., Antarctic sulphate budget, *Nature, 299*, 677-678, 1982.

Faivre-Pierret, R., SO_2, HCl and HF detection and dosing in the volcanic gas phase, in *Forecasting Volcanic Events*, edited by H. Tazieff and J. C. Sabroux, pp. 399-409, Elsevier, New York, 1983.

Gerlach, T., Etna's greenhouse pump, *Nature, 351*, 352-353, 1991a.

Gerlach, T. M., Present-day CO_2 emissions from volcanos, *Eos Trans. AGU, 72*, 249, 1991b.

Giggenbach, W. F., Geothermal ice caves on Mt Erebus, Ross Island, Antarctica, *N. Z. J. Geol. Geophys., 19*, 365-372, 1976.

Giggenbach, W. F., and D. S. Sheppard, Variations in the temperature and chemistry of White Island fumarole discharges 1972-85, in *The 1976-82 Eruption Sequence at White Island Volcano (Whakaari), Bay of Plenty, New Zealand*, edited by B. F. Houghton and I. A. Nairn, pp. 119-126, New Zealand Geological Survey, Lower Hutt, New Zealand, 1989.

Giggenbach, W. F., P. R. Kyle, and G. L. Lyon, Present volcanic activity on Mount Erebus, Ross Island, Antarctica, *Geology, 1*, 135-136, 1973.

Hofmann, D. J., and S. Solomon, Ozone destruction through heterogeneous chemistry following the eruption of El Chichón, *J. Geophys. Res., 94*, 5029-5041, 1989.

Holdsworth, G., and F. C. Ugolini, Fumarolic ice-towers on Mt Erebus, Ross Island, Antarctica, *J. Glaciol., 5*, 878-879, 1965.

Johnston, D. A., Volcanic contribution of chlorine to the stratosphere: More significant to ozone than previously estimated?, *Science, 209*, 491-493, 1980.

Kellogg, W. W., R. D. Cadle, E. R. Allen, A. L. Lazrus, and E. A. Martell, The sulphur cycle, *Science, 175*, 587-596, 1972.

Keys, J. R., Salts and their distribution in the McMurdo region, Antarctica, Ph.D. thesis, Victoria Univ., Wellington, New Zealand, 1980.

Keys, J. R., and K. Williams, Origin of crystalline, cold desert salts in the McMurdo region, Antarctica, *Geochim. Cosmochim. Acta, 45*, 2299-2309, 1981.

Kyle, P. R., K. Meeker, and D. Finnegan, Emission rates of sulfur dioxide, trace gases and metals from Mount Erebus, Antarctica, *Geophys. Res. Lett., 17*, 2125-2128, 1990.

Kyle, P. R., G. Zreda-Gostynska, L. Sybeldon, K. Meeker, D. Finnegan, and E. Gladney, Volcanic emissions from Mount Erebus, Ross Island, Antarctica, in Pre-Conference Abstracts, Symposium on Tropospheric Chemistry in the Antarctic Region, Boulder, Colorado, *Spec. Rep. 91-10*, p. 28, U.S. Army Cold Regions Res. and Eng. Lab., Hanover, N. H., June 1991.

Kyle, P. R., L. M. Sybeldon, W. C. McIntosh, and K. Meeker, Sulphur dioxide emission rates from Mount Erebus, Antarctica,

this volume.

Lambert, G., M.-F. Le Cloarec, and M. Pennisi, Volcanic output of SO_2 and trace metals: A new approach, *Geochim. Cosmochim. Acta, 52,* 39-42, 1988.

Le Cloarec, M.-F., G. Lambert, J. C. Le Roulley, and B. Ardouin, Long-lived radon decay products in Mount St. Helens emissions: An estimation of the magma reservoir volume, *J. Volcanol. Geotherm. Res., 28,* 85-89, 1986.

Le Guern, F., and A. Bernard, A new method for sampling and analysing volcanic sublimates--Application to Merapi Volcano, Java, *J. Volcanol. Geotherm. Res., 12,* 133-146, 1982.

LeMasurier, W. E., and J. W. Thomson (Eds.), *Volcanoes of the Antarctic Plate and Southern Oceans, Antarct. Res. Ser.,* vol. 48, 487 pp., AGU, Washington, D. C., 1990.

Lyon, G. L., and W. F. Giggenbach, Geothermal activity in Victoria Land, Antarctica, *N. Z. J. Geol. Geophys., 17,* 511-521, 1974.

Martin, D., B. Ardouin, G. Bergametti, J. Carbonelle, R. Faivre-Pierret, G. Lambert, M. F., Le Cloarec, and G. Sennequier, Geochemistry of sulfur in Mount Etna plume, *J. Geophys. Res., 91,* 12,249-12,254, 1986.

Meeker, K., The emission of gases and aerosols from Mount Erebus Volcano, Antarctica, M.S. thesis, 172 pp., N. M. Inst. of Mining and Technol., Socorro, Oct. 1988.

Meeker, K., P. R. Kyle, D. Finnegan, and R. Chuan, Chlorine and trace element emissions from Mount Erebus, Antarctica (abstract), in Proceedings of the General Assembly on Continental Magmatism: International Association of Volcanology and Chemistry of Earth's Interior, *Bull. 131,* p. 184, N. M. Bur. of Mines and Miner. Resour., Socorro, 1989.

Moore, J. A., and P. R. Kyle, Mount Erebus, in *Volcanoes of the Antarctic Plate and Southern Oceans, Antarct. Res. Ser.,* vol. 48, edited by W. E. LeMasurier and J. W. Thomson, pp. 103-108, AGU, Washington, D. C., 1990.

Natusch, D. F. S., H. B. Klonis, H. D. Axelrod, R. J. Teck, and J. P. Lodge, Sensitive method for measurement of atmospheric hydrogen sulphide, *Anal. Chem., 44,* 2067-2070, 1972.

Naughton, J. J., V. A. Lewis, D. Hammond, and D. Nishimoto, The chemistry of sublimates collected directly from lava fountains at Kilauea Volcano, Hawaii, *Geochim. Cosmochim. Acta, 38,* 1679-1690, 1974.

Nriagu, J. O., A global assessment of natural sources of atmospheric trace metals, *Nature, 338,* 47-49, 1989.

Palais, J. M., and B. W. Mosher, Elemental tracers of volcanic emissions in Antarctic aerosol and snow samples, Reviews *Antarct. J. U. S., 24,* 217-218, 1989.

Palais, J. M., R. Chuan, and M. J. Spencer, Soluble and insoluble impurities in snow samples from Ross Island, Antarctica, Review, *Antarct. J. U. S., 24,* 89-90, 1989.

Palais, J., B. W. Mosher, and D. Lowenthal, Sources of contaminants in Antarctic snow, in Pre-Conference Abstracts, Symposium on Tropospheric Chemistry in the Antarctic Region, Boulder, Colorado, *Spec. Rep. 91-10,* p. 45, U.S. Army Cold Regions Res. and Eng. Lab., Hanover, N. H., June 1991.

Polian, G., and G. Lambert, Radon daughters and sulfur output

from Erebus Volcano, Antarctica, *J. Volcanol. Geotherm. Res., 6,* 125-137, 1979.

Radke, L. F., Sulphur and sulphate from Mt Erebus, *Nature, 299,* 710-712, 1982.

Radke, L. F., Antarctic sulphate: Erebus considered, in Pre-Conference Abstracts, Symposium on Tropospheric Chemistry in the Antarctic Region, Boulder, Colorado, *Spec. Rep. 91-10,* p. 48, U.S. Army Cold Regions Res. and Eng. Lab., Hanover, N. H., June 1991.

Rose, W. I., R. L. Chuan, and P. R. Kyle, Rate of sulphur dioxide emission from Erebus Volcano, Antarctica, December 1983, *Nature, 316,* 710-712, 1985.

Rose, W. I., R. L. Chuan, W. F. Giggenbach, P. R. Kyle, and R. B. Symonds, Rates of sulfur dioxide and particle emissions from White Island Volcano, New Zealand, and an estimate of the total flux of major gaseous species, *Bull. Volcanol., 48,* 181-188, 1986.

Sheppard, D. S., and W. F. Giggenbach, Methods for the analysis of geothermal and volcanic waters and gases, *Rep. C.D. 2364,* Dep. of Sci. and Ind. Res., Wellington, New Zealand, Sept. 1985.

Stoiber, R. E., S. N. Williams, and L. L. Malinconico, Mount St. Helens, Washington, 1980 volcanic eruption: Magmatic gas component during the first 16 days, *Science, 208,* 1258-1259, 1980.

Stoiber, R. E., S. N. Williams, L. L. Malinconico, D. A. Johnston, and T. J. Casadevall, Mt. St. Helens: Evidence of increased magmatic gas component, *J. Volcanol. Geotherm. Res., 11,* 203-212, 1981.

Stoiber, R. E., S. N. Williams, and B. J. Huebert, Sulfur and halogen gases at Masaya caldera complex, Nicaragua: Total flux and variations with time, *J. Geophys. Res., 91,* 12,215-12,231, 1986.

Stoiber, R. E., S. N. Williams, and B. Huebert, Annual contribution of sulphur dioxide to the atmosphere by volcanoes, *J. Volcanol. Geotherm. Res., 33,* 1-8, 1987.

Symonds, R. B., P. R. Kyle, and W. I. Rose, SO_2 emission rates and the 1984 activity at Mt. Erebus Volcano, Antarctica (abstract), *Eos Trans. AGU, 66,* 417, 1985.

Varekamp, J. C., J. F. Luhr, and K. L. Prestegaard, The 1982 eruptions of El Chichón Volcano (Chiapas, Mexico): Character of the eruptions, ash-fall deposits, and gas phase, *J. Volcanol. Geotherm. Res., 23,* 39-68, 1984.

Varekamp, J. C., E. Thomas, M. Germani, and P. R. Busek, Particle geochemistry of volcanic plumes of Etna and Mount St. Helens, *J. Geophys. Res., 91,* 12,233-12,248, 1986.

D. S. Sheppard, Institute of Geological and Nuclear Sciences, Lower Hutt, New Zealand

F. Le Guern, CFR/Centre National de la Recherche Scientifique, Saclay, France

B. W. Christenson, Institute of Geological and Nuclear Sciences, Wairakei Research Centre, Taupo, New Zealand

DISPERSAL OF VOLCANO-DERIVED PARTICLES FROM MOUNT EREBUS IN THE ANTARCTIC ATMOSPHERE

R. L. Chuan

Femtometrics, Costa Mesa, California

Emission rates of up to 20 megagrams (Mg) per day of particles, smaller than about 50 μm, have been measured in the eruption plume from Mount Erebus. Being the only local source of volcanic aerosols, it is possible to trace their dispersal over long distances from the volcano. By matching the size distribution, particle morphology, and elemental composition of the aerosol in the ambient atmosphere to those measured directly in the plume, volcano-derived particles from Mount Erebus have been traced as far as the south pole and to an altitude of 8 km.

INTRODUCTION

Small particles emitted from Mount Erebus were directly measured by sampling at the ground level on the crater rim and by aerial sampling in the plume above the crater. Surface sampling was only feasible when there were no explosive eruptions, whereas aerial sampling was practical only when the emission rate was high enough to make it possible to collect measurable quantities of particles during a short passage through the plume with an aircraft. We have one good set of samples acquired by aircraft sampling in December 1983 when Mount Erebus had more frequent strombolian eruptions [*Chuan et al.,* 1986]. During later seasons Erebus was sampled directly at the crater, and several sets of samples were acquired. Ambient aerosols were also collected on aircraft flights from McMurdo Station to outlying stations (Table 1).

Both ground and aerial samples were collected with a quartz crystal microbalance cascade impactor (QCM), which measures in real time the aerosol mass concentration in segregated size bands and retains the particles for postsampling analysis by scanning electron microscopy (SEM) and energy dispersive X ray analysis [*Chuan,* 1975].

DESCRIPTION OF EREBUS PARTICLES

Differences in the particle types depend on the eruptive state of the volcano. During the 1983–1984 season, when strombolian eruptions were frequent, the dominant particles were glass shards, elemental sulfur crystals, silica and salts (KCl, K_2S, NaCl), some mantled in sulfuric acid, and oxides of iron and chromium. The highest aerosol mass concentration encountered in sampling through the plume was in excess of 300 μg m^{-3}, with a mass median diameter of over 10 μm. During noneruptive periods when the volcano was fuming, samples collected at the crater rim did not contain sulfuric acid or elemental sulfur. Instead, hydrated hydrogen chloride was often found. Crystalline elemental gold was also often present [*Meeker et al.,* 1991]. We have not seen elemental gold in samples collected at other active volcanoes and suggest it is a unique signature of the aerosol emissions from Mount Erebus. The aerosol mass concentration measured at the crater rim was highly variable and depended on the state of activity and wind, but it was generally of the order of a few hundred micrograms per cubic meter, with a mass median diameter of about 10 μm.

Particle flux was determined by flying through the plume and measuring aerosol concentration profiles. During December 1983 when small strombolian eruptions were common, the particle flux was thus determined to average 21 Mg d^{-1} [*Chuan et al.,* 1986]. For the same period the SO_2 flux measured by correlation spectrometer was 230 Mg d^{-1} [*Rose et al.,* 1985], giving an SO_2 to particle flux ratio of 14. If the same ratio is used for 1987 through the end of 1989 when the SO_2 flux ranged from 25 to 44 Mg d^{-1} [*Kyle et al.,* 1990, this

TABLE 1. Ambient Aerosol Characteristics

Data Set	Season/Date	Sampling Path	Wind, deg	Concentration, $\mu g\ m^{-3}$	MMD, μm	Aerosol Type	SO_2 Flux, $Mg\ d^{-1}$
				1983–1984			
225	Dec. 7, 1983	McM-Pole		11.6	12	1, 2, 3	230
				1986–1987			
268	Jan. 6, 1987	McM-Pole		0.2	0.2	1	25
				1987–1988			
286	Dec. 3, 1987	McM-Pole		0.3	2.0	1, 2, 3, 4	44
288	Dec. 21, 1987	McM-Pole		0.2	0.3	1, 3, 4, 5	
				1988–1989			
298	Dec. 24, 1988	McM-Siple		0.17	0.5	1	27
300	Dec. 28, 1988	McM-Byrd		0.24	0.2	1	
302	Jan. 3, 1989	McM-Pole	090	0.56	1.9	1, 4	
303	Jan. 5, 1989	McM-Pole	206	0.22	0.4	1	
304	Jan. 6, 1989	McM-Pole	285	0.56	3.2	1, 2, 3	
304	Jan. 6, 1989	Pole-McM	080	0.38	0.3	1	
306	Jan. 10, 1989	McM-Pole	060–340	0.66	3.3	1, 2, 4	
308	Jan. 13, 1989	McM-Byrd	330	0.2	0.2	1	

MMD, mass median diameter. SO_2 flux averaged over November and December. Aerosol types: 1, sulfuric acid (background aerosol of nonvolcanic origin); 2, salts; 3, silicates; 4, crystalline Au; 5, F. McM, McMurdo Station; Byrd Station; Siple, Siple Station; Pole, South Pole Station.

volume], the particle flux was an order of magnitude lower, at about 2 Mg d^{-1}.

During the 1983–1984 season when Erebus had frequent strombolian eruptions, only one long-distance sampling flight was made, from McMurdo to the south pole. In subsequent years when the volcano was relatively quiet, more than 10 long flights over different parts of the continent were made. The ambient aerosol concentration was from 0.1 to 1 $\mu g\ m^{-3}$, similar to the background aerosol concentration over the Antarctic continent. Thus concentration alone was not a sufficient criterion for identifying volcanic aerosols from Mount Erebus. Identifications were made using data on size distributions and particle composition. Since extensive
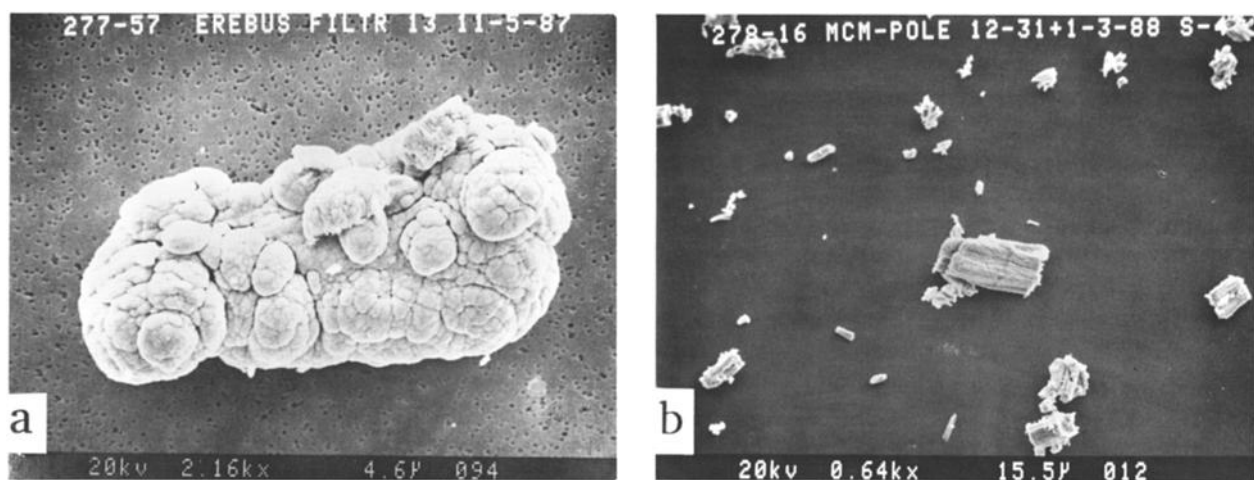
Fig. 1. Elemental crystalline gold particles from Mount Erebus emissions: (*a*) 45-μm gold particle recovered from snow pit 13 km from Erebus summit and (*b*) gold particles collected at 8 km altitude on flight from McMurdo to south pole. Crystals are viewed on sides.
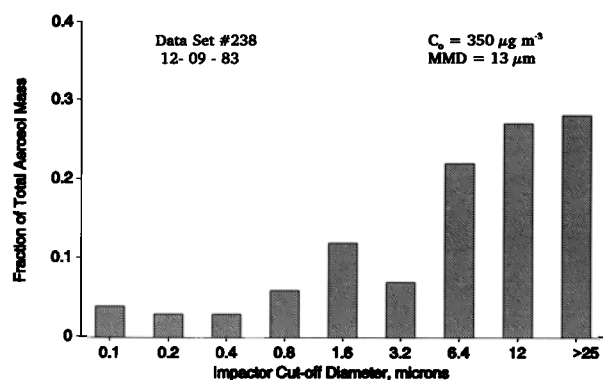
Fig. 2. Distribution of aerosol mass among nine size bands from 0.1 μm to larger than 25 μm, from direct sampling of plume from Mount Erebus during a period of relatively high activity of the volcano. The high average aerosol mass concentration of 350 μg m^{-3} and large mass median diameter of 13 μm of the particles are presumably related to the high activity, which also correlates with a high SO_2 emission rate of 230 Mg d^{-1} [*Rose et al.*, 1985].

analyses of a fairly large data base from over 20 aerial and crater rim samples have established crystalline elemental gold as a unique Erebus signature particle [*Meeker et al.*, 1991; R. L. Chuan and J. M. Palais, unpublished data, 1991], we have used it as the identifying particle to trace the dispersal of particles from Mount Erebus. Some examples of these gold particles are shown in Figure 1. The mass median diameter of the aerosol particles was used to supplement the matching of ambient atmosphere aerosols with Mount Erebus emissions, especially when a particular sample did not contain the signature gold particles. Figure 2 shows the aerosol size distribution for the plume during the active period of December 1983, for which the total aerosol mass concentration is 350 μg m^{-3}, and the mass median diameter is 13 μm. Some representative particles in this plume are shown in Figure 3.

During the less active period from 1985 through 1989 the particle flux directly from Erebus was too small to be measured with the techniques used here. However,

Fig. 3. (Opposite) Representative particles from Erebus plume during period of relatively high activity: (*a*) submicron sulfuric acid droplets and some silicate aggregates mantled in acid, (*b*) elemental sulfur crystals presumably formed by nucleation from vapor state, and (*c*) silicate aggregate particle covered with sulfuric acid. These three types of particles have only been found when Erebus is in an active state, with small explosive eruptions.
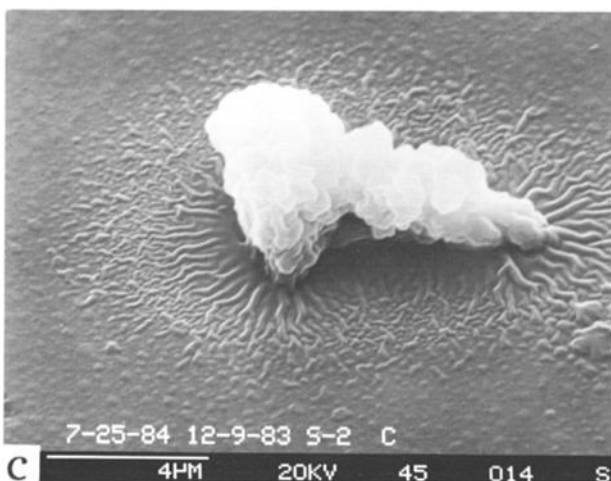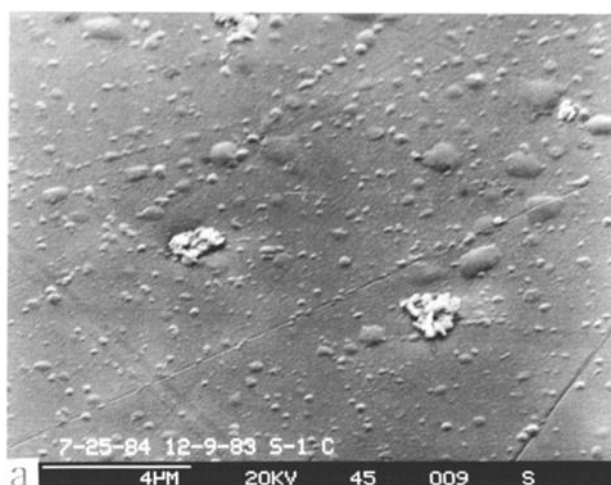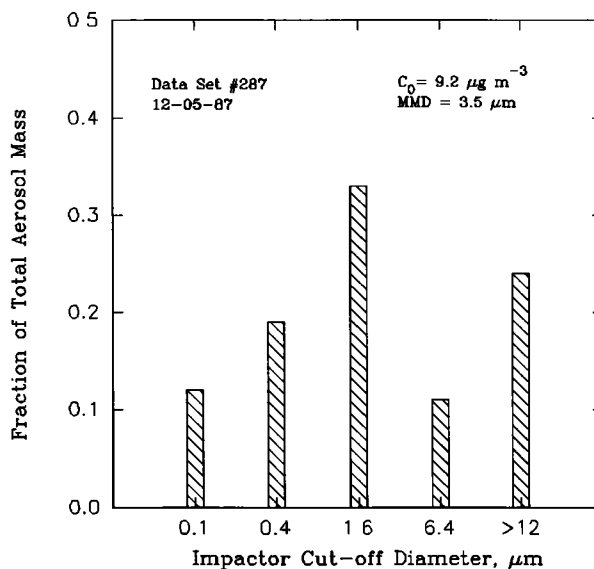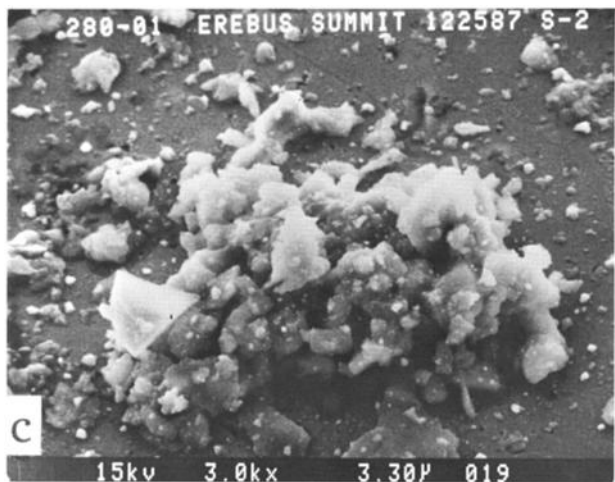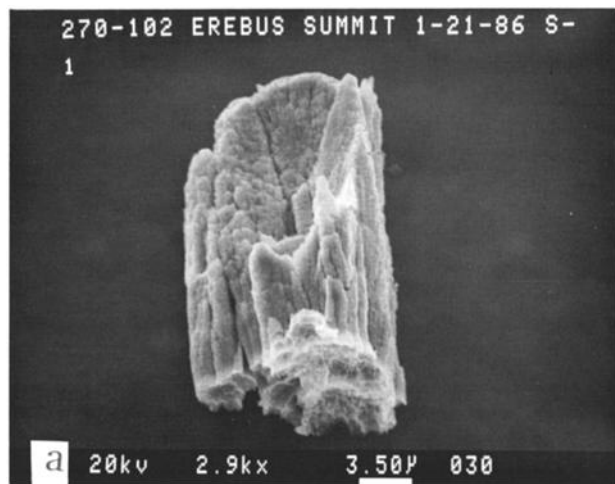
Fig. 5. Aerosol mass distribution in five size bands from 0.1 μm to larger than 12 μm, from direct sampling of Erebus plume during a period of low activity, characterized by a lower aerosol mass concentration of only 9 μg m^{-3}, compared to 350 μg m^{-3} in Figure 2, and a smaller mass median diameter of 3.5 μm, compared to the 13 μm from the plume during a more active period.

particle samples are obtained by stationary sampling at the crater rim. Some typical examples are shown in Figure 4. The size distribution, determined from aerial sampling along the visible plume, is shown in Figure 5. The total concentration for this case is 9.2 μg m^{-3}, and the mass median diameter is 3.5 μm.

BACKGROUND AEROSOL IN THE AMBIENT ATMOSPHERE

The data collected on a number of flights over the continent on days when the wind was such that there was little chance of encountering Erebus plume material

Fig. 4. (Opposite) Representative plume particles collected from the crater rim of Mount Erebus during a less active fuming state, characterized by SO_2 emission rates of less than 50 Mg d^{-1}: (a) crystalline gold collected from the plume and (b) mixture of salts. The cubic shapes are sodium chloride, while the pyramidal shapes are potassium chloride. These salts are abundant in the plume and constitute the majority of the aerosol mass. (c) Aggregates of chromium oxide, mixed with some silicates, are also shown.
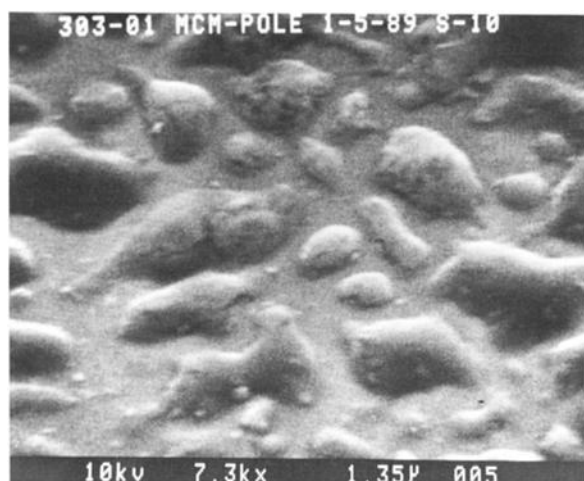
Fig. 6. Sulfuric acid aerosol droplets from the ambient atmosphere at 8 km altitude. These are the only particles recovered, which suggests the air mass traversed by the sampling flight was free of Erebus-generated particles.

indicated that the background is almost exclusively made up of sulfuric acid aerosol droplets, with a mass concentration of typically around 0.2 μg m^{-3} and a mass median diameter of about 0.2 to 0.4 μm. Figure 6 shows the sulfuric acid droplets collected on a flight between McMurdo and the south pole when the wind was from 206°. Most of the shapes shown in the SEM represent the coalescence of several single drops. Only the near circular shapes represent individual droplets.

DISPERSAL OF EREBUS-GENERATED PARTICLES OVER THE CONTINENT

Volcano-derived particles from Mount Erebus have been identified in six aircraft sampling flights (Table 1), using the criteria that the aerosol had a concentration higher than 0.5 μg m^{-3}, had a mass median diameter larger than 1 μm, and contained particles characteristic of Erebus emissions.

How far Erebus-generated particles are transported over the continent can be discerned by examining the spatial distribution of the aerosol known to contain such particles. Using the example of data set 306, we show in Figure 7 the aerosol concentration as a function of distance from McMurdo on a flight along longitude 165° to the south pole. Representative particles collected on this flight are shown in Figure 8. The crystalline Au and the potassium chloride particles are indicative of their Erebus origin, while the sulfuric acid droplets, in the final stage of the cascade impactor (for mean particle

diameter of 0.1 μm), are from the background. The aerosol mass concentration in this last stage, averaged over the flight, is 0.12 μg m^{-3}. It is thus seen that the total aerosol concentration remains above background over the entire course of the sampling flight, from 78°S to 88.7°S (where sampling was terminated prior to descent to South Pole Station). The presence of Erebus-generated particles is not ubiquitous over the continent, as evidenced by the apparent dependence of their presence on wind conditions. On this particular sampling flight the wind was generally from the north, swinging from 60° at the start of the flight to 340° for about the last 75% of the flight. On the other hand, during a southbound flight when the wind was from 285°, the aerosol contained Erebus particles, while on the northbound flight, when the wind had changed to 80°, the aerosol exhibited more of the characteristics of the background.

In earlier limited aerosol sampling at the south pole, *Shaw* [1983] had reported the anomalous presence of Cl and Si, which he speculated might indicate that the area was affected by emissions from Mount Erebus. The present results appear to support Shaw's surmise.

CONCLUSION

Under the right wind conditions, particles emitted by Mount Erebus can be transported great distances over the Antarctic continent. Erebus signature particles such as potassium chloride and elemental crystalline gold as large as 20 μm have been found in sampling flights at 8 km altitude. Within the affected air mass the total aerosol mass concentration can be twice the background level, as far away as the south pole.
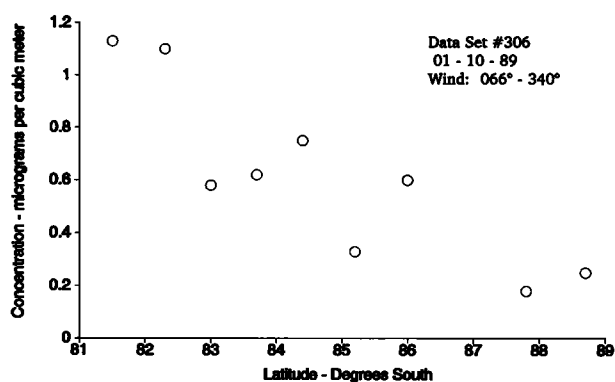
Fig. 7. Spatial variation of aerosol mass concentration between McMurdo and the south pole at 8 km altitude. The concentration decreases to near background value just before the flight begins descent to South Pole Station.
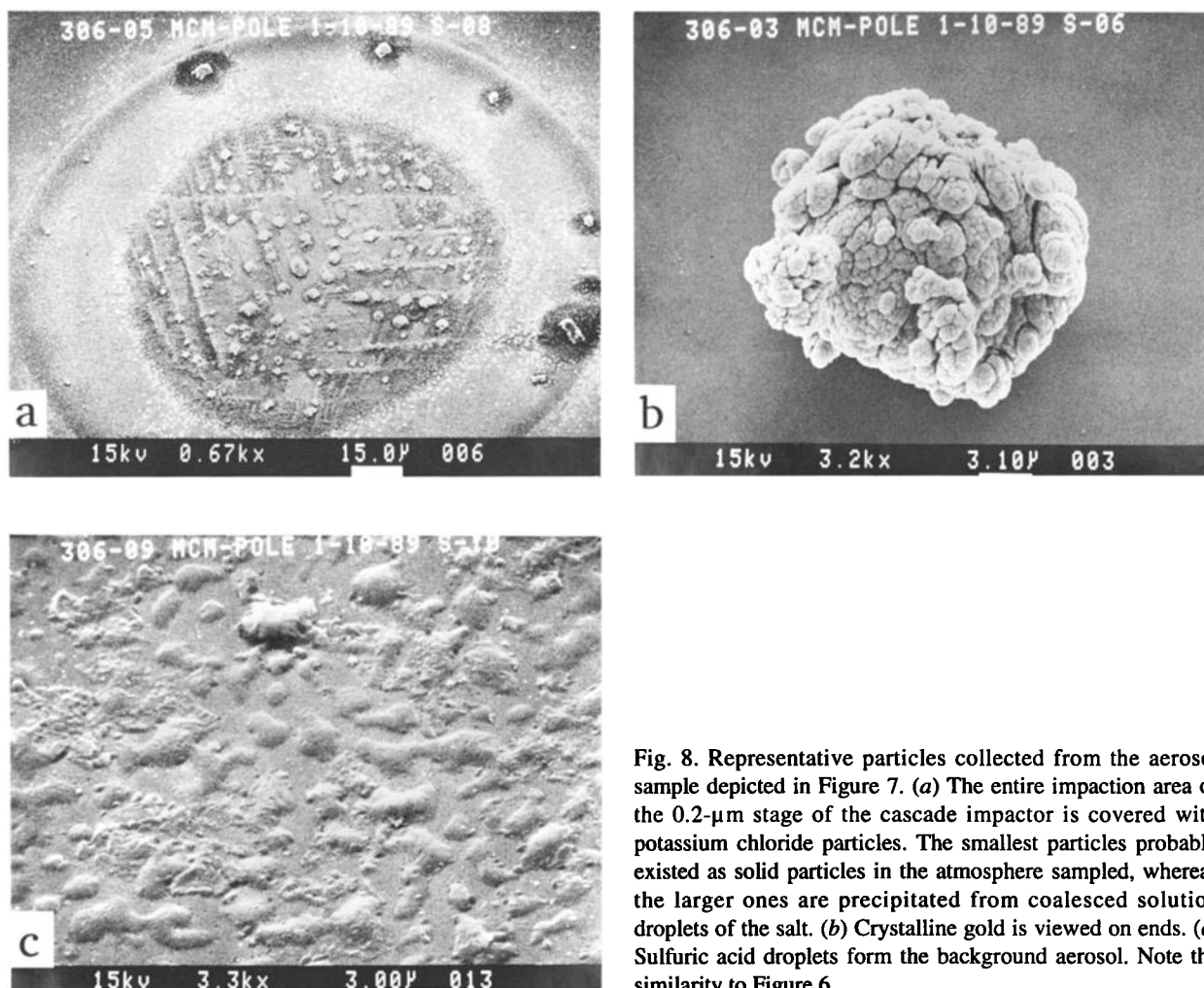
Fig. 8. Representative particles collected from the aerosol sample depicted in Figure 7. (*a*) The entire impaction area of the 0.2-μm stage of the cascade impactor is covered with potassium chloride particles. The smallest particles probably existed as solid particles in the atmosphere sampled, whereas the larger ones are precipitated from coalesced solution droplets of the salt. (*b*) Crystalline gold is viewed on ends. (*c*) Sulfuric acid droplets form the background aerosol. Note the similarity to Figure 6.

REFERENCES

Chuan, R. L., Rapid measurement of particulate size distribution in the atmosphere, in *Fine Particles: Aerosol Generation, Measurement, Sampling and Analysis*, edited by B. Y. H. Liu, pp. 763-775, Academic, San Diego, Calif., 1975.

Chuan, R. L., J. M. Palais, W. I. Rose, and P. R. Kyle, Particle sizes and fluxes of the Mt. Erebus volcanic plume, December, 1983, *J. Atmos. Chem.*, *4*, 467-477, 1986.

Kyle, P. R., K. Meeker, and D. Finnegan, Emission rates of sulfur dioxide, trace gases and metals from Mt. Erebus,

Antarctica, *Geophys. Res. Lett.*, *17*, 2125-2128, 1990.

Kyle, P. R., L. M. Sybeldon, W. C. McIntosh, K. Meeker, and R. Symonds, Sulfur dioxide emission rates from Mount Erebus, Antarctica, this volume.

Meeker, K. A., R. L. Chuan, P. R. Kyle, and J. M. Palais, Emission of elemental gold particles from Mount Erebus, Ross Island, Antarctica, *Geophys. Res. Lett.*, *18*, 1405-1408, 1991.

Rose, W. I., R. L. Chuan, and P. R. Kyle, Rate of sulfur dioxide emission from Erebus volcano, Antarctica, December, 1983, *Nature*, *316*, 710-712, 1985.

Shaw, G. E., X-ray spectrometry of polar aerosols, *Atmos. Environ.*, *17*, 329-339, 1983.

R. L. Chuan, P. O. Box 1183, Hanalei, HI 96714.

ELEMENTAL TRACERS OF VOLCANIC EMISSIONS FROM MOUNT EREBUS IN ANTARCTIC SNOW SAMPLES

Julie M. Palais and Byard W. Mosher

Glacier Research Group, University of New Hampshire, Durham

Douglas Lowenthal

Desert Research Institute, University of Nevada, Reno

Mount Erebus was evaluated as a source of trace elements and other impurities for the Antarctic environment. Snow samples were collected to determine whether a trace element signature, characteristic of Mount Erebus, could be identified in Antarctic snow samples. The snow was analyzed by instrumental neutron activation analysis for a suite of trace elements. The source of contaminants in the snow samples was determined using receptor-modeling estimates of source contributions. Most snow samples contained significant contributions from crustal sources and minor marine components. A signature characteristic of the volcanic gas plume of Mount Erebus was found mainly in snow samples collected in close vicinity to the volcano.

INTRODUCTION

Studies of atmospheric aerosol composition in remote regions of the world show enrichment of certain volatile trace elements (Zn, Cu, In, W, Sb, Se, Pb, Au, As, Cd, Br, and I) with respect to their composition in average crust or marine sources [*Zoller et al.,* 1974; *Duce et al.,* 1975, 1976; *Rahn,* 1976; *Maenhaut et al.,* 1979; *Cunningham and Zoller,* 1981]. It has generally been assumed that these elements are derived from either natural (e.g., volcanoes) or anthropogenic sources (e.g., coal-fired power plants, oil combustion, and nonferrous smelters) involving some type of high-temperature volatilization process [*Zoller et al.,* 1974; *Phelan,* 1983; *Rahn and Lowenthal,* 1984, 1985].

Because Antarctica is still believed to be relatively untouched by anthropogenic emissions [*Wolff and Peel,* 1985a, b; *Boutron and Patterson,* 1987; *Peel,* 1989], natural (volcanic) sources are generally considered to be the most likely candidates for the enriched elements measured in the atmospheric aerosol of Antarctica [*Cunningham and Zoller,* 1981].

Peel and Wolff [1982] and *Dick and Peel* [1985] determined the abundances of Cd, Cu, Pb, and Zn in Antarctic aerosol samples at sites in the Antarctic

Peninsula. An important aspect of this work was the simultaneous collection of aerosol and freshly fallen snow samples, to determine mechanisms for incorporation and removal of crustal and heavy metal components from the atmosphere. *Dick and Peel* [1985] concluded that there is little fractionation among the crustal, marine, and heavy metal components of the aerosol during precipitation, which is in agreement with theoretical predictions of *Junge* [1977]. Work of *Pourchet et al.* [1983] and *Zoller et al.* [1983] also supports a direct relationship between the concentrations of a variety of components in the air and those in the snow.

Mount Erebus (77.55°S, 167.17°E), the world's southernmost active volcano, located on Ross Island, Antarctica, is the principal source of volcanic emissions to the Antarctic atmosphere [*Rose et al.,* 1985; *Kyle et al.,* 1990]. The volcano is known to have a persistent volcanic plume emanating from the summit crater in which there has been an active lava lake since at least 1972 and possibly for more than a century [*Kyle et al.,* 1982]. In order to determine if Mount Erebus contributes significantly to the trace element composition of snow near the volcano, we conducted a snow-sampling program designed to determine whether a trace element signature, characteristic of Mount Erebus, could be

identified. Comparison of the elemental ratios in Erebus plume samples [*Meeker,* 1988; *Kyle et al.,* 1990] and snow samples collected near the volcano has allowed us to determine that, for certain elements, snow samples can provide good surrogates for aerosol measurements.

In this study, receptor modeling [*Kowalczyk et al.,* 1978; *Henry et al.,* 1984] was used to investigate the sources of contaminants in Antarctic snow samples. By applying techniques similar to those used by *Rahn and Lowenthal* [1984, 1985] for identifying characteristic signatures from regional pollution aerosols, we have developed a method for identifying the characteristic signature of Mount Erebus trace elements.

The regional elemental signatures used by *Rahn and Lowenthal* [1984, 1985] were determined empirically by calculating multielemental ratios of tracer concentrations in regionally representative aerosol samples. Because most samples were actually mixtures from several source regions, receptor modeling was used to apportion a sample of "unknown" origin among the various regional sources which may have contributed to it. In this study, source apportionment was done with a chemical mass balance model using source profiles to investigate the source of contaminants in Antarctic snow samples.

Studies by *Germani* [1980] and *Meeker* [1988] have provided information for determining the source profiles for the Erebus plume and Erebus magma. *Germani* [1980] sampled both particulate and vapor phase aerosol emissions from the plume of Mount Erebus. Volatile chalcophile elements, including As, Se, In, Cd, and Sb and the halogens F, Cl, and Br, were found to be enriched in the plume emissions. Other elements that were found to be enriched included Na, K, La, Ce, Sm, and Th. *Germani* [1980] concluded that the enrichment factors for the volatile elements that he examined were all greater than or equal to those determined for particles at the south pole. This led him to conclude that while the volcano may be a source of Se, As, Sb, Zn, S, Cu, Cs, Au, and Br in the south polar aerosol, the differences in the enrichment patterns suggest that Mount Erebus is not the only source of these elements.

Meeker [1988] and *Kyle et al.* [1990] measured aerosols and gas emissions from the active lava lake at Mount Erebus. SO_2 flux was measured with a correlation spectrometer [*Kyle et al.,* this volume], and particles were measured and collected using a quartz crystal microbalance cascade impactor (QCM) [*Chuan,* 1975, this volume]. The acidic volatiles and trace metals were sampled using particle and filters treated with [7]LiOH [*Finnegan et al.,* 1989]. The filter measurements gave evidence of vapor phase transport of metals and enrich-

ment of other elements (with respect to the Erebus phonolite magma), including Cl, F, As, S, Se, Zn, Sb, Hg, and In.

The results of these previous studies have provided background for our investigation of trace elements in snow samples in Antarctica. In addition to trying to establish whether a trace element signature characteristic of Mount Erebus could be identified in snow samples collected both near to and at distances from the volcano, one of the main objectives of this study was to develop the necessary analytical techniques for collecting, analyzing, and interpreting trace elements in snow samples measured by instrumental neutron activation analysis (INAA). These sampling techniques and analytical methods are discussed below.

SAMPLING AND ANALYTICAL METHODS

Most investigators have used graphite furnace atomic absorption analysis for trace element measurements. A few investigators have used instrumental neutron activation analysis for measurements of trace elements on snow and ice samples [*Briat,* 1974; *Echevin,* 1975; *Legrand et al.,* 1984; *De Angelis et al.,* 1984; *Koyama et al.,* 1988]. The elements most often analyzed in these studies include Cl, Na, Mn, Al, and V. In most of these studies, INAA was used mainly for intercalibration purposes, to check the concentrations of samples measured by other techniques (i.e., ion chromatography and graphite furnace atomic absorption).

In this study we have developed methods for snow sample collection, preparation, and analysis by instrumental neutron activation analysis after preconcentration by lyophilization (freeze-drying). Analysis by INAA has allowed us to obtain information on a larger suite of elements than is commonly possible using other techniques.

Sample Collection

During the 1988/1989 Antarctic field season, snow samples were collected at a number of sites around Ross Island, Antarctica, and in the vicinity of the south pole. Table 1 is a list of these samples, and Figure 1 shows the locations at which the samples were collected. Samples were collected at eight different locations in order to examine the spatial variability of trace elements in surface snow samples. The locations of sampling sites were chosen to be representative of different source regimes (e.g., crustal, marine, volcanic, pollution) in order to characterize "near-source" trace element concentrations in snow. All of the samples were collected in

TABLE 1. List of Samples, Their Locations, Elevations, and Distance From the Ross Sea

Location*	Elevation, m	Distance to Summit, km	Distance to Sea, km	Main Source
(1) Erebus upper hut	3400	0.5	15	volcanic
(2) Fang Glacier	2600	4	14	volcanic
(3) Terra Nova Saddle	1600	7.5	20	volcanic
(4) Bird Saddle	750	12.5	5	volcanic and marine
(5) Cape Crozier	0	90	25	marine?
(6) Newall Glacier	1700	110	55	crustal
(7) South pole	2800	1300	1300	crustal, marine and pollution (downwind of the station)

*Sample descriptions as follows: (1) Near upper hut on Mount Erebus. Sample collected in snowfield above the hut. (2) Sample collected in surface snow on Fang Glacier. (3) Sample TN Saddle collected in surface snow on the saddle between Mount Erebus and Mount Terra Nova. Samples with designation 0-50, 50-100, etc., collected at those depths in centimeters in a 2-m pit excavated on the Terra Nova Saddle. Sample 170-180 was observed to contain visible volcanic ash. (4) Sample collected in shallow snow pit from 10 to 50 cm. (5) Sample collected in surface snow at a site on the Ross Ice Shelf about 35 km due east of Cape Crozier. (6) Samples taken in snow pit at Newall Glacier: sample L1 taken in upper (31-56 cm) hard section of pit estimated to cover the years 1987-1988 and sample L2 taken in hard snow and hoar frost which contained some visible rock debris (121-138 cm) estimated to be from the years 1984-1985. (7) Samples were taken at three localities near the south pole: SPDow was taken about 1 km downwind of the station along the ski runway. SP19 km and SP38 km were collected in surface snow 19 and 38 km, respectively, from South Pole Station along the eastern margin of the clean air sector.

precleaned acid-washed 1-L polyethylene bottles, by people wearing full clean suits, including a face mask, gloves, and boot covers. The 1-L wide-mouth low-density polyethylene bottles which were used for sample collection were soaked for approximately 1 week in 1% Ultrex HNO_3. The bottles were then rinsed and soaked in deionized water (Millipore ultrapure, 18 Mohm resistance, 0.2-μm filter), dried in a class 100 laminar flow hood, and triple sealed in clean polyethylene bags for shipment to the field.

In order to eliminate possible seasonal variations in trace element concentrations at any one site, 1 year's worth of accumulation was integrated in each sample. Because some of the sampling sites had not been visited before, the accumulation rate was estimated on the basis of stratigraphic features such as depth hoar and hard-packed layers. A test of the interannual variability in trace element concentrations was also made. The Terra Nova Saddle, a site that had been visited before (and which is known to have an annual accumulation of about 50 cm of snow), was chosen for this test [Palais et al., 1990, this volume]. In addition, for two of the samples (Terra Nova Saddle (TN170-180) and Newall Glacier (L2)) we attempted to locate and sample a specific annual layer, namely, the 1984/1985 horizon, in which there might be evidence of fallout from the austral summer 1984/1985 eruptions of

Mount Erebus [Kyle, 1986].

Sample Preparation

Snow samples were concentrated and analyzed in a manner similar to that of Heaton et al. [1990]. A purified starch solution was first prepared by dissolving soluble starch in subboiling deionized water, treating the solution twice with mixed-bed ion exchange resin, and finally centrifuging to remove colloidal and undissolved material. Starch preparation and centrifuging was carried out in Ultrex (J. T. Baker) HNO_3 leached glass and plasticware. The final solution contained 0.12 g starch per 10 mL. Blank trace element values for the purified starch solution are given in Table 2.

In order to check the cleaning procedure of the 1-L polyethlene bottles, they were filled with deionized water, and starch was added, frozen, freeze-dried, and analyzed. These blanks were the same, within the analytical uncertainty, as pure starch solution which was analyzed.

The snow samples (1.6-1.9 L melted equivalent) were melted at room temperature in a laminar flow clean hood, and 20 mL of starch solution containing 0.51 μg Ta internal standard was added. The sample was then refrozen and freeze-dried. After freeze-drying, the starch residue containing the dissolved and particulate
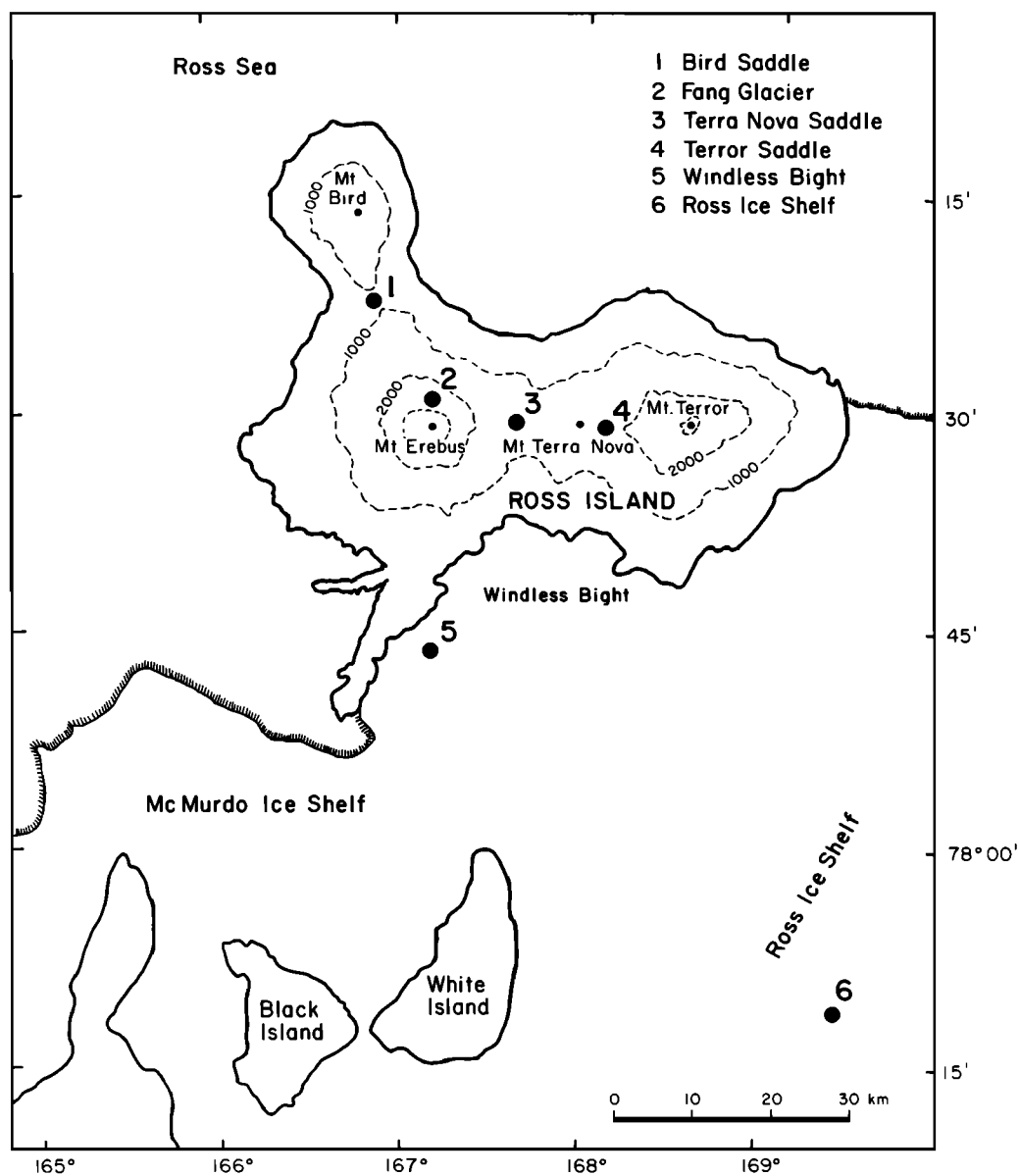
Fig. 1. Location map showing sample collection sites on Ross Island.

trace elements was recovered and placed in acid-cleaned vials for analysis. Starch preparation and sample handling were conducted in a class 100 laminar flow clean hood. The Ta internal standard determinations indicated 85-95% sample recovery, and all final concentrations have been corrected for recovery efficiency.

Sample Analysis

Starch samples were irradiated for 5 min at the Rhode Island Nuclear Science Center 2-MW research reactor at a

nominal thermal neutron flux of 4×10^{12} neutrons cm^{-2} s^{-1}. After irradiation, samples were counted for 400 s and 1000 s on two Ge(Li) gamma ray detectors (25% relative efficiency) in order to determine short-lived isotopes. A second irradiation of 28 hours was used to quantify long-lived isotopes. Samples and co-irradiated standards were counted on 35% efficiency Ge detectors 1 and 3 weeks after irradiation. The accuracy and precision of this analytical scheme has been examined thoroughly through the irradiation of National Institute of Standards and Technology (NIST) Standard Reference

Materials such as urban particulates, coal fly ash, orchard leaves, and bovine liver [*Rahn et al.,* 1986].

RESULTS

The Trace Element Data

Table 3 contains the elemental concentration (micrograms per liter) of some of the trace elements analyzed in the snow samples. Although concentrations were determined for over 40 elements, many were below detection in the majority of samples.

Major Anion and Cation Analyses

Limited analyses of the major anions and cations were made in bulk samples taken at the sites where the samples were collected for trace elements. The results of these measurements are shown in Table 4. Samples were measured for both anions and cations in all but the samples from Cape Crozier and the south pole. Most of the samples were collected so as to represent approximately 1 year of accumulation, except at Bird Saddle and the south pole, where the samples probably represent ~0.5 year of accumulation.

Major anion and cation analyses were made simply to get a general idea of their concentrations at each site. The interpretation of the major anion and cation composition of snow collected around Ross Island is complicated by the fact that there are at least two sources (marine and volcanic) of ions such as Na and Cl which are typically used as reference elements for the marine source [*Palais et al.,* this volume]. Therefore few conclusions can be drawn by examining the anion and cation analyses alone.

Source Apportionment Approach

Receptor modeling estimates source contributions by comparing elemental concentrations in a receptor sample with their compositions in various source emissions. Receptor-modeling techniques are described in detail by *Hopke* [1991]. Source apportionments in this study were done with the Chemical Mass Balance (CMB) model, first used by *Friedlander* [1973]. The Environmental Protection Agency's Chemical Mass Balance Receptor Model version CMB 7.0 [*Watson et al.,* 1989] software was used. CMB is a multiple-linear regression with source profile vectors as independent variables and the ambient concentration vector as the dependent variable. The regression is weighted by effective variances [*Watson et al.,* 1984], which depend on the uncertainties

TABLE 2. INAA Starch Blanks

Element	Blank, ng/g
Na	2860 ± 1080
Al	790 ± 230
Cl	2950 ± 1280
Au	0.39 ± 0.24
Sb	380 ± 200
La	12 ± 4
Cs	36 ± 10
Mg	<1600
Ca	<2750
Ti	<930
Cu	<250
V	<3
Dy	<2
Ba	<900
In	<1.5
Br	<100
Mn	<8
I	<100
Fe	<3700
Eu	<4
Tc	<90
Yb	<1.4
As	<10
W	<210
Sm	<0.6
Ce	<15
Lu	<2
Se	<10
Th	<5
Ir	<0.2
Cr	<45
Hf	<5
Nd	<500
Ag	<30
Ni	<1700
Tb	<6
Sc	<0.6
Rb	<200
Co	<10

$N = 12.$

of the ambient and source measurements and which are used to calculate uncertainties of the source strength estimates.

Two major assumptions underlying the CMB model are that (1) the major sources are identified and their emissions are characterized and (2) the source compositions are conserved (i.e., there is no fractionation and no reactions occur between the source and the receptor). The first assumption is extremely important and has

TABLE 3. Elemental Concentrations in Antarctic Snow Determined by Instrumental Neutron Activation Analysis

Sample	Na	Al	Cl	Ca	Sc	V	Cr	Mn	Fe	Co	As	Se	Br	La	Ce	Au
EREBUS	252.7	72.61	249.19	9.42	0.092	n.d.	0.49	7.64	543.3	0.09	4.762	1.074	0.33	5.2	9.73	0.00024
BIRDS ADD	1526.9	13.38	2620.6	65.05	0.006	n.d.	0.2	0.74	47.6	0.02	n.d.	0.864	3.43	0.13	0.21	0.00031
CAPECROZ	8.0	4.23	2.31	1.56	0.001	0.006	0.06	0.03	7.5	0.01	n.d.	0.148	0.45	0.91	0.01	0.00042
FANG	1078.9	1490.3	383.66	224.48	0.079	n.d.	0.27	30.61	1170.5	0.07	1.946	0.525	0.31	5.11	8.32	0.00037
NEWALL1	71.7	72.39	53.07	56.09	0.043	0.152	0.38	0.85	95.6	0.05	0.028	0.301	0.05	0.09	0.14	0.00014
NEWALL2	351.2	1299.6	79.05	1276.6	1.914	6.555	10.39	27.46	2686.9	1.83	n.d.	0.221	0.06	0.75	1.35	0.00012
SPOLE19KM	4.3	0.97	4.60	0.65	0.000	0.003	n.d.	0.01	5.4	n.d.	0.021	0.52	0.48	0.01	n.d.	0.00025
SPOLE38KM	4.7	0.74	2.11	0.94	0.000	0.002	n.d.	0.02	3.4	n.d.	0.011	0.122	0.67	0	n.d.	0.00014
SPOLEDOW	5.2	2.22	5.85	3.38	0.000	0.003	n.d.	0.11	3.2	0.01	n.d.	0.369	0.84	0	n.d.	0.00005
TN0-50	75.3	5.07	87.64	4.666	0.000	0.005	0.03	0.1	4.3	0.01	n.d.	n.d.	0.79	0.01	0.01	0.00098
TN50-100	51.6	12.85	54.45	4.23	0.000	0.002	0.05	0.13	4.8	0.01	n.d.	n.d.	1.38	0.03	0.02	0.00162
TN100-150	23.3	6.70	8.2	2.40	0.001	0.002	0.05	0.12	8.7	0.01	0.016	0.139	0.69	0.03	0.04	0.0004
TN150-200	73.3	73.27	13.96	10.76	0.003	n.d.	0.04	1.45	44.9	0.01	0.027	n.d.	0.44	0.3	0.27	0.00212
TN170-180	54.6	63.36	5.83	15.86	0.004	n.d.	0.16	1.27	53.3	0.01	0.014	0.184	0.16	0.22	0.34	0.0013
TNSADDLE	14.9	0.99	8.65	n.d.	0.000	0.003	n.d.	0.02	6	n.d.	n.d.	0.187	1.46	0	n.d.	0.00013

Concentrations are given in micrograms per liter; n.d. means not detected.

been met only to a first approximation in this study. The second assumption is more or less valid for primary trace elements in aerosol but may be less so for precipitation and particularly less so for snowpack. With this in mind, and because of the small number of samples available for this study, care should be taken not to overinterpret the results presented here.

The source profiles used in CMB modeling of Antarctic snow samples in this study are presented in Figure 2. Erebus plume and Erebus magma concentrations were taken from *Meeker* [1988]. An average crustal rock profile was taken from *Taylor and McLennan* [1985]. A local (Beacon) sandstone profile was taken from *Roser and Pyne* [1990]. Elemental concentrations not available in the sandstone profile were taken from *Taylor and McLennan*'s [1985] average crustal profile. A sea-salt profile was derived from bulk seawater concentrations presented by *Quinby-Hunt and Turekian* [1983].

The CMB model provides mass concentrations from various sources when the source composition profiles are expressed as fractions of total mass emissions. Because magma concentrations were given in units of parts per million, Erebus plume concentrations (micrograms per cubic meter) were scaled up by a factor of 940, the average of the ratios of Ca and Al concentrations in the plume to those in the magma. Similarly, bulk seawater concentrations were scaled to give Na a 30% composition in sea-salt emissions. These approximations allow direct comparison of source contributions in units of milligrams (mg) of total dissolved and particulate contaminants per liter of snow sample.

As shown in Figure 2, the elements measured reliably in most samples and sources were Na, Al, Cl, Ca, Sc, V, Cr, Mn, Fe, Co, As, Se, Br, La, Ce, and Au. All of these elements in the Erebus plume, the Erebus magma, average crustal rock, seawater, and local sandstone were initially input to the model. Elements with zero concentrations in samples were not used in the fits. After the initial runs (for a given sample), sources with negative coefficients were eliminated, as were poorly fit elements. Because the average crustal rock and local sandstone were statistically similar, both could not be included in the same CMB, and the one that resulted in the best fit was retained.

The results of the source apportionment analyses are given in Figure 3. Source contributions (milligrams per liter) from Erebus (plume plus magma), crust (rock plus sandstone), and sea salt are presented in stacked-bar charts (on a logarithmic scale). Figure 3 indicates the greatest contributions from Erebus in samples from Erebus, Fang, Bird Saddle, Cape Crozier, and TN 50-100 cm. Because these results cannot be objectively ver-

TABLE 4. Major Anion and Cation Analyses of Bulk Snow Samples Taken at the Same Sites as Trace Element Samples

Sample	Cl, μeq/L	NO₃, μeq/L	SO₄, μeq/L	Na, μeq/L	NH₄, μeq/L	K, μeq/L	Mg, μeq/L	Ca, μeq/L
CAPE CROZ	1.75	0.61	0.83	n.a.	n.a.	n.a.	n.a.	n.a.
SPole38km-B	2.08	0.65	0.85	n.a.	n.a.	n.a.	n.a.	n.a.
SPole38km-T	0.68	1.23	0.73	n.a.	n.a.	n.a.	n.a.	n.a.
SPole19km-B	0.62	2.34	0.96	n.a.	n.a.	n.a.	n.a.	n.a.
TN 0-25	7.52	0.34	12.48	6.57	0.50	0.33	1.50	0.80
TN25-50	0.62	0.56	7.88	0.43	0.29	0.10	0.17	0.25
TN50-75	1.04	0.53	11.13	0.78	0.49	0.18	0.25	0.25
TN75-100	6.96	0.40	11.13	5.83	0.31	0.26	1.25	0.45
TN100-125	1.75	0.84	10.10	1.30	0.31	0.28	0.33	0.20
TN125-150	3.94	1.26	8.04	4.87	0.35	1.95	0.58	0.80
TN150-175	5.77	1.89	18.06	13.22	1.67	2.95	1.08	2.60
TN175-200	0.90	0.44	7.21	1.70	0.30	0.26	0.25	0.55
BIRDSADD #1	695.77	0.79	244.79	466.96	0.00	10.72	92.83	23.50
BIRDSADD #2	79.86	0.76	45.94	74.57	0.00	1.90	14.50	3.10

Abbreviation n.a. means not analyzed.

ified, they are at best qualitative. On the other hand, the largest effect of Erebus is in fact predicted for the Erebus sample.

There appears to be significant crustal contributions to most samples. Although a sea-salt contribution was predicted for Bird Saddle on Ross Island, none was detected at Cape Crozier, also a coastal site. This may reflect an analytical problem or the possibility that the sea-salt contribution was assigned to Erebus in this sample, as both Erebus and sea-salt emissions are enriched in Cl.

The TN 50-100 apportionment, with the fourth-highest Erebus contribution, seems unrealistic. Arsenic, which is enriched in the Erebus plume, was not detected in this sample. The high Erebus contribution to this sample was probably due to its relatively enriched Au concentration and the fact that Cl was grossly overpredicted and was deleted from the fit. It is likely that some of the predicted Erebus contribution to this sample actually came from sea salt.

It is also interesting to note that sample 170-180 cm was found to contain a small contribution from Mount Erebus, as was expected. This interval was specially sampled because it was observed to contain visible volcanic ash, believed to be from the 1984/1985 period of increased eruptive activity at Mount Erebus.

DISCUSSION

One problem with least squares based source apportionment is that the solutions are not unique. This is especially true in our case because only a small number of elements were actually used in the fitting process. That is because most of the elements were fit quite poorly. Unrepresentative or missing source profiles can seriously bias CMB estimates. It is also likely that the Erebus aerosol plume may not be representative of the more aged material in deposition. This might explain the general underfitting of elements like As and Se. A more realistic sea-salt profile could be obtained from aerosol samples collected on the coast. The sandstone profile is probably representative, but it would be appropriate for future studies to obtain analyses from a variety of exposed Antarctic soils.

The conclusions to be drawn from these apportionments are for the most part qualitative. Future source apportionment studies of Antarctic air or snow should concentrate on properly characterizing source emissions. Better data for As, a more aged plume profile, and better soil and sea-salt profiles would probably improve this type of analysis. Future studies should attempt to evaluate effects of local and distant anthropogenic sources as well as examine some secondary species such as sulfuric acid (H_2SO_4) and methane sulphonic acid.

CONCLUSIONS

The elements arsenic and gold were found to be highly enriched in the volcanic plume [Meeker, 1988] and were likewise found to be prominent in the snow samples collected at sites near the volcano and downwind from it. This supports the work of Meeker et al. [1991],

EREBUS PLUME
Kim Meeker: Thesis

1E6 PPM of Mass Emissions

CRUSTAL
Taylor and McLennan

1E6 PPM of Mass Emissions

EREBUS MAGMA
Kim Meeker: Thesis

1E6 PPM of Mass Emissions

ANTARCTIC SANDSTONE

PPM of Mass Emissions

Fig. 2. Source profiles used in CMB modeling of Antarctic snow samples.

SEASALT
Quinby-Hunt and Turekian
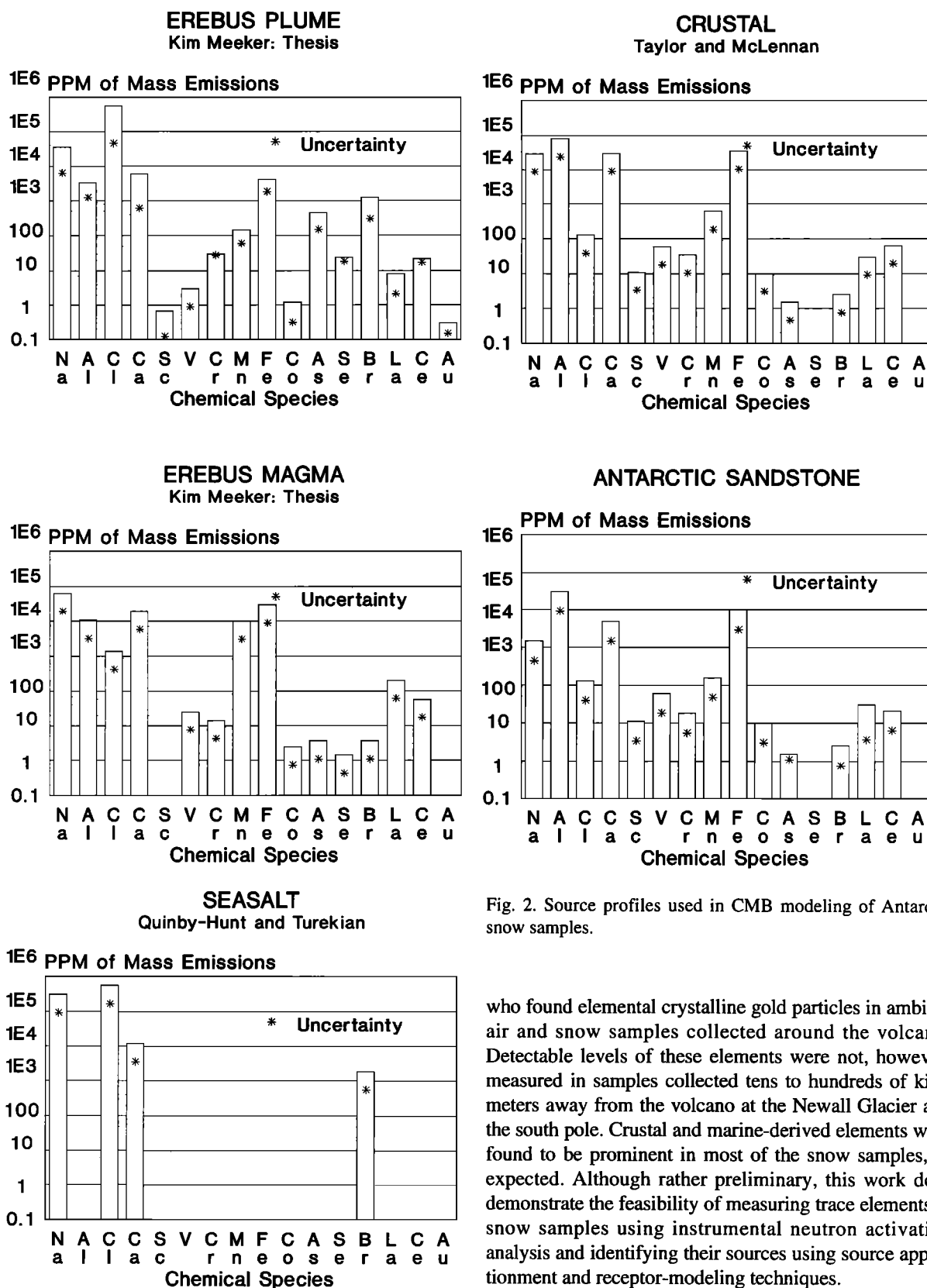
1E6 PPM of Mass Emissions

who found elemental crystalline gold particles in ambient air and snow samples collected around the volcano. Detectable levels of these elements were not, however, measured in samples collected tens to hundreds of kilometers away from the volcano at the Newall Glacier and the south pole. Crustal and marine-derived elements were found to be prominent in most of the snow samples, as expected. Although rather preliminary, this work does demonstrate the feasibility of measuring trace elements in snow samples using instrumental neutron activation analysis and identifying their sources using source apportionment and receptor-modeling techniques.

Source Contributions to Mass
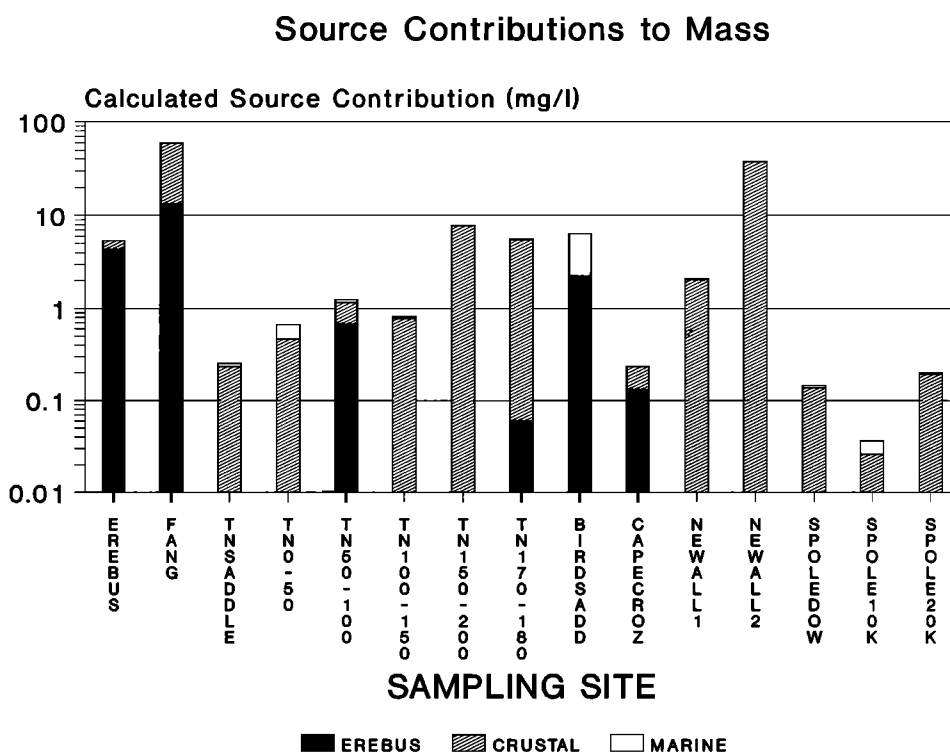
Fig. 3. Source contributions (milligrams per liter) from Erebus (plume plus magma), crust (rock plus sandstone), and sea salt presented in stacked-bar charts (on a logarithmic scale).

REFERENCES

Boutron, C. F., and C. C. Patterson, Relative levels of natural and anthropogenic lead in recent Antarctic snow, *J. Geophys. Res., 92,* 8454–8464, 1987.

Briat, M., Dosage du chlore, du sodium et du magnesium par activation neutronique dans le neve Antarctique: Origine et retombee de ces elements, *Publ. 166,* 111 pp., Centre Natl. de la Rech. Sci. Lab. de Glaciol., Verrières-le-Buisson, France, 1974.

Chuan, R. L., Rapid measurement of particulate size distribution in the atmosphere, in *Fine Particles, Aerosol Generation, Measurement, Sampling, and Analysis,* edited by B. Y. H. Liu, pp. 763–775, Academic, San Diego, Calif., 1975.

Chuan, R. L., Dispersal of volcano-derived particles from Mount Erebus in the Antarctic atmosphere, this volume.

Cunningham, W. C., and W. H. Zoller, The chemical composition of remote area aerosols, *J. Aerosol Sci., 12,* 367–384, 1981.

DeAngelis, M., M. Legrand, J. R. Petit, N. I. Barkov, Ye. S. Korotkevitch, and V. M. Kotlyakov, Soluble and insoluble impurities along the 950 m deep Vostok ice core (Antarctica)—Climatic implications, *J. Atmos. Chem., 1,* 215–239, 1984.

Dick, A. L., and D. A. Peel, Trace elements in Antarctic air and snowfall, *Ann. Glaciol., 7,* 12–19, 1985.

Duce, R. A., G. L. Hoffman, and W. H. Zoller, Atmospheric trace metals at remote northern and southern hemisphere sites: Pollution or natural?, *Science, 187,* 59–61, 1975.

Duce, R. A., G. L. Hoffman, B. J. Ray, I. S. Fletcher, G. T. Wallace, J. L. Fashing, S. R. Piotrowicz, P. R. Walsh, E. J. Hoffman, J. M. Miller, and J. L. Heffter, Trace metals in the marine atmosphere: Sources and fluxes, in *Marine Pollutant Transfer,* edited by H. Windom and R. A. Duce, pp. 77–120, D. C. Heath, Lexington, Mass., 1976.

Echevin, M., Contribution to the chemistry of Antarctic snow: Trace element dosage by neutron activation, *Draft Transl. 423,* 80 pp., Cold Regions Res. and Eng. Lab., Hanover, N.

H., 1975.

Finnegan, D. L., J. P. Kotra, D. M. Hermann, and W. H. Zoller, The use of 7LiOH-impregnated filters for the collection of acidic gases and analysis by intrumental neutron activation analysis, *Bull. Volcanol., 51*, 83–87, 1989.

Friedlander, S. K., Chemical element balances and identification of air pollution sources, *Environ. Sci. Technol., 7*, 235–240, 1973.

Germani, M. S., Selected studies of four high temperature air-pollution sources, Ph.D. thesis, Univ. of Md., College Park, May 1980.

Heaton, R. W., K. A. Rahn, and D. H. Lowenthal, Determination of trace elements, including regional tracers, in Rhode Island precipitation, *Atmos. Environ., 24*, 147–153, 1990.

Henry, R. C., C. W. Lewis, and H. J. Williamson, Review of receptor model fundamentals, *Atmos. Environ., 18*, 1507–1515, 1984.

Hopke, P. K., Receptor modelling for air quality management, in *Science and Technology*, vol. 7, *Data Handling*, edited by P. K. Hopke, Elsevier, New York, 1991.

Junge, C. E., Processes responsible for the trace content in precipitation, in Isotopes and Impurities in Snow and Ice, Proceedings of the IUGG Symposium, Grenoble, *IAHS Publ., 118*, 63–77, 1977.

Kowalczyk, G. S., C. E. Choquette, and G. E. Gordon, Chemical element balances and identification of air pollution sources in Washington, D. C., *Atmos. Environ., 12*, 1143–1153, 1978.

Koyama, M., J. Takada, K. Kamiyama, N. Fujii, J. Inoue, K. Issiki, and E. Nakayama, Neutron activation analysis of snow and ice in Antarctica, *J. Radioanal. Nucl. Chem., 124*, 235–249, 1988.

Kyle, P. R., Volcanic activity of Mount Erebus, 1984–1986, *Antarct. J. U. S., 21*, 7–8, 1986.

Kyle, P. R., R. R. Dibble, W. F. Giggenbach, and J. H. J. R. Keys, Volcanic activity associated with the anorthoclase phonolite lava lake, Mount Erebus, Antarctica, in *Antarctic Geoscience*, edited by C. Craddock, pp. 735–745, University of Wisconsin Press, Madison, 1982.

Kyle, P. R., K. Meeker, and D. Finnegan, Emission rates of sulfur dioxide, trace gases and metals from Mount Erebus, Antarctica, *Geophys. Res. Lett., 17*, 2125–2128, 1990.

Kyle, P. R., L. M. Sybeldon, W. C. McIntosh, K. Meeker, and R. Symonds, Sulfur dioxide emission rates from Mount Erebus, Antarctica, this volume.

Legrand, M., M. DeAngelis, and R. J. Delmas, Ion chromatographic determination of common ions at ultratrace levels in Antarctic snow and ice, *Anal. Chim. Acta, 156*, 181–192, 1984.

Maenhaut, W., W. H. Zoller, R. A. Duce, and G. L. Hoffman, Concentration and size distribution of particulate trace elements in the south polar atmosphere, *J. Geophys. Res., 84*, 2421–2431, 1979.

Meeker, K., The emission of gases and aerosols from Mount Erebus Volcano, Antarctica, M.S. thesis, 172 pp., N. M. Inst. of Mining and Technol., Socorro, Oct. 1988.

Meeker, K. A., R. L. Chuan, P. R. Kyle, and J. M. Palais, Emission of elemental gold particles from Mount Erebus, Ross Island, Antarctica, *Geophys. Res. Lett., 18*, 1405–1408, 1991.

Palais, J. M., R. Chuan, and M. J. Spencer, Soluble and insoluble impurities in snow samples from Ross Island, Antarctica, *Antarct. J. U. S., 24*, 89–90, 1989.

Palais, J. M., M. J. Spencer, and R. L. Chuan, Glaciochemical studies of aerosol fallout from Mount Erebus, this volume.

Peel, D. A., Trace metals and organic compounds in ice cores, in *The Environmental Record in Glaciers and Ice Sheets*, edited by H. Oeschger and C. C. Langway, pp. 207–223, John Wiley, New York, 1989.

Peel, D. A., and E. W. Wolff, Recent variations in heavy metal concentrations in firn and air from the Antarctic Peninsula, *Ann. Glaciol., 3*, 255–259, 1982.

Phelan, J. M., Volcanoes as a source of volatile trace elements in the atmosphere, Ph.D. thesis, Univ. of Md., College Park, Dec. 1983.

Pourchet, M., F. Pinglot, and C. Lorius, Some meteorological applications of radioactive fallout measurements in Antarctic snows, *J. Geophys. Res., 88*, 6013–6020, 1983.

Quinby-Hunt, M. S., and K. K Turekian, Distribution of elements in sea water, *Eos Trans. AGU, 64*, 130-132, 1983.

Rahn, K. A., The chemical composition of the atmospheric aerosol, technical report, 265 pp., Grad. Sch. of Oceanogr., Univ. of R. I., Kingston, 1976.

Rahn, K. A., and D. H. Lowenthal, Elemental tracers of distant regional pollution aerosols, *Science, 223*, 132–139, 1984.

Rahn, K. A., and D. H. Lowenthal, Pollution aerosol in the northeast: Northeastern-mid-western contributions, *Science, 228*, 275–284, 1985.

Rahn, K. A., K. R. Wunschel, and D. H. Lowenthal, Elemental tracers applied to transport of aerosol from midwest to northeast, project report, Environ. Prot. Agency, Washington, D.C., 1986. (Available as *PB 86-168 812/S* from Natl. Tech. Inf. Serv., Springfield, Va.)

Rose, W. I., Jr., R. L. Chuan, and P. R. Kyle, Rates of sulfur dioxide emissions from Erebus Volcano, Antarctica, *Nature, 316*, 710–712, 1985.

Roser, B. P., and A. R. Pyne, Wholerock geochemistry, in Antarctic Cenozoic History From the CIROS-1 Drillhole, McMurdo Sound, *Bull.*, 245 pp., 175–184, Dep. of Sci. and Ind. Res., Wellington, New Zealand, 1990.

Taylor, S. R., and S. M. McLennan, *The Continental Crust: Its Composition and Evolution*, 312 pp., Blackwell Scientific, Boston, Mass., 1985.

Watson, J. G., J. A. Cooper, and J. J. Huntzicker, The effective variance weighting for least squares calculations applied to the mass balance receptor model, *Atmos. Environ., 18*, 1347–1355, 1984.

Watson, J. G., J. E. Chow, D. A. Core, P. L. Dubose, R. C. Hanraham, R. C. Henry, T. G. Pace, N. F. Robinson, H. J. Williamson, and L. Wijnberg, *Receptor Model Technical Series*, vol. III, *CMB User's Manual, Version 7.0*, U.S. Environmental Protection Agency, Research Triangle Park, N. C., 1989.

Wolff, E. W., and D. A. Peel, Closer to a true value for heavy metal concentrations in recent Antarctic snow by improved contamination control, *Ann. Glaciol., 7,* 61–69, 1985*a*.

Wolff, E. W., and D. A. Peel, The record of global pollution in polar snow and ice, *Nature, 313,* 535–540, 1985*b*.

Zoller, W. H., E. S. Gladney, and R. A. Duce, Atmospheric concentrations and sources of trace metals at the south pole, *Science, 183,* 198–200, 1974.

Zoller, W. H., W. C. Cunningham, and A. M. Sulek, Scavenging of aerosols by ice crystals: A comparison of atmospheric aerosol and ice chemistry, paper presented at the Symposium on Polar Meteorology and Climatology, Int. Union of Geod. and Geophys. XVIII Gen. Assem., Hamburg, Aug. 15–27, 1983.

D. Lowenthal, Desert Research Institute, University of Nevada, Reno, NV 89506.

B. W. Mosher, Glacier Research Group, University of New Hamsphire, Durham, NH 03824.

J. M. Palais, Office of Polar Programs, National Science Foundation, 4201 Wilson Boulevard, Room 755, Arlington, VA 22230.

GLACIOCHEMICAL STUDIES OF AEROSOL FALLOUT FROM MOUNT EREBUS

J. M. Palais, M. J. Spencer, and R. L. Chuan

Glacier Research Group, University of New Hampshire, Durham

Six snow pits were sampled on and around Ross Island and analyzed for major cations, anions, microparticles, and oxygen isotopes to assess the geochemical impact of Mount Erebus on the local atmosphere and snow chemistry. The sources, background concentrations, and seasonal variations of impurities in the snow around Mount Erebus have been evaluated. Although there is some evidence that emissions from Mount Erebus affect the chemistry of snow at sites on and around Ross Island, the volcanic signature is not unambiguous. Chloride and sulfate are the most characteristic products found in the snow that were emitted from Mount Erebus.

INTRODUCTION

Measurements of gaseous and particulate aerosols from Mount Erebus conducted since 1979 have documented both a variable emission rate and an unusual suite of compounds originating from the volcano [*Polian and Lambert*, 1979; *Radke*, 1982; *Rose et al.*, 1985; *Chuan et al.*, 1986; *Meeker et al.*, 1987, 1991; *Kyle et al.*, 1990; *Chuan*, this volume]. Recent work by *Zreda-Gostynska et al.* [1993], *Kyle et al.* [1990], and *Meeker et al.* [1987, 1991] has shown that Mount Erebus is an important source of halogen gases and other trace elements to the Antarctic atmosphere. As part of a larger study to assess the geochemical impact of Mount Erebus on the local atmospheric chemistry, a series of six snow pits were sampled on and around Ross Island and analyzed for major anions, cations, and microparticles. Prior to this study, little was known about either the snow accumulation rates or the chemical composition of snow on Ross Island. These results provide the first detailed information on these and other matters related to the impact of Mount Erebus on the glaciochemistry in the Ross Island region of Antarctica.

SAMPLING AND ANALYSIS

Snow pits were sampled during the 1987/1988 and 1988/1989 austral summer seasons at Bird Saddle, Terra Nova Saddle, Windless Bight, Fang Glacier, Terror Saddle, and the Ross Ice Shelf (Figure 1). General site and sampling information is provided in Table 1. The sampling sites located off of Ross Island at the Ross Ice Shelf and Windless Bight are at sea level whereas the Ross Island sampling sites cover a range of elevations.

The sampling techniques that were used have been described in detail by *Mayewski et al.* [1990]. Briefly, a 2-m pit was excavated with a regular shovel, and the wall to be sampled was cleaned by further digging and scraping with a precleaned plastic shovel and lexan tools. Personnel working in the pits wore complete clean room clothing on top of their cold weather gear, including full body suit, hood, face mask, and plastic gloves. Samples were collected using a precleaned lexan scraper and placed into precleaned plastic specimen cups. One sample was taken for major anion, cation, and particle analysis, and a separate but adjacent sample was taken for the oxygen isotope analyses. All samples were returned frozen from the field and were stored at -20°C until just prior to analysis.

The samples were analyzed for anions and cations using Dionex models 2010 and 4040 ion chromatographs. Details of the anion technique are described by *Mayewski et al.* [1987]. The cations were analyzed in a single chromatographic run using Dionex Fast Cation I and Fast Cation II columns with 18 mM HCl/DAP eluent. The results are expressed as microequivalents per kilogram (μeq kg^{-1}).

The oxygen isotope analyses were performed at the Quaternary Isotope Laboratory, University of Washington, using a Micromass 903 automated mass spectrometer with an on-line water/CO$_2$ equilibration

115
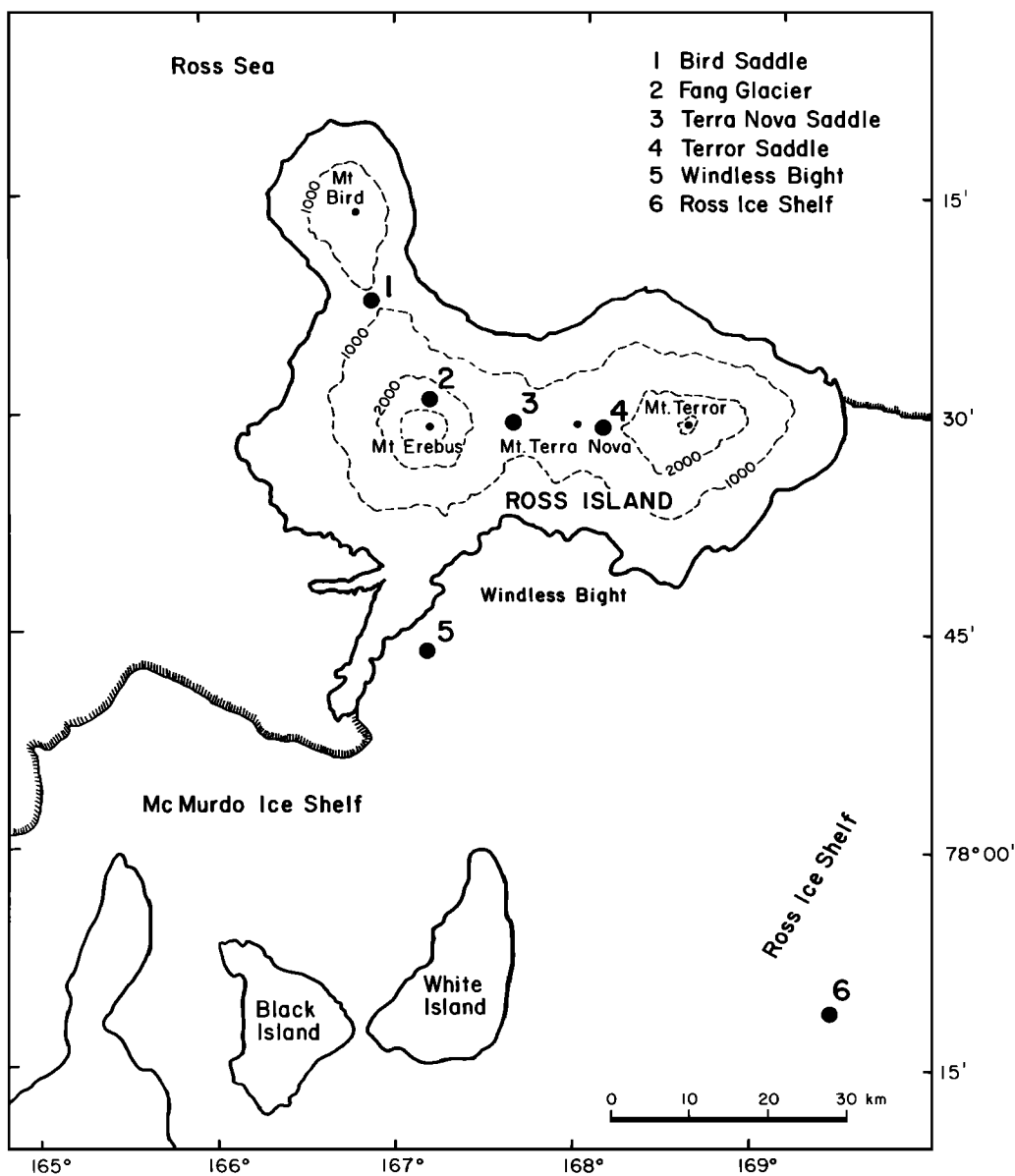
Fig. 1. Map showing the locations of the six sampling sites in the Ross Island region of Antarctica.

system. The results are expressed as the relative difference between the $^{18}O/^{16}O$ ratio of the sample and that of standard mean ocean water (V-SMOW), given in parts per mil (‰). Standard deviations for a single measurement are less than 0.1‰ [*Grootes et al.*, 1990].

In addition to analyses for major anions and cations, the concentration of insoluble microparticles in the size range 0.65-13.22 µm in the meltwater samples was determined for the snow pits using an Elzone model 280

PC particle counter. The methods of sample handling and analysis are described by *Fiacco* [1991].

BACKGROUND

In order to assess the geochemical impact of Mount Erebus on the glaciochemistry of snow around Ross Island, it is necessary to first understand the sources, the

TABLE 1. General Site and Sampling Information

Snow Pit	Sampling Year	Depth, cm	Sample Interval, m	Elevation, m	Distance to Summit, km	Distance to Sea, km	Accumulation Estimate of Snow, cm yr^{-1}
Bird Saddle	1987/1988	2	2.25	750.	12.5	5.0	50–60
Terra Nova Sadl	1987/1988	2	2.25	1600.	7.5	20.0	40–50
Error	1988/1989	1	2.50	1600.	17.5	15.0	—
Windless Bight	1987/1988	2	2.25	0.	29.0	15.0	40–60
Ross Ice Shelf	1988/1989	2	2.50	0.	90.0	70.0	30–50
Fang	1988/1989	1	2.50	2600.	4.0	15.0	10–20

background concentrations, and the seasonal variations of impurities in the snow. The chemistry of Mount Erebus emissions and the general meteorology of the Ross Island region also need to be examined. These topics are discussed briefly below.

Glaciochemistry on the Ross Ice Shelf

Previous studies of snow chemistry and accumulation rates on the Ross Ice Shelf were performed at a number of sites further south and east of Ross Island [*Warburton and Linkletter*, 1978; *Herron and Langway*, 1979; *Warburton et al.*, 1981; *Warburton and Young*, 1981]. More recently, *Zeller et al.* [1986] studied the nitrate flux at Windless Bight, very near to one of the sampling sites examined in this study.

Herron and Langway [1979] used the seasonal variations in the concentration of sodium in shallow cores from the Ross Ice Shelf to date the cores and determine the annual accumulation rate of snow. They concluded that the concentrations of Na, Mg, Ca, and K varied seasonally with the maximum concentration occurring in the autumn. The chemical variations were believed to be caused by meteorological events (cyclonic storms) which have a higher frequency in the autumn. The minimum sea ice extent (i.e., more open water) at that time was also believed to favor an aerosol more enriched in marine-derived elements such as Na, Mg, Ca, and K.

Zeller et al. [1986] analyzed snow pit and firn core samples from a site at Windless Bight on the Ross Ice Shelf and concluded that the nitrate concentrations vary in an annual cycle with sharp (2–3 month) summer peaks and broad (9–10 month) winter troughs. *Neubauer and Heumann* [1988] found a weak seasonal variation in nitrate concentration of samples from shallow firn cores and snow pits on the Riiser Larsen and Ekstrom ice shelves (along the Weddell Sea). Summer concentration

maxima occurred in only three out of seven snow pits. *Neubauer and Heumann* [1988] concluded that there is not a simple relationship between the concentration of nitrate in Antarctic snow and the Antarctic atmosphere because of postdepositional diagenetic modifications such as evaporation, photochemical decomposition, and depth hoar formation. *Parker et al.* [1982], *Legrand and Delmas* [1986], *Mayewski and Legrand* [1990], and *Legrand and Kirchner* [1990] have also discussed the sources and seasonal variations of nitrate in Antarctic snow.

Glaciochemical studies at other Antarctic coastal sites have examined the concentrations and sources of the major anions and cations occurring in Antarctic snow [*Aristarain et al.*, 1982; *Legrand and Delmas*, 1985, 1988; *Wagenbach et al.*, 1988]. These studies as well as others based on analyses of snow samples from inland sites such as South Pole [*Delmas et al.*, 1982; *Legrand and Delmas*, 1984], and Dome Charlie (Dome C) [*Legrand*, 1987] suggest that in coastal areas, snow contains primarily sea salt and two acids (H_2SO_4 and HNO_3), whereas in more central locations, the sea-salt contribution decreases markedly [*Legrand*, 1987]. The background sulfate (as H_2SO_4) has a variety of sources but is believed to be primarily derived from dimethyl sulfide (DMS) gas derived from marine organisms [*Legrand and Feniet-Saigne*, 1991; *Legrand et al.*, 1991]. The source(s) of nitrate in Antarctic snow is still widely debated and may come from biomass burning, lightening, galactic cosmic rays, and surface sources [*Legrand and Delmas*, 1986; *Legrand and Kirchner*, 1990; *Mayewski and Legrand*, 1990].

In addition to H_2SO_4 and HNO_3, HCl is occasionally also present at more interior locations [*Legrand and Delmas*, 1988]. These studies suggest summer concentration maxima for SO_4^{2-} and NO_3^- and fall/winter maxima for Na^+ and Cl^-, with no clear seasonal variation for NH_4^+

and K+ [*Legrand and Delmas*, 1984, 1988; *Wagenbach et al.*, 1988].

Local Meteorology of Ross Island and Vicinity

The surface wind field of the northwestern portion of the Ross Ice Shelf is vastly modified by the mountainous topography of Ross Island [*Bromwich*, 1988]. Winds approach the island from the south and then blow around the steep island barrier. A calm zone is produced on the windward side of the island, hence the name Windless Bight. The incident wind results from both barrier wind and katabatic forcing.

Of greater interest for this study, however, are the prevailing winds at altitude, since we are interested in the effect of Mount Erebus on the local glaciochemistry of Ross Island. Although quite variable, in general, the plume is most frequently observed to extend into the quadrant northeast of the volcano, implying southerly to southwesterly winds.

Emissions of Mount Erebus

Except for two occasions in the past two decades during which emissions of gases and particles from Mount Erebus have been measured, the volcano has been relatively quiescent. *Radke* [1982] conducted aircraft sampling of sulphate in the plume of the volcano. During December 1983, continuous plume measurements were carried out [*Rose et al.*, 1985; *Chuan et al.*, 1986] showing SO_2 flux of 230 Mg d^{-1} and particle flux of 22 Mg d^{-1}. The increased eruptive activity during early spring of 1984 was not monitored. Since that time, extensive measurements have been made of SO_2 flux [*Kyle et al.*, this volume] and of acid gases and trace metals [*Kyle et al.*, 1990; *Zreda-Gostynska et al.*, 1993]. The SO_2 flux has varied between about 16 and 71 Mg d^{-1}. Some of the particle flux in the plume does not exit the crater. Fallout occurs within the crater as evaporites (of salts) nucleate and aggregate into particles larger than about 100 μm. Thus many of the salts found in and near the crater are not found in the aerial plume samples [*Keys*, 1980; *Chuan et al.*, 1986; *Chuan*, this volume]. Most of the particles between 100 μm and 20 μm fall within about 50 km of Erebus; their presence is detectable in the snow. On the other hand, micron and submicron particles traverse great distances and are so dispersed that their eventual fall to the surface is not easily detectable [*Chuan*, this volume].

Possible Complications

The ability to identify a clear volcanic signal in snow can be complicated by a number of factors.

Depending on the sources that contribute to the chemistry of the snow in the pit (e.g., marine, volcanic) and the elements that are considered characteristic of those sources (e.g., Cl, Na, SO_4), there may be problems with swamping of the volcanic signal by the local background and problems with identifying an unambiguous volcanic signal. The latter problem is particularly severe on Ross Island since many of the elements that are considered characteristic of marine impurities (Cl, Na, SO_4) are also considered characteristic of Mount Erebus. Fractionation on emission/deposition, chemical reactions, postdepositional alteration in the snowpack, and dating uncertainties can all further complicate the interpretation of snow pit data and make it difficult to find an unambiguous signature in the snow pits from Mount Erebus.

DETAILED SNOW PIT CHEMISTRY

In this section we present the major anions, cations, microparticles, and oxygen isotope profiles for five of the six snow pits which we sampled, along with the dating that we have assigned to each snow pit. The Terror Saddle pit, which only extended to 1 m, is not presented for detailed discussion because the section was too shallow and the concentrations too low to identify any clear trends. Figures 2-6 show the chemical profiles and dating for the Bird Saddle, Terra Nova Saddle, Windless Bight, Ross Ice Shelf, and Fang Glacier snow pits, respectively.

Where possible, seasonal variations of oxygen isotopes were used for dating and thus for determining annual accumulation of snow for each site. In some cases, other parameters were used to constrain the dating of each pit. Table 1 lists the average annual accumulation rate estimates made for each sampling site, based on the dating given for each pit. These snow pits and the results of the analyses made on the samples collected from them are discussed in more detail below.

Bird Saddle

The Bird Saddle snow pit site is located at approximately 750 m elevation in the saddle between Mount Bird and Mount Erebus. The oxygen isotope profile for this site (Figure 2) shows broad maxima representing snow accumulated during spring and summers and well-defined, narrow troughs which represent winter accumulation. This identification of summer- and winter-deposited snow has allowed a relative dating of the snow pit from the surface down and an estimate of annual accumulation of snow in the range of 50–60 cm.
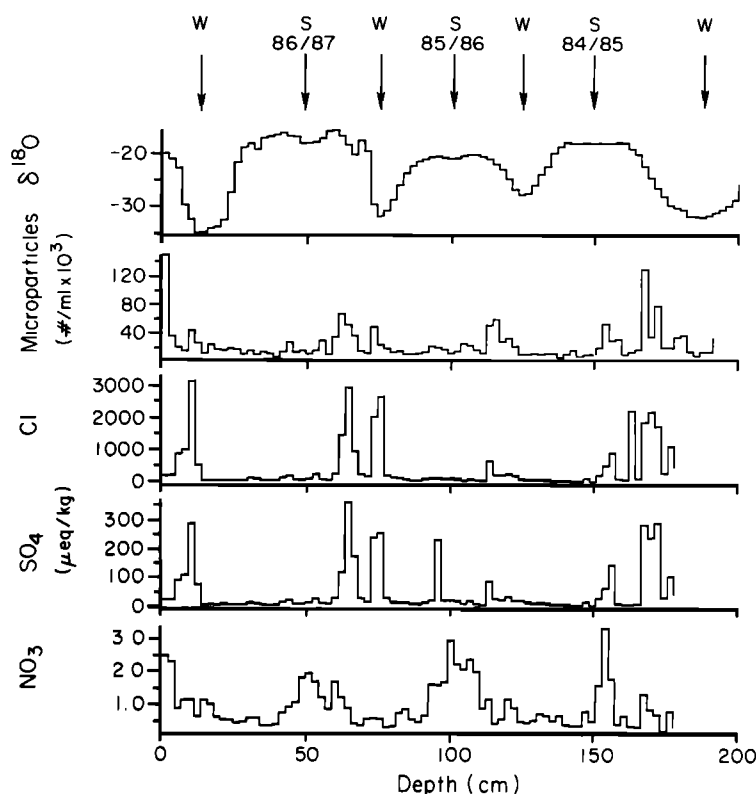
Fig. 2. The chemical profiles and dating for the Bird Saddle snow pit.

The Bird Saddle record also shows well-preserved seasonality for the microparticles (spring peaks) as well as for the anions (nitrate summer peaks, sulfate and chloride late winter/spring peaks). Superimposed on this seasonality is an apparent influence from Mount Erebus, as discussed below. Cations were not measured for this snow pit because of lack of sample.

Terra Nova Saddle

The Terra Nova Saddle snow pit was at an elevation of about 1600 m in the saddle between Mount Erebus and Mount Terra Nova. Figure 3 shows the chemical profiles for this pit, including oxygen isotopes, microparticles, anions, and cations. The oxygen isotope profile is irregular but still shows distinct seasonal variations which we have used to date the snow pit layers and estimate the annual accumulation of snow (~40-50 cm of snow).

The chloride, sodium, and magnesium concentrations in the Terra Nova pit, which are believed to be derived principally from sea salt, all show similar variations with sharp peaks occuring during the fall/winter time period. The close correspondence between the sodium and the chloride is a clear indication of a direct marine source for these two species with very little atmospheric or postdepositional fractionation. Sulfate peaks occur in the spring and fall with occasional winter peaks. As discussed below, some of these peaks (see especially the peak at 150 cm) may be related to Mount Erebus volcanism. The ammonium and potassium concentrations in the Terra Nova Saddle pit are relatively low, except for a few sporadic peaks which occur near the top of the pit and again near the bottom whose source is unknown. The potassium may be from Mount Erebus dust. The calcium concentrations are quite variable with depth and do not show any correlation with the other impurities measured.

The nitrate seasonality in the Terra Nova Saddle pit is irregular, with spring, winter, and occasional summer peaks. The oxygen isotope record shows two types of winters, short and long. There appear to be winter peaks in nitrate during the long winter events but not during the "short winter" episodes.

Deviations from a strict summer nitrate seasonal peak have been documented for other Antarctic sites.
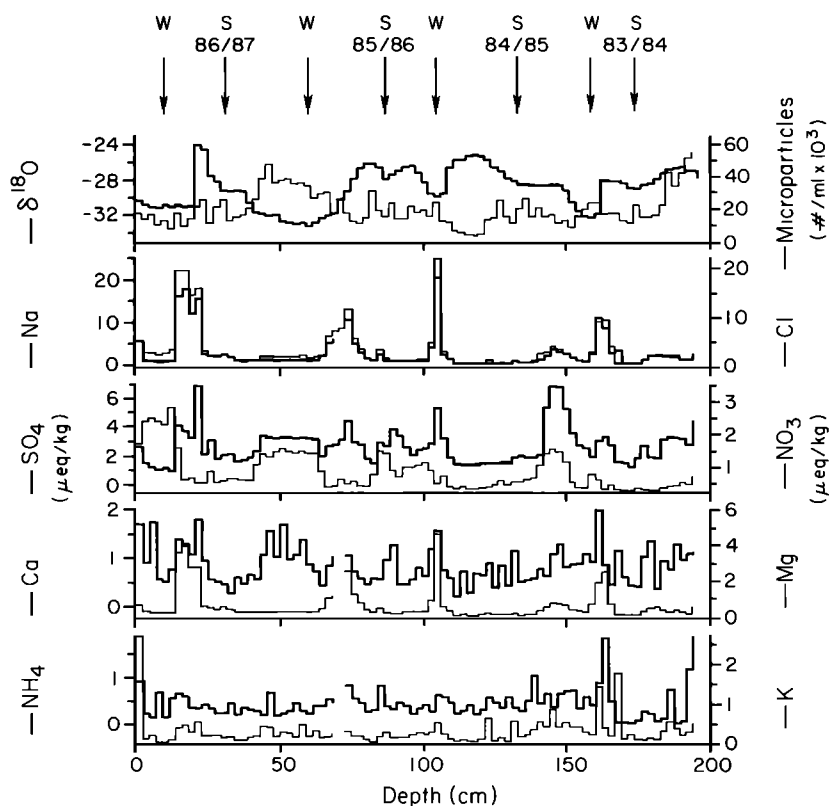
Fig. 3. The chemical profiles and dating for the Terra Nova Saddle snow pit.

Wagenbach et al. [1988] observed a bimodal seasonal variation in the nitrate concentration of aerosols sampled in coastal regions of the Antarctic, with maxima in July-September (winter/spring) and in November-December (summer). *Legrand and Kirchner* [1990] observed summer maxima in nitrate in snow at the south pole; however, they also observed winter peaks in years 1982, 1976, 1975, and 1973 which coincided with a large delay in the spring stratospheric warming. *Mayewski and Legrand* [1990] suggest that the spring maximum of nitrate during the years 1985-1988 has been increasing because of the more persistent polar stratospheric clouds (PSCs) and increased denitrification of the lower stratosphere. Deposition of nitrate from PSCs would therefore lead to winter/spring nitrate peaks, as seen in the Terra Nova Saddle pit.

Windless Bight

Figure 4 presents the analyses of samples taken from the snow pit excavated at Windless Bight. This site was at sea level on the Ross Ice Shelf east of Hut Point Peninsula. The oxygen isotope analyses display fairly

regular seasonal variations, allowing the samples to be dated with depth and giving an estimate of the annual accumulation rate of snow in the range of 40-60 cm.

The nitrate concentration maxima are not well defined but seem to occur for the most part during the summer. Sulfate and chloride concentrations in the Windless Bight pit, like those in the Terra Nova Saddle pit, occur at various times throughout the year and do not seem to exhibit a strong seasonal cycle. Sodium, on the other hand, follows chloride very closely (except for one peak during the winter of 1987 (40-50 cm)), suggesting a sea-salt origin for both. Calcium, magnesium, and potassium show similar temporal variations, with peaks that occur at various times throughout the year. The ammonium concentrations remain relatively low throughout the snow pit and show little correlation to other parameters.

Ross Ice Shelf

Figure 5 shows the results of anion and cation analyses for the Ross Ice Shelf pit. This site was at sea level on the Ross Ice Shelf southeast of Mount Erebus. The
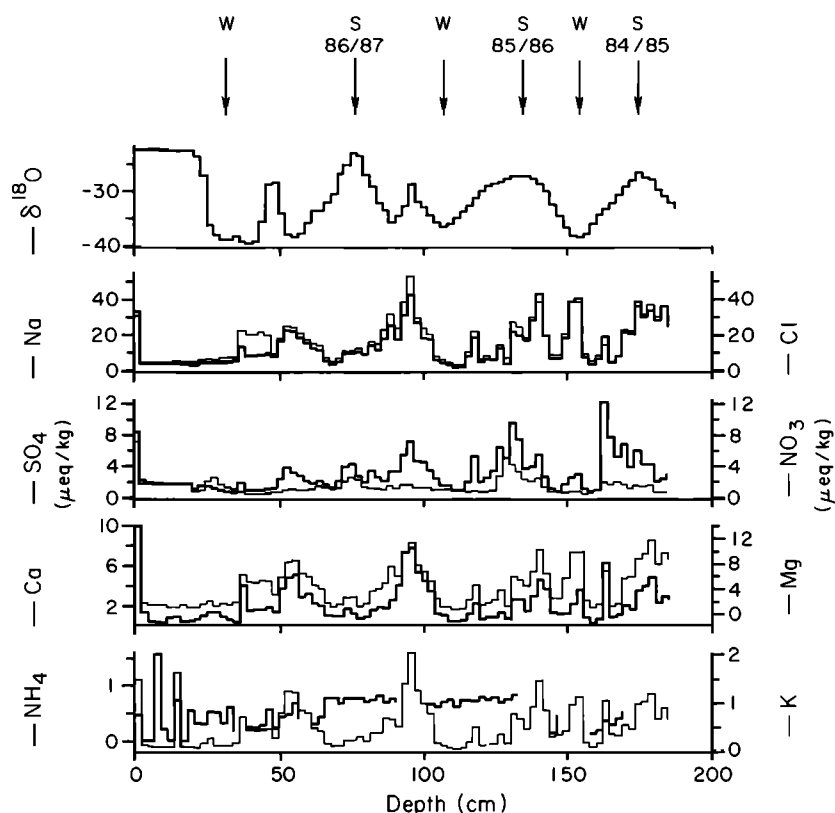
Fig. 4. The chemical profiles and dating for the Windless Bight snow pit.

oxygen isotope analyses display fairly regular seasonal variations (as was the case for the Windless Bight pit), allowing the samples to be dated with depth and giving an estimate of the annual accumulation rate of snow in the range of 30–50 cm.

The nitrate concentration maxima are very well defined in the Ross Ice Shelf pit and occur during the summer, as seen by comparison with the oxygen isotope profile. Chloride, sulfate, sodium, magnesium, and potassium show high summer concentrations with some sporadic peaks at other times. Ammonium concentrations remain relatively low throughout the profile, except for a few sporadic peaks, two of which coincide with summer peaks of the other anions and cations. Microparticle concentrations measured in the Ross Ice Shelf pit are quite low, with small irregular peaks throughout the year which do not seem to correlate with any one anion or cation.

Fang Glacier

A 2-m snow pit was excavated on the Fang Glacier (Figure 6) in an area of extremely icy, granular snow which contained a lot of visible windblown volcanic rock and dust particles. The sampling was very difficult, and because the value of the site was uncertain (both because of the abundance of the windblown volcanic material and because of apparent recrystallization/melting of the snowpack), it was decided to only sample the pit down to 1 m. The oxygen isotope record in the Fang snow pit is not well defined, and it is not possible to extract from it a clear seasonal signal. This also seems to be the case for the anions, cations, and microparticles.

The dating of this snow pit is based on the identification of an elevated level of anions, cations, and microparticles at a depth of 80–90 cm and the suggestion that this is related to the larger eruptions of Mount Erebus which took place in late 1984 [Kienle et al., 1985]. On the basis of the identification of that horizon as corresponding with approximately the summer of 1984/1985, and recognizing several slight increases in sodium and perhaps nitrate between that peak and the surface, we estimated a time scale for this pit.

Although this is not a well-dated pit, we present the
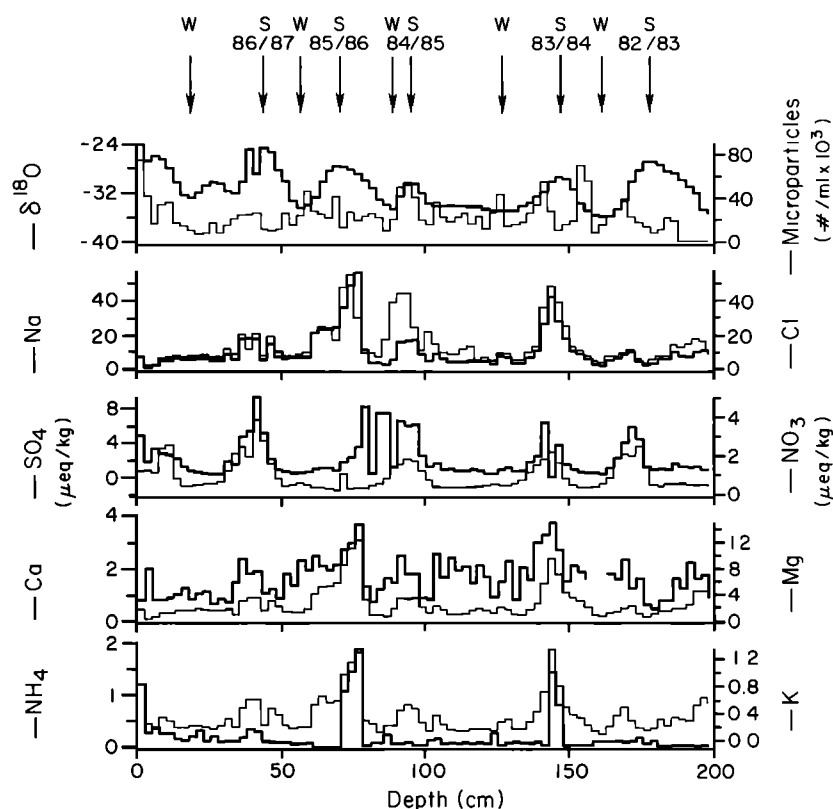
Fig. 5. The chemical profiles and dating for the Ross Ice Shelf snow pit.

data primarily to provide baseline information on the concentrations of the parameters which we measured in samples close to the summit of Mount Erebus. The influence of Mount Erebus on the glaciochemistry at this site seems clear from the elevated concentrations of the parameters measured in this pit, compared with the other pits.

SUMMARY OF REGIONAL GLACIOCHEMISTRY

In order to summarize the glaciochemistry in the Ross Island region, as determined from our snow pit studies, the average species concentration for each snow pit was calculated. Comparisons of the average values for the various sites are presented in Figures 7 and 8. On the basis of the average anion and cation concentration plots shown in Figure 7, four of the snow pits fall into two pairs having similar chemistry (pair one: Windless Bight and Ross Ice Shelf; pair two: Terra Nova Saddle and Terror Saddle). The anion concentrations in the other two snow pits (Fang and Bird Saddle) are 1 to 2 orders of magnitude higher than in the other four snow pits; however, because the microparticle concentrations

(Figure 8) are so much higher at Fang (probably because of the proximity of exposed rocks) than at Bird Saddle, different sources may contribute to the impurities at these two sites.

Figure 9 shows the average sea-salt and non-sea-salt contributions for each of the anions and cations as a function of sample location. Seawater contributions to the total concentration of the various species were calculated by using the Cl, Na, and Mg concentrations for each sample. The species that predicted the lowest sea-salt contribution was used to calculate the sea-salt component for all of the other species using the relative abundances in sea salt. This seawater contribution is, however, a maximum estimate of the real sea-salt input since all three of these species have additional sources which may be of importance.

Because no cations were measured in the Bird Saddle samples, the percent sea-salt and non-sea-salt contributions cannot be calculated for most of the parameters measured in this pit. However, the Bird Saddle samples have higher chloride and lower sulfate concentrations than those at Fang. Since the ratio of Cl/SO_4^{2-} in seawater is higher than that in the Erebus plume (Table 2), this
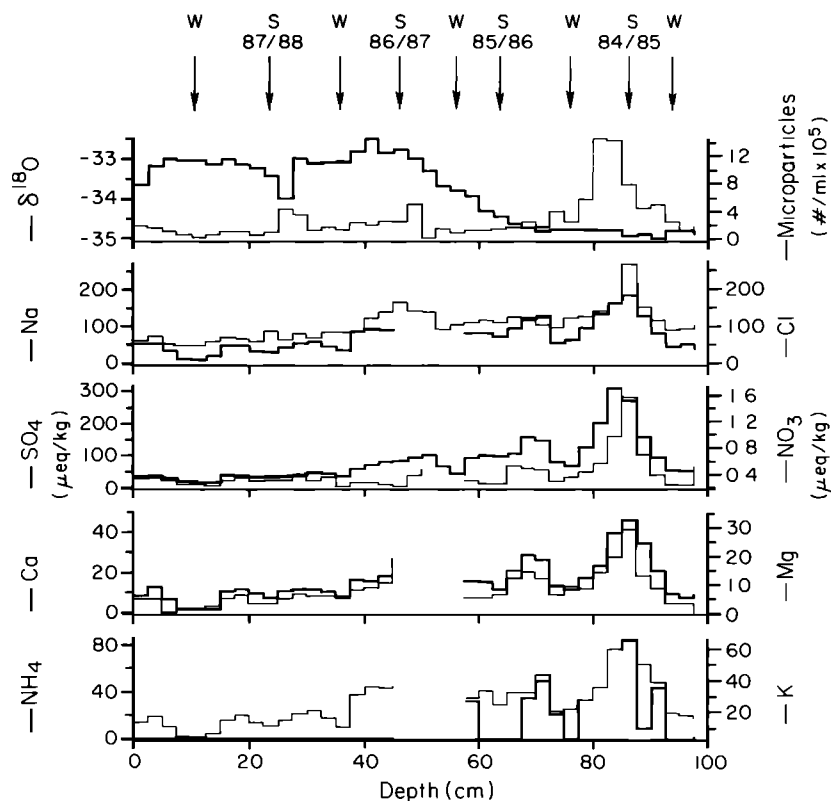
Fig. 6. The chemical profiles and dating for the Fang Glacier snow pit.

suggests a greater influence of sea salt at this site. As much as 70% of the sulfate at the Bird site may be derived from sea salt, in contrast to only about 7% at the Fang site (Figure 9). The combination of low elevation and short distance to the ocean at Bird Saddle also supports a large sea-salt influx at this site. In fact, at certain times of the year the distance from open ocean to this site is extremely short since small polynyas can form just off the coast of Ross Island west of Bird Saddle [*Bromwich*, 1988].

Terra Nova and Terror saddles have the lowest concentrations of soluble salts of any of the pits. The low $Cl/SO_4{}^{2-}$ suggests that sea salt is less important at these sites than at Bird Saddle. The total amount of sea salt is low, both because of the expected decrease with elevation (above the marine boundary layer) and because of the prevailing winds from the south which prevent sea salt from reaching these sites.

The Ross Ice Shelf and Windless Bight sites show concentrations in the middle of the range for the six snow pits. Since the sea salt concentrations are higher than for the Terra Nova Saddle and the Terror Saddle sites, this suggests that elevation and meteorological

blocking are more effective controls on sea-salt influx than distance from the sea. At the Windless Bight and Ross Ice Shelf sites, sulfate and potassium originate primarily from sea salt, in contrast to the other sites which are dominated by non-sea-salt influences (Mount Erebus?) (Figure 9). The calcium concentrations still show the dominance of non-sea-salt sources.

Table 3 summarizes the observations which were made above regarding the seasonality of anions, cations, and particles at the sites in the Ross Island region. Although the oxygen isotopes exhibit fairly regular seasonal variations in all of the pits, the timing of the anion, cation, and particle concentration peaks is sufficiently irregular in most cases to prohibit using these impurities as reliable proxies for dating purposes. Nitrate, along with the oxygen isotopes, is by far the most reliable seasonal indicator, peaking in summer snow in almost all cases.

EREBUS INFLUENCE ON LOCAL GLACIOCHEMISTRY

The most recent eruptions of Mount Erebus of any intensity occurred during the austral spring/summer of
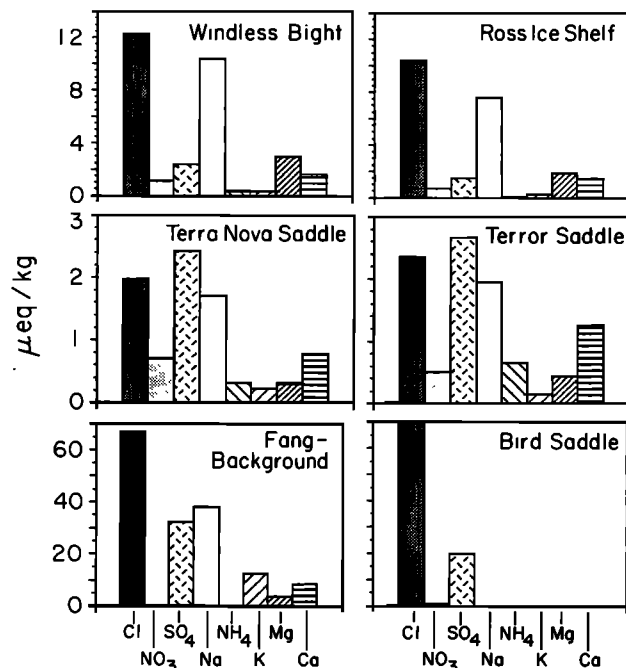
Fig. 7. Average anion and cation concentrations for the various snow pits. For the Fang snow pit the average is for the period winter 1987 to winter 1988 only.

Fig. 8. Average microparticle concentrations and oxygen isotope levels as a function of snow pit location.

1984/1985. The eruptions are believed to be the most significant since the discovery and naming of the volcano by James Clark Ross in 1841 [*Kienle et al.*, 1985]. During the eruptions over 10^5 m^3 of material was erupted. The former lava lake was totally buried but since then has been exhumed, and a smaller lava lake reformed at the same location [*Kyle et al.*, 1990].

Since the Fang site is the closest to Mount Erebus and is directly downwind from the summit, the Fang snow pit record is considered most likely to show evidence of an influence from Mount Erebus on the snow chemistry. As discussed above, the elevated concentrations of the chemical parameters, including microparticles, are attributed to the eruption of Mount Erebus during the spring/summer of 1984/1985.

In order to quantify the volcanic inputs, the section between the winter of 1984 and the winter of 1985 can be compared to the section between the winter of 1987 and the winter of 1988. The differences between the average values for the chemical species between these two time periods then correspond to the eruptions' input. The values calculated for each of the chemical species measured in the snow pit are presented in Table 2 under the heading Fang volcanic (parts per billion). In the table the snow pit sulfate values have been converted to elemental concentrations of sulfur in order to facil-

itate comparisons with the various source materials. The greatest total volcanic input is seen for chloride, in agreement with previous work documenting the high halogen content of Mount Erebus emissions [*Kyle et al.*, 1990; *Zreda-Gostynska et al.*, 1993]. Significant volcanic input is also seen for sulfur and sodium.

It is interesting to note a nitrate increase in the interval interpreted to correspond to spring/summer 1984/1985. The source of the apparent increase in nitrate is uncertain, but one possibility is that sal ammoniac (ammonium chloride), a common salt around volcanic vents, could occur in the Erebus vent and could have been blown out in the eruption. Partial oxidation of the ammonium could lead to increased nitrate in the snow at this depth. This interpretation is supported by the increase in ammonium at this depth.

In order to compare the composition of the Fang volcanic inputs to the composition of the noneruptive plume and to various source material, the ratio of the Fang volcanic influx to other Erebus source materials was calculated for each element. *Kyle et al.* [1990] and *Bigelow* [1985] present elemental concentrations for whole-rock analyses of Erebus bombs as well as results for analyses of inclusion and matrix glass which can be
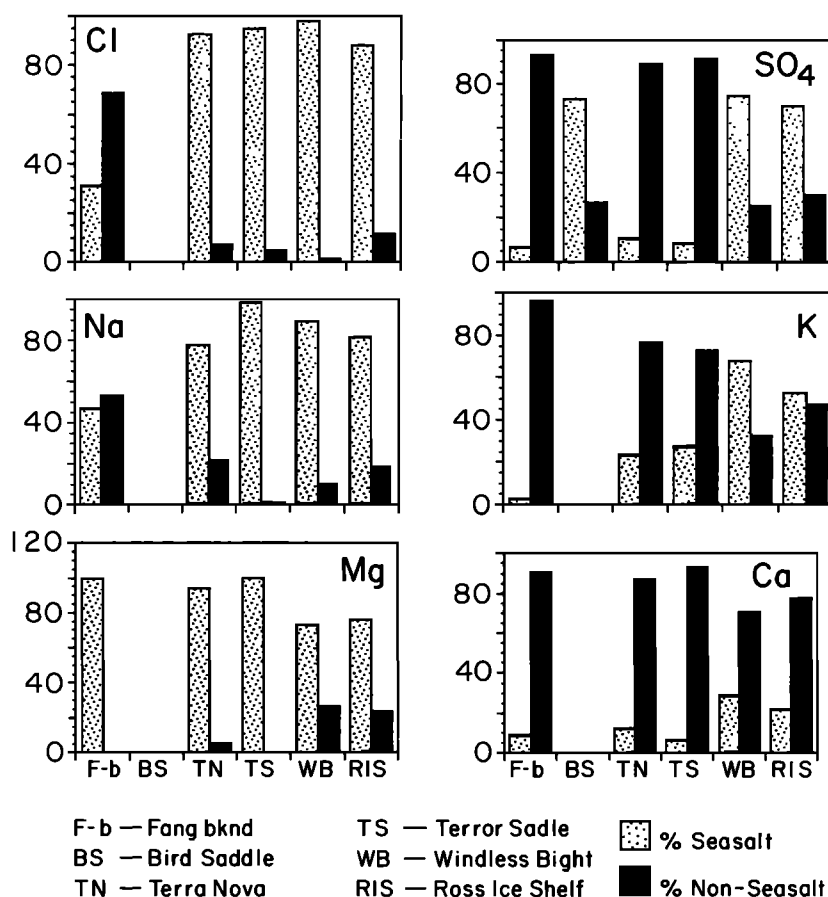
Fig. 9. Average sea-salt and non-sea-salt contributions for each of the anions and cations as a function of sample location.

used for these comparisons. These data are presented in Table 2.

The ratios of the Fang snow pit concentrations to the concentration of the other source materials for each element give information about the relative enrichment at Fang with respect to the source materials. Because it is not possible to convert all of the source composition data to similar units, the absolute values of these ratios are not important; rather, the variations of the ratios from one element to the others is what is important. For instance, the Fang snow pit data match the noneruptive volcanic plume data most closely since the numbers are all about the same. Relative to the plume, the volcanic input at Fang is slighty lower for chloride than for sulfur, sodium, calcium, and potassium. This comparison suggests that the gases emitted during the 1984/1985 eruption, recorded in the Fang snow pit, were more sulfur rich than those during subsequent noneruptive periods.

The source of the cations in the Fang pit is most like-

ly dust particles associated with the eruption, which is supported by the large increase in microparticles at the depth corresponding to the eruption fallout. The Fang cation abundances resemble the matrix glass most closely, as evidenced by the small variation in the Fang/matrix glass ratios. This suggests that the erupted material has undergone little fractionation from the source melt. Once again the eruption input (as evidenced by the Fang snow pit concentration) is more elevated for sulfur than for chlorine.

Examination of the other snow pits reveals perturbations in various parameters during the 1984/1985 time period which we also attribute to the eruptions of Mount Erebus. These perturbations are most evident in the Bird Saddle pit for SO_4^{2-}, Cl^- and microparticles, in the Terra Nova Saddle and Windless Bight pits for SO_4^{2-}, and in the Ross Ice Shelf pit for SO_4^{2-} and Cl^-. Except for the Fang site, where the volcanic perturbation is significant relative to the concentrations during noneruptive periods, most of the above mentioned chemical perturba-

TABLE 2. Concentration of Elements in Various Samples and in the 1984/1985 Volcanic Layer From the Fang Snow Pit

	Sodium	Magnesium	Calcium	Potassium	Chlorine	Sulfur
	Snow Pit Data					
Fang volcanic, ppb[a]	1,660	108	340	1,050	2,750	2,020
	Source Composition					
EB: whole rock, ppm[b]	63,275	5,160	19,000	37,940	1,110	260
EB: matrix glass, ppm[c]	66,800	5,100	13,930	45,900	1,560	330
EB: inclusion glass, ppm[c]	67,800	5,190	12,300	48,000	2,140	440
Plume samples, μg m[-3b]	96.6	NA	14.8	85.4	1,385	132
Seawater, ppm[d]	10,770	1,290	412	380	9,344	904
Whole rock/seawater	6	4	46	100	0.057	0.288
	Snow Pit/Source Ratios					
Fang/whole rock (×10^{-6})	26.3	20.9	1,709	27.7	2,495	7,777
Fang/matrix glass ((×10^{-6})	24.9	21.15	24.37	22.9	1,760	6,127
Fang/inclusion glass (×10^{-6})	24.5	20.79	27.6	21.9	1,283	4,596
Fang/plume (×10^{-6})	17.22	—	22.9	12.3	1.98	15.32
Fang/seawater (×10^{-6})	154	83.6	824	2,766	1.42	2,236

Abbreviations defined as follows: EB, Erebus bomb; NA, not analyzed.
[a]This study.
[b]*Kyle et al.* [1990].
[c]*Bigelow* [1985].
[d]*Krauskopf* [1979].

tions are relatively minor and are not identifiable unambiguously from the natural chemical variability from other sources.

CONCLUSIONS

Snow pit studies performed at a number of sites on and around Ross Island have provided some of the first data on glaciochemistry from this region. In addition to providing baseline information on snow chemistry in the Ross Island region for comparison with future work, these pit studies have allowed an assessment of the influence of Mount Erebus on the local glaciochemistry. Although there is some evidence that Mount Erebus emissions affect the chemistry of snow at sites on and around Ross Island, the volcanic signature is not unambiguous. Chloride and sulfate seem to be the most characteristic of emissions from Mount Erebus; however, because they have both a marine and a volcanic source, there are problems with swamping of the volcanic signal

TABLE 3. Seasonality of Anions, Cations, and Particles in Snow Pits From the Ross Island Region

Species	Terra Nova Saddle	Bird Saddle	Windless Bight	Ross Ice Shelf	Fang
Nitrate	Sp, W, I, Su	Sp/Su	Su	Su	Sp/Su
Chloride	F/W, I, Sp	W/SP	Sp/Su	Su	Su, I
Sulfate	Sp, F, I	W/SP	Su/F, Sp, I	Su, I	SP, Su
Sodium	F/W, I, Sp	NA	Sp/Su	Su	Sp, F
Magnesium	F/W, I, Sp	NA	Sp/Su	Su	Sp, F
Potassium	I	NA	Sp, I	Su, I	Sp, F
Ammonium	F, I	NA	I	SU, I	I
Calcium	I	NA	Sp/F, I	Su, I	Sp, F
Particles	I	Sp	NA	I	Sp, I

Abbreviations defined as follows: Sp, spring peak; Su, summer peak; F, fall peak; W, winter peak; I, irregular, seasonally not well defined; and NA, not analyzed.

by the local marine background and with identifying, unambiguously, the source of the impurities.

In this study we were unable to measure fluoride in the samples since the techniques were not developed in our laboratory. Future studies of this kind should make a greater effort to measure fluoride in the snow since it is likely to be one of the best tracers of emissions from Mount Erebus [Kyle et al., 1990] and would not have the complication of multiple sources, as is the case for sulfur and chlorine.

REFERENCES

Aristarain, A. J., R. J. Delmas, and M. Briat, Snow chemistry on James Ross Island (Antarctic Peninsula), *J. Geophys. Res.*, *87*, 11,004–11,012, 1982.

Bigelow, E. A., Techniques of volatile analysis in volcanic glass by quadropole mass spectrometry and application to Mount Erebus, Antarctica, M.S. thesis, N. M. Inst. of Mining and Technol., Socorro, 1985.

Bromwich, D. H., A satellite study of barrier-wind airflow around Ross Island, *Antarct. J. U. S.*, *23*(5), 167–169, 1988.

Chuan, R. L., Dispersal of volcano-derived particles from Mount Erebus in the Antarctic atmosphere, this volume.

Chuan, R. L., J. Palais, W. I. Rose, and P. R. Kyle, Particle sizes and fluxes of the Mount Erebus volcanic plume, December, 1983, *J. Atmos. Chem.*, *4*, 467–477, 1986.

Delmas, R. J., M. Briat, and M. Legrand, Chemistry of south polar snow, *J. Geophys. Res.*, *87*, 4314–4318, 1982.

Fiacco, R. J., Microparticles as a paleo-volcanic indicator in the 1989 GISP2 firn and ice core, M.S. thesis, 138 pp., Univ. of N. H., Durham, May 1991.

Grootes, P. M., M. Stuiver, T. L. Saling, P. A. Mayewski, M. J. Spencer, R. B. Alley, and D. Jenssen, A 1400-year oxygen isotope history from the Ross Sea area, Antarctica, *Ann. Glaciol.*, *14*, 94–98, 1990.

Herron, M. M., and C. C. Langway, Jr., Dating of Ross Ice Shelf cores by chemical analysis, *J. Glaciol.*, *24*, 345–357, 1979.

Keys, J. R., Salts and their distrbution in the McMurdo region, Antarctica, Ph.D. dissertation, Victoria Univ. of Wellington, Wellington, New Zealand, 1980.

Kienle, J., C. A. Rowe, P. R. Kyle, W. C. McIntosh, and R. R. Dibble, Eruption of Mount Erebus and Ross Island seismicity, 1984–1985, *Antarct. J. U. S.*, *20*, 25–28, 1985.

Krauskopf, K. B., *Introduction to Geochemistry*, 617 pp., McGraw-Hill, New York, 1979.

Kyle, P. R., K. Meeker, and D. Finnegan, Emission rates of sulfur dioxide, trace gases and metals from Mount Erebus,

Antarctica, *Geophys. Res. Lett.*, *17*, 2125–2128, 1990.

Kyle, P. R., L. M. Sybeldon, W. C. McIntosh, K. Meeker, and R. Symonds, Sulfur dioxide emission rates from Mount Erebus, Antarctica, this volume.

Legrand, M., Chemistry of Antarctic snow and ice, *J. Phys.* , *48*(C1), 77–86, 1987.

Legrand, M. R., and R. J. Delmas, The ionic balance of Antarctic snow: A 10-year detailed record, *Atmos. Environ.*, *18*, 1867–1874, 1984.

Legrand, M. R., and R. J. Delmas, Spatial variations of snow chemistry in Terre Adelie (East Antarctica), *Ann. Glaciol.*, *7*, 20–25, 1985.

Legrand, M. R., and R. J. Delmas, Relative contributions of tropospheric and stratospheric sources to nitrate in Antarctic snow, *Tellus, Ser. B*, *38*, 236–249, 1986.

Legrand, M. R., and R. J. Delmas, Formation of HCl in the Antarctic atmosphere, *J. Geophys. Res.*, *93*, 7153–7168, 1988.

Legrand, M., and C. Feniet-Saigne, Methanesulfonic acid in south polar snow layers: A record of strong El Nino?, *Geophys. Res. Lett.*, *18*, 187–190, 1991.

Legrand, M., and S. Kirchner, Polar atmospheric circulation and chemistry of recent (1957–1983) south polar precipitation, *Geophys. Res. Lett.*, *15*, 879–882, 1990.

Legrand, M., C. Feniet-Saigne, E. S. Saltzman, C. Germain, N. I. Barkov, and V. N. Petrov, Ice core record of oceanic emissions of dimethylsulphide during the last climatic cycle, *Nature*, *350*, 144–146, 1991.

Mayewski, P. A., and M. R. Legrand, Recent increase in nitrate concentration, of Antarctic snow, *Nature*, *346*, 258–260, 1990.

Mayewski, P. A., M. J. Spencer, W. B. Lyons, and M. S. Twickler, Seasonal and spatial trends in south Greenland snow chemistry, *Atmos. Environ.*, *21*, 863–869, 1987.

Mayewski, P. A., M. J. Spencer, M. S. Twickler, and S. Whitlow, A glaciochemical survey of the summit region, Greenland, *Ann. Glaciol.*, *14*, 186–190, 1990.

Meeker, K. A., P. R. Kyle, and R. Chuan, Particle emissions from Mount Erebus during the 1986–1987 field season, *Antarct. J. U. S.*, *22*, 247–248, 1987.

Meeker, K., R. Chuan, P. Kyle, and J. Palais, Emission of elemental gold particles from Mount Erebus, Ross Island, Antarctica, *Geophys. Res. Lett.*, *18*, 1405–1408, 1991.

Neubauer, J., and K. G. Heumann, Nitrate trace determinations in snow and firn core samples of ice shelves at the Weddell Sea, Antarctica, *Atmos. Environ.*, *22*, 537–545, 1988.

Palais, J. M., R. Chuan, and M. J. Spencer, Soluble and insoluble impurities in snow samples from Ross Island, Antarctica, *Antarct. J. U. S.*, *24*, 89–90, 1989.

Parker, B. C., E. J. Zeller, and A. J. Gow, Nitrate fluctuations in Antarctic snow and firn: Potential sources and mechanisms of formation, *Ann. Glaciol.*, *3*, 243–248, 1982.

Polian, G., and G. Lambert, Radon daughters and sulfur output from Erebus Volcano, Antarctica, *J. Volcanol. Geotherm. Res.*, *6*, 125–137, 1979.

Radke, L. F., Sulphur and sulphate from Mount Erebus,

Nature, *299*, 710–712, 1982.

Rose, W. I., R. L. Chuan, and P. R. Kyle, Rate of sulphur dioxide emissions from Erebus Volcano, Antarctica, December, 1983, *Nature*, *316*, 710–712, 1985.

Wagenbach, D., U. Gorlach, K. Moser, and K. I. Munnich, Coastal Antarctic aerosol: The seasonal pattern of its chemical composition and radionuclide content, *Tellus, Ser. B*, *40*, 426–436, 1988.

Warburton, J. A., and G. O. Linkletter, Atmospheric processes and the chemistry of snow on the Ross Ice Shelf, Antarctica, *J. Glaciol.*, *20*, 149–162, 1978.

Warburton, J. A., and L. G. Young, Estimating ratios of snow accumulation in Antarctica by chemical methods, *J. Glaciol.*, *27*, 347–357, 1981.

Warburton, J. A., J. V. Molenar, C. R. Cornish, M. S. Owens, and L. G. Young, Time-related changes in snow chemistry—Ross Ice Shelf, Antarctica, *Cold Reg. Sci. Technol.*, *4*, 27–39, 1981.

Zeller, E. J., G. A. M. Dreschhoff, and C. M. Laird, Nitrate flux on the Ross Ice Shelf, Antarctica and its relation to solar cosmic rays, *Geophys. Res. Lett.*, *13*, 1264–1267, 1986.

Zreda-Gostynska, G., P. R. Kyle, and D. L. Finnegan, Chlorine, fluorine, and sulfur emissions from Mount Erebus, Antarctica, and estimated contributions to the Antarctic atmosphere, *Geophys. Res. Lett.*, *20*, 1959–1962, 1993.

R. L. Chuan, P.O. Box 1183, Hanalei, HI 96714.

J. M. Palais, Office of Polar Programs, National Science Foundation, 4201 Wilson Boulevard, Room 755, Arlington, VA 22230.

M. J. Spencer, Glacier Research Group, University of New Hampshire, Durham, NH 03824.

CRYSTALLIZATION PROCESSES OF ANORTHOCLASE PHENOCRYSTS IN THE MOUNT EREBUS MAGMATIC SYSTEM: EVIDENCE FROM CRYSTAL COMPOSITION, CRYSTAL SIZE DISTRIBUTIONS, AND VOLATILE CONTENTS OF MELT INCLUSIONS

Nelia W. Dunbar

Department of Geoscience, New Mexico Institute of Mining and Technology, Socorro

Katharine V. Cashman and Roslyn Dupré

Department of Geological and Geophysical Sciences, Princeton University, Princeton, New Jersey

Mount Erebus, Antarctica, is a large, active, phonolitic volcano that contains an actively convecting and continuously degassing phonolite lava lake. Bombs emitted during eruptions contain strikingly large anorthoclase feldspar phenocrysts, which appear to be the product of a two-stage growth process. Initial crystal growth produces a spongy core, containing abundant melt inclusions (MI), followed by deposition of fine laminae that form the crystal rims. Crystal size distributions suggest that these crystals have low nucleation rates, but nucleate and grow continuously through time. Trace and major element systematics, combined with Normarski imaging, suggest that crystal cores are a result of rapid growth, whereas the rims are the result of slow growth coupled with repeated resorption episodes. The MI found in anorthoclase crystals are compositionally similar to matrix glass. The volatile contents of MI are low, suggesting that the crystals grew from degassed magma at depths of between 400 m and the surface. Degassing of the magma during ascent may trigger rapid, low-pressure crystallization.

INTRODUCTION

Mount Erebus, on Ross Island, Antarctica, is a large (3794 m) active volcano that contains a convecting phonolite lava lake. Eruptive activity at Mount Erebus is typified by small daily strombolian eruptions, some of which eject bombs onto the crater rim. Anomalously energetic explosive activity occurred in September 1984, with bombs up to 10 m in diameter thrown over a kilometer into the air, landing several hundred meters beyond the crater rim. The phonolite bombs are highly vesicular and contain unusually large anorthoclase feldspar crystals (up to 9 cm in length), as well as clinopyroxene crystals. Olivine, magnetite, pyrrhotite, and apatite are also present in minor quantities and represent primary phases that crystallized from the present phonolitic magma [*Kyle*, 1977].

Anorthoclase megacrysts are characteristic features of anorthoclase phonolite (kenyte) lavas (e.g., Mount Kenya, Mount Kilimanjaro). The unusually large size of the crystals poses an interesting question as to their origin: Are they the result of long residence times in the magmatic reservoir, or are they the result of unusual crystallization kinetics (low nucleation densities combined with rapid growth)? Measured crystal size distributions (CSDs) place constraints on the history of crystal growth in shallow magmatic systems [e.g., *Marsh*, 1988a; *Cashman*, 1990]. Analysis of the form of the anorthoclase CSDs, the overall number density and average size of crystals in the magma, and the zoning patterns of individual crystals of different sizes are combined to provide constraints on crystallization in the Erebus system.

Additional information on the process of crystallization lies in the volatile history of the phonolitic magma. Investigation of melt inclusions (MI) in the Mount Erebus phenocrysts was undertaken to determine the preeruptive volatile contents of the phonolitic magma,

129

with the goal of complimenting studies of active magmatic degassing [*Meeker*, 1988; *Kyle et al.*, 1990]. Both the anorthoclase and the pyroxene phenocrysts contain up to 30% MI. Because MI are trapped within phenocrysts, quench rapidly, and do not degas during the eruptive process, they can be used as indicators of the volatile composition of a magma at the time of crystal growth [*Roedder*, 1984]. Volatiles in magma not trapped within MI are lost by degassing during magmatic convection of the lake and eruptions, thus leaving no direct method to determine the preeruptive volatile composition of the magma. By comparing the volatile contents of MI and degassed magma (matrix glass), it is possible to assess changes in magmatic volatile contents resulting from volcanic eruptions [e.g., *Devine et al.*, 1984].

Although it is difficult to uniquely constrain the rate or exact location and timing of crystallization, the results of combined MI, anorthoclase composition, and CSD data provide evidence that (1) nucleation and growth of anorthoclase crystals have occurred in two stages, with earlier growth of chemically homogeneous, MI-rich cores followed by finely oscillatory zoned rims, (2) CSDs show no evidence for anomalous accumulation or depletion of crystals, and (3) MI are composed of volatile-poor melt that is chemically similar to matrix glass. A model for crystallization in the shallow magmatic reservoir at Mount Erebus that satisfies these observations is one of rapid anorthoclase crystal growth resulting from volatile exsolution at relatively shallow levels in the magmatic system, followed by near-surface convection and additional crystal growth in the lava lake that occupies the Inner Crater of the volcano.

BACKGROUND

Textural Evidence for Processes of Crystallization

Detailed investigation of crystal compositional zoning combined with measured size distribution characteristics of a given phase has the potential to provide important information on the relative importance of nucleation and growth throughout the crystallization interval [e.g., *Cashman*, 1990], and the patterns of crystallization and the frequency of episodes of rapid growth and/or resorption during the formation of a single crystal [e.g., *Pearce and Kolisnik*, 1990]. Used together, these techniques have the potential to elucidate the importance of physical changes in the system (e.g., episodes of magmatic convection, mixing, degassing) as recorded by the chemical response to change.

Unambiguous interpretation of zoning profiles in crystals remains elusive despite substantial effort devoted to this problem in igneous petrology. Recent advances such as the application of Nomarski interference contrast microscopy [*Anderson*, 1984], laser interferometry [*Pearce*, 1984], and analysis of trace element distributions [*Blundy and Shimizu*, 1991] have significantly increased our understanding of zoning patterns, and thus something of their origins. For example, *Pearce and Kolisnik* [1990] identify two main types of crystal zoning patterns in plagioclase: type 1 zoning is characterized by small zone widths (<10 μm), small changes in composition (<10% An), and euhedral interfaces. Greater widths (up to 100 μm), large and abrupt changes in compositions (up to 37% An), and irregular interfaces, which probably result from dissolution, constitute type 2 zones. *Pearce and Kolisnik* [1990] interpret these differences in zoning style to reflect fundamental differences in zoning origin. Ubiquitous type 1 zones are probably the result of local disequilibrium at the crystal-melt interface, whereas episodic type 2 zones represent changes in the physical conditions of crystallization such as those resulting from convective overturn, mixing, or eruption.

The rate at which crystallization proceeds in a magmatic system is controlled by the balance between the kinetics of crystallization and the rate at which the magma is supersaturated in the crystallizing component. Supersaturation can occur through cooling, depressurization, and/or degassing. A method of determining crystallization rates in magmas is the measurement of the size distribution of crystals in systems where crystallization times are known [*Marsh*, 1988a, b; *Cashman and Marsh*, 1988]. Such measurements suggest that crystal growth rates for plagioclase in basaltic melts are controlled by cooling rates and are commonly 10^{-10} to 10^{-11} cm/s for conditions of shallow magmatic cooling (summarized by *Cashman* [1992]). *Mangan* [1990] extended this work using measured size distributions of phenocrystic olivine to determine average crystal residence times (magma storage time) at shallow levels prior to the 1959 eruption of Kilauea Volcano. The only constraints on crystal growth rates in alkalic magmas are those of *Peterson* [1990], who estimated growth rates of 5 x 10^{-11} cm/s for combeite growth in nephelinite of Ol Doinyo Lengai. The form of the measured CSD also allows assessment of physical perturbations to the crystallizing system, such as crystal depletion or accumulation resulting from settling, mixing of magmas containing two very different crystal populations, or significant crystal growth without nucleation of new crys-

tallites [*Marsh*, 1988*a, b*; *Cashman*, 1990].

Melt Inclusions

Melt inclusions are small samples of magma that are trapped within crystals during crystalline growth [*Roedder*, 1984]. If unaltered, MI provide direct samples of preeruptive magma and contain the volatile content of the magma at the time that the crystal grew. MI can contain any phases which were present in the melt at the time of crystal growth (e.g., melt, exsolved fluid, and crystals). Contraction bubbles sometimes form during cooling of a MI after eruption when differential contraction causes the melt to shrink more than the surrounding crystal while the glass is still plastic [*Roedder*, 1984]. While these contraction bubbles are likely to contain a volatile phase, probably dominated by H_2O or CO_2, exsolved gas generally represents a small proportion of the total volatile content of the MI [*Anderson et al.*, 1989].

A number of factors may cause MI compositions to deviate from true melt compositions. First, additional host crystal may be deposited on the crystal walls if a crystal which trapped a droplet of pristine magma remains at high temperature. The remaining glass will be enriched or depleted in elements that are respectively incompatible or compatible in the crystal. "Postentrapment crystallization" has been recognized by a number of workers [*Watson*, 1976; *Anderson and Wright*, 1972]. The extent of postentrapment crystallization in a MI can be assessed by detailed major and trace element characterization of the inclusions. If the major and trace element chemistry of the inclusion agrees closely with the major element chemistry of the crystal-free whole rock (or inferred melt composition), insignificant postentrapment crystallization has taken place [e.g., *Beddoe-Stephens et al.*, 1983]. Another potential problem with MI is that the melt may be altered just prior to trapping. Rapid crystal growth may prevent elements from diffusing efficiently toward or away from the crystal-magma interface, thus forming an envelope of anomalous melt around the growing crystal. Comparison of MI composition with inferred melt composition and detailed investigation of crystal composition near MI allows recognition of this problem.

ANALYTICAL METHODS

Three volcanic bombs were analyzed for their crystal content: two erupted in September 1984 and one in December 1988. The matrix glass of the bombs is extremely fragile and easily desegregated. All individual anorthoclase crystals with lengths of 0.3 to 8 cm contained in a given bomb were separated by hand from the glassy matrix. Separation of whole crystals allowed crystal long, intermediate, and short axes to be measured by hand with calipers (measurements are accurate to within 0.01 cm), thus avoiding the problem of converting size measurements in two dimensions to three dimensions [*Cashman and Marsh*, 1988]. In the separation process it was noted that a significant proportion (up to one third) of crystals in each bomb showed a single fracture perpendicular to their long axis. Apparently, this breakage occurred as a result of eruption, as careful dissection of individual bombs showed matching pieces separated by vesicles. For this reason the crystal size plots shown are for measured crystal widths, a dimension still measurable after breakage. Crystal frequency plots are created assuming that the total number of crystals in a given size class is equal to the number of unbroken crystals in the size class plus one half the number of broken crystals (as a large percentage of the broken crystals contain only a single fracture). We consider it important to include these crystals as larger crystals were more prone to breakage during eruption than smaller crystals; thus neglecting them would tend to skew the measured population to the smaller sizes. Lava volume (vesicle-free) for each sample was determined by weighing the glass and crystals separately, assuming densities of 2.7 g/cm^3 (glass) and 2.58 g/cm^3 (anorthoclase).

Selected crystals from each sample were sectioned parallel to their long axis and perpendicular to their short axis. Both large (5–6 cm) and small (1–2 cm) crystals were examined from each sample. Crystal zoning patterns were imaged using Nomarski interference contrast microscopy [*Anderson*, 1983]; Nomarski work was done in the laboratory of T. H. Pearce, Queens University, Canada. Polished thin sections were etched with concentrated HBF_4 (fluoroboric acid) to preferentially etch the more calcic zones; etching times were of the order of 10 min (in contrast to the usual 30-s etch for plagioclase), a result of the low anorthite content of the anorthoclase crystals. Selected crystals were also analyzed for compositional profiles. All electron microprobe work was done at Rutgers University on a JEOL 8600 superprobe at operating conditions of 15 kV and 15 nA.

The major and trace element composition of MI and the trace element compositions of some feldspar and pyroxene phenocrysts were determined by electron microprobe and ion microprobe, respectively. Major
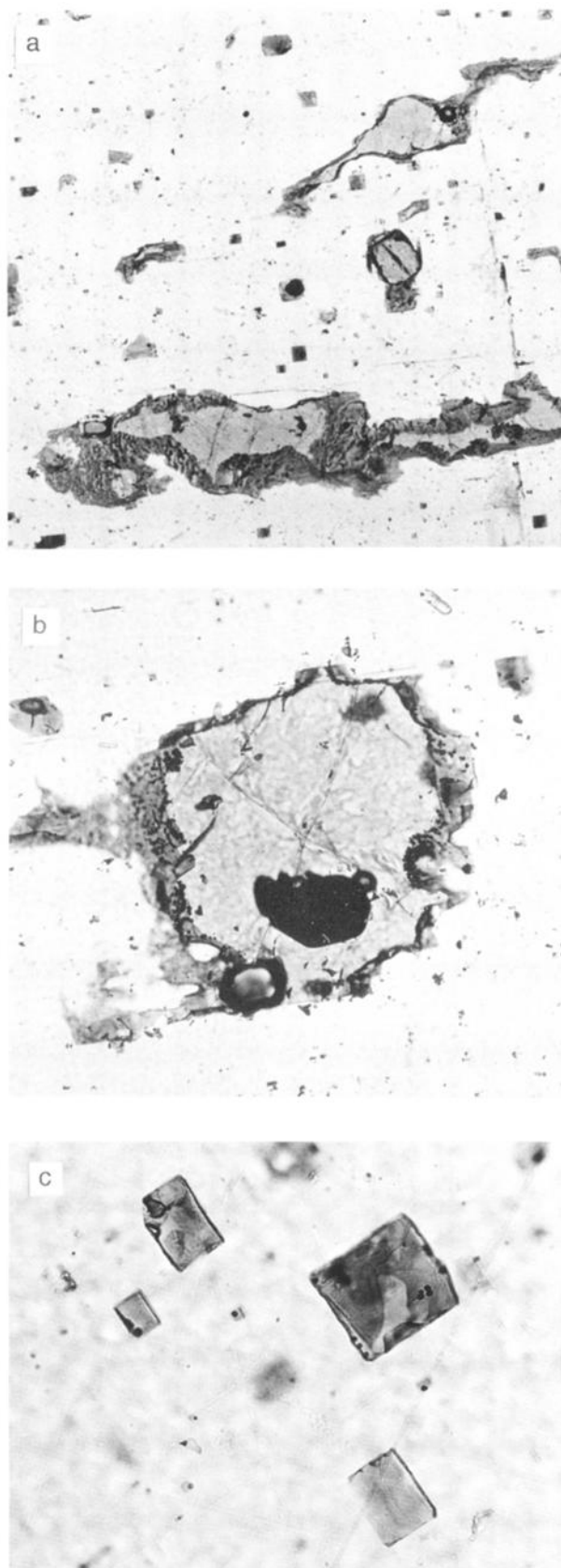
element analyses were made using JEOL 733 micro-probe at Victoria University (New Zealand) and a JEOL 8600 microprobe at Arizona State University, using standard techniques for glass analysis. Trace element analyses were made with a Cameca 3f ion microprobe at Arizona State University. Analytical techniques used are detailed by *Hervig et al.* [1989] and *Dunbar et al.* [1989]. Matrix glass (crystal-free glass that forms the matrix of eruptive bombs) represents the composition of crystal-free magma and was analyzed in microsamples by ion microprobe and in bulk by X ray fluorescence and instrumental neutron activation analysis in order to check ion microprobe analyses. Analyses made by ion microprobe represent true crystal-free melt composition, whereas analyses by the other techniques may include some small crystals.

The H_2O and F contents of MI from Mount Erebus were determined using ion microprobe analysis. This technique involves bombarding the sample with an ion beam, sputtering positive or negative ions off the sample surface, and analyzing these secondary ions [*Morrison and Slodzian*, 1975]. Volatile elements H (presumed to occur only in H_2O) and F can be analyzed by this technique with accuracies of ±0.1 wt % and ±100 ppm or better, respectively. The application of ion microprobe analyses of MI is discussed in detail by *Hervig et al.* [1989] and *Dunbar et al.* [1989].

Volatile elements Cl and S were analyzed by electron microprobe [*Dunbar et al.*, 1989]. The essential points in the use of electron microprobe for volatile analyses are that the beam must be widened to at least 20 μm to reduce volatilization and count times must be long (e.g., 150 s on the peak and 75 s on the background) as a result of low abundances of these elements. Detection limits for both S and Cl are about 50 ppm [*Devine et al.*, 1984].

Finally, thermal information about a host magma can be determined by MI analysis. Temperature measurements involve heating the MI on a heating stage and can determine the minimum temperature at which the MI was trapped (homogenization temperature, T_h) [*Roedder*, 1984]. The homogenization temperature is the temperature at which all phases present homogenize to a

Fig. 1. (Opposite) Photomicrographs of MI in an anorthoclase phenocryst from Mount Erebus. (*a*) The general distribution of MI within feldspar matrix is shown. Two end-member types of MI are apparent, those which are large and irregular and those which are small and rectangular (field of view is 2 mm). (*b*) Large, irregular MI, including a number of small bubbles (field of view is 2 mm), and (*c*) small, negative crystal-shaped MI, with a single, small bubble (field of view is 0.5 mm), are also shown.
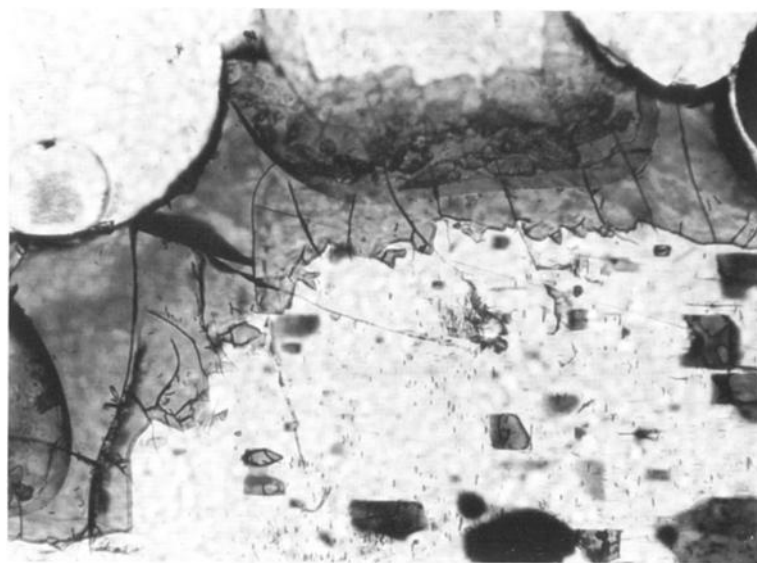
Fig. 2. Photomicrograph illustrating the extremely irregular interface between the anorthoclase crystals and the surrounding melt (matrix glass). Plane-polarized light; field of view in approximately 0.5 cm in the long dimension.

single phase [*Roedder*, 1984]. A number of studies have been made of MI-trapping temperatures which appear to have yielded accurate results [e.g., *Clochiatti et al.*, 1976; *Chaigneau et al.*, 1980; *Belkin et al.*, 1985; *Corti-ni et al.*, 1985].

GENERAL OBSERVATIONS

Individual anorthoclase crystals were sectioned both parallel and perpendicular to their long axes. Large (<3 cm in length) crystals are composed of a MI-rich, "spongy" core, which represents most of the crystal volume. Melt inclusions represent up to 30% of the crystal volume and occur in two morphologies: large and irregularly shaped (up to 1000 μm in the longest direction) or small and euhedral (up to 100 μm in diameter) (Figure 1). MI are composed of brownish-green glass and commonly contain both small crystals of phenocryst phases (clinopyroxene, olivine, titanomagnetite, apatite) and small bubbles that are probably the result of differential shrinkage of glass and crystal during quenching. Bubbles are most abundant in the irregular MI (Figure 1b); these bubbles are generally clustered around the edge of the MI. All crystals also have finely zoned rims, obvious in thin section as defined by bands of small (up to 100 μm), euhedral MI (Figure 1c). The boundary between the homogeneous crystal core and the finely zoned rim is commonly marked by very large, irregular MI. Small (1–2 mm) anorthoclase crystals commonly

show fine-scale zoning throughout their length and show little evidence for the homogeneous core of the larger crystals. In these smaller crystals, growth was very asymmetric with growth zones very thin or even missing perpendicular to the long axis of growth. All crystals exhibit euhedral morphologies, although the crystal-melt boundary is commonly irregular in detail (Figure 2). Crystal boundary irregularities such as those shown in Figure 2 will promote MI entrapment when euhedral crystal growth resumes. Thus the internal structure of the feldspar crystals suggests at least two growth stages: (1) growth of the homogeneous cores accompanied by the entrapment of large MI and (2) growth of finely zoned rims with periodic entrapment of euhedral MI.

Nomarski interference images illustrate the extreme complexities of the zoning patterns that characterize the anorthoclase rims. The most prominent zoning in the rims is termed "hieroglyphic texture" by *Pearce and Kolisnik* [1990]. Bands of extremely irregular hieroglyphic zoning are commonly punctuated by thin, regular "type 1" zones (Figure 3). Note the MI are contained within the hieroglyphic bands, and the thin regular zones display the same wavy morphology that is seen at the current crystal boundaries. Alternating type 1 and hieroglyphic zoning bands are observed throughout the length of many of the smaller crystals (Figure 4) with growth predominantly along the long axis. In the smaller crystals some zones appear to have been sharply truncated (resorbed) parallel to the long axis. In all crystals
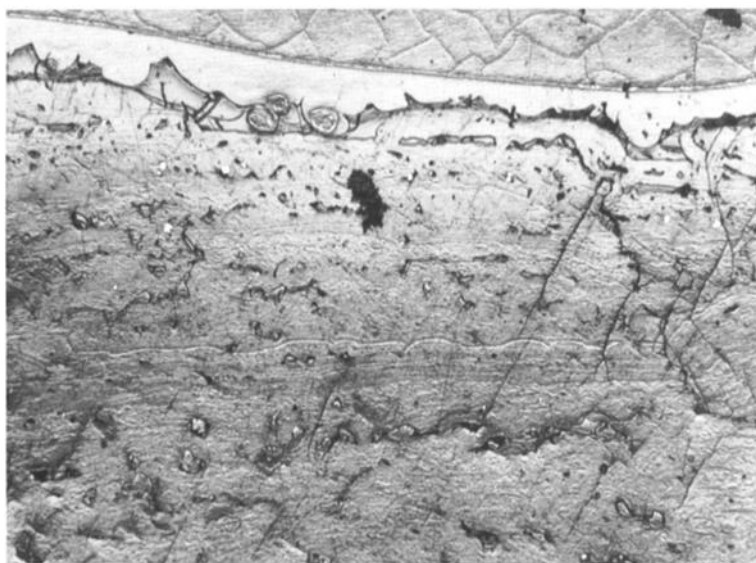
Fig. 3. Photomicrograph taken using Nomarski interference contrast microscopy illustrating typical rim zoning patterns. Note especially (1) the larger MI along the outer rim zone, (2) the convoluted zoning around the MI and in another interior zone, and (3) the very irregular boundary of both the internal zones and again of the crystal-melt interface. Scale is approximately 0.5 cm in the long dimension.

this type of zoning has a rough periodicity of 300–500 μm. We emphasize that the large size of even our "smaller" crystal population allowed sectioning of these crystals exactly through the crystal long axis; thus the observed zoning is not an artifact of the sectioning process.

MAJOR AND TRACE ELEMENT COMPOSITIONS OF ANORTHOCLASE AND MI

Electron microprobe compositional scans were collected on several individual anorthoclase crystals to assess the extent of chemical variation in the rim zones
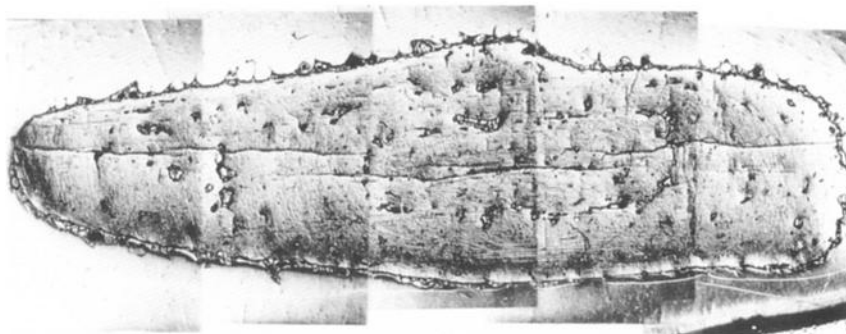
Fig. 4. Composite photomicrograph showing zoning patterns typical of the smaller crystals. Note (1) extreme elongation in the long axis direction, (2) apparent truncation of some growth zones perpendicular to the long axis, (3) delineation of interior crystal core by extensive MI, (4) again, uneven boundaries at the crystal-melt interface, and (5) alternation between regular, type 1 zones and uneven "hieroglyphic" texture; the typical cycle is approximately 300-500 μm in length. The entire crystal is approximately 1.5 cm long.
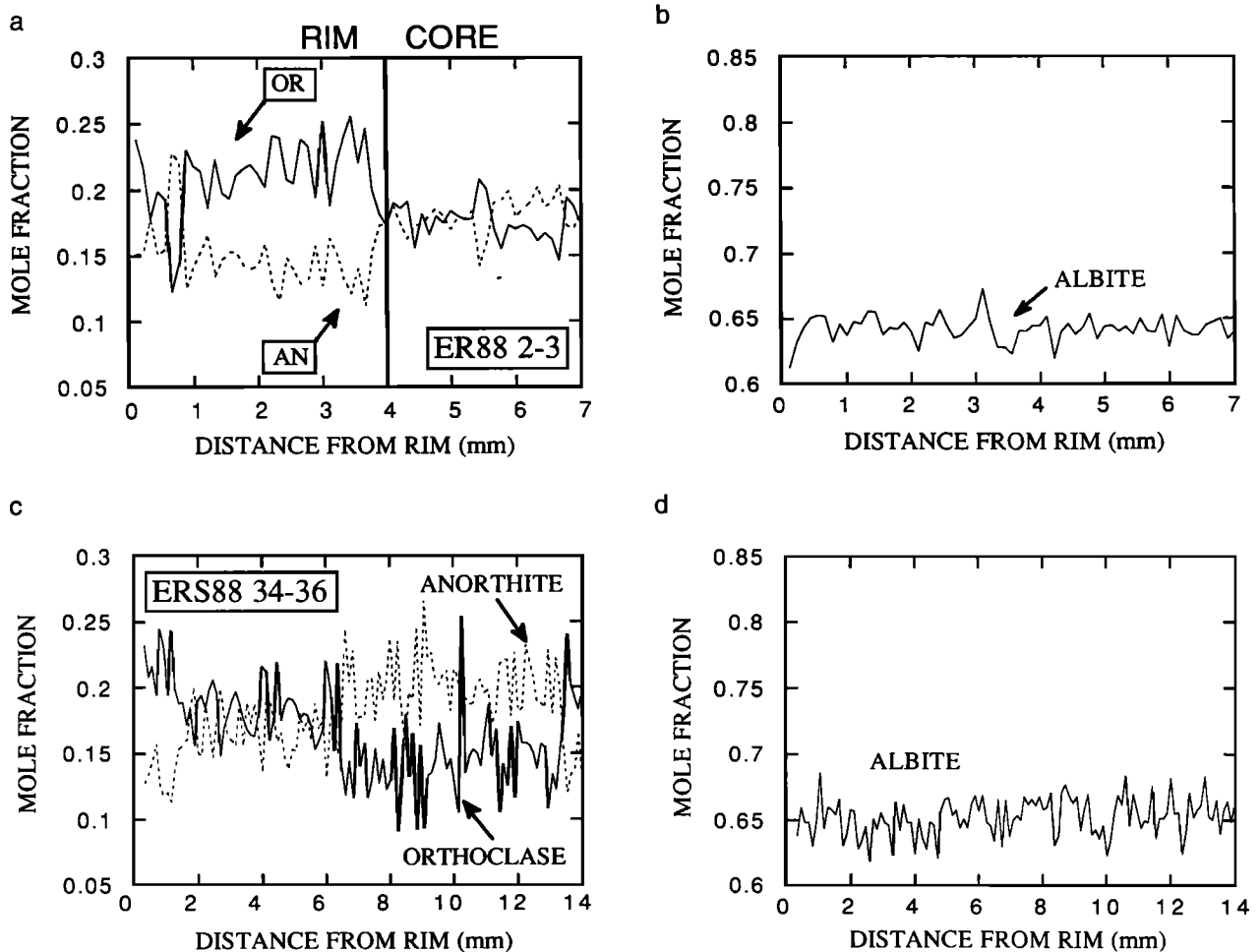
Fig. 5. Typical electron microprobe scans across the rim of (a)-(b) a large crystal and (c)-(d) a core-to-rim traverse of a smaller crystal. The larger crystal (ER88) is 3 cm wide by 6 cm long; shown here is a traverse across the outer 7 mm of the rim and into the crystal core. The region of the traverse is pictured in Figure 5b (to the left of the obvious bend). The smaller crystal is 2.2 cm in length and 0.75 cm wide; the traverse shown includes about half the length of crystal. Note the large variations in Or and An content in both crystals relative to the constant Ab content.

delineated by the small MI. As illustrated above, the zoning seen in Nomarski interference microscopy is morphologically complex; this complexity was borne out in our inability to correlate individual compositional zones, even from two transects across the rim of the same crystal. There are generalizations that can be made, however, concerning patterns of zoning in the anorthoclase crystals.

First, compositional zoning exists as variations in anorthite and orthoclase components of the anorthoclase; the albite (Ab) component is relatively constant at mole fraction Ab 0.65 ± 0.02 across all crystals, small

and large (Figure 5). Second, rim compositions are distinct from core compositions in the extent of compositional zoning apparent in electron microprobe traverses (Figure 5). Crystal cores in all large 1984 and 1988 crystals analyzed are relatively unzoned, with mole fraction An and Or between 0.15 and 0.2. In contrast, crystal rims' orthoclase (Or) and anorthite (An) mole fractions vary inversely between 0.1 and 0.27. In general, rim compositions are characterized by high Or contents (0.2–0.27), although there are places where Or and An are reversed. Rim widths as denoted by a change in zoning pattern are 2–4 mm (Figure 5).

TABLE 1. Average Major, Volatile, and Trace Element Abundance of Melt Inclusions, Matrix Glass, and Phenocrysts From Anorthoclase Phonolite Bombs From Mount Erebus

| | Melt Inclusions | | Matrix | Whole | Phenocrysts | |
	Feldspar	Pyroxene	Glass	Rock*	Feldspar†	Pyroxene
	Major Elements, wt %					
SiO_2	54.8	54.5	55.0	55.93	61.61	49.95
Al_2O_3	20.5	20.4	20.2	19.74	22.32	4.14
TiO_2	1.0	1.0	1.0	1.10	0.19	1.91
FeO	5.2	5.6	5.6	4.59	0.18	8.99
MgO	0.8	0.9	0.9	1.23	0.27	12.49
CaO	2.0	2.1	1.9	3.20	3.35	20.62
Na_2O	9.4	9.6	9.5	7.77	7.49	1.01
K_2O	5.7	5.4	5.5	4.33	3.17	0.99
	Volatile Elements, wt %					
H_2O	0.2 (0.02)	0.1 (0.05)	0.1 (0.08)			0
F	0.27 (0.04)	0.29 (0.05)	0.30 (0.02)			0.06
S	0.065 (0.008)	0.053 (0.07)				
Cl	0.17 (0.014)	0.18 (0.015)	0.18 (0.01)		0	0
	Trace Elements, ppm					
Li	45 (13)	36 (3)	35 (1)		1 (1)	
B	32 (7)	15 (2)	16 (4)		15 (6)	
P	1940 (250)	1371 (122)	1963 (280)		140 (19)	
Rb	145 (18)	142 (11)	163 (15)	19	18 (3)	
Y	66 (4)	60 (9)	51 (5)	49	1 (1)	
Sr	199 (73)	182 (25)	219 (14)	990	2242 (77)	
Zr	1572 (122)	1607 (150)	1335 (39)	855	3 (2)	
Nb	396 (31)	372 (22)	379 (27)	236	1 (1)	
Ba	485 (152)	480 (36)	536 (4)	1064	2688 (213)	
Ce	287 (20)	320 (57)	299 (26)	204.2	29 (4)	
Th	29 (6)	23 (8)	26 (6)	17.5	2 (1)	
n (electron probe)	9	8	3	†	5	
n (ion probe)	9	4	3	6	unavailable	

Major elements, Cl, and S were analyzed by electron microprobe; all other analyses are made by ion microprobe. Errors of determination for electron microprobe are as follows, based on counting statistics: $SiO_2 \pm 1\%$; $Al_2O_3 \pm 1\%$; $TiO_2 \pm 3\%$; FeO $\pm$ 2%; MgO $\pm$ 15%; CaO $\pm$ 10%; $Na_2O \pm 1\%$;$K_2O \pm 1\%$. Errors for Cl and S, based on replicate analyses of a standard, are both around $\pm$ 100 ppm. Ion microprobe errors are ± 0.1 wt % of H_2O and $\pm$ 15% for F and other trace elements. Number of analyses range between 1 and 10 for each mean value shown. Standard deviations of analysis sets are given in parentheses.

*Analyses from *Kyle et al.* [1993].

†Major element analysis from *Kyle* [1977].

Smaller crystals (crystal length <1 cm) from both 1984 and 1988 lavas are characterized by pronounced zoning seen throughout most of their length, both as denoted by small MI and as delineated in Nomarski images (e.g., Figure 4). In some cases the entire length of the crystal shows zonation (Figures 4, 5c, and 5d), while in others there appears to be a distinct boundary between core and rim similar to that shown in Figure 5a for the outside centimeter of a larger crystal. In the latter case the apparent rim along the long axis of the smaller crystals is again 2–4 mm in width. Chemical zoning patterns suggest that these crystals experienced the same patterns of growth as the

larger crystals, with the conditions that promoted zonation characteristic of rim growth prevalent for a greater proportion of the period of small crystal growth.

Clinopyroxene major element compositions are constant at $En_{57-58}Fs_{15-16}Wo_{17-18}$ for crystals included in large anorthoclase crystals as well as for phenocryst phases in the magma (Table 1). Olivine compositions are similarly constant at Fo_{53-54}, in agreement with analyses reported by *Kyle* [1977].

Major element compositions of MI in anorthoclase and pyroxene are shown in Table 1 to be virtually identical to the matrix glass composition. While MI compositions are
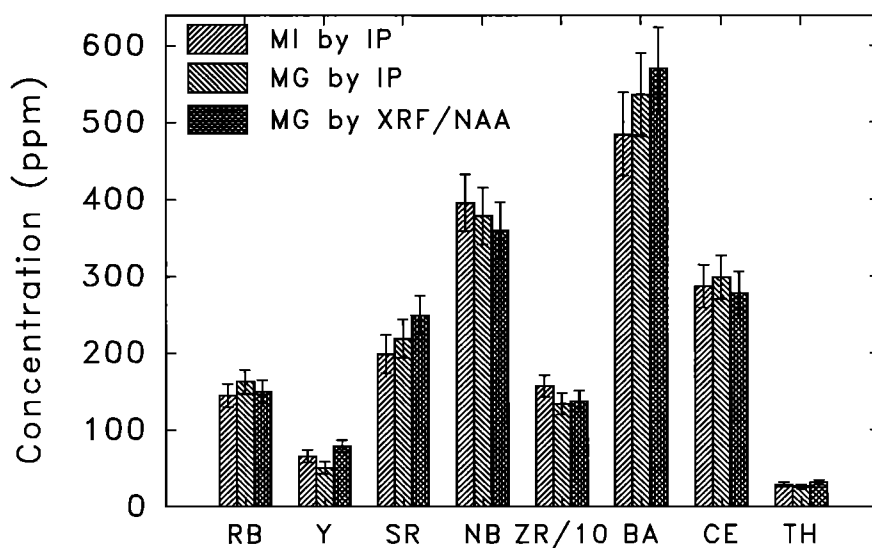
Fig. 6. Histogram of trace element composition of MI and matrix glass from Mount Erebus. Compositions of MI are measured by ion microprobe, and those of matrix glass are measured by both ion microprobe and neutron activation analysis.

slightly variable across a single crystal, the variations represent no discernible pattern, an observation consistent with that of *Kyle* [1977]. Note that MI compositions are similar to whole rock analyses of anorthoclase bombs presented by *Kyle* [1977], shown in Table 1. The main difference between matrix glass and whole rock compositions is the higher total alkali content of the matrix glass relative to that of the whole rock. This similarity in composition exists despite ~35% crystallization (weight percent; based on weight ratios of separated crystals and glass from individual volcanic bombs) and illustrates the near-eutectic composition of the anorthoclase magma.

Minor and trace elements show an even greater consistency between the matrix glass and the MI compositions (Table 1, Figure 6). Again, there does not appear to be any significant variation of MI composition from core to rim of the phenocrysts, nor is there any systematic difference between the compositions of large and small MI. The compositional similarity between MI and matrix glass from the Erebus magmatic system suggests that the MI are representative of preeruptive magma and that no significant alteration has affected the MI, either preentrapment or postentrapment. In some MI, there is evidence of a small amount of postentrapment crystallization (Figure 7). Absence of measurable depleted zones around anorthoclase crystals in erupted lava suggests that this is not a likely problem for the larger MI. The anorthoclase crystal compositions are enriched approximately 10 times in Sr and Ba with respect to

glass. However, some MI in feldspar are slightly depleted in Sr and Ba as compared to matrix glass. This slight depletion could be caused by some crystallization of feldspar onto the interior walls of the MI after entrapment, and by the Sr and Ba content of the crystal, which is so high that the glass would become disproportionally depleted in these components. For example, the three points in Figure 7 that are depleted in Ba and Sr compared to matrix glass composition are located at the edge of the MI, near the crystal-melt interface. The limited amount of postentrapment crystallization would have little effect on the volatile content of MI.

VOLATILE CONTENTS OF MELT INCLUSIONS

Ion microprobe analyses of MI from anorthoclase and pyroxene phenocrysts reveal that the H_2O content of these inclusions is low (Table 1). The relative abundance of volatile components within MI from the Mount Erebus anorthoclase and pyroxene phenocrysts is unusual, because the Cl and F contents of the glass are higher than H_2O, the volatile component that generally dominates the gas phase in volcanic systems. The H_2O content of the glass ranges between 0.1 and 0.3 ($\pm$0.1) wt %, the Cl contents between 0.20 and 0.25 ($\pm$0.01) wt %, and the F contents between 0.30 and 0.35 ($\pm$0.03) wt %. The S contents are lower, between 0.05 and 0.07 ($\pm$0.01) ppm.

Although the MI from Mount Erebus appear repre-
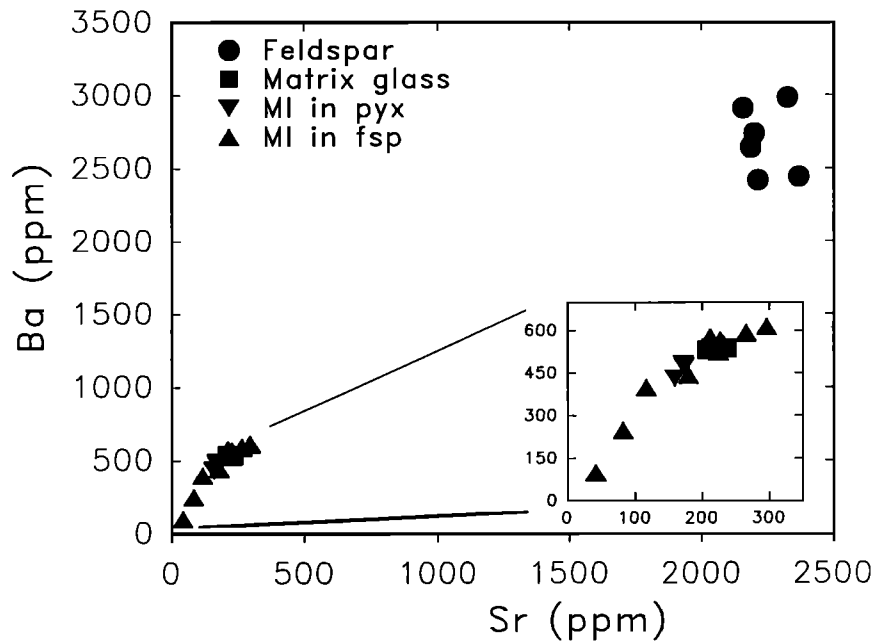
Fig. 7. Ba versus Sr composition of anorthoclase feldspar, MI in anorthoclase feldspar and pyroxene phenocrysts, and matrix glass as determined by ion microprobe analysis. Error of analysis is ±10%.

sentative of the magmatic composition at the time that the phenocrysts grew, an unusual feature of the Mount Erebus magmatic system is that the volatile contents of MI and degassed matrix glass are virtually identical (Figure 8). In many other magmatic systems, MI are enriched in volatile components with respect to matrix
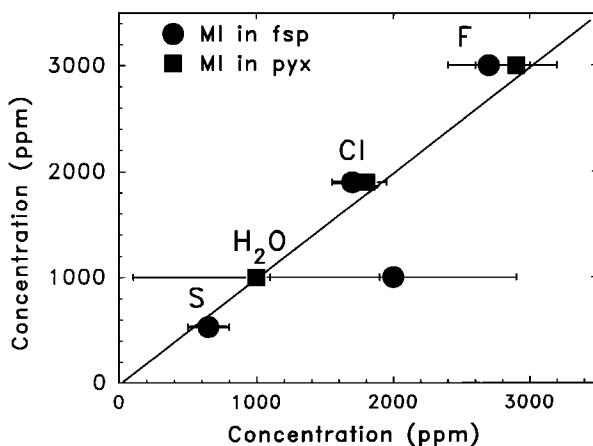
Fig. 8. Diagram showing the mean H_2O, F, Cl, and S contents of MI in feldspar and pyroxene versus matrix glass, as analyzed by electron and ion microprobe. Errors are ±0.1 wt %, ±0.03 wt %, ±0.01 wt %, and ±0.01 wt % for H_2O, F, Cl, and S, respectively. The volatile contents of the MI are similar to that of matrix glass. A 1:1 correlation line is drawn. Note that only H_2O deviates from the 1:1 line, but not significantly because of the large analytical error.

glass, as would be expected if the matrix glass represents degassed primary magmatic composition [Devine et al., 1984]. The magma in the Erebus magmatic system is obviously not gas-free at depth, as continuous degassing from the lava lake is observed, and outputs of volcanic S, Cl, and F of several hundred milligrams per day have been measured [Kyle et al., 1990]. Episodic strombolian eruptions from both the lava lake and a nearby vent typify slowly convecting systems [Wilson and Head, 1981] and are clearly driven by bubble rise and escape. Although it has not been measured directly, H_2O certainly exsolves from Erebus magma, as evidenced by the large steam plume visible at Mount Erebus. On the basis of known gas emission from other volcanoes [Gerlach, 1982; Giggenbach, 1975], CO_2 is likely to be emitted as well. Yet the similarity of volatile contents between the matrix glass and the MI suggests that no significant gas is being lost between the times of crystallization and eruption. There are three possible reasons for this. First, the MI could have trapped magma which was not representative of bulk magma. This is unlikely because of the strong similarity between major and trace element composition of MI and matrix glass. Second, the MI could have degassed after entrapment, either by vesiculation or by leaking of volatile species through cracks in the host crystal [Bacon, 1989; Skirius et al., 1990]. The former process is unlikely to have affected the volatile composition of MI from Mount Erebus, because the bubble/glass ratio of most MI is

low. Furthermore, there is no apparent difference between the volatile content of large MI containing many shrinkage bubbles and that of smaller MI containing one or none. Volatile leaking through cracks in the host crystal is also thought to be unlikely. Cracks in MI are not observed petrographically (Figure 1), although they could be present but not easily visible. Further evidence against the presence of cracks is that when MI were heated repeatedly to high temperature, the homogenization temperatures did not change. This suggests that the MI remained compositionally intact during the heating process, because variations in the homogenization temperature would have been observed if glass and/or vapor leaked out existing cracks. The third and most plausible explanation for the low volatile contents of MI is that the anorthoclase feldspar and clinopyroxene phenocrysts grew under near-surface, low-pressure conditions in the magmatic system, thereby trapping partially to fully volatile depleted magma.

Volatile solubility in a melt is a direct function of pressure. Therefore if the solubility of a given volatile component in the Erebus phonolitic magma is known, depth of crystallization can be estimated. Solubilities of Cl, F, and S in magmas are poorly understood [*Holloway*, 1981] and are therefore not useful in this context. The behavior of H_2O in magmatic systems has been studied in some detail [*Burnham*, 1979; *Stolper*, 1982; *Silver and Stolper*, 1985, 1989]. *Burnham* [1975, 1979] presents an empirical model for calculation of H_2O solubility in a given magmatic composition. Phonolite magma at Erebus is outside the range of compositions for which the solubility calculations are most appropriate, so the calculation represents an approximation of the true H_2O solubility (Figure 9). Although this is only an estimate, the extremely low mea-
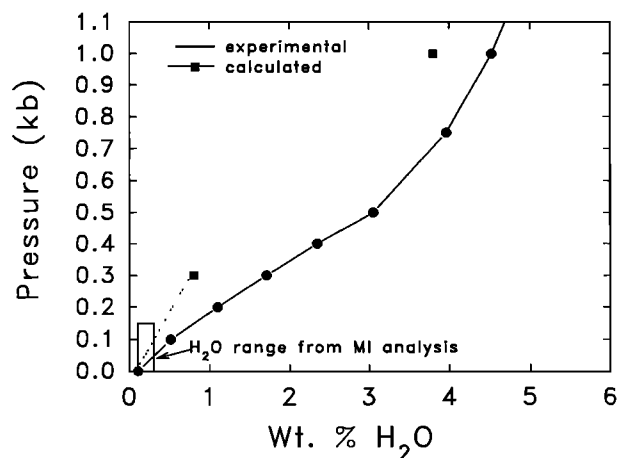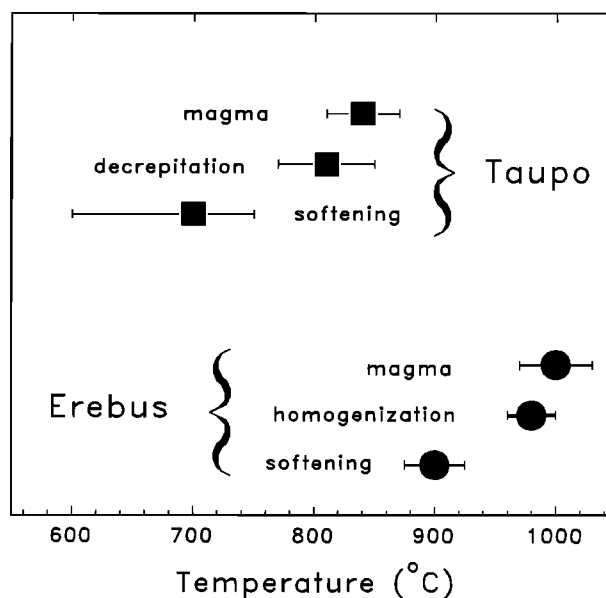
Fig. 10. Glass softening, homogenization/decrepitation, and magmatic temperature measurements for MI from Mount Erebus and the Taupo Volcanic Zone, New Zealand. Softening and homogenization/ decrepitation temperatures are measured by microthermometry heating stage, and magmatic temperatures are from *Kyle* [1977] and *Dunbar* [1988].

sured H_2O contents of MI certainly reflect equilibration at shallow (<1 km) conditions.

Solubility of H_2O in the Erebus phonolite was determined experimentally by heating an experimental charge containing rock powder and water to magmatic temperatures and known pressure. Experiments were made in a tantalum-zirconium-molybdenum (TZM) cold seal vessel, with rapid-quench capabilities [*Rudert et al.*, 1976]. Gold capsules were used to avoid iron loss. Several percent of H_2O were added to the experimental charge to assure saturation. Once the run had equilibrated (run times between 5 and 20 hours) and the charge was rapidly quenched, the H_2O content of the resultant glass was measured by ion microprobe. Two determinations made to date (Figure 9) suggest that the calculated H_2O slightly overestimates true solubility.

Homogenization temperatures (T_h) were determined for a number of MI in anorthoclase crystals (Figure 10). Measurements were made of both irregular and negative crystal shape MI, and no differences were found between the two. In the case of the Erebus MI the T_h of ~985°C is close to the magmatic temperature of 1000°C determined by other means [*Kyle*, 1977], suggesting that the inclusions have not undergone any type of alteration after entrapment. MI could be heated and recooled repeatedly without altering the T_h, suggesting that the crystal containing the MI was not cracked, and there-

Fig. 9. Calculated and experimental H_2O solubility in a Mount Erebus composition phonolitic glass (calculations following *Burnham* [1975, 1979]).
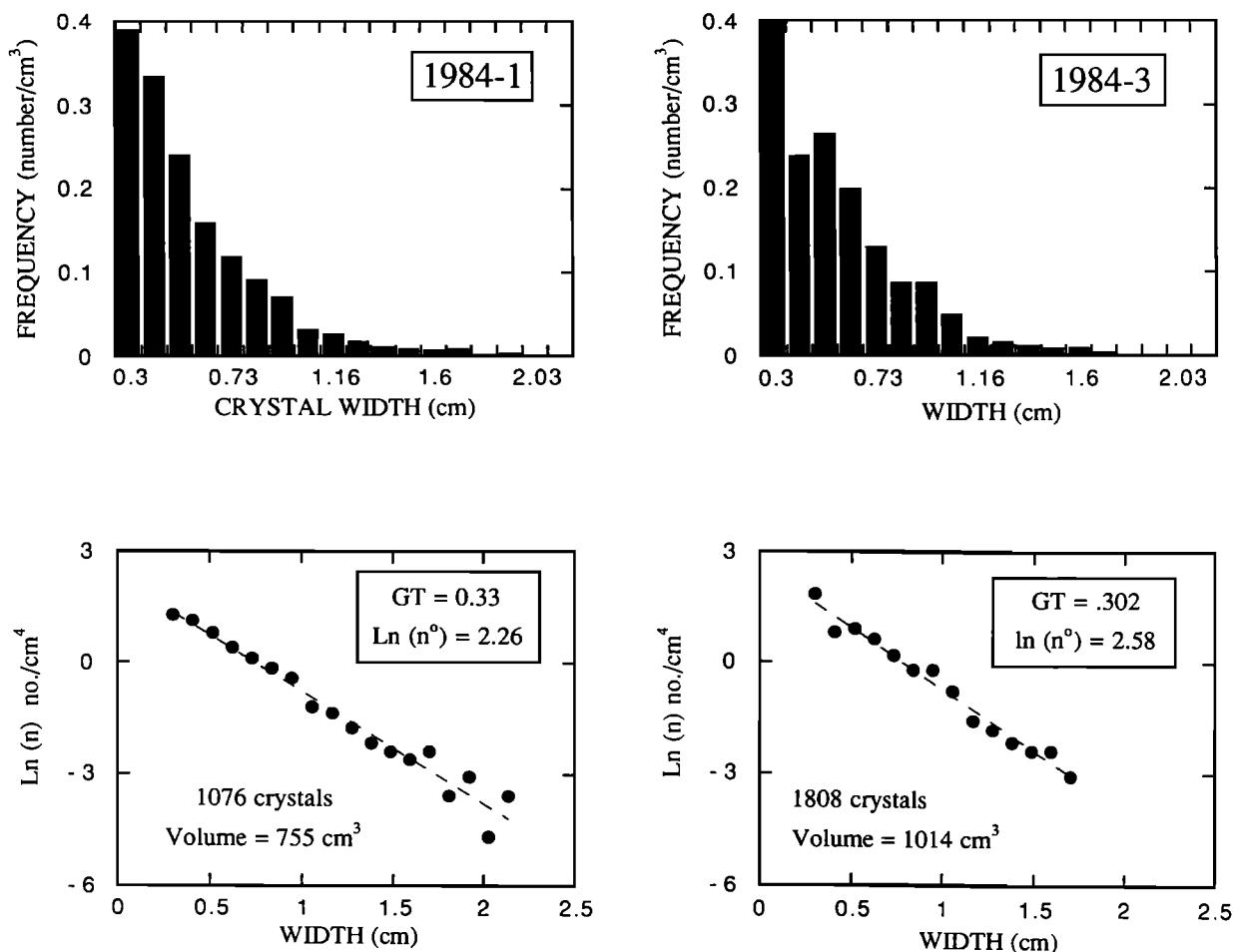
Fig. 11. Histograms and CSD plots of anorthoclase crystal distributions in two 1984 bombs (1984-1 and 1984-3) and one 1988 bomb. All measurements are of crystal widths. Size distributions show the greatest number density of crystals in the smallest size classes, with progressively decreasing numbers in larger size classes. CSD plots (ln (n) versus L, as discussed in text) are linear; $G\tau$ values as determined from CSD slopes range from 0.30 to 0.36. Nuclei population density $(n°)$ is the intercept at size $L = 0$. Linear distributions imply that crystallization has been continuous through time; absence of obvious accumulation in the larger size classes suggests that accumulation of anorthoclase crystals has not been an important factor in generating current Erebus lavas.

fore that the MI were well enclosed by their crystalline host.

When heated, MI from the Taupo plinian eruption (New Zealand) show a marked contrast in behavior to those from Mount Erebus. The MI from the rhyolitic Taupo plinian eruption are volatile-rich [*Dunbar et al.*, 1989] and are prone to decrepitation upon heating to magmatic temperature. *Chaigneau et al.* [1980] suggested that volatile-rich MI tend to decrepitate during the heating process because of high pressure generated by solution of the volatile component. By analogy, the consistent homogenization behavior of the MI from Mount Erebus would suggest that these MI are volatile-poor.

CRYSTAL SIZE DISTRIBUTIONS

Quantitative textural measurements can be used to constrain magmatic processes related to original conditions of crystallization in addition to redistribution of those crystals by gravitational settling and magma mixing [*Cashman*, 1990]. Crystal size distribution (CSD) measurements on samples from active volcanic systems [*Cashman and Marsh*, 1988; *Cashman*, 1992, 1993; *Maaloe et al.*, 1989; *Peterson*, 1990] have illustrated the use of quantitative textural measurements to estimate in situ crystallization rates in active volcanic systems. Measured CSDs in these systems can be fit by the equa-
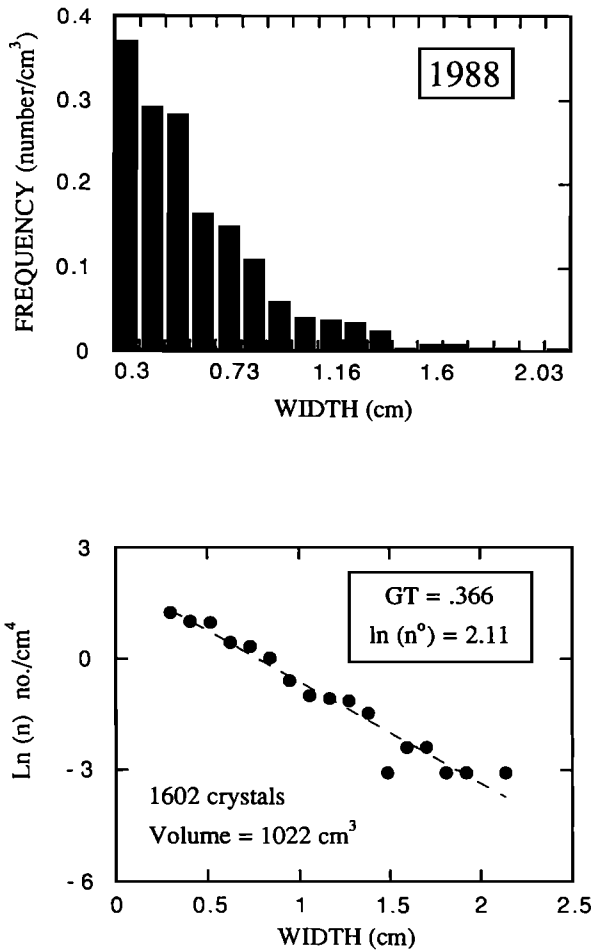
Fig. 11. (continued)

tion

$$n = n° \exp\ [-L/(G\tau]$$

where L is crystal size (measured as long axis, short axis, diameter, etc.), G is linear crystal growth rate, τ is average growth time, and n is the number density of crystals as a function of linear crystal size (= dN/dL, where N is the number of crystals in a given size class per unit volume); $n°$ is then the intercept at size $L = 0$, or the nuclei population density [Randolph and Larson, 1971; Marsh, 1988a]. Expression of size as a negative exponential distribution allows determination of the characteristic crystal size (L_c = $G\tau$ on a length-weighted basis, $2G\tau$ on an area-weighted basis, $3G\tau$ on a mass-weighted basis). If the average time for crystal growth is known, the average growth rate can then be determined. Plagioclase growth rates in active volcanic systems

appear to vary by only an order of magnitude (10^{-10} to 10^{-11} cm/s) over a broad range of magma compositions and conditions of crystallization [Cashman, 1990, 1993a]. This result suggests that the size distribution of crystals in a volcanic rock is a measure of its residence time in a subliquidus (crystallizing) magmatic system [Mangan, 1990].

Measured CSDs for Erebus samples are shown in Figure 11. Histograms of the frequency of occurrence of crystals of a specific width show a negative exponential distribution that translates to a linear distribution on a plot of ln (n) versus L. Two separate 1984 bombs and one 1988 bomb show no significant variations in the form of their CSDs. The average $G\tau$ is 0.33 cm; thus the average crystal size on a mass-weighted basis is $3G\tau$, or 1 cm. As mentioned above, this average crystal size is unusually large relative to most other lavas [Cashman, 1990]. If crystal growth rates approximate those of feldspar in other volcanic systems ($G = 1 \times 10^{10}$ cm/s), this average size implies that the average crystal age is approximately 100–300 years. Note that this is a minimum age, both because the parameter measured was crystal width (the average length is commonly twice to 3 times the width) and because, as discussed above, there is abundant evidence for an unknown amount of crystal dissolution during formation.

Linear size distributions shown in Figure 11 suggest that crystal nucleation and growth in the Erebus magmatic system have been continuous through time. Moreover, the observed distribution of crystal sizes implies that crystal accumulation through anorthoclase flotation, as would be expected through examination of the density differences between anorthoclase and liquid, has not occurred to a significant extent. If anorthoclase flotation had been important, a deviation in the size distribution pattern of crystals in the larger size ranges would be expected [Marsh, 1988a, b].

Finally, low crystal number densities (N_T = $n°G\tau$ = 2–3 cm^{-3}) imply extremely low nucleation rates in the Erebus magmatic system. In this regard, it is interesting to note that the most common megacrysts in silicic plutonic rocks are orthoclase feldspar. One explanation for megacryst occurrence is difficulty in nucleation requiring enhanced growth at the few nucleation sites to maintain chemical equilibrium.

IMPLICATIONS FOR CRYSTALLIZATION PROCESSES IN THE EREBUS MAGMATIC SYSTEM

Observations of anorthoclase chemistry, morphology, and size distributions combined with measurements of
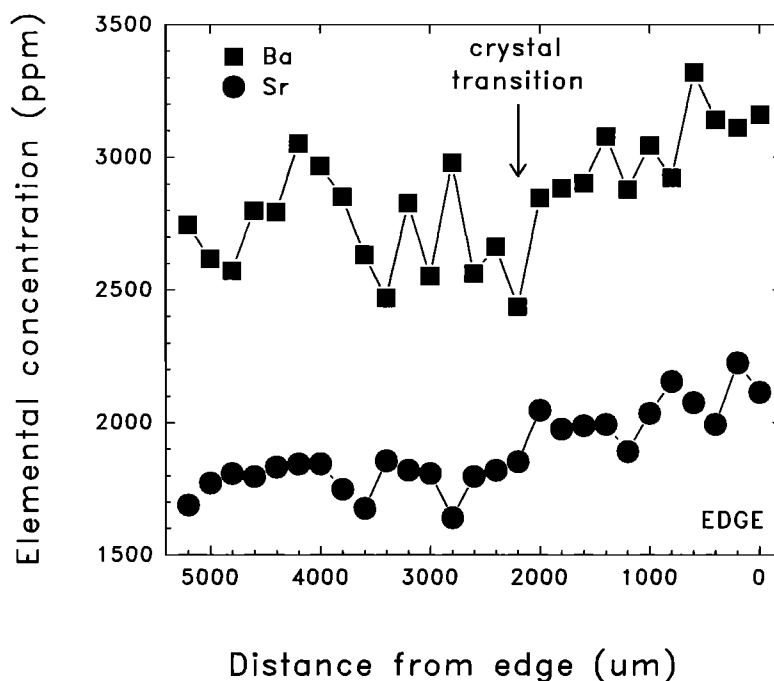
Fig. 12. Ion microprobe determinations of Ba and Sr composition in a stepwise scan across the outer 5 mm of anorthclase feldspar. Step size is 200 μm. Error of analyses is ±10%. The transition in crystalline structure from "spongy" MI-rich core to finely laminated outer crystalline layers is indicated.

MI composition allow constraints to be placed on conditions of anorthoclase crystallization in the Erebus magmatic system. Most important of these observations are the evidence for two stages of anorthoclase growth and the degassed nature of MI composition.

Anorthoclase Size Distributions, Morphology, and Chemistry

Anorthoclase is the dominant phenocryst phase in the Erebus phonolite, constituting 25 to 40 vol % of the magma [Kyle, 1977]. Anorthoclase crystals exhibit a continuous distribution in sizes from microphenocryst (of the order of a few millimeters in length) up to megacrysts measuring several centimeters in length. Measured crystal widths yield CSDs that are similar for all three samples (Figure 11). CSDs show little evidence of anorthoclase accumulation, consistent with Kyle's [1977] observation that Erebus phonolites do not contain a pronounced Eu anomaly. The absence of crystal accumulation is reasonable given the similarities in densities between anorthoclase and the residual liquid, combined with observed convection rates at the surface of the crater lava lake of 0.05–0.1 m/s [Kyle et al., 1982], rates that are high enough to keep crystals in suspension.

Large (>2 cm) anorthoclase crystals are composed of a structurally homogeneous, MI-rich core, surrounded by finely zoned laminar and "hieroglyphic textured" rims. The break between the core and the rim morphologies is sharp and is often marked by large MI (Figure 3). Rim zones are highlighted by trains of small euhedral MI; Normarski imaging shows that included MI mark zones of convoluted growth patterns. Outer boundaries of crystals of all sizes are irregular (Figures 2 and 3), although it is difficult to ascertain whether these are growth or dissolution features. Smaller crystals (<2 cm) appear to be composed predominantly of rimlike growth morphologies with alternating bands of laminar and convoluted zoning. Thus smaller crystals appear to have grown at the same time as the rims of larger crystals, an observation that supports the observation of continuous crystal size distributions.

The morphological difference between crystal cores and rims suggests that they grew in a two-stage process. Both the "spongy" appearance of the cores and the apparent homogeneity of the crystalline material suggest that this was the product of a relatively rapid growth. The convoluted nature of the rim zoning implies quite a different growth process. While the origin of hieroglyphic zoning is uncertain [Pearce and Kolisnik, 1990], apparent erosion into underlying zones implies some

component of dissolution. In addition, the blocky and irregular nature of the parts of the current crystal-melt interface (Figure 2) suggests that rapid, skeletal growth may also be important. Thus, periodic zoning in the Erebus anorthoclase probably represents cycles of growth and dissolution resulting from convection in the near-surface magmatic system, as seen in the current lava lake.

Morphological zoning patterns are concident with chemical zoning denoted by variations in mole fraction Or and An. The crystalline cores contain subequal proportions of Or and An, whereas the rims are commonly relatively enriched in mole fraction Or. Ion microprobe step scan analyses of the outer 5 mm of a single large anorthoclase crystal show similar compositional variations in minor elements Ba and Sr between a crystal core and a rim (Figure 12). While core contents of Sr and Ba are relatively constant in the interior of the crystal, an abrupt increase in both Ba and Sr contents occurs at the break between the homogeneous core and the finely zoned rim. Both Ba and Sr continue to increase slightly to the crystal rim. There is a suggestion of variation of Ba and Sr on a 300- to 500-μm scale, similar to the rim zoning periodicity noted with Normarski imaging and major element step scans. Other elements analyzed in this step scan (Rb, Ce, P, Ti, and Zr) are low and homogeneous for the entire 5 mm, with the exception of P, which decreases slightly in the outer 2 mm of the crystal rim. The observed increase in Ba and Sr is thus consistent with the observed major element variation and may actually reflect the role of minor elements in major element partitioning suggested by Smith and Brown [1988].

While we have no unique explanation for the observed zoning patterns, the data presented above demonstrate a clear link between morphological changes in zoning patterns (related to the physical environment in which crystallization occurred) and measured variations in major and minor element chemistry (related to partitioning of elements between crystal and melt at the crystalline interface). We speculate that the observed relationship between chemistry and morphology may be controlled by changes in crystal growth mechanism. The crystal core morphology appears skeletal in form and implies rapid (diffusion controlled) growth. In contrast, rim-zoning patterns imply slower (interface controlled) growth periodically interrupted by dissolution. Interface-controlled growth would be expected to incorporate Ba and Sr more selectively into the crystal structure than would be diffusion-controlled growth. Additionally, periodic resorption may create anomalous enrichment of compatible elements at the crystal-melt interface. Thus variation patterns of Ba and Sr are also

consistent with a model of multiple episodes of crystal resorption and growth during formation of crystal rims.

Melt Inclusion Chemistry and Volatile Contents

The MI study provides several important constraints on the timing and location of anorthoclase growth within the magmatic system. First, while the composition of MI in anorthoclase megacrysts is somewhat variable, (1) compositional variations show no systematic relationship to MI location within a crystal [Kyle, 1977], (2) compositional variations are small, (3) MI compositions are similar in feldspar and pyroxene, and (4) the average MI composition is indistinguishable from that of matrix glass (cf. Table 1). Additionally, MI have extremely low volatile contents that also closely resemble that of matrix glass.

The evolved nature of the MI chemistry suggests that anorthoclase was the last phase to crystallize from the phonolitic melt. Note in particular that the MI (and matrix) glass is strongly depleted in MgO and enriched in Na_2O relative to whole rock composition, although the anorthoclase megacrysts are depleted in MgO and similar in Na_2O to the whole rock composition. This suggests significant olivine crystallization prior to anorthoclase crystallization. This conclusion is consistent with the presence of included crystals of olivine in anorthoclase megacrysts. It is also consistent with 1-bar phase relationships presented by Sack et al. [1987] for alkalic lavas. Mount Erebus anorthoclase phonolite compositions plot on the pseudoeutectic point in their OL-DI-NEPH normative projection. In thin section, included olivine crystals commonly showed embayed textures. This observation supports not only an interpretation of early crystallization of olivine in this system but also the suggestion of Sack et al. [1987] that the apparent eutectic is really a peritectic point in natural liquids. The similarity of MI major element chemistry in both anorthoclase and Ca-pyroxene suggests that the pyroxene also crystallized after most of the olivine crystallization.

The low volatile content of MI in anorthoclase and pyroxene phenocrysts from the Mount Erebus magmatic system suggests that the crystals were growing at low (<300 bars) pressures. The highest observed H_2O content in a MI is 0.3 wt %, but the uncertainty in H_2O solubility in phonolitic magmas prohibits the determination of precise equilibration depths. Furthermore, because the preeruptive volatile content of the Erebus magma is unknown, it is impossible to assert that H_2O degassing occurs simply in response to reduced pressure as the magma rises in the conduit. Magmatic H_2O may also partition into a vapor phase composed predominantly of

another species, such as CO_2 [*Holloway*, 1976]. In this case, H_2O degassing would not follow the solubility relationship described in Figure 9, and some of the preeruptive H_2O content could be lost at greater depths. However, measured gas compositions at many other volcanoes suggest that H_2O is the primary gas phase [*Giggenbach*, 1975; *Gerlach*, 1982; *Anderson*, 1974; *Newman and Chesner*, 1989], suggesting that partitioning of H_2O into a CO_2-rich vapor would not be a dominant effect. On the basis of this information we make the simplifying assumptions that the Erebus magma contained >0.3 wt % H_2O at depth and that H_2O degassing followed normal solubility relationships. Given this information, and on the basis of a combination of calculated and experimental solubility determinations, crystallization probably took place at less than 400 m depth in the magmatic system. Water lost to a CO_2-rich vapor phase would increase this estimated crystallization depth.

SUMMARY

On the basis of the evidence presented here, we suggest that anorthoclase crystallization occurs in response to depressurization-induced degassing, possibly at depths as shallow as 400 m. Relatively homogeneous crystals with large and numerous trapped MI suggest that crystal growth is initially rapid. All crystals examined in this study have 2- to 4-mm oscillatory-zoned rims indicative of multiple episodes of dissolution and precipitation, probably in response to shallow magmatic convection. We suggest that this zoning pattern occurs in response to shallow magmatic convection, as observed in the current magma lake [*Kyle et al.*, 1982]. The alternating bands of hieroglyphic and type 1 zoning at a periodicity of ~500 μm indicate that convection was fairly regular. Convection apparently prevented extensive flotation of anorthoclase crystals and promoted maintenance of a constant magma composition and crystal content through time [*Kyle*, 1977]. If anorthoclase growth rates are similar to rates of feldspar growth in basaltic systems, core growth would require crystallization times of the order of a few hundred years. If crystal growth in the phonolite magma is an order of magnitude faster, then crystallization times would be correspondingly shorter. In comparison, preliminary analyses by *Reagan et al.* [1992] based on ^{238}U series geochronology suggest that anorthoclase cores have ages of ~3000 years, although they allow that rim growth could have occurred over the past several tens of years. The postulated age break between the core and the rim growth is puzzling if anorthoclase crystallization

is truly occurring at a shallow level in the Erebus magmatic system. Evidence supporting shorter time scales of crystallization includes observation of a semipermanent, convecting, actively degassing lava lake that must serve to cool and degas the upper part of the system over short time periods. We anticipate that improved geochronology, combined with estimates of crystal circulation time within the magmatic system, based on calculated convective cell overturn rates, may help resolve these differences.

REFERENCES

Anderson, A. T., Chlorine, sulfur and water in magmas and oceans, *Geol. Soc. Am. Bull.*, *85*, 1485–1492, 1974.

Anderson, A. T., Oscillatory zoning of plagioclase: Nomarski interference contrast microscopy of etched sections, *Am. Mineral.*, *68*, 125–129, 1983.

Anderson, A. T., Probable relations between plagioclase zoning and magma dynamics, Fuego Volcano, Guatemala, *Am. Mineral.*, *69*, 660–676, 1984.

Anderson, A. T., and T. L. Wright, Phenocrysts and glass inclusions and their bearing on oxidation and mixing of basaltic magmas, Kilauea Volcano, Hawaii, *Am. Mineral.*, *57*, 188–216, 1972.

Anderson, A. T., S. Newman, S. Williams, T. Druitt, C. Skirius, and E. Stolper, H_2O, CO_2, Cl and gas on the plinian and ash-flow Bishop rhyolite, *Geology*, *17*, 221–225, 1989.

Bacon, C. R., Crystallization of accessory phases in magmas by local saturation adjacent to phenocrysts, *Geochim. Cosmochim. Acta*, *53*, 1055–1066, 1989.

Beddoe-Stephens, B., J. A. Aspden, and T. J. Shepherd, Glass inclusions and melt compositions of the Toba Tuffs, northern Sumatra, *Contrib. Mineral. Petrol.*, *83*, 278–287, 1983.

Belkin, H. E., B. De Vivo, E. Roedder, and M. Cortini, Fluid inclusion geobarometry from ejected Mt. SommaVesuvius nodules, *Am. Mineral.*, *70*, 288–303, 1985.

Blundy, J. D., and N. Shimizu, Trace element evidence for plagioclase recycling in calc-alkaline magmas, *Earth Planet. Sci. Lett.*, *102*, 178–197, 1991.

Burnham, C. W., Water and magma; a mixing model, *Geochim. Cosmochim. Acta, 39,* 1077–1084, 1975.

Burnham, C. W., Importance of volatile constituents, in *Evolution of Igneous Rocks, Fiftieth Anniversary Perspectives,* edited by H. D. Yoder, pp. 439–482, Princeton University Press, Princeton, N. J., 1979.

Cashman, K. V., Textural constraints on the kinetics of crystallization of igneous rocks, in Modern Methods of Igneous Petrology: Understanding Magmatic Processes, edited by J. Nicholls and J. K. Russell, *Rev. Mineral., 24,* 259–314, 1990.

Cashman, K. V., Groundmass crystallization of Mount St. Helens dacite, 1980–1986: A tool for interpreting shallow magmatic processes, *Contrib. Mineral. Petrol., 109,* 431–449, 1992.

Cashman, K. V., Relationship between crystallization and cooling rate -insight from textural studies of dikes, *Contrib. Mineral. Petrol., 113,* 126–142, 1993.

Cashman, K. V., and B. D. Marsh, Crystal size distribution (CSD) in rocks and the kinetics and dynamics of crystallization, 11, Makaopuhi lava lake, *Contrib. Mineral. Petrol., 99,* 292–305, 1988.

Chaigneau, M., D. Massare, and R. Clochiatti, Contributions a l'etude des inclusions vitreuses et des elements volatiles contenus dans les phenocristaux des quartz des roches volcaniques acides, *Bull. Volcanol., 43,* 233–240, 1980.

Clochiatti, R., C. Desnoyers, J. C. Sabroux, H. Tazieff, and S. Wilhelm, Relations entre les anorthoses de I'Erebus et leurs inclusions vitreuses, *Bull. Soc. Fr. Mineral. Cristallogr., 99,* 98–110, 1976.

Cortini, M., A. Lima, and B. De Vito, Trapping temperatures of melt inclusions from ejected Vesuvian mafic xenoliths, *J. Volcanol. Geotherm. Res., 26,* 167–172, 1985.

Devine, J. D., H. Sigurdsson, and A. N. Davis, Estimates of sulfur and chlorine yield to the atmosphere from volcanic eruptions and potential climatic effects, *J. Geophys. Res., 89,* 6309–6325, 1984.

Dunbar, N. W., Pre-eruptive volatile contents and degassing systematics of rhyolitic magmas from the Taupo Volcanic Zone, New Zealand, Ph.D. thesis, N. M. Inst. of Mining and Technol., Socorro, 1988.

Dunbar, N. W., R. L. Hervig, and P. R. Kyle, Determination of pre-eruptive H_2O, F and Cl contents of silicic magmas using melt inclusions: Examples from Taupo volcanic center, New Zealand, *Bull. Volcanol., 51,* 177–184, 1989.

Gerlach, T. M., Interpretation of volcanic gas data from tholeiitic and alkaline mafic lavas, *Bull. Volcanol., 45,* 235–244, 1982.

Giggenbach, W., Variations in the carbon, sulfur and chlorine contents of volcanic gas discharges from White Island, New Zealand, *Bull. Volcanol., 39,* 1–13, 1975.

Harris, D. M., and A. T. Anderson, Volatiles H, O, CO_2 and Cl in a subduction related basalt, *Contrib. Mineral. Petrol., 87,* 120–128, 1984.

Hervig, R. L., N. W. Dunbar, H. R. Westrich, and P. R. Kyle, Pre-eruptive water content of rhyolitic magmas as determined by ion microprobe analyses of melt inclusions in

phenocrysts, *J. Volcanol. Geotherm. Res., 36,* 293–302, 1989.

Holloway, J. R., Fluids in the evolution of granitic magmas: Consequences of finite CO_2 solubility, *Geol. Soc. Am. Bull., 87,* 1513–1518, 1976.

Holloway, J. R., Volatile interactions in magma, in *Thermodynamics of Melts and Minerals,* edited by R. C. Newton, A. Navrotsky, and B. J. Wood, pp. 273–293, Springer-Verlag, New York, 1981.

Kyle, P. R., Mineralogy and glass chemistry of recent volcanic ejecta from Mt. Erebus, Ross Island, Antarctica, *N. Z. J. Geol. Geophys., 20,* 1123–1146, 1977.

Kyle, P. R., R. R. Dibble, W. F. Giggenbach, and J. Keys, Volcanic activity associated with the anorthoclase phonolite lava lake, Mount Erebus, Antarctica, in *Antarctic Geosciences,* 1st ed., vol. 1, edited by C. Craddock, pp. 735–745, University of Wisconsin Press, Madison, 1982.

Kyle, P. R., K. Meeker, and D. Finnegan, Emission rates sulfur dioxide, trace gases and metals from Mount Erebus, Antarctica, *Geophys. Res. Lett., 17,* 2125–2128, 1990.

Kyle, P. R., J. A. Moore, and M. F. Tbirlwall, Petrologic evolution of anorthoclase phonolite lavas at Mount Erebus, Ross Island, Antarctica, *J. Petrol., 33,* 849–875, 1992.

Maaloe, S., O. Tumyr, and D. James, Population density and zoning of olivine phenocrysts in tholeiites from Kauai, Hawaii, *Contrib. Mineral. Petrol., 101,* 176–186, 1989.

Mangan, M. T., Crystal size distribution systematics and the determination of magma storage times: The 1959 eruption of Kilauea Volcano, Hawaii, *J. Volcanol. Geotherm. Res., 44,* 295–302, 1990.

Marsh, B. D., Crystal size distributions (CSD) in rocks and the kinetics and dynamics of crystallization, I, Theory, *Contrib. Mineral. Petrol., 99,* 277–291, 1988a.

Marsh, B. D., Crystal capture, sorting, and retention in convecting magma, *Geol. Soc. Am. Bull., 100,* 549–552, 1988b.

Meeker, K. A., The emission of gases and aerosols from Mount Erebus Volcano, Antarctica, M.S. thesis, N. M. Inst. of Mining and Technol., Socorro, 1988.

Morrison, G. H., and G. Slodzian, Ion microscopy, *Anal. Chem., 47,* 933A–943A, 1975.

Newman, S., and C. Chesner, Volatile compositions of glass inclusions from the 75 ka Toba Tuff, Sumatra, *Geol. Soc. Am. Abstr. Programs, 21,* A271, 1989.

Pearce, T. H., Optical dispersion and zoning in magmatic plagioclase: Laser interference observations, *Can. Mineral., 22,* 383–390, 1984.

Pearce, T. H., and A. M. Kolisnik, Observations of plagioclase zoning using interference imaging, *Earth Sci. Rev., 29,* 9–26, 1990.

Peterson, T. D., Petrology and genesis of natrocarbonatite, *Contrib. Mineral. Petrol., 105,* 143–155, 1990.

Randolph, A. D., and M. A. Larson, *Theory of Particulate Processes,* 251 pp., Academic, San Diego, Calif., 1971.

Reagan, Z. M. K., A. M. Volpe, and K. V. Cashman, [238]U- and [232]Th-series chronology of phonolitic fractionation at Mount Erebus, Antarctica, *Geochim. Cosmochim. Acta, 56,* 1401–1407, 1992.

Roedder, E., Fluid inclusions, *Rev. Mineral., 12*, 1–644, 1984.

Rudert, V. I., I. Chou, and H. P. Eugster, Temperature gradients in rapid-quench cold-seal pressure vessels, *Am. Mineral., 61*, 1012–1015, 1976.

Sack, R. O., D. Walker, and I. S. E. Carmichael, Experimental petrology of alkalic lavas: Constraints on cotectics of multiple saturation in natural basic liquids, *Contrib. Mineral. Petrol., 96*, 1–23, 1987.

Silver, L., and E. Stolper, A thermodynamic model for hydrous silicate melts, *J. Geol., 93*, 161–178, 1985.

Silver, L., and E. Stolper, Water in albite glass, *J. Petrol., 30*, 667–709, 1989.

Skirius, C. M., J. W. Peterson, and A. T. Anderson, Homogenizing rhyolitic glass inclusions from the Bishop Tuff, *Am. Mineral., 75*, 1381–1398, 1990.

Smith, J. V., and W. L. Brown, *Feldspar Mineralogy*, 1st ed., vol. 1, Springer-Verlag, New York, 1988.

Stolper, E., Water in silicate glasses: An infrared spectroscopy study, *Contrib. Mineral. Petrol., 81*, 1–17, 1982.

Watson, E. B., Glass inclusions as samples of early magmatic liquid: Determinative method and application to a South Atlantic basalt, *J. Volcanol. Geotherm. Res., 1*, 73–84, 1976.

Wilson, L., and J. W. Head, Ascent and eruption of basaltic magma on the Earth and Moon, *J. Geophys. Res., 86*, 2971–3001, 1981.

K. V. Cashman, Department of Geological Sciences, University of Oregon, Eugene, OR 97403.

N. W. Dunbar, Department of Geoscience, New Mexico Institute of Mining and Technology, Socorro, NM 87801.

R. Dupré, Department of Geological and Geophysical Sciences, Princeton University, Princeton, NJ 08544.

MINERALOGY AND GEOCHEMISTRY OF EJECTA ERUPTED FROM MOUNT EREBUS, ANTARCTICA, BETWEEN 1972 AND 1986

D. A. Caldwell and P. R. Kyle

Department of Geoscience, New Mexico Institute of Mining and Technology, Socorro, New Mexico

Short-term variations in the magmatic composition were examined by analyzing olivine, clinopyroxene, magnetite, anorthoclase, and glass separated from bombs erupted from Mount Erebus between 1972 and 1986. Olivine, clinopyroxene, and glass show uniform compositions. Individual anorthoclase megacrysts show erratic zoning indicative of their complex growth histories. Magnetite has a constant composition in bombs erupted from 1972 until 1978, but then it shows a steady decline in ulvöspinel content. A decrease in temperature of 10° to 15°C, at constant oxygen fugacity, can account for the change in magnetite composition. To account for the increased size and frequency of strombolian eruptions in late 1984, we propose a model in which a batch of new volatile-rich phonolite was injected into the magma chamber. This provided the volatiles which drove the eruptions, but the magma itself did not reach the lava lake until after 1986 and before 1988.

INTRODUCTION

Mount Erebus (77°32′S, 167°9′E, 3794 m), Ross Island, Antarctica, contains a persistent convecting, anorthoclase phonolite lava lake. The lake, discovered in 1972 [*Giggenbach et al.*, 1973], has undergone changes in size and patterns of eruptive activity over the last 20 years [*Kyle et al.*, 1982; *Dibble et al.*, 1984]. Small strombolian eruptions from the lava lake and an adjacent explosive vent (informally called the active vent) occurred at a frequency of 2 to 6 per day between 1972 and 1984. These eruptions occasionally ejected bombs onto the main crater rim 220 m above the lava lake.

On September 13, 1984, strombolian eruptions abruptly increased in frequency and size. Bombs up to 10 m long were thrown nearly 1 km from the vent. The Inner Crater was profoundly affected, largely through infilling by erupted materials, and the lava lake was completely buried by ejecta. By January 1985, eruptive activity had returned to pre–September 1984 levels, when a small lava lake was exhumed from under the ejecta infilling the Inner Crater. Since January 1985, eruptive activity at Mount Erebus has decreased to levels lower than those seen between 1972 and 1984.

The anomalous frequency and high energy of the eruptions between September and December 1984 suggest that a fundamental change had occurred in the magmatic system. One possible driving mechanism for the more violent eruptions in late 1984 was injection of a new batch of volatile-rich magma into the magma chamber system. Such a batch of magma might be detected by small differences in the chemical compositions of the phenocryst phases or the magma itself.

The purpose of this study was to examine glass, olivine, clinopyroxene, anorthoclase, and magnetite separates from bombs collected between 1972 and 1986 to characterize the composition of the material and search for evolutionary trends or abrupt changes in composition which may coincide with the 1984 eruptive activity.

SAMPLE COLLECTION AND PREPARATION

From 1972 to 1991 the summit of Mount Erebus was visited annually by geologic research teams. Bombs with fresh, unaltered appearance were collected from the main crater rim and/or crater floor during many of these visits. Upon eruption, the exterior of bombs exhibit resinous to vitreous, iridescent luster. This luster is completely lost within a few weeks of eruption through reaction with the acid volcanic gas plume. The relative degree of the alteration is usually a reliable indicator of

the elapsed time since eruption.

Glass and minerals were separated from volcanic bombs erupted from the lava lake and associated vents. Anorthoclase phenocrysts were hand picked from bombs. The remaining glassy material was crushed with a mortar and pestle and sieved to pass 40 mesh. Magnetite was extracted with a hand magnet, and the glass was separated from the olivine and clinopyroxene using a Franz isodynamic magnetic separator. Microprobe grain mounts were then made of each group of separates. Standard microprobe mounts were made of anorthoclase crystals cut perpendicular to the C axis.

ANALYTICAL METHODS

Major element analyses of glass, anorthoclase, olivine, clinopyroxene, and magnetite were determined by electron microprobe. Analyses were made on a JEOL 733 Superprobe at Victoria University of Wellington, New Zealand. Instrumental parameters used in this study are presented in Table 1. Data were reduced using the *Bence and Albee* [1968] technique. An estimate of the analytical precision for the microprobe analyses is given in Table 2.

For glass analyses, the beam was defocused to 20 micrometers (μm) and the beam current was set at 80 nanoamps (nA) to limit the volatilization of sodium. Similar settings were used for the anorthoclase and magnetite analyses. A 1-mm beam was used for olivine and pyroxene analyses.

Major and trace element analyses of whole rock and bulk glass separates were also made by X ray fluorescence (XRF) on a Philips PW1404 automatic sequential X ray spectrometer at Victoria University of Wellington, New Zealand, and a Rigaku 3062 XRF at New Mexico Institute of Mining and Technology (NMIMT) using standard techniques [*Norrish and Hutton*, 1969; *Norrish and Chappell*, 1977]. Selected whole rock and matrix glass samples were analyzed at NMIMT by instrumental neutron activation analysis [*Kyle et al.*, 1992].

RESULTS AND DISCUSSION

Olivine

Representative microprobe analyses of olivine crystals separated from bombs erupted between 1972 and 1986 are given in Table 3. The olivine typically contains about 2.5 wt % MnO; so analyses have been recalculated into three end-members: forsterite (Fo), fayalite (Fa),

TABLE 1. Instrumental Parameters Used in the Electron Microprobe Analyses of Glass, Anorthoclase, Magnetite, Olivine, and Pyroxene Separates Taken From Bombs Erupted Between 1972 and 1986 at Mount Erebus

	Beam Diameter, μm	Current, nA	Analysis Time
Glass	20	80	4 counts at 3 s
Anorthoclase	20	80	3 counts at 10 s
Magnetite	20	80	4 counts at 15 s
Olivine	1	120	3 counts at 10 s
Pyroxene	1	120	3 counts at 10 s

An accelerating voltage of 15 kV was used for all analyses.

and tephroite (Te) (Figure 1). The majority of the analyses plot at $Fa_{46}Fo_{51}Te_3$. Taken as a group, the analyses define a weak trend from Fo_{53} to Fo_{50}. Olivine from 1975 bombs shows the greatest variation and helps define the observed trend (Figure 1). For most other years the variation in olivine composition is within the expected analytical error.

There are no significant compositional differences in olivine from bombs erupted between 1972 and 1986 (Figure 1). Olivines in recent ejecta are identical in composition to those found in older anorthoclase phonolite lavas exposed on the flanks of Mount Erebus [*Moore*, 1987; *Kyle et al.*, 1992]. Similar compositions are shown by olivine which occurs as inclusions in the anorthoclase phenocrysts and in older bombs scattered around the summit of Mount Erebus [*Kyle*, 1977].

TABLE 2. Estimated Errors in Electron Microprobe Analyses of Phonolite Glass Based on the Pooled Standard Deviations of Replicate Analyses

	Estimated Errors, wt %
SiO_2	0.29
Al_2O_3	0.17
TiO_2	0.09
FeO	0.22
MnO	0.15
MgO	0.05
CaO	0.10
Na_2O	0.22
K_2O	0.15

TABLE 3. Average Electron Microprobe Analyses of Olivine Separated From Bombs Erupted Between 1972 and 1986 From Mount Erebus

	1972 (2)*	1975 (8)	1977 (1)	1978 (1)	1979 (5)	1981 (2)	1982 (4)	1983 (2)	1984 (9)	1985 (3)	1986 (4)
SiO_2	34.97	35.09	35.08	34.83	34.84	34.24	34.72	34.75	34.76	34.73	34.60
FeO	37.64	38.66	38.29	38.70	37.67	38.20	38.13	37.69	37.86	37.87	38.36
MnO	2.41	2.50	2.34	2.31	2.43	2.49	2.45	2.52	2.47	2.52	2.29
MgO	23.47	23.53	23.68	23.47	23.55	23.60	23.56	23.68	23.68	23.74	23.46
CaO	0.47	0.50	0.48	0.50	0.48	0.49	0.51	0.51	0.50	0.51	0.50
Total	98.96	100.3	99.87	99.81	98.97	99.02	99.37	99.15	99.27	99.37	99.21

*Number of analyses averaged.

Clinopyroxene

Clinopyroxene is common as a phenocryst phase in the bombs. Prismatic crystals of clinopyroxene reaching 20 mm in length can occur as synneusis intergrowths with anorthoclase found in crystal lag screes on the upper slopes of Mount Erebus. This lag results from physical weathering and disintegration of the fragile glassy groundmass surrounding more resistant phenocrystic phases in bombs which litter the crater rim and adjacent slopes.

Representative microprobe analyses of clinopyroxene separated from bombs erupted between 1972 and 1986 are given in Table 4. End-member compositions have been calculated using the procedure of Papike et al. [1974] and are plotted in Figure 1. The analyses show a weak iron enrichment trend of increasing ferrosilite ($Fs_{15.5}$ to Fs_{19}) coupled with decreasing wollastonite (Wo_{48} to $Wo_{45.5}$) and slight variations in enstatite (En_{37} to En_{35}) (Figure 1). The

clinopyroxenes have a mean composition of $Wo_{47}En_{36}Fs_{17}$.

Microprobe analyses of four larger clinopyroxenes intergrown with anorthoclase have slightly higher Fs and lower Wo contents than clinopyroxenes found in the recent bombs (Figure 2). The differences are not considered significant. Weak oscillatory zoning is seen in a 6-mm traverse from core to rim across one crystal.

Clinopyroxene compositions show no systematic differences in any of the bombs examined (Figures 1 and 2). Clinopyroxene in older anorthoclase phonolite lavas on the slopes of Mount Erebus, as inclusions in anorthoclase and in older bombs, is similar to that found in the bombs [Kyle, 1977; Moore, 1986; Kyle et al., 1992]. Compositional variations in clinopyroxene from the basanite to anorthoclase phonolite suite of lavas which occur on Mount Erebus are very small [Kyle et al., 1992]. The low Fe and Na contents of clinopyroxene from the bombs are surprising consider-

TABLE 4. Average Electron Microprobe Analyses of Pyroxene Separated From Bombs Erupted Between 1972 and 1986 From Mount Erebus

	1972 (8)*	1975 (9)	1977 (2)	1978 (5)	1981 (4)	1982 (3)	1983 (2)	1984 (8)	1985 (3)	1986 (3)
SiO_2	50.08	50.74	50.89	50.89	50.59	50.51	50.48	50.67	51.18	50.89
Al_2O_3	2.51	2.74	2.46	2.27	2.59	2.46	2.66	2.35	2.21	2.52
TiO_2	1.19	1.43	1.28	1.25	1.28	1.30	1.40	1.22	1.22	1.33
FeO	9.24	9.56	9.42	9.49	9.40	9.60	9.06	9.32	9.01	9.81
MnO	0.68	0.66	0.59	0.61	0.62	0.64	0.61	0.55	0.55	0.70
MgO	12.14	11.74	11.96	12.27	12.11	12.11	12.17	12.11	12.38	12.04
CaO	21.30	21.24	21.69	21.98	21.65	22.09	21.98	22.05	22.18	21.45
Na_2O	0.99	1.15	0.83	0.85	0.95	0.92	0.95	0.83	0.51	0.98
Total	98.72	99.26	99.12	99.61	99.19	99.63	99.31	99.10	99.24	99.72

* Number of analyses averaged.
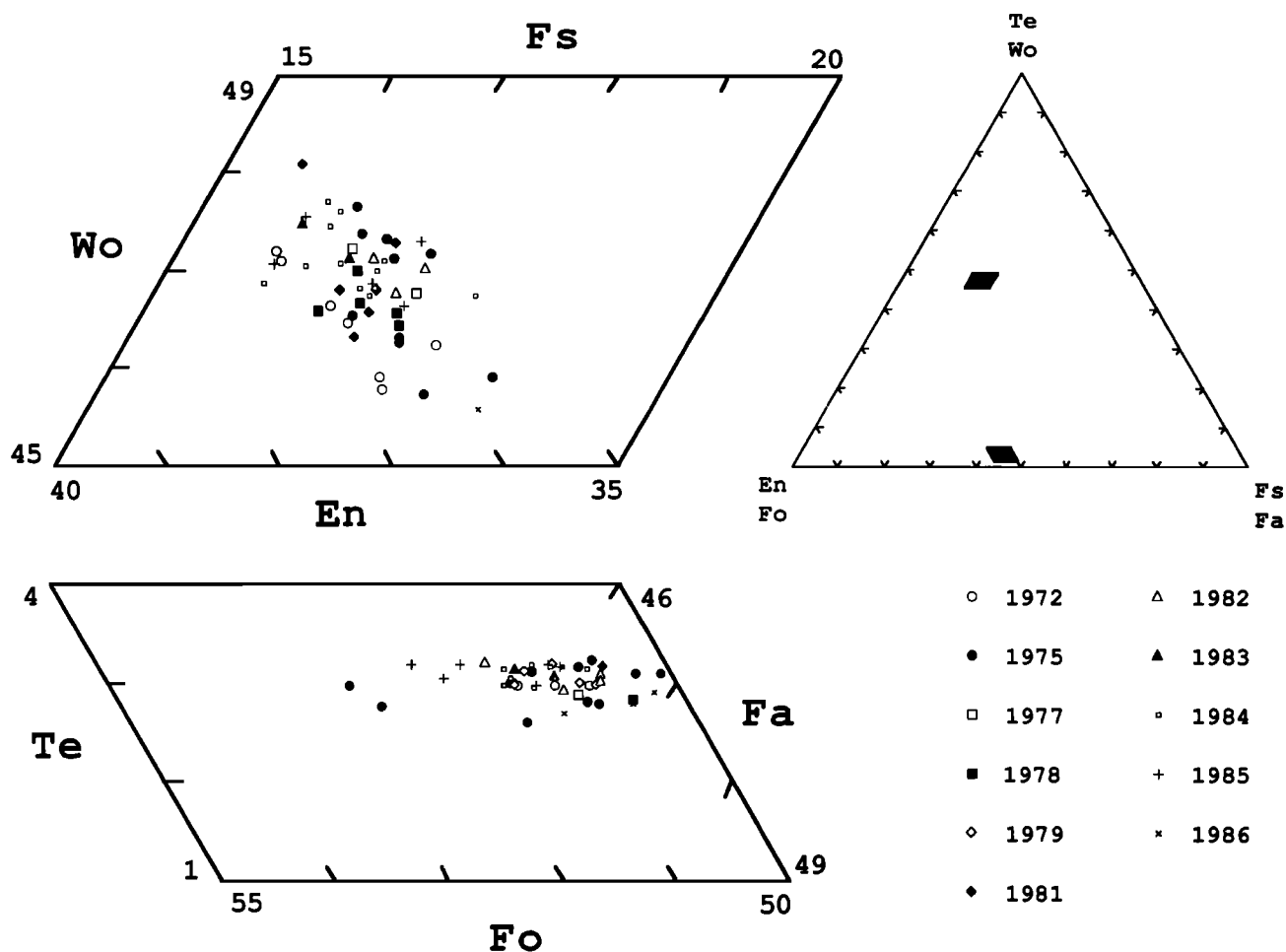
Fig. 1. Electron microprobe analyses of olivine and clinopyroxene in bombs erupted from Mount Erebus between 1972 and 1986. Pyroxene end members (Wo, Fs, En) were calculated after charge balance estimations of Fe^{3+} [Papike et al., 1974]. Olivine is plotted in terms of the calculated end-members tephroite (Mn_2SiO_4), fayalite (Fe_2SiO_4), and forsterite (Mg_2SiO_4).

ing the extreme evolved nature of the phonolitic host magma. Oxygen fugacity in the melt may be buffered by olivine and magnetite, thus limiting the formation of Fe^{3+} and suppressing the formation of the Na-rich acmite component in the clinopyroxene.

Temperatures calculated using the olivine-clinopyroxene geothermometer [Powell and Powell, 1974] are 990°C [Kyle, 1977] and agree with measurement of melt inclusion homogenization temperatures [Dunbar et al., this volume] and a direct optical pyrometer measurement on the lava lake [Kyle et al., 1982].

Anorthoclase

Large euhedral anorthoclase phenocrysts are ubiquitous in the older lavas and recent bombs erupted from

Erebus [Kyle, 1977]. Williams et al. [1954, p. 156] report that the anorthoclase phenocrysts were erupted as lapilli, but this is not supported by observations of eruptions over the last 20 years. It is likely that the anorthoclase which makes up a lag deposit around the crater rim was not recognized as such during visits by British explorers in 1908 and 1912, but was inferred to have been erupted as lapilli.

Dupre [1990] and Dunbar et al. [this volume] have measured crystal size distributions in two bombs erupted in 1984 and a third erupted in 1988. Most of the crystals in these three samples were less than 2 cm in length, with the majority being between 0.4 and 0.8 cm long. However, the lag scree around the summit crater often yields crystals up to 10 cm in length.

Thirty-two anorthoclase phenocrysts from bombs
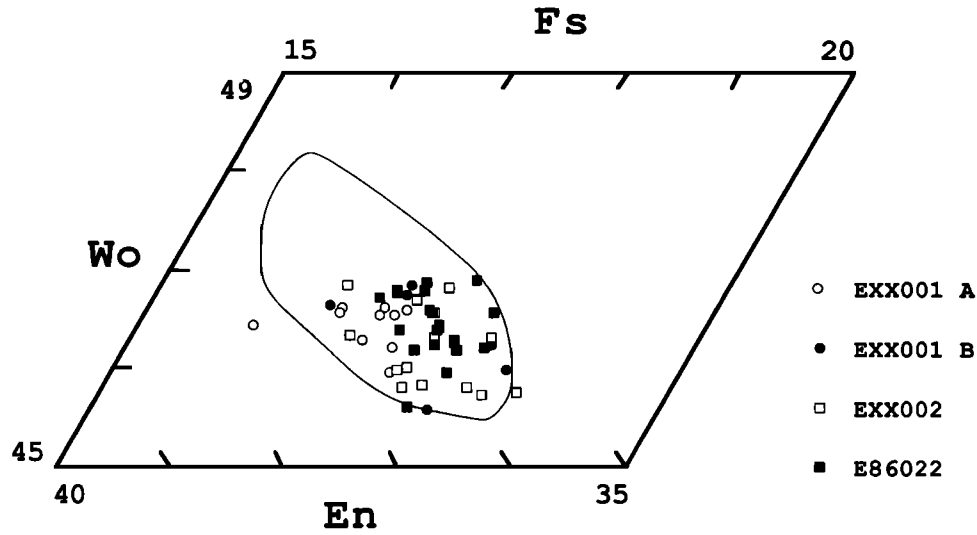
Fig. 2. Electron microprobe analyses of four larger clinopyroxene crystals intergrown with anortho-clase. The field shows the range of compositions for clinopyroxene from the bombs (see Figure 1).
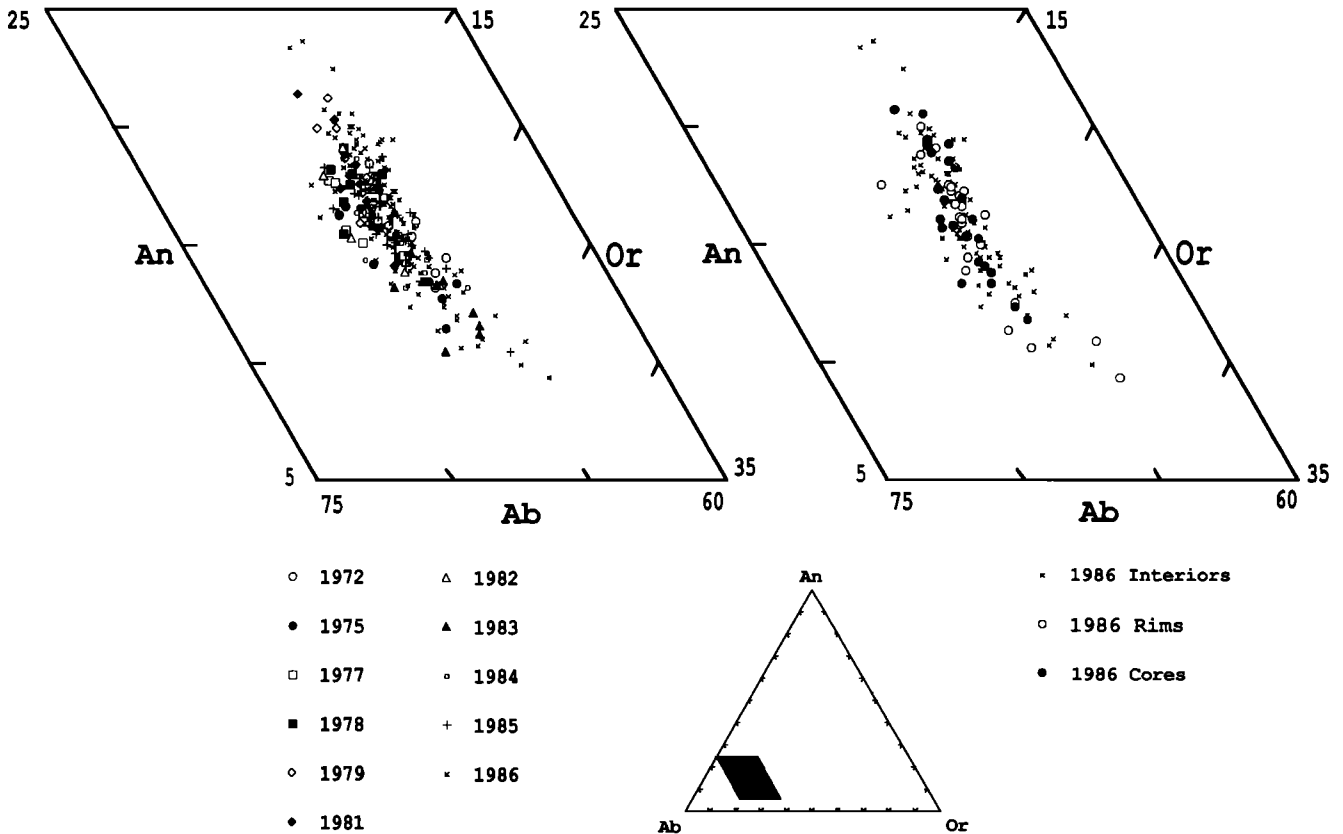
Fig. 3. Electron microprobe analyses of anorthoclase phenocrysts in bombs erupted from Mount Erebus between 1972 and 1986. Upper right-hand plot shows anorthoclase separated from bombs erupted in 1986. The zonation in anorthoclase is not systematic; there is an overlap in compositions of analyses made at core, rim, and intermediate positions on crystals.

TABLE 5. Average Electron Microprobe Analyses of Magnetites Separated From Bombs Erupted Between 1972 and 1986 From Mount Erebus

	1972 (6)*	1975 (12)	1977 (6)	1978 (4)	1979 (6)	1981 (4)	1982 (6)	1983 (4)	1984 (2)	1985 (4)	1986 (4)
TiO_2	25.03	25.10	24.96	25.07	24.96	24.59	24.65	24.51	24.75	24.26	24.13
Al_2O_3	2.39	2.33	2.32	2.30	2.27	2.37	2.38	2.29	2.33	2.29	2.32
Fe_2O_3	19.51	19.51	19.43	19.38	20.18	20.45	19.87	20.48	20.09	20.55	20.64
FeO	48.51	48.64	48.41	48.43	48.67	48.29	48.16	47.99	48.52	47.82	47.80
MnO	1.79	1.78	1.69	1.76	1.75	1.63	1.74	1.70	1.54	1.57	1.39
MgO	2.90	2.88	2.89	2.93	2.90	2.88	2.83	2.92	2.88	2.85	2.87
Total	100.1	100.2	99.70	99.87	100.7	100.2	99.63	99.89	100.1	99.34	99.15

*Number of analyses averaged.

erupted between 1972 and 1986 were examined. A detailed study was made of anorthoclase from bombs erupted in 1986 (Figure 3). Microprobe traverses, averaging nine analyses, were made from the rim to the core of each crystal. The average distance between analyses (stepping distance) was typically ~500 μm. The anorthoclase has a near-constant albite composition of Ab_{67}, whereas the variation in anorthite is An_{23} to An_{12} and orthoclase variation is from Or_9 to Or_{21}.

Chemical zonation ($An_{12-23}Ab_{65-69}Or_{9-21}$) is present in all the anorthoclase (Figure 3), with many showing oscillatory character. Major element zonation patterns do not appear to be related to common growth histories. No trends or patterns of chemical zonation common to multiple crystals taken from single bombs are noted.

Similarly, no systematic variation in zonation patterns is seen over time.

Core areas of the phenocrysts often appear "spongy," containing many large irregular melt inclusions. The rim areas have a small-scale melt-inclusion/host-crystal banding. The core morphology may reflect a phase of fast initial growth, whereas the finely banded rim may represent slower growth in the lava lake [Reagan et al., 1992; Dunbar et al., this volume]. The observed zonation in these phenocrysts is probably related to growth rates and differences in elemental diffusion rates.

Magnetite

Average electron microprobe analyses of magnetite in bombs erupted from Mount Erebus between 1972 and 1986 are given in Table 5. The FeO and Fe_2O_3 contents and the magnetite composition, expressed as ulvöspinel (Usp) content, were determined following the method of Stormer [1983]. In a plot of magnetite composition versus the year of eruption (Figure 4), a marked break in the slope of the composition curve occurs at 1978, and by 1986 a ~2 wt % decrease in Usp content is noted. This trend is reflected in the analyses by decreasing TiO_2 contents (Table 5). Magnetites collected in 1984 deviate from the trend and have higher Usp contents relative to the years before and after. As the 1984 data are based on only two analyses, the significance of the deviation is difficult to judge.

Among the minerals analyzed, only magnetite shows any systematic variation in composition with time (Figure 4). Because magnetite reequilibrates quickly under magmatic conditions [Lindsley, 1976], variation in the Mount Erebus magnetite compositions presents an
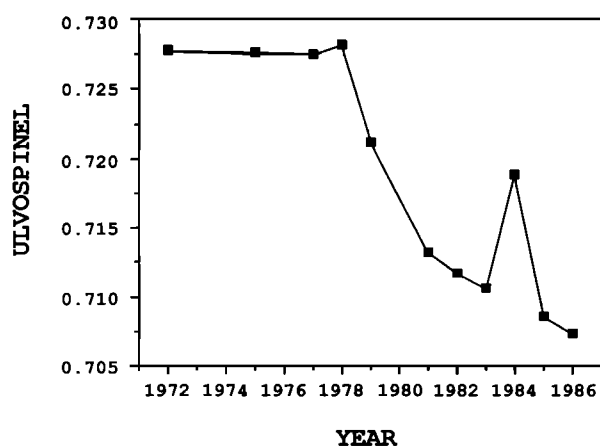
Fig. 4. Average ulvöspinel content (in weight fraction) calculated from microprobe analyses of magnetite in bombs erupted from Mount Erebus between 1972 and 1986.
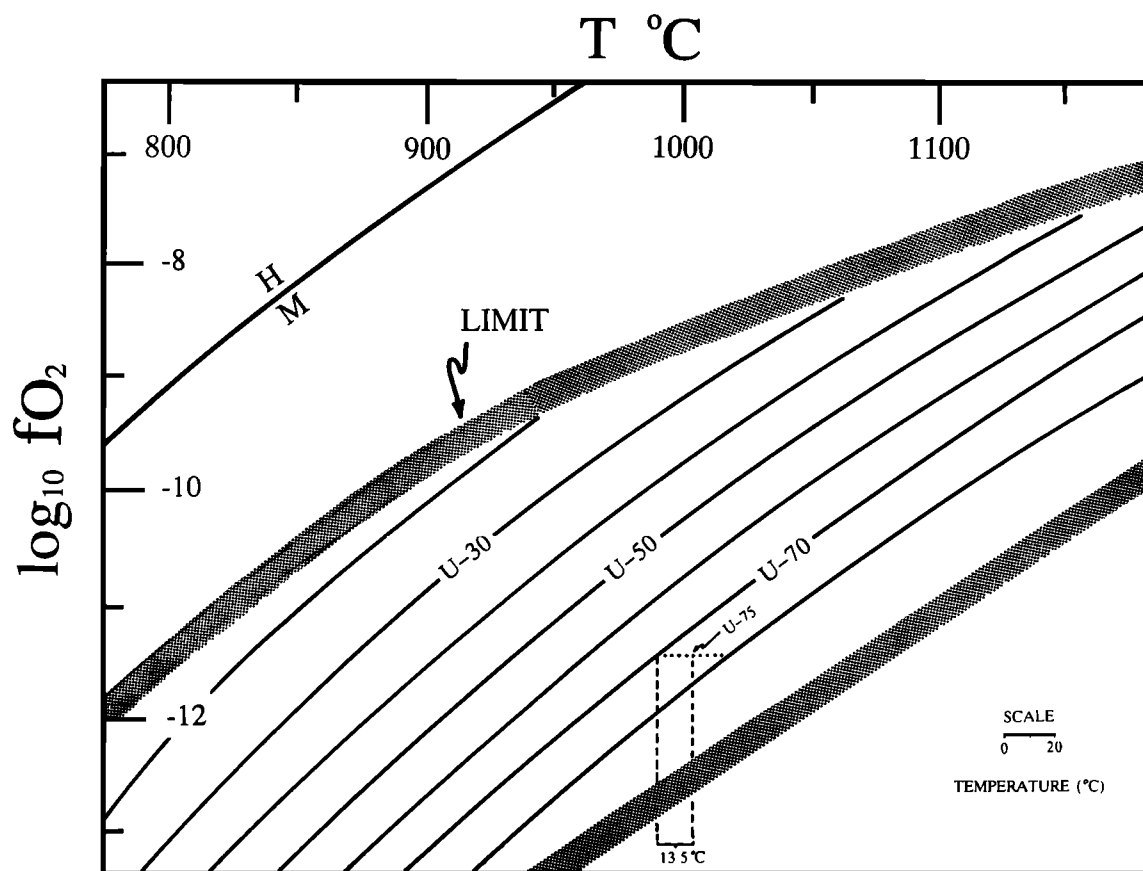
Fig. 5. Variation in magnetite composition plotted on a temperature versus oxygen fugacity diagram. Ulvöspinel contents expressed as percentages are shown by the lines labeled U. At constant oxygen fugacity the change in magnetite composition from Usp_{70} to Usp_{75} would correspond to a temperature change of about 13°C. Figure after *Spencer and Lindsley* [1981].

accurate, quenched record of the magmatic conditions immediately preceding eruption. The change in the ulvöspinel trend between 1978 and 1979 coincides with the cessation of lake growth seen over the 1970s [*Kyle et al.*, 1982, unpublished observations, 1985] and may be the result of some progressive, physiochemical change in this system.

Temperature and oxygen fugacity fo_2 were examined as the two variables most likely to affect the chemistry of the Mount Erebus magnetite. Degassing of the magma in the lava lake may affect the fo_2 of the magma. Degassing of sulphur (S) at a constant temperature could influence the fo_2 according to the following reaction:

$$3FeS + 2O_2(g) = Fe_3O_4 + 3/2\ S_2(g)$$
pyrrhotite   magnetite
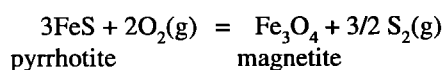
This reaction would be driven to the right by loss of S

as S_2 gas, resulting in a decrease in the fo_2 of the magma, and a corresponding increase in ulvöspinel component in the magnetite [*Spencer and Lindsley*, 1981] (Figure 5). This result is opposite to that observed in Mount Erebus magnetites and suggests that fo_2 in the lava lake has probably remained relatively constant. Constant fo_2 is consistent with the lack of any significant Na enrichment in the clinopyroxene.

Alternatively, a relatively small decrease in temperature, while holding fo_2 constant, could account for the observed decrease in ulvöspinel. At a starting temperature of 1000°C and log fo_2 of -12.2, typical of Mount Erebus magma [*Kyle*, 1977], cooling by 10°–15°C could account for the observed change in magnetite composition [*Spencer and Lindsley*, 1981] (Figure 5). This interpretation is preferred for the observed trend of decreasing TiO_2 in Mount Erebus magnetites.

It is unclear whether the anomalously high ulvöspinel percentage in 1984 represents a true anomaly associated

TABLE 6. Whole Rock, Major Element Analyses (in Weight Percent) of Recent Volcanic Ejecta From Mount Erebus

	1 25726 1972	2 25724 1972/1973	3 25721 1974/1975	4 2E2 1974/1975	5 2E6 1974/1975	6 25723 1975/1976	7 77015 1977/1978	8 77016 1977/1978	9 78003 1977/1978	10 78004 1977/1978	11 78200 1978/1979	12 78325 1978/1979
SiO_2	55.16	56.13	56.41	56.36	56.19	55.96	55.59	56.64	56.18	56.43	56.84	56.01
TiO_2	1.06	0.95	0.91	0.93	0.95	0.98	0.99	0.92	0.99	0.93	0.84	0.93
Al_2O_3	19.72	20.04	20.20	20.20	20.13	19.92	19.89	20.26	20.14	20.15	19.67	19.98
FeO^*	5.19	4.82	4.48	4.71	4.78	4.94	5.00	4.57	4.88	4.56	4.33	4.78
MnO	0.23	0.21	0.22	0.21	0.21	0.22	0.22	0.21	0.22	0.21	0.29	0.33
MgO	0.97	0.84	0.82	0.83	0.83	0.89	0.91	0.83	0.82	0.87	0.87	1.00
CaO	2.64	2.68	2.74	2.65	2.63	2.65	2.55	2.68	2.57	2.69	2.67	2.66
Na_2O	8.68	8.41	8.59	8.59	8.45	8.48	8.68	8.57	8.67	8.73	7.95	8.28
K_2O	4.70	4.50	4.47	4.57	4.59	4.57	4.70	4.52	4.72	4.53	4.38	4.58
P_2O_5	0.44	0.39	0.38	0.38	0.39	0.42	0.40	0.38	0.40	0.37	0.37	0.39
LOI	0.19	0.00	0.07	0.07	0.01	0.00	0.00	0.00	0.00	0.07	0.00	0.00
Total	98.97	98.97	99.20	99.50	99.16	99.03	98.93	99.53	99.51	99.47	98.21	98.94

*Total Fe as FeO.
LOI, loss on ignition at 1000°C.

with the 1984 eruptive event or normal statistical variance due to small sample population (two analyses). Additional analyses will be needed to clarify this point.

Whole Rock

Major and trace element analyses of whole rock samples have been made of a select number of bombs erupted in the 1970s and early 1980s (Tables 6, 7, and 8). Major element compositions of the bombs are typical of anorthoclase phonolite lavas from the flanks of Mount Erebus [Kyle et al., 1992]. Small variations, outside of analytical error, are shown for most elements.

Chondrite-normalized rare earth element (REE) plots (Figure 6) of two whole rock samples (Table 7) show strong light REE enrichment and a small positive Eu anomaly. For the other trace elements analyzed in the whole rock samples, only Sr and Zr show significant variations (Table 8). Sr ranges from 843 to 997 ppm, whereas Zr ranges from 917 to 1000 ppm.

The range in whole rock major and trace element analyses are not considered significant in terms of small, subtle variations in the anorthoclase phonolite magma composition; rather, they are more likely to be an artifact of sample collection and transportation and analytical uncertainties. Preparation of bomb samples for whole rock analysis is difficult because of their strongly vesicular and porphyritic nature. The large, dense anorthoclase phenocrysts are easily fractionated and can be lost from the fragile, low-density pumiceous matrix during handling, transport, and sample preparation. Because the anorthoclase can reach up to 10 cm in length and have typical modal abundances of 30–40%, it is necessary to grind over 5 kg of samples. Even with such large samples it is difficult to guarantee that it is representative.

The anorthoclase phenocrysts contain over 2500 ppm Sr [Kyle, 1977], whereas the matrix (groundmass) glass has a low Sr content of about 250 ppm (Table 9). The variation in Sr content of the whole rock samples, therefore, reflects variations in anorthoclase contents. Conversely, Zr is an incompatible element in the phonolite magma and is concentrated in the matrix glass where it typically ranges from 1300 to 1400 ppm (Table 9). In the whole rock samples an inverse correlation is seen between Sr and Zr. As the relative abundance of anorthoclase increases, so does the Sr content of the sample, which in turn reduces the amount of matrix glass, resulting in decreased Zr content.

Whole rock samples, therefore, do not provide an ideal means to examine the magma composition and its possible evolution with time. However, although fraught

TABLE 7. Instrumental Neutron Activation Analyses of Whole Rock Samples of Bombs Erupted From Mount Erebus

	1 78325 1978/1979	2 81003 1980/1981
FeO*	4.40	4.73
Na₂O	8.71	8.42
Sc†	2.40	2.79
Cr	3.1	1.0
Co	—	2.4
Rb	116	108
Sb	0.35	0.31
Cs	1.33	1.36
Ba	1045	1026
La	130.5	130.1
Ce	247	246
Sm	14.78	14.92
Eu	4.72	4.74
Tb	1.74	1.78
Yb	5.44	5.46
Lu	0.733	0.784
Hf	21.4	21.07
Ta	15.6	15.6
Th	19.5	19.2
U	6.7	5.2

*Total Fe as FeO. FeO and Na₂O in weight percent.
†Trace elements in ppm.

with sampling and analytical problems, whole rock analyses do show that as a first-order observation, the bulk composition of the phonolite magma remained unchanged during the 1970s. No significant changes in composition should be expected, considering the general uniformity in composition of older lavas. Analyses of lava flow samples from the summit area (P. R. Kyle, unpublished data, 1992) and the base and flanks of the volcano [Kyle et al., 1992] show them to be similar in mineralogy and composition. It is apparent that Mount

Erebus has erupted anorthoclase-phyric phonolite, similar in mineralogy and composition to that occurring in the present lava lake, for ~1,000,000 years. The magmatic evolution of the phonolite by fractionational crystallization from a mantle-derived basanite parent [Kyle et al., 1992] has occurred in a uniform manner throughout the life of the volcano.

Glass

XRF and instrumental neutron activation major and trace element analyses of bulk matrix glass samples separated from bombs are given in Tables 9 and 10. Microprobe analyses of matrix glass separates from bombs erupted between 1972 and 1986 are given in Table 11 and represent the average of 9–14 (mean 12) separate spot analyses.

XRF analyses show scatter outside that expected from analytical error alone (Table 9). However, the analyses show no systematic trends with time. The largest variation is shown by Sr which ranges from 222 to 301 ppm.

Chondrite–normalized REE plots (Figure 6) of bulk matrix glass separates (Table 10) show a small spread. The glass has higher REE abundances than the whole rock samples with the exception of Eu. There is a pronounced negative Eu anomaly in the glass. REE analyses of the anorthoclase [Kyle and Rankin, 1976; Sun and Hanson, 1976] show them to have large positive Eu anomalies. The negative Eu anomaly in the glass, therefore, results from anorthoclase crystallization. The heavy REE are more enriched than the light REE in the glass relative to the whole rock samples. This pattern probably reflects clinopyroxene crystallization.

There are minor variations in trace element concentrations in analyses of bulk glass samples, especially for Sr. Most of this scatter is due to incomplete separation of phenocrysts and microphenocryst phases from the

TABLE 8. Whole Rock, Trace Element Analyses (in ppm) of Recent Volcanic Ejecta From Mount Erebus

	1 2E2 1974/1975	2 2E6 1974/1975	3 25723 1975/1976	4 78200 1978/1979	5 78325 1978/1979	6 79301 1979/1980	7 81003 1980/1981	8 81410 1981/1982	9 82420 1982/1983
Rb	103	107	110	103	104	112	107	104	105
Sr	922	879	863	971	977	843	879	961	924
Y	57	58	60	57	56	60	59	55	57
Zr	929	957	989	919	917	1000	963	923	946
Nb	246	254	262	243	243	266	256	243	251
Mo	17	18	18	17	17	18	17	17	17
Pb	2	3	–	1	1	2	2	1	2
Th	20	20	18	19	19	22	20	18	19

TABLE 9. Major (in Weight Percent) and Trace Element (in ppm) Analyses of Bulk Samples of Glass Separated From Bombs Erupted Between 1974 and 1986 From Mount Erebus

	1	2	3	4		5		6	7	8	9	10	11
	2E2G	25723G	77015G	78003G		78325G		79301G	79302G	80401G	81003G	81005G	82415G
	1974/1975	1975/1976	1977/1978	1977/1978	$n=3$	1978/1979	$n=3$	1979/1980	1979/1980	1980/1981	1980/1981	1980/1981	1982/1983
SiO_2	56.04	54.69	55.06	55.16	±0.09	55.35	±0.08	55.91	54.59	54.52	55.28	55.01	55.18
TiO_2	0.95	1.09	1.02	0.97	±0.01	0.98	±0.00	0.99	0.98	0.97	0.98	0.97	1.02
Al_2O_3	19.67	19.20	19.32	19.22	±0.06	19.34	±0.00	19.40	19.17	19.14	19.43	19.29	19.54
$FeO*$	4.97	5.80	5.61	5.61	±0.06	5.37	±0.005	5.42	5.49	5.46	5.39	5.34	5.55
MnO	0.23	0.27	0.26	0.27	±0.005	0.26	±0.00	0.25	0.26	0.26	0.26	0.26	0.27
MgO	0.87	0.97	0.90	1.06	±0.03	0.84	±0.01	0.83	0.86	0.86	0.85	0.83	0.88
CaO	2.49	2.16	2.08	2.12	±0.02	1.96	±0.00	1.90	2.00	2.04	1.98	1.99	2.12
Na_2O	8.53	8.90	8.92	9.01	±0.19	9.07	±0.03	8.93	9.06	9.05	9.04	8.61	9.06
K_2O	4.83	5.39	5.43	5.41	±0.03	5.51	±0.01	5.49	5.52	5.49	5.49	5.45	5.48
P_2O_5	0.39	0.44	0.39	0.38	±0.01	0.32	±0.00	0.29	0.39	0.39	0.32	0.36	0.35
Total	98.97	98.91	98.99	98.85		99.00		99.42	98.32	98.19	99.02	98.10	99.46
Rb	148	150	145	148		150		149	147	151	148	148	151
Sr	256	244	301	243		254		256	229	247	260	264	258
Y	80	80	79	77		77		76	77	79	77	78	79
Zr	1368	1385	1337	1388		1376		1387	1406	1383	1354	1369	1379
Nb	365	369	357	370		366		369	376	368	361	365	368
Mo	26	26	26	26		26		26	26	27	26	26	26
Pb	7	7	14	6		8		7	6	11	9	10	11
Th	32	33	32	33		33		34	34	33	32	34	36

	12	13	n=3	14	n=3	15	n=3	16	17	18	19	20	21
	82418G	83207G		83208G		83220G		84500G	84501G	84505G	85009G	85010G	86007G
	1982/1983	1983/1984		1983/1984		1983/1984		1984/1985	1984/1985	1984/1985	1985/1986	1985/1986	1986/1987
SiO_2	55.00	55.22	±0.09	55.33	±0.13	55.14	±0.08	55.24	55.16	55.27	55.14	54.88	54.26
TiO_2	0.98	0.97	±0.01	0.96	±0.01	0.98	±0.01	0.99	0.98	0.97	0.99	1.00	1.03
Al_2O_3	19.30	19.43	±0.12	19.31	±0.12	19.41	±0.03	19.33	19.45	19.37	19.31	19.29	18.80
$FeO*$	5.40	5.43	±0.06	5.38	±0.02	5.39	±0.02	5.57	5.41	5.36	5.44	5.60	6.09
MnO	0.26	0.26	±0.00	0.26	±0.00	0.26	±0.00	0.27	0.26	0.26	0.26	0.27	0.30
MgO	0.90	0.88	±0.02	0.98	±0.02	0.91	±0.01	0.94	0.92	0.85	0.90	0.90	1.30
CaO	2.08	2.11	±0.01	2.28	±0.00	2.14	±0.01	2.16	2.10	2.15	2.09	2.14	2.33
Na_2O	9.32	9.04	±0.02	8.86	±0.05	9.00	±0.23	9.02	9.03	9.10	9.08	8.67	8.96
K_2O	5.49	5.44	±0.00	5.29	±0.00	5.48	±0.00	5.45	5.43	5.45	5.45	5.49	5.27
P_2O_5	0.41	0.41	±0.00	0.43	±0.00	0.43	±0.00	0.47	0.40	0.44	0.42	0.46	0.54
Total	99.12	99.19		99.08		99.14		99.44	99.14	99.23	99.08	98.70	98.88
Rb	151	147	±1	143		148		150	147	148	148	152	145
Sr	248	295	±2	368		281		263	301	288	275	222	292
Y	80	79	±0.05	77		79		82	78	80	80	84	82
Zr	1387	1347	±1	1294		1356		1370	1346	1359	1360	1399	1340
Nb	371	359	±0.2	344		352		365	352	362	362	373	356
Mo	26	26	±0.3	25		26		26	26	26	26	27	26
Pb	7	6	±2	8		7		7	6	6	6	6	5
Th	33	32	±1	30		34		34	31	33	32	33	31

*Total Fe as FeO.

Standard deviations on replicate analyses are listed for selected sample; n, number of analyses. All analyses by XRF.

TABLE 10. Instrumental Neutron Activation Analyses of Bulk Samples of Glass Separated From Bombs
Erupted Between 1974 and 1986 From Mount Erebus

	1 25721G 1974/1975	2 2E2G 1974/1975	3 2E6G 1974/1975	4 77015G 1977/1978	5 77016G 1977/1978
FeO*	5.97	5.68	5.86	5.53	6.33
Na$_2$O	9.34	9.30	9.28	9.32	8.83
Sc†	3.72	3.74	3.60	3.16	4.05
Cr	<10	<10	<10	<10	<10
Co	2.7	2.9	3.1	2.1	3.6
As	3.1	2.9	3.2	3.2	3.1
Rb	148	142	146	149	139
Sb	0.54	0.53	0.49	0.50	0.48
Ba	445	460	366	416	418
Cs	2.02	1.86	1.94	1.96	1.77
La	169	161	159	162	167
Ce	337	322	318	322	335
Sm	20.4	19.3	19.1	18.8	20.4
Eu	4.17	4.07	3.89	3.93	4.26
Tb	2.51	2.45	2.46	2.45	2.58
Yb	7.41	7.31	7.31	7.42	7.32
Lu	1.05	1.01	1.02	1.04	0.98
Hf	30.9	30.4	30.4	31.3	29.2
Ta	25.8	25.4	25.4	26.1	24.3
Th	29.2	29.0	28.6	29.7	27.8
U	7.1	7.8	7.7	7.9	7.6

	6 78003G 1977/1978	7 78004G 1977/1978	8 78200G 1978/1979	9 78325G 1978/1979	10 79301G 1979/1980
FeO*	5.92	6.47	5.40	5.35	5.74
Na$_2$O	9.34	8.92	9.14	9.16	8.94
Sc†	3.51	3.35	3.06	3.06	3.35
Cr	<10	<10	<10	<10	<10
Co	3.0	4.0	2.1	2.3	2.6
As	3.6	2.9	3.1	2.6	2.6
Rb	143	158	141	142	137
Sb	0.52	0.47	0.48	0.48	0.47
Ba	433	414	431	426	420
Cs	1.83	2.19	1.92	1.85	1.81
La	163	156	157	157	157
Ce	319	303	307	304	309
Sm	19.5	18.5	18.2	18.4	18.6
Eu	3.99	3.92	3.77	3.76	3.93
Tb	2.43	2.39	2.31	2.34	2.36
Yb	7.12	6.95	7.20	7.26	6.83
Lu	1.03	1.01	1.00	1.00	0.93
Hf	30.3	29.3	30.3	30.0	29.1
Ta	25.3	25.0	25.3	25.4	24.6
Th	28.9	27.7	28.9	28.8	27.8
U	7.7	7.4	7.7	8.1	7.3

*Total Fe as FeO. FeO and Na$_2$O in weight percent.
†Trace elements in ppm.

TABLE 10. (continued)

	11 79302G 1979/1980	12 80300G 1980/1981	13 81003G 1980/1981	14 81005G 1980/1981	15 83211G 1983/1984
FeO*	5.80	5.97	5.47	5.81	5.32
Na$_2$O	9.29	9.09	9.36	9.23	—
Sc†	3.71	3.64	3.11	4.19	3.10
Cr	<10	<10	<10	<10	<10
Co	2.5	2.8	2.1	2.7	2.1
As	3.3	3.3	3.2	2.7	—
Rb	143	143	150	139	143
Sb	0.51	0.49	0.50	0.50	0.40
Ba	417	440	457	463	480
Cs	1.82	1.80	1.98	1.94	1.88
La	164	162	158	160	159
Ce	325	324	317	315	314
Sm	19.7	19.3	18.6	19.4	18.77
Eu	3.98	4.11	3.98	4.01	3.75
Tb	2.42	2.47	2.38	2.44	2.25
Yb	7.16	7.06	7.22	7.04	7.53
Lu	1.04	1.01	1.00	0.98	1.07
Hf	30.7	30.2	30.8	29.6	29.9
Ta	25.8	25.0	25.7	24.7	22.3
Th	29.5	28.5	29.2	28.1	27.7
U	7.5	7.8	7.8	8.2	7.8

	16 84500G 1984/1985	17 85009G 1985/1986	18 86022G 1986/1987	19 89001G 1989/1990
FeO*	5.42	5.46	5.74	5.32
Na$_2$O	9.01	9.08	9.16	9.21
Sc†	2.97	2.92	2.99	2.88
Cr	—	2.6	1.4	1.7
Co	2.2	2.3	2.4	2.1
As	—	—	—	—
Rb	144	140	142	146
Sb	0.43	0.34	0.44	0.40
Ba	488	582	448	458
Cs	1.84	1.78	1.86	1.94
La	167	156	167	158
Ce	320	306	322	312
Sm	19.66	18.38	19.68	18.60
Eu	3.85	3.92	3.86	3.74
Tb	2.34	2.16	2.34	2.24
Yb	7.46	7.14	7.35	7.44
Lu	1.04	1.01	1.03	1.01
Hf	29.8	28.4	29.6	29.4
Ta	21.6	21.15	21.6	22.3
Th	27.4	27.1	27.2	28.0
U	10.5	8.1	9.2	9.0

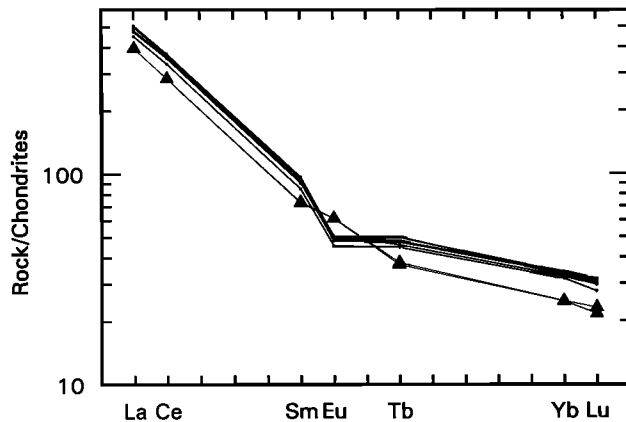*Total Fe as FeO. FeO and Na$_2$O in weight percent.
†Trace elements in ppm.

Fig. 6. Chondrite-normalized plot of rare earth element abundances in whole rock (triangles) and matrix glass (small dots) samples of volcanic bombs erupted from Mount Erebus.

glass separates. The variations in Sr can be explained by minor contamination of the glass by anorthoclase.

Matrix glass analyses were made to examine potential crystallization of the phonolite magma within the chamber and conduit system. In a phenocryst-rich magmatic system such as that at Mount Erebus, crystallization may be occurring. The current activity has been monitored for nearly 20 years with no obvious visual change in the character of the magma. However, over this 20-year period there has been ample time for crystallization to occur, which would not be apparent in hand specimen samples. Crystallization of the main phenocryst phases anorthoclase, clinopyroxene, olivine, and magnetite would modify the composition of the residual phonolitic magma. This residual magma is represented by the matrix glass forming the bombs.

The data in Table 2, and the standard deviations given for replicate analyses in Table 9, suggest that the electron microprobe analyses (Table 11) are less precise than the XRF analyses. However, it is apparent that the averaged electron microprobe analyses of the matrix glass are all identical within analytical error (Table 11). The microprobe analyses generally agree well with the bulk XRF analyses. Surprisingly, the microprobe analyses have systematically higher Na_2O contents. Electron microprobe analyses are frequently plagued by sodium loss from volatilization by the electron beam. However, the low beam current and enlarged beam used in this study overcame this difficulty. The higher Na_2O contents in the microprobe analyses probably represent inherent differences between XRF and electron microprobe standardization and data reduction techniques.

Electron microprobe analyses of the matrix glass from bombs erupted between 1972 and 1986 (Table 11)

are amazingly uniform. The simplest interpretation is that during this time the magma was not modified by crystallization of the observed phenocryst phases. On the basis of measured crystal size distributions and assumed crystal growth rates, Dunbar et al. [this volume] suggest that the average anorthoclase has a minimum approximate age of 100–300 years. Reagan et al. [1992], using a glass-anorthoclase (^{226}Ra)/Ba versus (^{230}Th)/Ba isochron plot, suggest that the average age of the anorthoclase is 2380 years. On the basis of these observations it is, therefore, not surprising that we observed no evidence for crystallization over a 14-year period.

MAGMATIC EVOLUTION

Careful and systematic analyses of olivine and clinopyroxene, whole rock and matrix glass samples from bombs erupted from Mount Erebus show no evidence for variations in composition over a 15-year period. Variations in magnetite compositions may be due to temperature changes and reflect slight cooling of the magmatic system over a 7-year period. Our data suggest that the significant increase in the number and size of strombolian eruptions during the period September to December 1984 was not a result of injection of a new batch of chemically different magma. The larger size of the eruptions implies a significant increase in the volatile content of the magma. Higher volatile content would result in saturation at deeper levels and the ascent of larger gas bubbles which would give larger explosions. If the volatiles were introduced into the magmatic system by injection of new magma, then this magma either (1) was identical in composition to that which already existed in the system or (2) had not yet reached the lava lake by late 1986, and thus was not available to be erupted as bombs or to be sampled for chemical analysis.

Reagan et al. [1992] have shown statistical differences in (^{230}Th)/(^{232}Th) and (^{238}U)/(^{232}Th) ratios in matrix glass from bombs erupted in 1984 and 1988. They suggest that between 1984 and 1988 a new magma batch was mixed into the lava lake. In our analyses of mineral, whole rock, and glass samples from bombs collected through 1986 we see no evidence of chemical changes. It does remain, however, a possibility that the 1984 eruptions were a consequence of an injection of a new volatile-rich batch of magma. The volatiles, especially CO_2, would exsolve and become decoupled from the magma and then rise rapidly to the surface. The degassed new magma batch would then mix with the existing magma and slowly convect to the surface. If

TABLE 11. Average Electron Microprobe Analyses of Matrix Glass Separated From Bombs Erupted Between 1972 and 1987 From Mount Erebus

	1972/1973 (13)*	1975/1976 (13)	1977/1978 (14)	1978/1979 (13)	1979/1980 (12)	1981/1982 (12)	1982/1983 (10)	1983/1984 (14)	1984/1985 (13)	1985/1986 (9)	1986/1987 (10)
SiO_2	55.38	55.54	55.60	55.65	55.66	55.45	55.29	55.96	55.88	55.74	55.60
Al_2O_3	19.02	19.03	19.45	19.49	19.33	19.39	19.23	19.59	19.53	19.37	19.41
TiO_2	1.03	1.02	1.04	1.06	1.09	1.00	1.06	1.04	1.01	1.07	1.05
FeO†	5.37	5.47	5.37	5.30	5.51	5.41	5.46	5.35	5.26	5.28	5.42
MnO	0.19	0.17	0.19	0.22	0.24	0.19	0.20	0.21	0.19	0.37	0.30
MgO	0.82	0.80	0.81	0.81	0.83	0.81	0.81	0.83	0.84	0.79	0.84
CaO	1.90	1.93	1.84	1.96	1.91	1.91	1.90	1.86	1.85	1.98	1.81
Na_2O	9.67	9.46	9.31	9.44	9.41	9.38	9.36	9.56	9.47	9.40	9.41
K_2O	5.20	5.32	5.35	5.10	5.22	5.27	5.19	5.34	5.39	5.42	5.31
Total	98.58	98.74	98.96	99.03	99.20	98.81	98.50	99.74	99.42	99.42	99.15

*Number of analyses averaged.
†Total Fe as FeO.

this is the case, our data suggest that it may have taken 2–4 years for this magma to reach the surface where it was erupted and sampled in 1988. This implies the Erebus lava lake is underlain by a large magma chamber complex which is only slowly convecting from depth. Convective overturn of the magmatic system may take many years.

REFERENCES

Bence, A. E., and A. L. Albee, Empirical correction factors for the electron microanalysis of silicates and oxides, *J. Geol.*, *76*, 382–402, 1968.

Dibble, R. R., J. Kienle, P. R. Kyle, and K. Shibuya, Geophysical studies of Erebus volcano, Antarctica, from 1974–1981, *N. Z. J. Geol. Geophys.*, *27*, 425–455, 1984.

Dunbar, N., K. V. Cashman, and R. Dupre, Crystallization processes of anorthoclase phenocrysts in the Mount Erebus magmatic system: Evidence from crystal composition, crystal size distributions and volatile contents of melt inclusions, this volume.

Dupre, R. M., The origin of anorthoclase megacrysts from Mount Erebus, Ross Island, Antarctica, B.S. thesis, Princeton Univ., Princeton, N. J., 1990.

Giggenbach, W. F., P. R. Kyle, and G. Lyon, Present volcanic activity on Mt. Erebus, Ross Island, Antarctica, *Geology*, *1*, 135–136, 1973.

Kyle, P. R., Mineralogy and glass chemistry of recent volcanic ejecta from Mt. Erebus, Ross Island, Antarctica, *N. Z. J. Geol. Geophys.*, *20*, 1123–1146, 1977.

Kyle, P. R., and P. C. Rankin, Rare earth element geochemistry of Late Cenozoic alkaline lavas of the McMurdo Volcanic Group, Antarctica, *Geochim. Cosmochim. Acta*, *40*, 1497–1507, 1976.

Kyle, P. R., R. R. Dibble, W. F. Giggenbach, and J. Keys,

Volcanic activity associated with the anorthoclase phonolite lava lake, Mt. Erebus, Antarctica, in *Antarctic Geoscience*, edited by C. Craddock, pp. 735–745, University of Wisconsin Press, Madison, 1982.

Kyle, P. R., J. A. Moore, and M. F. Thirlwall, Petrologic evolution of anorthoclase phonolite lavas at Mount Erebus, Ross Island, Antarctica, *J. Petrol.*, *33*, 849–875, 1992.

Lindsley, D. H., Experimental studies of oxide minerals, in *Oxide Minerals*, *Rev. in Mineral.*, vol. 3, edited by D. Rumble, pp. 61–84, Mineralogical Society of America, Washington, D. C., 1976.

Moore, J. A., Mineralogy, geochemistry and petrogenesis of the lavas of Mount Erebus, Antarctica, M.S. thesis, N. M. Inst. of Min. and Technol., Socorro, 1987.

Norrish, K., and B. W. Chappell, X-ray fluorescence spectrometry, in *Physical Methods in Determinative Mineralogy*, 2nd ed., edited by J. Zussman, pp. 210–272, Academic, San Diego, Calif., 1977.

Norrish, K., and J. T. Hutton, An accurate X-ray spectrographic method for the analysis of a wide range of geochemical samples, *Geochim. Cosmochim. Acta*, *33*, 431–453, 1969.

Papike, J. J., K. L. Cameron, and K. Baldwin, Amphibole and pyroxenes: Characterization of other than quadrilateral components and estimates of ferric iron from microprobe data, *Geol. Soc. Am. Abstr. Programs*, *6*, 1053–1054, 1974.

Powell, M., and R. Powell, An olivine-clinopyroxene geothermometer, *Contrib. Mineral. Petrol.*, *48*, 249–263, 1974.

Reagan, M. K., A. M. Volpe, and K. V. Cashman, ^{238}U- and ^{232}Th-series chronology of phonolite fractionation at Mount Erebus, Antarctica, *Geochim. Cosmochim. Acta*, *56*, 1401–1407, 1992.

Spencer, K. J., and D. H. Lindsley, A solution model for coexisting iron-titanium oxides, *Am. Mineral.*, *66*, 1189–1201, 1981.

Stormer, J. C., The effects of recalculation on estimates of temperature and oxygen fugacity of multicomponent iron-titanium oxides, *Am. Mineral.*, *68*, 586–594, 1983.

Sun, S.-S., and G. N. Hanson, Rare earth element evidence for differentiation of McMurdo volcanics, Ross Island, Antarctica, *Contrib. Mineral. Petrol.*, *54*, 139–155, 1976.

Williams, H., F. J. Turner, and C. M. Gilbert, *Petrography*, W. H. Freeman, San Francisco, Calif., 1954.

D. A. Caldwell, P.O. Box 3105, Elko, NV 89801.

P. R. Kyle, Department of Geoscience, New Mexico Institute of Mining and Technology, Socorro, NM 87801.